PERMANENT DEFORMATION BEHAVIOUR OF FLEXIBLE PAVEMENTS

PHILIPPUS CORNELIUS PETRUS LOOTS SCHUTTE

A dissertation submitted in partial fulfilment of the requirements for the degree of

MASTER OF ENGINEERING (TRANSPORTATION ENGINEERING)

in the

FACULTY OF ENGINEERING, BUILT ENVIRONMENT AND INFORMATION TECHNOLOGY

UNIVERSITY OF PRETORIA

August 2018

DISSERTATION SUMMARY

PERMANENT DEFORMATION BEHAVIOUR OF FLEXIBLE PAVEMENTS

P.C.P.L. SCHUTTE

Supervisor: Professor W.J.vdM. Steyn

Department: Civil Engineering

University: University of Pretoria

Degree: Master of Engineering (Transportation Engineering)

Permanent deformation (rutting) is a pavement distress condition visible in the surfacing layer of a pavement. It occurs along the wheel path and results from the accumulation of load-induced permanent deformation developed from all individual pavement layers, including the subgrade. It is one of the major distress conditions in flexible pavements. Plenty of research regarding permanent deformation in flexible pavements exists, but it is mainly focused on asphalt surface layers and granular base, subbase, and subgrade layers.

The South African National Roads Agency Ltd (SANRAL) completed the construction of seven flexible pavement sections on the R104, between the east of Pretoria and Bronkhorstspruit, during 2013. In-situ pavement response and environmental related data have been collected from these test sections ever since on a number of occasions. The seven flexible pavement structures include a natural gravel (G4) base, a high-quality graded crushed stone (G1) base, a Foam Treated Base (FTB), an Emulsion Treated Base (ETB), a Cement Treated Base (CTB), a Bitumen Treated Base (BTB), and a High Modulus Asphalt (HiMA)/Enrobés à Module Elevé (EME) base.

The permanent deformation behaviour of different flexible pavements relative to each other was investigated by processing, validating, and analysing the relevant in-situ pavement response and environmental related data collected from each of the SANRAL test sections. With the focus on total and base layer deformation, it was found that in terms of a short-term loading response and under normal operating conditions, bituminous pavements show superior performance to cement/bitumen stabilised pavements, while the latter performs better than granular pavements. CTB and ETB

pavements are very similar with FTB pavements closely behind. The only granular exceptions are inverted crushed stone pavements, which should closely follow bituminous pavements at the top end of the performance range. For permanent deformation behaviour in terms of a longer-term recovering response, it was found that bituminous pavements tend to recover a larger amount of the permanent deformation attained after load application than granular pavements, probably due to the delayed elasticity (visco-elastic properties) of bituminous materials.

The possibility of a transfer function for linking the permanent deformation behaviour of a pavement to its structural integrity was also investigated by determining a representative pavement number for each of the SANRAL test sections. It was found that the permanent deformation behaviour of flexible pavements relates relatively well to their structural integrity as a general decrease in permanent deformation (rut rate) was observed with an increase in pavement number. A negative power function for linking permanent deformation behaviour to structural integrity was proposed ($y = 76.657x^{-0.752}$, $R^2 = 0.77$).

Additionally, it was found that post-compaction trafficking has a significant effect on the permanent deformation behaviour of flexible pavements during the initial stages of their life cycle; temperature variations can have a major influence on the in-situ performance and behaviour of bituminous layers, and the permanent deformation behaviour of flexible pavements correlates positively with the corresponding dynamic response as an increase in permanent deformation (rut rate) was observed with an increase in maximum dynamic deflection (positive linear function, $y = 0.0361x - 2.5687$, $R^2 = 0.92$).

DECLARATION

I, the undersigned hereby declare that:

- I understand what plagiarism is and I am aware of the University's policy in this regard;
- The work contained in this dissertation is my own original work;
- I did not refer to work of current or previous students, lecture notes, handbooks or any other study material without proper referencing;
- Where other people's work has been used this has been properly acknowledged and referenced;
- I have not allowed anyone to copy any part of my dissertation;
- I have not previously in its entirety or in part submitted this dissertation at any university for a degree.

Signature of student: 

Name of student: **P.C.P.L. SCHUTTE**

Student number: **12021084**

Date: **30/08/2018**

ACKNOWLEDGEMENTS

I wish to express my appreciation to the following organisations and persons who made this dissertation possible:

a) Professor W.J.vdM. Steyn, my supervisor for this dissertation, for his interest, guidance and mentoring during this study.

b) The South African National Roads Agency Limited (SANRAL) for making their R104 experimental site available for testing.

c) The University of Pretoria (UP) for collecting the necessary data from the SANRAL experimental site.

d) Mrs. Cora Bezuidenhout at UP for her library assistance throughout the course of this dissertation.

e) Mr. Colin Fisher at CSIR for his assistance with the strata data.

f) Mr. Andrew Mackellar at SANRAL for assisting me with my numerous questions regarding the SANRAL TSD, in-situ sensors and collected data.

g) My family and friends for their ongoing support, interest and motivation.

h) My friend, Bernard Jansen van Vuuren, for his insights and advice.

i) My sister, Dr. Marietjie Schutte-Smith, for proofreading large parts of this dissertation.

j) My Lord and Saviour for providing me with the willpower and wisdom to take on and complete this project.

TABLE OF CONTENTS

1. INTRODUCTION 1

1.1. Background 1

1.2. Objectives of the Study 2

1.3. Scope of the Study 3

1.4. Methodology 3

1.5. Layout of the Dissertation 4

2. LITERATURE STUDY 5

2.1. Introduction 5

2.2. Fundamental Behaviour of Pavement Materials 5

2.2.1. Plasticity 6

2.2.2. Shakedown Concept 9

2.3. Parameters Affecting Permanent Deformation 12

2.3.1. Effect of Density 12

2.3.2. Effect of Moisture Content 13

2.3.3. Effect of Temperature 16

2.4. Background on Flexible Pavement Materials 18

2.4.1. G4 Natural Gravel 19

2.4.2. G1 Crushed Stone 20

2.4.3. Bitumen Stabilised Material 21

2.4.4. Cemented Material 23

2.4.5. Asphalt 24

2.5. Permanent Deformation of Flexible Pavement Materials 26

2.5.1. Natural Gravel 31

2.5.2. Crushed Stone 31

2.5.3. Bitumen Foam Treated Material 32

2.5.4. Bitumen Emulsion Treated Material 33

2.5.5. Cemented Material 33
2.5.6. Large Aggregate Mixes 34
2.5.7. High Modulus Asphalt 35
2.6. Pavement Instrumentation 36
2.6.1. Multi-Depth Deflectometer 36
2.6.2. Strata Gauge 40
2.7. Traffic Speed Deflectometer 42
2.7.1. Pavement Response Analysis 43
2.7.2. Static vs Dynamic Response Analysis 44
2.8. Multi-Layer Elastic Theory 46
2.8.1. Moduli Back-Calculation 47
2.8.2. CHEV Computer Program 48
2.9. Pavement Number Design Method 51
2.9.1. Applicability and Limitations 51
2.9.2. Rules of Thumb 52
2.9.3. Effective Long-Term Stiffness (ELTS) 53
2.9.4. Modular Ratio Limit 54
2.9.5. Maximum Allowable Stiffness 54
2.9.6. Base Confidence Factor 54
2.9.7. Design Equivalent Material Class 55
2.10. Summary 55
3. METHODOLOGY 58
3.1. Introduction 58
3.2. SANRAL Experimental Site Setup 58
3.2.1. Material Properties 60
3.2.2. Instrumentation 61
3.2.3. Test Section Summary 62
3.3. Methods for Data Collection 67

3.3.1. Analysis of MDD Data 67
3.3.2. Moduli Back-Calculation Method 71
3.3.3. Pavement Number Calculation Method 72
3.4. Summary 75
4. DATA COLLECTION 76
4.1. Introduction 76
4.2. Collected Data 76
4.2.1. MDD Data 77
4.2.2. Temperature Data 79
4.2.3. Moisture Data 82
4.2.4. Density Data 85
4.3. Calculated Data 87
4.3.1. Permanent Deformation Behaviour 87
4.3.2. Back-Calculated Layer Moduli 89
4.3.3. Calculated Pavement Numbers 90
4.4. Summary 92
5. DISCUSSION 93
5.1. Introduction 93
5.2. Permanent Deformation Behaviour 93
5.3. Permanent Deformation vs Structural Integrity 96
5.3.1. Moduli Back-Calculation 98
5.3.2. Pavement Number Calculation 98
6. CONCLUSIONS AND RECOMMENDATIONS 99
6.1. Introduction 99
6.2. Conclusions 99
6.3. Recommendations 100
7. REFERENCES 102
8. APPENDICES 109

8.1. Appendix A: MDD Data 109

8.2. Appendix B: Moisture Data 113

8.3. Appendix C: Density Data 117

8.4. Appendix D: Moduli Back-Calculation Data 121

8.5. Appendix E: Pavement Number Data 131

LIST OF FIGURES

Figure 2-1: Permanent deformation mechanisms (Garba, 2002). 6

Figure 2-2: Permanent deformation development phases (AASHTO, 2004). 7

Figure 2-3: Structural vs non-structural permanent deformation (Gibb, 1996). 8

Figure 2-4: Approximation of Young's modulus by the resilient modulus (Theyse et al., 2011). 8

Figure 2-5: Permanent deformation under cyclic loading (Taherkhani, 2006). 9

Figure 2-6: Shakedown theory concept (Theyse et al., 2007) 10

Figure 2-7: Traffic moulding process (Kleyn and Steyn, 2015 & 2010). 11

Figure 2-8: Effect of increased density on permanent deformation (Barksdale, 1972). 12

Figure 2-9: Impact of internal moisture on granular materials (Kolisoja and Dawson, 2004). 14

Figure 2-10: Influence of drainage on permanent deformation (Dawson, 1990) 15

Figure 2-11: Thornthwaite's Moisture Index for South Africa (SANRAL, 2014). 15

Figure 2-12: HWTTs for standard HMA mix at different temperatures (Steyn et al., 2008). 17

Figure 2-13: Effect of temperature on different HMA mixes (Al-Mosawe, 2016) 17

Figure 2-14: Completed, slushed G1 base (Kleyn, 2012). 20

Figure 2-15: Slushing process (Boudreau et al., 2016). 21

Figure 2-16: Bitumen emulsion and foamed bitumen production (Asphalt Academy, 2009). 22

Figure 2-17: Aggregate-binder bond of BSMs (Asphalt Academy, 2009). 22

Figure 2-18: Typical cement treated base (AG Peltz, n.d.). 23

Figure 2-19: Typical bitumen treated base (Pavement Interactive, 2012a). 24

Figure 2-20: Aggregate packing theory (SANRAL, 2014) 25

Figure 2-21: Typical high modulus asphalt base (Nkgapele et al., 2012) 25

Figure 2-22: Change in permanent deformation of granular layers (Jordaan, 2006). 27

Figure 2-23: Change in effective elastic modulus of granular layers (Jordaan, 2006). 27

Figure 2-24: Change in permanent deformation of cemented layers (Jordaan, 2006). 28

Figure 2-25: Change in effective elastic modulus of cemented layers (Jordaan, 2006). 28

Figure 2-26: Change in permanent deformation of bituminous layers (Jordaan, 2006). 29

Figure 2-27: Change in effective elastic modulus of bituminous layers (Jordaan, 2006). 29
Figure 2-28: Rut depth vs deflection plot for Road P6/1 (Jordaan, 2006). 30
Figure 2-29: Rut depth vs deflection plot for Road P21/1 (Jordaan, 2006). 30
Figure 2-30: Components of a MDD module (De Beer et al., 1989). 37
Figure 2-31: Measured MDD deflections on an asphalt base pavement (De Beer et al., 1989). 38
Figure 2-32: Measured MDD deflections on a granular base pavement (De Beer et al., 1989). 39
Figure 2-33: Measured MDD deflections on a cemented base pavement (De Beer et al., 1989). 39
Figure 2-34: Quasi-continuous deflection basins for a set of five MDDs. 40
Figure 2-35: CPN MC-S-24 dual probe strata gauge (InstroTek, n.d.). 41
Figure 2-36: Principle of TSD operation (Krarup, 2012). 42
Figure 2-37: Greenwood TSD owned by SANRAL (Krarup, 2012). 43
Figure 2-38: Static and dynamic components of tyre load (Steyn, 2001). 44
Figure 2-39: Change in mean and COV of tyre load population (Steyn, 2001). 45
Figure 2-40: Manual iterative procedure for calculating layer moduli (Scullion et al., 1988). 48
Figure 2-41: CHEV input screen. 50
Figure 2-42: CHEV output. 50
Figure 2-43: ELTS example for a lightly cemented material (Asphalt Academy, 2009). 53
Figure 2-44: Permanent deformation performance rank for 13 APT test sections. 57
Figure 2-45: Expected permanent deformation performance rank for different base materials. 57
Figure 3-1: Transverse cross-section of testing facility. 58
Figure 3-2: Location and longitudinal cross-section of SANRAL testing facility. 59
Figure 3-3: Emu strain coils, pressure cells, big mat stress sensors, and strain gauges. 61
Figure 3-4: MDDs, pressure films, pressure cells, and strain gauges. 62
Figure 3-5: Schematic location of sensors in Section 1. 63
Figure 3-6: Schematic location of sensors in Section 2. 63
Figure 3-7: Schematic location of sensors in Section 3. 64
Figure 3-8: Schematic location of sensors in Section 4. 64
Figure 3-9: Schematic location of sensors in Section 5. 65

Figure 3-10: Schematic location of sensors in Section 6. 65
Figure 3-11: Schematic location of sensors in Section 7a. 66
Figure 3-12: Schematic location of sensors in Section 7b. 66
Figure 3-13: Typical vertical strain response output from a MDD module. 68
Figure 3-14: Typical TSD loading sequence. 69
Figure 3-15: Analysis of collected MDD data for permanent deformation behaviour. 69
Figure 3-16: Target transverse location of the TSD trail dual wheel. 70
Figure 3-17: Subgrade stiffness adjustment based on cover thickness (Asphalt Academy, 2009). 74
Figure 3-18: Layer thickness adjustment factor for cemented layers (Asphalt Academy, 2009). 75
Figure 4-1: Measured MDD deflections from Section 1. 78
Figure 4-2: Flooded manhole and water-damaged Smartreader unit (Steyn and Coetzer, 2015). 79
Figure 4-3: Monthly average plot of temperature data. 81
Figure 4-4: Test-specific temperature data. 82
Figure 4-5: Water-damaged Decagon unit (Steyn and Coetzer, 2015). 82
Figure 4-6: Section 1 moisture content with depth. 83
Figure 4-7: Average section moisture content per measuring date. 84
Figure 4-8: Section 1 dry density with depth. 85
Figure 4-9: Average section dry density per measuring date. 86
Figure 4-10: CHEV output for Section 1. 89
Figure 4-11: Measured versus calculated depth deflections for Section 1 90
Figure 5-1: Permanent deformation per cycle vs pavement number. 97
Figure 5-2: Permanent deformation per cycle vs dynamic deflection. 97
Figure 8-1: Measured MDD deflections from Section 2. 109
Figure 8-2: Measured MDD deflections from Section 3. 110
Figure 8-3: Measured MDD deflections from Section 4. 110
Figure 8-4: Measured MDD deflections from Section 5. 111
Figure 8-5: Measured MDD deflections from Section 6. 111
Figure 8-6: Measured MDD deflections from Section 7a. 112

Figure 8-7: Measured MDD deflections from Section 7b. 112
Figure 8-8: Section 2 moisture content with depth. 115
Figure 8-9: Section 3 moisture content with depth. 115
Figure 8-10: Section 4 moisture content with depth. 116
Figure 8-11: Section 5 moisture content with depth. 116
Figure 8-12: Section 2 dry density with depth. 119
Figure 8-13: Section 3 dry density with depth. 119
Figure 8-14: Section 4 dry density with depth. 120
Figure 8-15: Section 5 dry density with depth. 120
Figure 8-16: CHEV output for Section 2. 121
Figure 8-17: CHEV output for Section 3. 122
Figure 8-18: CHEV output for Section 4. 122
Figure 8-19: CHEV output for Section 5. 123
Figure 8-20: CHEV output for Section 6. 123
Figure 8-21: CHEV output for Section 7a. 124
Figure 8-22: CHEV output for Section 7b. 124
Figure 8-23: Measured versus calculated depth deflections for Section 2. 127
Figure 8-24: Measured versus calculated depth deflections for Section 3. 127
Figure 8-25: Measured versus calculated depth deflections for Section 4. 128
Figure 8-26: Measured versus calculated depth deflections for Section 5. 128
Figure 8-27: Measured versus calculated depth deflections for Section 6. 129
Figure 8-28: Measured versus calculated depth deflections for Section 7a. 129
Figure 8-29: Measured versus calculated depth deflections for Section 7b. 130

LIST OF TABLES

Table 2-1: Thornthwaite's Moisture Index values for climatic regions (SANRAL, 2014). 16

Table 2-2: TRH14 material classification system (SANRAL, 2014; TRH14, 1985). 19

Table 2-3: BSM characteristics (Asphalt Academy, 2009). 23

Table 2-4: Rutting behaviour of bitumen foam treated base test sections (Gonzalez et al., 2009). 33

Table 2-5: Rutting behaviour of rehabilitated ETB test section (Horak and Rust, 1992). 33

Table 2-6: Rutting behaviour of CTB test section (Metcalf et al., 1999). 34

Table 2-7: Rutting behaviour of rehabilitated BTB test section (Van der Merwe et al., 1992). 34

Table 2-8: EME mix and bitumen characteristics (Rohde et al., 2008). 35

Table 2-9: EME1 mix and bitumen characteristics (Perret et al., 2004). 35

Table 2-10: Resilient moduli and Poisson's ratios according to the SAMDM (SANRAL, 2014). 47

Table 2-11: Typical axle and wheel load configurations for design (Theyse et al., 2011). 49

Table 2-12: Summary of previous permanent deformation studies. 56

Table 3-1: Material properties of flexible pavement sections. 60

Table 3-2: Types of sensors monitored on the R104 experimental site. 61

Table 3-3: Structural properties of flexible sections. 62

Table 3-4: Step by step flow diagram of methodology for data collection. 67

Table 3-5: Climate adjustment factors (Asphalt Academy, 2009). 73

Table 3-6: Modular ratio limit and base confidence factor values (Asphalt Academy, 2009). 74

Table 3-7: Data summary. 75

Table 4-1: Representative test runs for seven SANRAL test sections. 76

Table 4-2: Cut-out of MDD data from Section 1. 77

Table 4-3: MDD order rearrangement and operational status. 79

Table 4-4: Cut-out of temperature data from SANRAL experimental site. 80

Table 4-5: Test-specific temperature data. 81

Table 4-6: Section 1 moisture content with depth. 83

Table 4-7: Average section moisture content per measuring date. 84

Table 4-8: Section 1 dry density with depth. 85
Table 4-9: Average section dry density per measuring date. 86
Table 4-10: First and last second, static MDD vertical response averages. 87
Table 4-11: Short-term loading response per section. 88
Table 4-12: Longer-term recovering response per section. 88
Table 4-13: Measured versus calculated depth deflections for Section 1. 89
Table 4-14: Back-calculated layer moduli per section. 90
Table 4-15: Calculation of subgrade ELTS for Section 1. 91
Table 4-16: Calculation of ELTS for individual layers of Section 1. 91
Table 4-17: Calculation of pavement number for Section 1. 91
Table 4-18: Pavement number values per section. 91
Table 4-19: Deformation data summary. 92
Table 4-20: Environmental related data summary. 92
Table 5-1: Permanent deformation performance rank for seven flexible pavements. 94
Table 8-1: Section 2 moisture content with depth. 113
Table 8-2: Section 3 moisture content with depth. 113
Table 8-3: Section 4 moisture content with depth. 114
Table 8-4: Section 5 moisture content with depth. 114
Table 8-5: Section 2 dry density with depth. 117
Table 8-6: Section 3 dry density with depth. 117
Table 8-7: Section 4 dry density with depth. 118
Table 8-8: Section 5 dry density with depth. 118
Table 8-9: Measured versus calculated depth deflections for Section 2. 125
Table 8-10: Measured versus calculated depth deflections for Section 3. 125
Table 8-11: Measured versus calculated depth deflections for Section 4. 125
Table 8-12: Measured versus calculated depth deflections for Section 5. 125
Table 8-13: Measured versus calculated depth deflections for Section 6. 126
Table 8-14: Measured versus calculated depth deflections for Section 7a. 126

Table 8-15: Measured versus calculated depth deflections for Section 7b. 126
Table 8-16: Calculation of subgrade ELTS for Section 2. 131
Table 8-17: Calculation of ELTS for individual layers of Section 2. 131
Table 8-18: Calculation of pavement number for Section 2. 131
Table 8-19: Calculation of subgrade ELTS for Section 3. 132
Table 8-20: Calculation of ELTS for individual layers of Section 3. 132
Table 8-21: Calculation of pavement number for Section 3. 132
Table 8-22: Calculation of subgrade ELTS for Section 4. 133
Table 8-23: Calculation of ELTS for individual layers of Section 4. 133
Table 8-24: Calculation of pavement number for Section 4. 133
Table 8-25: Calculation of subgrade ELTS for Section 5. 134
Table 8-26: Calculation of ELTS for individual layers of Section 5. 134
Table 8-27: Calculation of pavement number for Section 5. 134
Table 8-28: Calculation of subgrade ELTS for Section 6. 135
Table 8-29: Calculation of ELTS for individual layers of Section 6. 135
Table 8-30: Calculation of pavement number for Section 6. 135
Table 8-31: Calculation of subgrade ELTS for Section 7a. 136
Table 8-32: Calculation of ELTS for individual layers of Section 7a. 136
Table 8-33: Calculation of pavement number for Section 7a. 136
Table 8-34: Calculation of subgrade ELTS for Section 7b. 137
Table 8-35: Calculation of ELTS for individual layers of Section 7b. 137
Table 8-36: Calculation of pavement number for Section 7b. 137

LIST OF ABBREVIATIONS

°C	-	degrees Celsius
%	-	per cent
υ	-	Poisson's ratio
ε	-	strain
σ	-	stress
AASHTO	-	American Association of State Highway and Transportation Officials
ACB	-	Asphalt Concrete Base
ALF	-	Accelerated Loading Facility
APT	-	Accelerated Pavement Testing
ATB	-	Asphalt Treated Base
BTB	-	Bitumen Treated Base
BCF	-	Base Confidence Factor
BSM	-	Bitumen Stabilised Material
CBR	-	California Bearing Ratio
cm	-	centimetres
COV	-	Coefficient of Variance
CSIR	-	Council for Scientific and Industrial Research
CTB	-	Cement Treated Base
DBM	-	Dense Bitumen Macadam
DCP	-	Dynamic Cone Penetrometer
DEMAC	-	Design Equivalent Material Class
E	-	Young's modulus
ELTS	-	Effective Long-Term Stiffness
EME	-	Enrobés à Module Elevé (HiMA)
ETB	-	Emulsion Treated Base
FAS-FDR	-	Recycled Asphalt Pavement from Full-Depth Reclamation

FTB	-	Foam Treated Base
FWD	-	Falling Weight Deflectometer
GVM	-	Gross Vehicle Mass
HiMA	-	High Modulus Asphalt
HMA	-	Hot-Mix Asphalt
HVS	-	Heavy Vehicle Simulator
kN	-	kilonewtons
km	-	kilometres
kPa	-	kilopascals
LAMBs	-	Large Aggregate Mixes for Bases
LVDT	-	Linear Variable Differential Transformer
MDD	-	Multi-Depth Deflectometer
MESA	-	Million Equivalent Standard Axles
nm	-	nanometres
m	-	metres
mm	-	millimetres
µm	-	micrometres
MPa	-	megapascals
M_r	-	resilient modulus
PN	-	Pavement Number
RA	-	Reclaimed Asphalt
SANRAL	-	South African National Roads Agency Limited
SMA	-	Stone Mastic Asphalt
SN	-	Structural Number
TRH	-	Technical Recommendations for Highways
TSD	-	Traffic Speed Deflectometer
UP	-	University of Pretoria

1. INTRODUCTION

1.1. Background

Pavement response is the manner in which a pavement reacts to applied stresses and determines how it will behave structurally. Pavement response data are often used to determine the cause of pavement distress as well as the effectiveness and timing of maintenance actions. This allows for more structurally suitable designs as well as informed maintenance decisions.

There is a general tendency in pavement design to collect more site specific data. Generally, surface based tests and inspections are adopted to determine the serviceability of a specific pavement. These tests and inspections, however, produce only the most basic data regarding the pavement's response to loading and its structural integrity. This is where in-situ sensors prove to be valuable, especially for flexible pavement analysis, as the pavement structure can be studied to a greater extent.

In-situ pavement instrumentation has recently become an important tool to monitor in-situ material performance and measure pavement response to loading. Parameters that are measured in the field include the stress, strain, deflection, temperature, moisture content, etc. at almost any location within the pavement structure. With various Accelerated Pavement Testing (APT) transportation projects currently implemented worldwide, numerous sensors have become available to monitor the health and performance of pavements.

Typical in-situ pavement response and environmental related data such as in-depth deflection, temperature, moisture content, density, etc. have been collected from 10 test sections on the R104, between the east of Pretoria and Bronkhorstspruit, since 2013 on a number of occasions. It is a SANRAL driven initiative that consists of seven flexible pavement sections and three rigid pavement sections. The need exists to conduct detailed analyses on the collected data from the seven flexible pavement sections and study the permanent deformation behaviour of different flexible pavements.

Permanent deformation (rutting) is a pavement distress condition visible in the surfacing layer of a pavement. It occurs along the wheel path and results from the accumulation of load-induced permanent deformation developed from all individual pavement layers, including the subgrade. It is one of the major distress conditions in flexible pavements. Plenty of research regarding permanent deformation in flexible pavements exists, but it is mainly focused on asphalt surface layers and granular base, subbase, and subgrade layers (Steyn, 2012). This is where the SANRAL experimental site proves to be useful as a variety of flexible pavement structures can be studied under similar conditions.

The flexible pavement structures are all 100 m in length and differ from each other primarily in layer thickness and base layer component. The different base layer constituents include a natural gravel (G4) base, a high-quality graded crushed stone (G1) base, a Foam Treated Base (FTB), an Emulsion Treated Base (ETB), a Cement Treated Base (CTB), a Bitumen Treated Base (BTB), and a High Modulus Asphalt (HiMA)/Enrobés à Module Elevé (EME) base. During response-to-loading testing, loading is provided in the form of a Traffic Speed Deflectometer (TSD), which drives over the respective sections at a constant speed while applying three axle loads to the underlying pavement structure.

Horak et al. (2015) showed that elastic response data (collected using the FWD) can be related to the structural integrity of a pavement section by using the deflection bowl information to determine an effective Pavement Number (PN). This effective PN value correlated quite well with the calculated (actual) PN value, which meant it can be used as a benchmark analysis approach on both project and network level. During preliminary analyses of flexible pavements, sections of the pavement that are either high or low in effective PN relative to the rest of the pavement can be identified.

The PN value of a pavement is a measure of its structural integrity and subsequently is an indication of its remaining life/structural capacity (Asphalt Academy, 2009). The structural capacity has shown to be a good indicator of the required maintenance and expected performance of a pavement. A correlation between response data and PN value can, therefore, assist in making timely and informed maintenance decisions as pavement sections that are low in structural capacity can readily be identified.

Hence, it may be useful to examine how well plastic response data, derived from in-situ pavement response data (i.e. Multi-Depth Deflectometer [MDD] data), relates to the structural integrity of a pavement by using in-situ pavement response data (i.e. dynamic MDD depth deflections) to calculate a representative PN value.

1.2. Objectives of the Study

The objectives of the study are:

a) To investigate and compare the permanent deformation behaviour of various flexible pavement structures through the analysis of in-situ pavement response and environmental related data, and

b) To develop a possible transfer function for linking the permanent deformation behaviour of a pavement to its structural integrity by determining a representative pavement number.

1.3. Scope of the Study

The overall scope of the study focuses on investigating the permanent deformation behaviour of a number of specific flexible pavements, with special attention to the base layer and the pavement structure as a whole. It falls within the scope and extent of the study to:

a) Indicate the current understanding of permanent deformation in flexible pavements as well as various other concepts related to it, by means of a literature study;

b) Develop a better understanding regarding the permanent deformation behaviour of different kinds of flexible pavements in terms of a short-term loading response between the beginning and the end of a load cycle;

c) Develop a better understanding regarding the permanent deformation behaviour of different kinds of flexible pavements in terms of a longer-term recovering response between the end of a load cycle and the beginning of the next, and

d) Identify a possible relationship between the permanent deformation behaviour of a pavement and its structural integrity in terms of a pavement number value.

It falls outside the scope and extent of the study to:

a) Study the permanent deformation behaviour of rigid pavements;

b) Use the TSD data to make inferences about the permanent deformation behaviour;

c) Make any comparisons between the TSD measured data and the in-situ pavement response data, and

d) Investigate or improve existing models of permanent deformation in pavements.

1.4. Methodology

A summarised procedure for conducting the study includes the following:

a) In-situ pavement response and environmental related data are collected by the University of Pretoria (UP) from the various flexible pavement test sections at the SANRAL experimental site on the R104. All in-situ sensors have already been installed prior to the study (during construction in 2013).

b) The relevant data (MDD, temperature, moisture, and density) are processed and a validation check is performed to assess the credibility of each data type before it is used.

c) The vertical response data (MDD data) are examined through a process whereby only the static, non-loading state between successive load applications (TSD passes), portion of the data is utilised. Conservatively, the first and last second of a TSD test run are chosen to represent this portion of data in order to ensure static, non-loading conditions for analysis.

d) With the first and last second representing vertical response data before and after load application respectively, a conclusion can be drawn regarding any permanent response as a result of the applied load (short-term loading response).

e) Considering the last second of a test run relative to the first second of the next test run, a conclusion can be drawn regarding any permanent response recovered as a result of the time delay between TSD test runs (longer-term recovering response).

f) The permanent deformation behaviour is compared across the entire range of test sections between individual layers as well as the complete pavement structures, taking note of any environmental related factors (temperature, moisture, and material density) that might have had an influence.

g) It is determined whether this permanent deformation behaviour can be related to the structural integrity of a pavement. Layer moduli are back-calculated from the original vertical response data (MDD data) and used to determine a representative PN value for the pavement.

1.5. Layout of the Dissertation

The dissertation consists of the following chapters:

- Chapter 1: Introduction;
- Chapter 2: Literature Study;
- Chapter 3: Methodology;
- Chapter 4: Data Collection;
- Chapter 5: Discussion;
- Chapter 6: Conclusions and Recommendations;
- Chapter 7: References, and
- Chapter 8: Appendices.

2. LITERATURE STUDY

2.1. Introduction

The headlines discussed in this chapter cover the main aspects of the topic that is investigated, which are:

- Fundamental behaviour of pavement materials;
- Parameters affecting permanent deformation in pavements;
- Background on flexible pavement materials;
- Permanent deformation of flexible pavement materials;
- Pavement instrumentation used for pavement analysis;
- Traffic speed deflectometer and its loading regime;
- Multi-layer elastic theory, and
- Pavement number design method.

2.2. Fundamental Behaviour of Pavement Materials

Road building materials are mainly categorised into three groups. These three groups are granular materials, cemented materials, and bituminous materials. There are three fundamental types of material behaviour that are relevant to the understanding of these road building materials, namely: elasticity, plasticity, and viscosity. However, there are very few road building materials that only follow one discrete mode of material behaviour; a combination of the behavioural types is usually required to model the behaviour more accurately. Typical examples include:

- Elastic material behaviour for cemented materials;
- Elasto-plastic material behaviour for granular materials;
- Visco-elastic material behaviour for bituminous binders, and
- Visco-elasto-plastic material behaviour for bituminous materials (asphalt, seals, etc.).

When a wheel load is applied to the surface of a flexible pavement, it tends to deform the material elements of the pavement structure. Various factors such as material properties, temperature, load intensity, loading time, etc. affect the magnitude of the deformation attained. When the wheel load is removed, a part of this deformation will be recovered, but some of it will remain in the material. The recovered deformation can be attributed to the elastic and delayed elastic components of the pavement materials, while the remaining deformation is due to the plastic and viscous components (Brown, 1978; Battiato et al., 1977).

2.2.1. Plasticity

Plasticity describes the behaviour of a material that accumulates non-recoverable (permanent) deformation or plastic strain when subjected to traffic load. Permanent deformation (or rutting) is a longitudinal surface depression that forms within the wheel tracks of a pavement and, in most cases, is accompanied by pavement upheaval along the sides of the depression. Permanent deformation can occur in any layer of a pavement structure. The net result is visible in the surfacing layer and represents the accumulation of permanent deformation developed from all individual pavement layers, including the subgrade (Barksdale, 1972).

The development of permanent deformation is described by two main mechanisms, namely consolidation (densification) and shear deformation (plastic flow not associated with volume change). *Densification* is the primary mechanism of permanent deformation during the initial phase of a pavement's life and is often the result of poor compaction during construction. This compaction inadequacy causes the aggregate skeleton to become more closely packed together during the early life of the structure. *Shear deformation* is the main subsequent cause of permanent deformation with the formation of shoulders on either side of the depression usually being the result. The volume decrease underneath the tyres is approximately the same as the volume increase in the adjacent upheaval zones. It is considered the primary mechanism of permanent deformation for the greater part of a pavement's lifetime (Werkmeister, 2003; Eisenmann and Hilmer, 1987). Figure 2-1 illustrates the mechanisms of permanent deformation in flexible pavements.

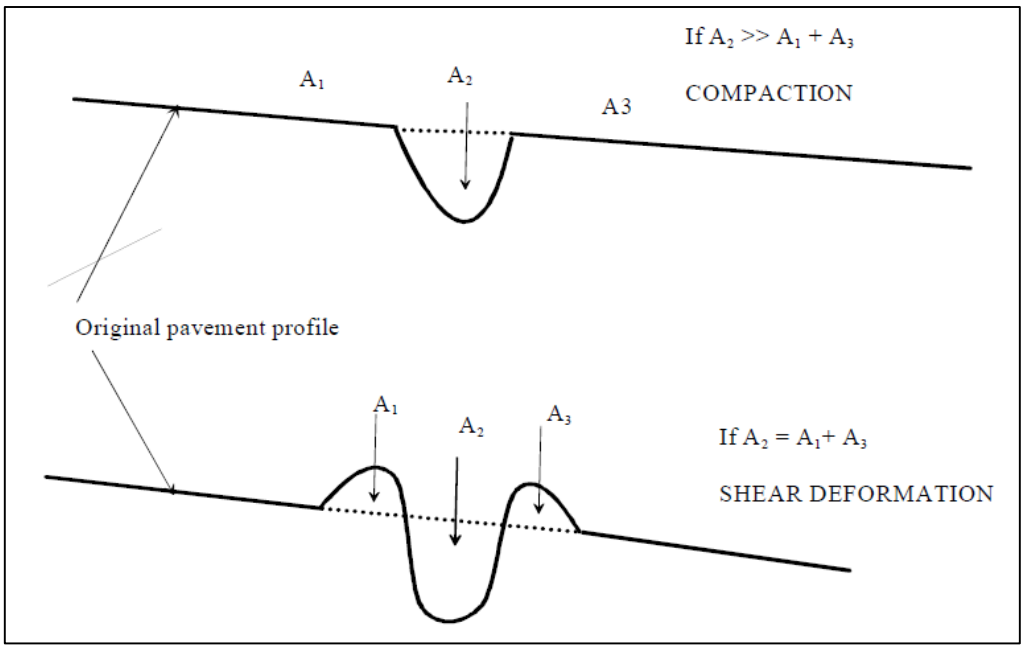

Figure 2-1: Permanent deformation mechanisms (Garba, 2002).

Generally, permanent deformation can be considered in three phases (Figure 2-2):

1) *Primary Phase* – This phase is associated with the change in volume of the material (densification). It represents a compaction regime where the pavement is considered to experience additional compaction through traffic loading. The compaction normally results in an improved aggregate interlock and consequently decreases the rut rate (the slope of the permanent deformation curve).

2) *Secondary Phase* – This phase shows a constant, slow rate of increase in permanent deformation associated with an increase in shear deformation at the same rate.

3) *Tertiary Phase* – This phase represents a catastrophic range of permanent deformation associated with shear deformation under no volume change. This involves large scale aggregate movements as the rut rate gradually begins to increase again (AASHTO, 2004).

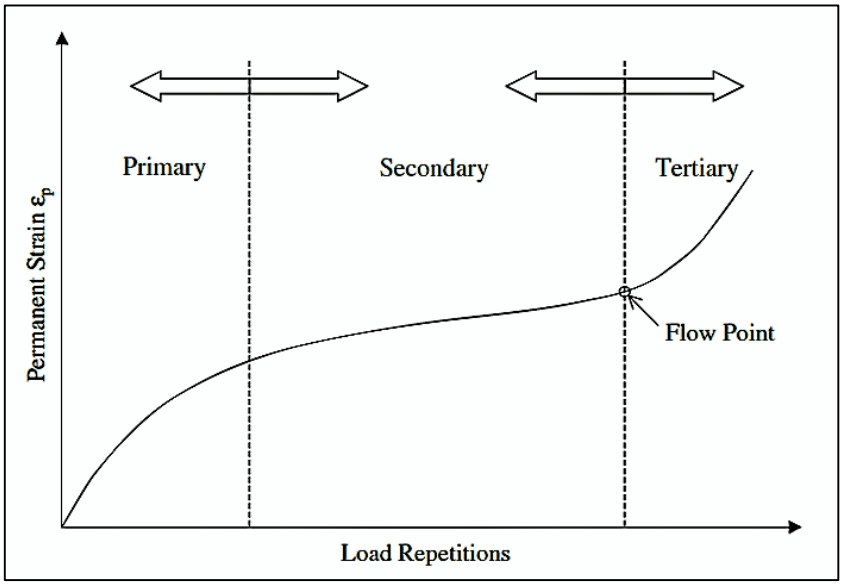

Figure 2-2: Permanent deformation development phases (AASHTO, 2004).

Permanent deformation in pavements can be classified as structural, non-structural, or a combination of both. *Structural* permanent deformation is the result of a weak support layer (usually the subgrade) that propagates upwards through a pavement structure and reflects in the surface, regardless of the stiffness of the surfacing layer. *Non-structural* permanent deformation is related to the properties of the surfacing layer (normally asphalt mixtures). It occurs due to the shortage of shear strength to withstand the vertical repeated load. Figure 2-3 provides a visual illustration of structural versus non-structural permanent deformation. Structural permanent deformation generally tends to provide a much broader rut width on the surface in comparison with non-structural permanent deformation (Gibb, 1996).

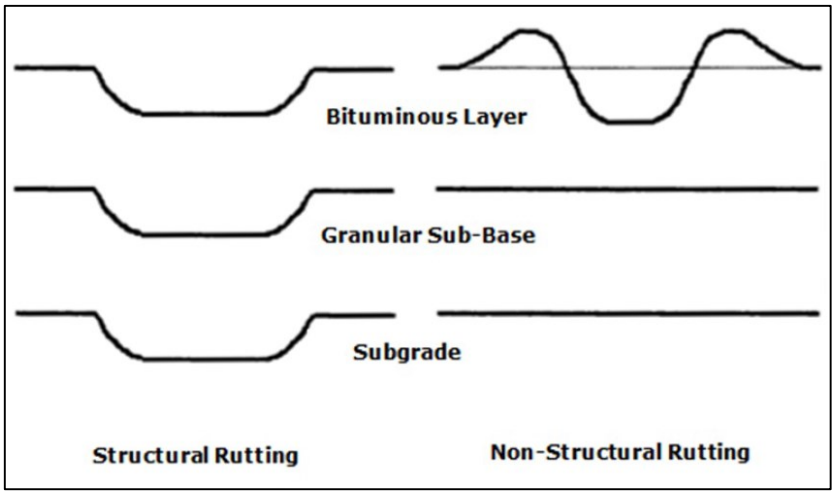

Figure 2-3: Structural vs non-structural permanent deformation (Gibb, 1996).

When applying a wheel load to a flexible pavement, more than often a non-linear stress-strain curve in the form of a hysteresis loop is produced upon removal of the load. The loop represents the permanent (non-recoverable) and resilient (elastic) strains for the load cycle. It is this elastic strain that is related to a resilient modulus (M_r), which replaces the initial elastic modulus in order to describe the recoverable behaviour of a material subjected to cyclic loading. The resilient modulus is known to be non-linear and strongly dependent on the stress state (Uthus, 2007; Lekarp, 1999). The approximation of Young's modulus by the resilient modulus is illustrated in Figure 2-4. The hysteresis loop for a single load cycle applied to a visco-elasto-plastic material is shown. Figure 2-5 illustrates the accumulation of permanent deformation due to the plastic component of each load cycle under repeated cyclic loading.

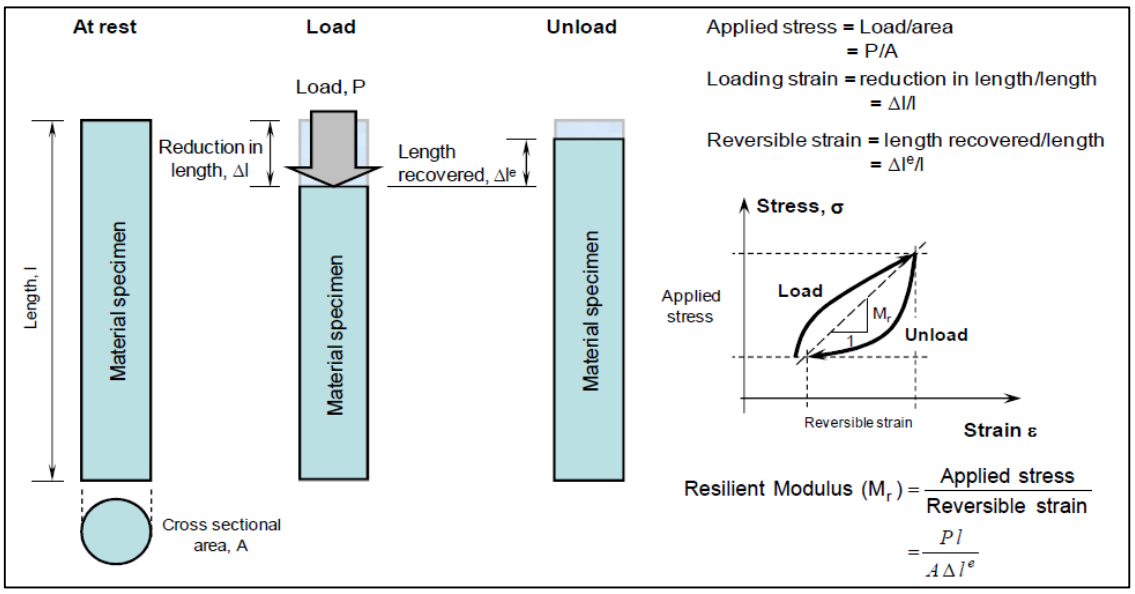

Figure 2-4: Approximation of Young's modulus by the resilient modulus (Theyse et al., 2011).

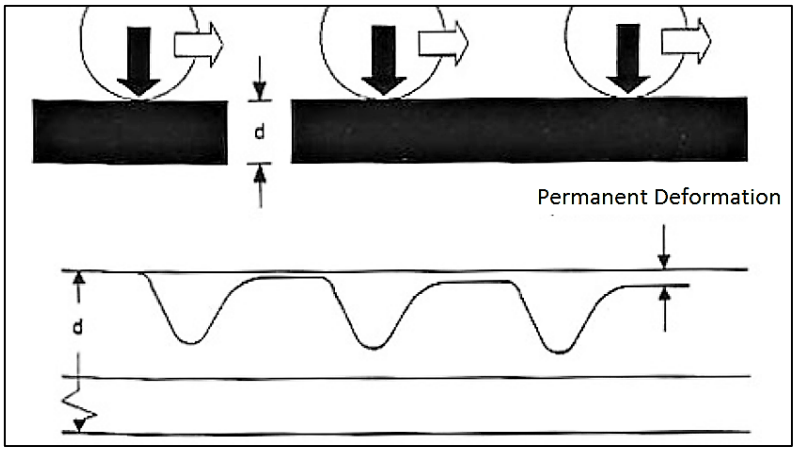

Figure 2-5: Permanent deformation under cyclic loading (Taherkhani, 2006).

According to current permanent deformation prediction models, permanent deformation development will stagnate over time with increasing load repetitions. However, this only applies for stresses below a certain limit, the "Plastic Shakedown Limit". When stresses exceed this limit, an unstable condition is reached and further permanent deformation takes place as previously shown in Figure 2-2. Due to the stress dependency of many materials used in pavement construction (predominantly gravels and crushed stones), recent development of models has mainly been based on the shakedown concept. The shakedown concept is used to describe the plastic behaviour of conventional engineering structures under repeated cyclic loading (Theyse et al., 2007; Arnold, 2004).

2.2.2. Shakedown Concept

The shakedown concept describes plastic behaviour under repeated cyclic loading. The level of applied stress defines the type of plastic strain behaviour that can be expected. From an engineering perspective, the level of stress that results in a decreasing permanent deformation rate is ideal as it represents stable conditions. These stable conditions are considered as shakedown; therefore, a shakedown limit stress exists at the boundary between the points where shakedown occurs and does not occur. The concept suggests that there are three ranges of material response under cyclic loading (Figure 2-6):

1) *Plastic Shakedown* – The response shows a high plastic strain rate for a finite number of load cycles during the initial compaction period. After compaction, the incremental plastic strain rate decreases with the increasing number of load applications until it finally approaches zero. The material response becomes completely resilient and no further plastic strain occurs. The material is said to have "shaken down". The maximum stress level at which plastic shakedown is attainable is said to be the "plastic shakedown limit".

2) *Plastic Creep* – The initial behaviour is like plastic shakedown during the compaction period. After this, the plastic strain per load cycle is either slowly decreasing or remains constant. The material response does not become entirely resilient; however, after a large amount of load cycles, it may be possible. The maximum stress level at which plastic creep is attainable is said to be the "plastic creep limit".

3) *Incremental Collapse* – The applied repeated stress is relatively large. An initial compaction period may be observed after which the plastic strain rate increases with increasing load cycles (Korkiala-Tanttu, 2009; Theyse et al., 2007; Arnold, 2004).

The basic assumption is that plastic strain under repeated cyclic loading can be classified as one of three types. The long-term plastic strain rate is either decreasing with increasing load cycles (plastic shakedown), remaining constant with increasing load cycles (plastic creep), or increasing with increasing load cycles (incremental collapse). The structure under consideration can be modelled as a homogeneous elastic/plastic material, in which case it will eventually either shakedown or fail. The ultimate response will be purely elastic (reversible), or the structural response will remain plastic (irreversible) regardless of the number of load cycles (Arnold, 2004). Figure 2-6 provides a graphical illustration of the shakedown theory concept.

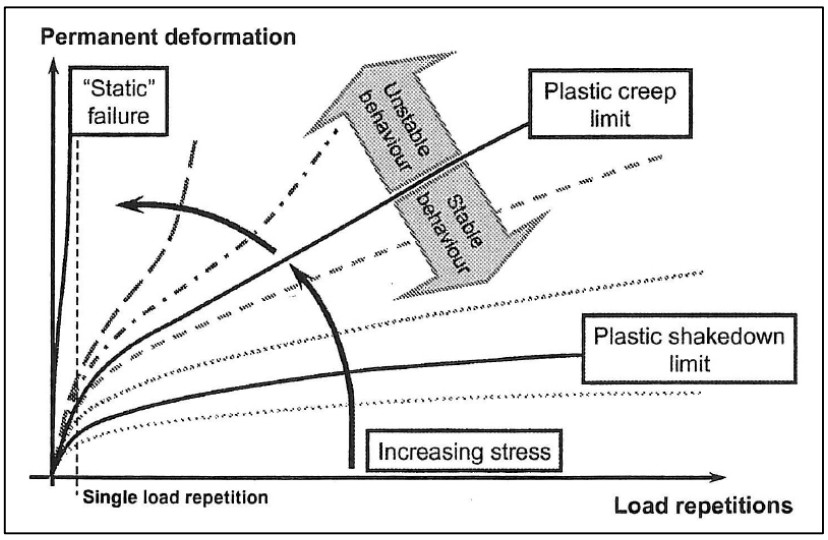

Figure 2-6: Shakedown theory concept (Theyse et al., 2007).

The shakedown concept goes hand in hand with the traffic moulding phenomenon, which is the changing (moulding of) properties and behaviour of a pavement due to applied traffic loads and changing climate conditions (temperature and moisture levels). Traffic moulding can either lead to structural failure or result in an increased bearing capacity and improved strength-balance, which compares to incremental collapse and plastic shakedown respectively.

The phenomenon is monitored and verified by means of DCP strength profiles, which is indicative of the strength transition throughout the pavement structure (pavement strength-balance). A strength-balanced pavement refers to a pavement with ideal strength transition when the design load stresses the structure over the entire effective pavement depth to the same level of maximum elastic strain. Pavement strength-balance, over the life cycle of a pavement, can be related to two distinct states. Traffic moulding continues until the pavement either reaches a state of improved, stable bearing capacity and possibly some form of strength-balance capable of withstanding the current traffic load without change (stable state), or it does not develop sufficient strength and continues being moulded until total structural failure (unstable state) (Kleyn and Steyn, 2015 & 2010). Figure 2-7 illustrates a schematic flow diagram of the traffic moulding process.

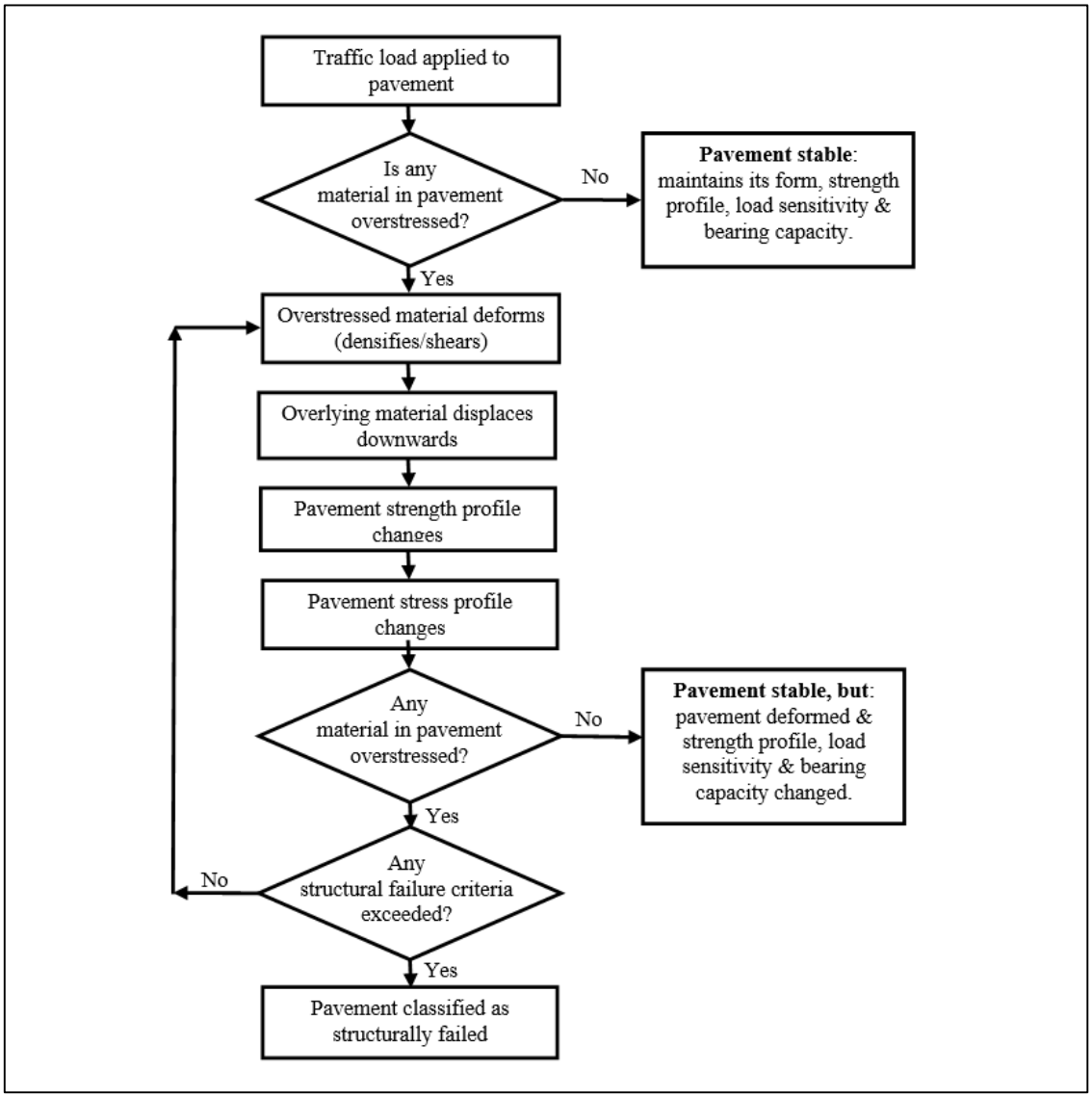

Figure 2-7: Traffic moulding process (Kleyn and Steyn, 2015 & 2010).

2.3. Parameters Affecting Permanent Deformation

For design purposes, it is important to take into account how the deformation behaviour of pavement materials is affected by changes in different influencing factors. The resilient and permanent deformation of pavement materials are affected by several factors that are either material or structural related. Three of the most important factors are:

- Effect of density; } Material
- Effect of moisture content, and
- Effect of temperature. } Structural

2.3.1. Effect of Density

The density of the grain skeleton is a very important influencing factor when considering the development of permanent deformation in pavement materials. The resistance to permanent deformation under cyclic loading can be greatly improved by an increased density. The general trend is that the resilient modulus increases with an increase in density as the additional compaction results in greater particle contact (Werkmeister, 2003). Barksdale (1972) studied the effect of density on the deformation behaviour of several granular materials and reported an average of 185% more permanent strain when the material was compacted at 95% instead of 100% of the maximum dry density (Standard Proctor Density) (Figure 2-8).

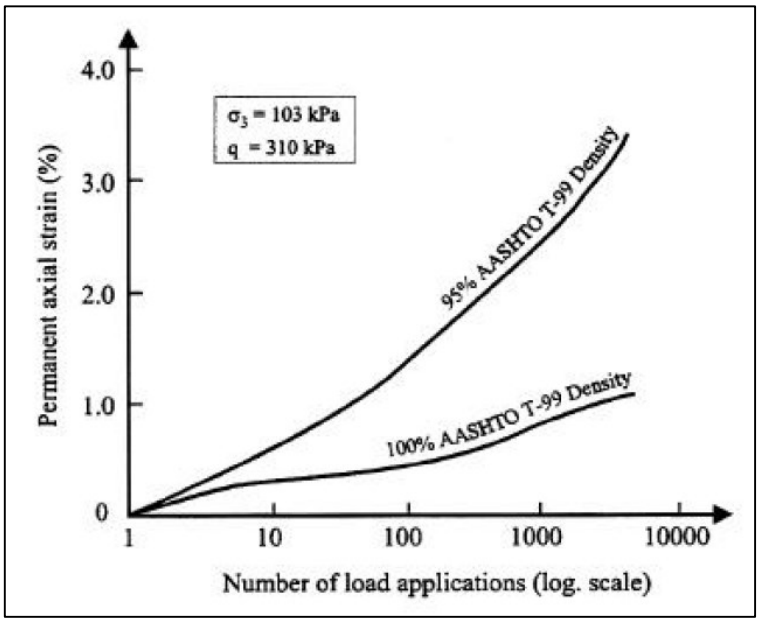

Figure 2-8: Effect of increased density on permanent deformation (Barksdale, 1972).

Increasing the density promotes a reduction in permanent deformation for crushed aggregates in particular. For rounded aggregates, however, the effect of an increased density is not as significant as for angular aggregates. This is because rounded aggregates are initially at a higher compacted density than angular aggregates for the same level of compaction (Holubec, 1969).

An increase in density is almost always beneficial to road building materials as it results in increased grain packing, reduced permeability, and increased strength. An exception, however, is asphalt materials where too high densities can result in all of the voids being filled with binder. The stone particles start losing contact with one another and they begin to "float" in the binder. At this stage, the strength of the asphalt does not depend on the aggregate interlock and the particles packing together as much but rather on the viscosity of the binder (SANRAL, 2014).

2.3.2. Effect of Moisture Content

The presence of moisture in a pavement system is probably the most important environmental consideration. Even though moisture helps with compaction during construction, a too high content thereof promotes particles sliding over one another, which results in a weakened material. Water is probably a pavement engineer's "Number One Enemy" as moisture ingress into the pavement system, either from above or below, decreases its structural capacity significantly. For very thick bound material layers like thick cemented or bituminous layers, this effect may be less significant than on unbound granular materials, but it still remains a problem (SANRAL, 2014).

The moisture content in a pavement system will change from the day it was built due to moisture ingress as a result of seasonal changes or capillary action. When there is a build-up of excess moisture, the pavement may develop excess pore water pressure as the amount of suction between the grains reduces. This usually occurs in granular materials due to a combination of low permeability, poor drainage, and a high degree of saturation. The result is a reduced effective stress, which consequently reduces the material's stiffness and its resistance to deformation (Thom and Brown, 1987; Barksdale, 1972; Haynes and Yoder, 1963).

Due to the recurring stresses from traffic loading, the water between the particles (inside the pores) becomes pressurised. This pore pressure then counteracts the externally applied stresses that are pushing the particles together. The friction and contact pressure between the particles decrease, and a reduced stiffness is the result (Kolisoja and Dawson, 2004). Figure 2-9 illustrates the impact of internal moisture in a granular material.

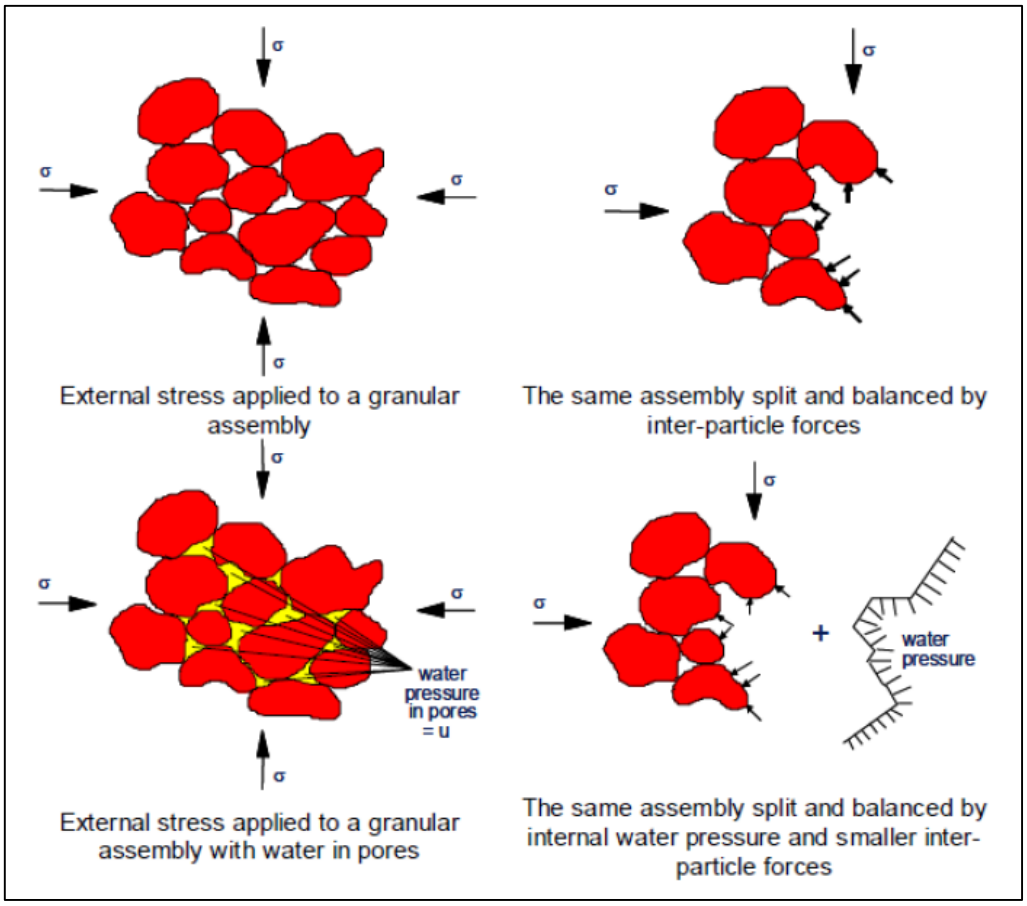

Figure 2-9: Impact of internal moisture on granular materials (Kolisoja and Dawson, 2004).

Numerous researchers have confirmed that a granular material's resistance to deformation is affected by the material's internal moisture content. The general thought is that a decrease in resistance to deformation can be expected with an increase in moisture content. Hicks and Monismith (1971) showed that an increase in moisture beyond the optimum moisture content resulted in a reduced resilient modulus and subsequently a lower resistance to deformation. Thom and Brown (1987) found that only a small increase in moisture content can bring about a dramatic increase in permanent deformation. Haynes and Yoder (1963) reported that the permanent deformation rose by more than 100% when an 80% instead of 60% degree of saturation was used. Barksdale (1972) observed a more modest increase in permanent deformation of 68% for tests on soaked specimens versus partially saturated specimens.

An experiment by Dawson (1990) shows how the change in moisture content can affect the deformation behaviour of a granular material. He investigated the influence of drainage on permanent deformation by testing two samples that started at the same moisture content but with different drainage regimes. The one was allowed to drain like a proper functioning pavement, while the other was not allowed to drain and encountered a significantly larger growth in permanent deformation (Figure 2-10).

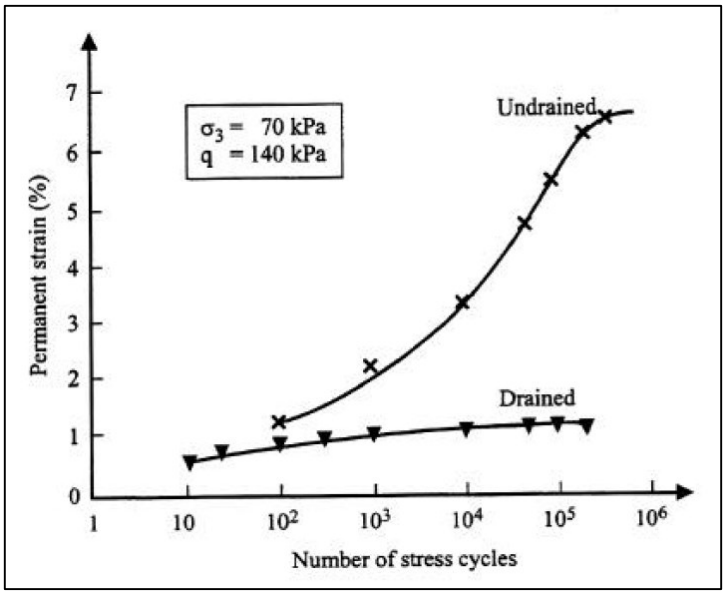

Figure 2-10: Influence of drainage on permanent deformation (Dawson, 1990).

In South Africa, the Thornthwaite Moisture Index is the preferred method for classifying climatic zones for moisture. Thornthwaite's Moisture Index is a function of evapo-transpiration, which in turn is dependent on the rainfall and vegetation of the region under consideration. It provides a measure of the soil water storage and therefore indicates a moisture surplus or deficit (SANRAL, 2014). A map of the index is shown in Figure 2-11 and the index values are given in Table 2-1.

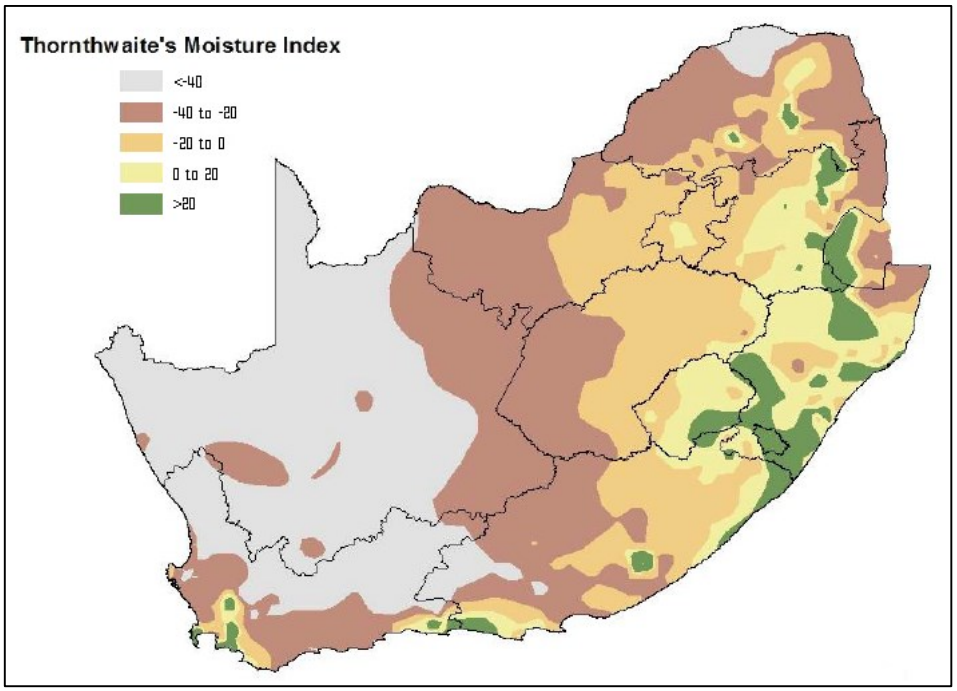

Figure 2-11: Thornthwaite's Moisture Index for South Africa (SANRAL, 2014).

Table 2-1: Thornthwaite's Moisture Index values for climatic regions (SANRAL, 2014).

Index Range	Climatic Region	
< - 40	Arid	Dry
- 40 to - 20	Semi-Arid	
- 20 to 0	Dry Sub-Humid	Moderate
0 to 20	Moist Sub-Humid	
20 to 100	Humid	Wet
> 100	Perhumid	

2.3.3. Effect of Temperature

Temperature variations normally only influence the strength of temperature susceptible materials, such as bituminous materials (usually asphalts). Temperature has been reported to have a significant effect on the permanent deformation behaviour of bituminous materials due to their visco-elastic properties. The presence or absence of direct sunlight as well as the ambient air temperature are responsible for the natural temperature variation the material experiences throughout the course of a day (Steyn and Denneman, 2008; Croney and Bulman, 1972). The typical effects of varying temperatures can be summarised as follows:

- Increased (high) temperatures:
  - Decrease in binder viscosity;
  - Softening of binder and asphalt concrete;
  - Decrease in material stiffness;
  - Higher stresses transferred to underlying layers, and
  - Increase in development of total permanent deformation.
- Decreased (low) temperatures:
  - Increase in binder viscosity;
  - Stiffening of binder and asphalt concrete;
  - Increase in material stiffness;
  - Lower stresses transferred to underlying layers, and
  - Decrease in development of total permanent deformation.

Steyn et al. (2008) compared the permanent deformation behaviour of a standard Hot-Mix Asphalt (HMA) mix with that of a rut resistant HMA mix and studied the effect of the change in aggregate grading between the two mixes. During the Hamburg Wheel Track Tests (HWTTs) conducted as part of the laboratory evaluation of the standard HMA mix, a clear increase in permanent deformation was observed with increased temperature (Figure 2-12).

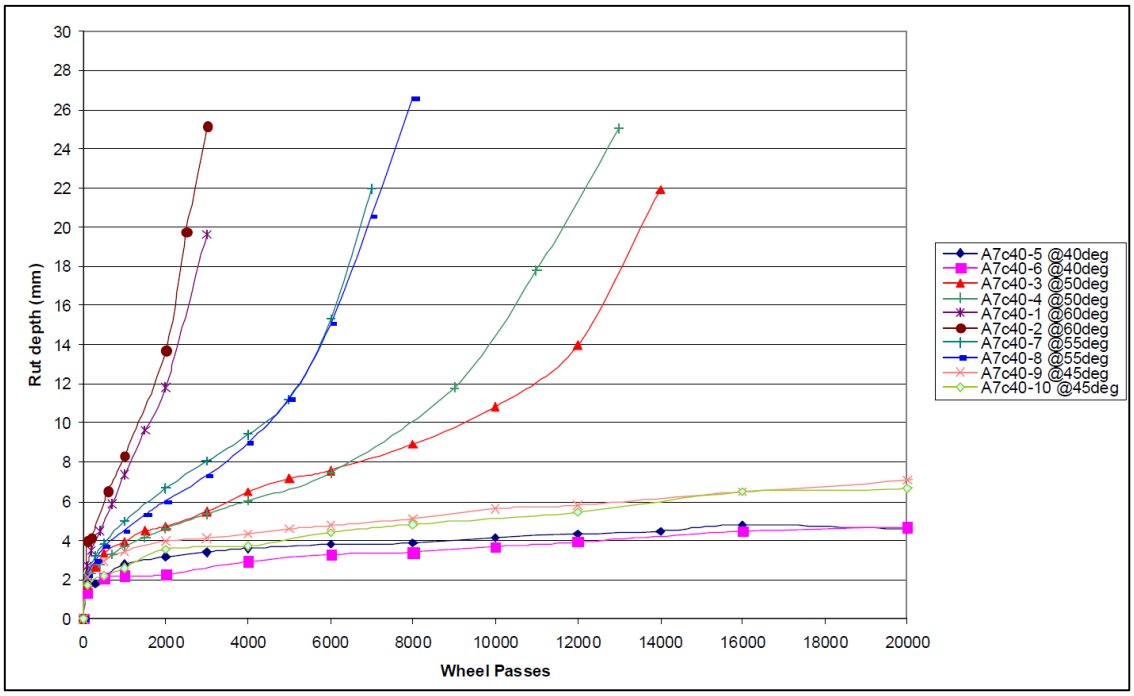

Figure 2-12: HWTTs for standard HMA mix at different temperatures (Steyn et al., 2008).

Al-Mosawe (2016) studied the effect of temperature in relation to permanent deformation on a variety of HMA mixes (different aggregate grading) at three different temperatures, 30°C, 40°C, and 50°C (Figure 2-13). The general observation was that the resistance to permanent deformation decreased as the temperature was increased. At a low temperature (30°C), all of the mixes showed minimal strain after the prescribed 5000 load cycles were applied. At a high temperature (50°C), all of the mixes, except mix 13 with its excellent aggregate packing characteristics, reached the maximum strain limit of 8% well before even half of the prescribed load cycles were applied.

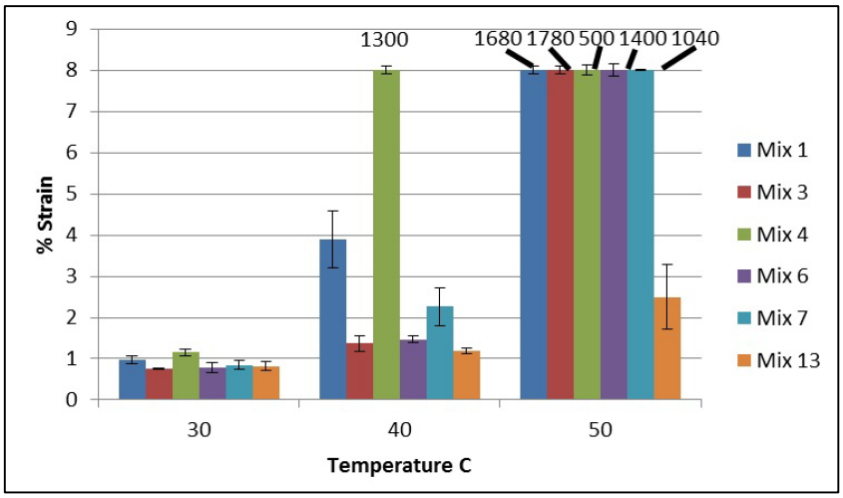

Figure 2-13: Effect of temperature on different HMA mixes (Al-Mosawe, 2016).

Both studies support the fact that resistance to permanent deformation is controlled by the binder of the HMA mix to a certain level of binder stiffness, which is dependent on the binder temperature. However, it is also shown that the aggregate grading can play a major role in the resistance to permanent deformation of the HMA mix if a very good aggregate packing (interlock) is obtained, even under severe temperature conditions.

2.4. Background on Flexible Pavement Materials

Road pavements are normally classified according to the type of materials used in the upper layers of the pavement structure, especially the surfacing layer. Flexible pavements usually have an asphalt or seal surfacing and are called flexible for the reason that they can bend on the supporting layers. In these types of pavements, the material quality gradually decreases from the surfacing down through all the structural layers to the subgrade at the bottom. Flexible pavements are typically deep pavements as the strength is distributed throughout the entire pavement structure (SANRAL, 2014; AASHTO, 1993).

The pavement structure of a road pavement is a combination of layers placed on top of the subgrade. The various layers present in a conventional pavement structure include a surfacing layer, a base layer, a subbase layer, a selected subgrade layer, and the existing subgrade. The base layer is a load spreading layer and probably the most important structural element of the pavement. It must provide the necessary support for the surfacing and distribute the applied tyre pressures and wheel loads uniformly over the underlying layers and subgrade (SANRAL, 2014; AASHTO, 1993).

The base layer can either comprise a bound or unbound material. Bound materials are typically asphalt or stabilised (bitumen or cement) granular materials. Unbound materials, on the other hand, are represented by crushed stone or gravel. In South Africa, these materials are commonly classified according to the TRH14 material classification system due to its compatibility with local materials. Table 2-2 provides the TRH14 classification for some frequently used road building materials. Typical base materials (relevant to this study) used in design and construction include:

- G4 natural gravel; } Unbound
- G1 crushed stone; }
- Bitumen stabilised material; }
- Cemented material, and } Bound
- Asphalt. }

Table 2-2: TRH14 material classification system (SANRAL, 2014; TRH14, 1985).

Surfacing		
AC	Asphalt Surfacing – Continuously Graded	Asphalt **(A)**
AG	Asphalt Surfacing – Gap-Graded	
AS	Asphalt Surfacing – Semi-Gap-Graded	
AO	Asphalt Surfacing – Open-Graded	
S1	Surface Treatment – Single Seal	Seal **(S)**
S2	Surface Treatment – Multiple Seal	
S3	Sand Seal	
S4	Cape Seal	
S5	Slurry Seal – Fine Grading	
S6	Slurry Seal – Coarse Grading	
Layered Material (Untreated)		
G1	Graded Crushed Stone	Granular **(G)** Material
G2	Graded Crushed Stone	
G3	Graded Crushed Stone	
G4	Natural Gravel	
G5	Natural Gravel	
G6	Natural Gravel	
G7	Gravel-Soil	
G8	Gravel-Soil	
G9	Gravel-Soil	
G10	Gravel-Soil	
Layered Material (Treated)		
C3	Cemented Natural Gravel	Cemented **(C)** Material
C4	Cemented Natural Gravel	
BT1	Bituminous Treated Crushed Stone	Bituminous **(B)** Material
BT2	Bituminous Treated Natural Gravel	
BT3	Bituminous Treated Cohesionless Sand	
BC	Bitumen Hot-Mix, Continuously Graded	
BS	Bitumen Hot-Mix, Semi-Gap-Graded	

2.4.1. G4 Natural Gravel

A G4 material is classified according to the TRH14 manual as a gravel of relatively high quality. The term “natural gravel” indicates that the material is produced through a weathering process where materials decompose, disintegrate, or abrade during transportation to resemble a natural, partially crushed material. This material shows stress-dependent elasto-plastic behaviour (described by the shakedown theory concept) and, under recurring stresses, permanent deformation can occur through shear and/or densification (TRH14, 1985).

The effectiveness of stress-dependent materials as pavement layers is highly dependent on the supporting layers. The support beneath a stress-dependent material layer affects the stress condition in the layer, which in turn affects the layer's stiffness response. For example, a strong supporting layer will enhance compressive stresses in the supported layer, which forces the particles against one another. This increases the zones of contact (denser aggregate packing) and inter-particle friction, resulting in a higher stiffness value (SANRAL, 2014).

2.4.2. G1 Crushed Stone

A G1 material is classified according to the TRH14 manual as a high-quality graded crushed stone. It is obtained through crushing of solid quarried rock, clean rock from mine rock dumps, or clean boulders. No clay minerals susceptible to rapid chemical weathering may be present; it must be non-plastic. At construction, it is placed at nearly saturation moisture content and a process called slushing is performed in order to achieve the required density for the G1 material (TRH14, 1985). Figure 2-14 illustrates a typical G1 base that has undergone slushing.

Figure 2-14: Completed, slushed G1 base (Kleyn, 2012).

Slushing is a key component of inverted pavement construction whereby excess fines are expelled from the unbound aggregate base in order to achieve the optimum fine to coarse soil matrix (Figure 2-15). This is done through high speed rolling of the saturated material as water migrates to the surface by capillary action carrying excess fines. A well-stabilised subbase is essential to contend with the excessive moisture and high compaction energy. As the excess fines are removed, the larger particles are consolidated, resulting in a greater density and stiffness (Kleyn, 2012). Like all other granular materials, this material also exhibits a stress-dependent elasto-plastic type of behaviour (described by the shakedown theory concept).

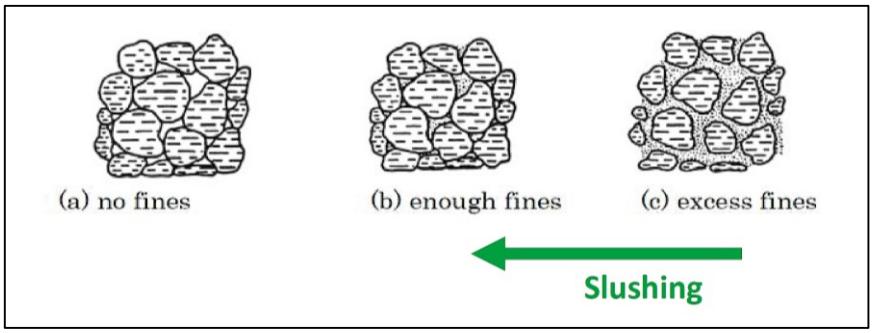

Figure 2-15: Slushing process (Boudreau et al., 2016).

2.4.3. Bitumen Stabilised Material

Bitumen Stabilised Materials (BSMs) are granular materials, previously cemented materials, or Reclaimed Asphalt (RA) layers treated with a bitumen stabilising agent in the form of an emulsion or foam. Small amounts of active filler (cement or hydrated lime) can also be added to the mix to assist in dispersing the bitumen and improve the retained strength under saturated conditions. However, the cement content must be smaller than 1 per cent and should not exceed the percentage of the bitumen stabiliser; otherwise, the material should be considered a cemented material.

This stabilising process provides some additional strength and flexibility to the parent material but primarily reduces its moisture susceptibility. The difference between the two stabilisation techniques is:

- *Bitumen emulsion treatment* occurs when small bitumen droplets are suspended in water containing an emulsifier in order to create a charged bitumen emulsion of reduced viscosity (Figure 2-16). When this emulsion is mixed with the parent material, the charged bitumen droplets are attracted to the aggregate particles, focusing on the smaller fractions due to their surface area and charge concentration features. Some of the larger particles are also painted by the bitumen emulsion. This aggregate-binder bond is illustrated in Figure 2-17 (Asphalt Academy, 2009).
- *Foamed bitumen treatment* occurs when hot bitumen, water, and air are rapidly mixed to produce bitumen bubbles called foamed bitumen (Figure 2-16). When these bubbles come in contact with the parent material, they burst into tiny splinters. These splinters disperse exclusively to the finer particles to form a mastic (mix of fines and bitumen). This is because the bitumen splinters only possess enough heat energy to warm and adhere to the smallest particles. When compacted, the bitumen particles in the mastic are pressed against the larger aggregate particles to form localised bonds (“spot welds”) as illustrated in Figure 2-17 (Asphalt Academy, 2009).

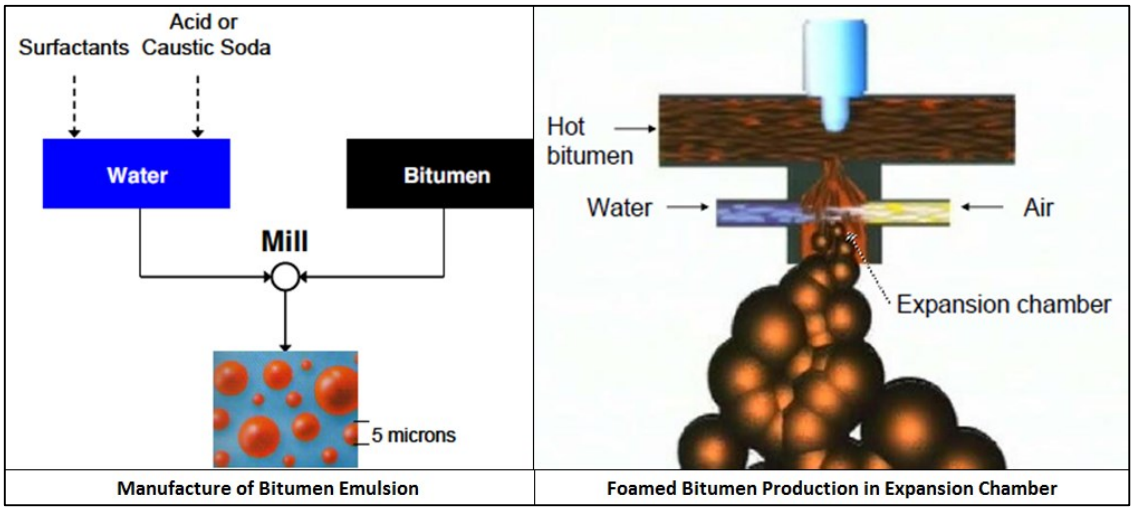

Figure 2-16: Bitumen emulsion and foamed bitumen production (Asphalt Academy, 2009).

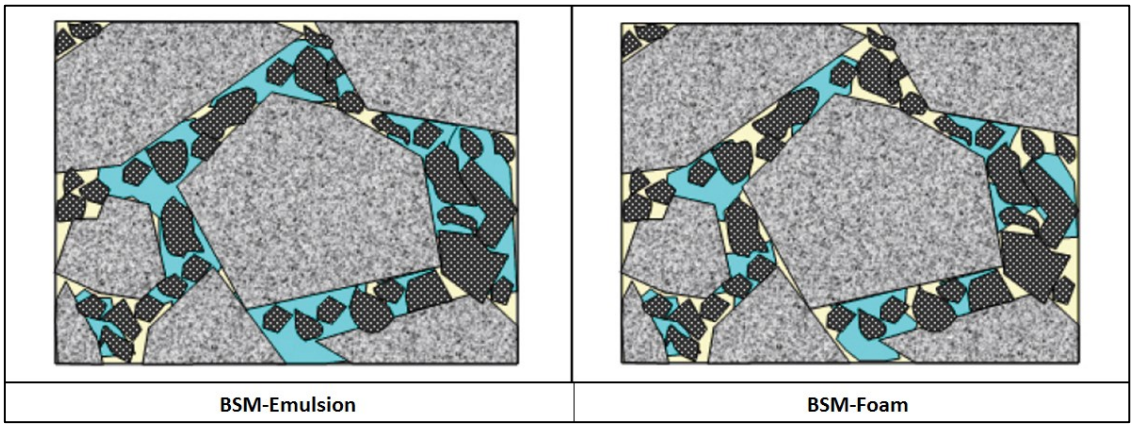

Figure 2-17: Aggregate-binder bond of BSMs (Asphalt Academy, 2009).

In a BSM, the bitumen stabilising agent is dispersed selectively amongst the finer soil particles and leaves the coarse particles mainly uncoated. Due to this pattern of bitumen dispersion, a BSM can be classified as a non-continuously bound material when compacted to form a pavement layer. This is due to the dispersed bitumen droplets forming localised bonds between material particles. BSMs rather exhibit a granular type of behaviour in nature but with considerably improved shear properties, durability, and reduced moisture sensitivity (SANRAL, 2014).

BSMs can be classified into three classes, namely BSM1, BSM2, and BSM3. These three classes are similar to the BT1, BT2, and BT3 classes from the TRH14 classification system. The classification is mainly based on the quality of the parent material and the design traffic. Table 2-3 contains all the relevant characteristics of each BSM class, which includes the parent material, its use in the pavement structure, and the design traffic application.

Table 2-3: BSM characteristics (Asphalt Academy, 2009).

	BSM1	BSM2	BSM3
Parent Material	Graded Crushed Stone / RA	Graded Natural Gravel / RA	Soil-Gravel and/or Sand
Use	Base Layer	Base Layer	Base Layer
Design Traffic	> 6 MESA	< 6 MESA	< 1 MESA

2.4.4. Cemented Material

Cement treated pavement layers can range from weakly cemented natural gravels (C3 and C4) to strongly cemented crushed stone (C1 and C2). Depending on the properties of the parent material, it can either be cement treated or lime treated. Cement is particularly effective for stabilising medium to low plasticity materials, while lime is more suitable for fine clayey materials (TRH4, 1996; TRH13, 1986). Figure 2-18 illustrates a typical CTB layer during construction as well as the finished product after curing.

Figure 2-18: Typical cement treated base (AG Peltz, n.d.).

Like concrete, cemented materials initially show elastic behaviour and have limited tensile strength as cracking occurs under repeated flexure. Cracking also occurs due to shrinkage during drying. These materials degrade in service and after numerous years reach an equivalent granular state, which resembles an elasto-plastic like type of behaviour. Some of the most common advantages of cement stabilisation are:

- Overall strength and durability of the parent material is increased;
- Resistance to the effects of water is improved;
- Ability to dry out wet soils, and
- Ability to improve the workability of clayey materials.

Cemented layers also have good load-spreading properties, which help improve the structural capacity of pavements. Cement treatment is overall a very effective and economical stabilisation technique. Material properties can be improved significantly with the addition of a relatively small amount of stabilising agent (TRH4, 1996; TRH13, 1986).

2.4.5. Asphalt

Asphalt is a premix of high-quality aggregate or RA with bitumen binder and filler. Due to the bitumen content, HMA materials have strong visco-elastic material properties and are highly temperature dependent. Under recurring axle loads an asphalt layer may crack and/or deform. At low temperatures asphalt tends to crack, and at high temperatures it usually shows signs of deformation (rutting). This behaviour is also heavily dependent on the type and quality of the supporting layers (TRH4, 1996).

In some situations where high base stiffness is required, as for heavily trafficked roads, base layers can be constructed using a variety of HMA mixes (BC and BS). They are commonly known as Asphalt Concrete Bases (ACBs), Asphalt Treated Bases (ATBs), Bitumen Treated Bases (BTBs), or Large Aggregate Mixes for Bases (LAMBs). Base course HMA mixes normally contain larger nominal maximum aggregate sizes in relation to surface course mixes and are subject to more lenient specifications. They are also more open graded, typically coarse continuous (like Dense Bitumen Macadam (DBM) for example) or Stone Mastic Asphalt (SMA) type grading with significantly larger maximum aggregate sizes (> 25 mm) (SANRAL, 2014; Pavement Interactive, 2012a & b). Figure 2-19 shows a typical BTB after construction.

Figure 2-19: Typical bitumen treated base (Pavement Interactive, 2012a).

Stone-skeleton packing, consequently, is the preferred aggregate packing type for asphalt bases due to the prime layer requirements. However, an exception is High Modulus Asphalt (HiMA) /Enrobés à Module Elevé (EME) bases. They are basically sand-skeleton types, which naturally exhibit a denser aggregate packing matrix. Aggregate packing plays an important role with regards to the ultimate stiffness an asphalt mix can end up with. Greater stiffness values can be obtained by selecting a dense aggregate packing. In conjunction with their sand-skeleton aggregate packing, EME bases also contain a high proportion of very hard (15-25 pen) binder, which enables them to yield great stiffness moduli (SANRAL, 2014). Figures 2-20 and 2-21 respectively illustrate the aggregate packing theory and a typical EME base after construction.

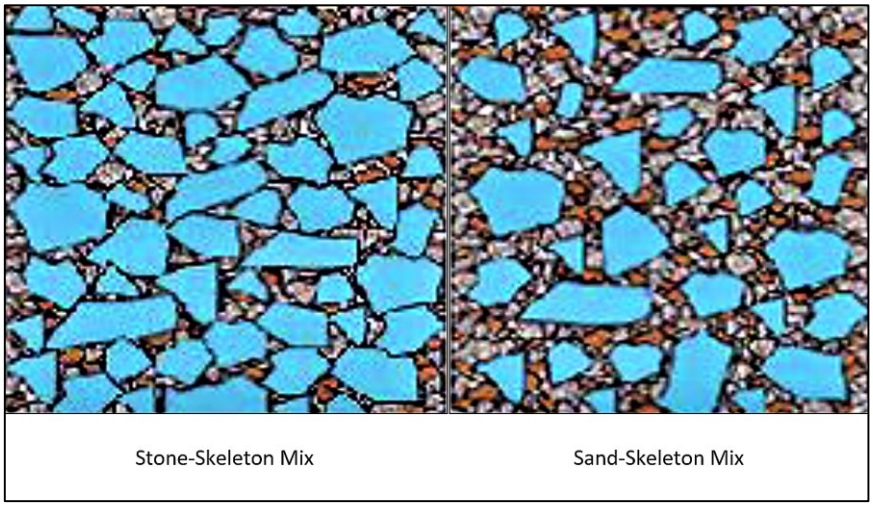

Figure 2-20: Aggregate packing theory (SANRAL, 2014).

Figure 2-21: Typical high modulus asphalt base (Nkgapele et al., 2012).

The performance of bituminous bases is highly dependent on the properties of the supporting layers as mentioned before. Although a bituminous base is a layer of high strength, an optimum balance between it and the underlying support is important for minimising fatigue cracking. This is usually done by providing a support layer of fairly high stiffness and sufficient thickness, normally in the form of a cementitious subbase layer (TRH8, 1987). Asphalt bases are designed to meet three main requirements:

- Distribute the carried loads from above to the underlying layers;
- Provide resistance to permanent deformation, and
- Provide a structure with long-lasting durability (SANRAL, 2014).

Even though relatively high air voids and low binder content are acceptable, a near impermeable base layer is still the target product in order to restrict water ingress to the underlying layers as effectively as possible (TRH8, 1987).

2.5. Permanent Deformation of Flexible Pavement Materials

All the different material layers used in flexible pavements can be categorised into three basic groups, namely granular pavement layers, cemented pavement layers, and bituminous pavement layers. Each one of these groups is unique in the way it behaves under traffic loading in terms of permanent deformation and effective elastic modulus.

The general behaviour of granular pavement layers in terms of permanent deformation and effective elastic modulus is illustrated in Figures 2-22 and 2-23 respectively. Phase 1 represents a phase of post-compaction deformation. High-strength layers may de-densify and lose strength, while low-strength layers may show an increase in strength due to densification (traffic moulding) (Jordaan, 2006).

After a phase of initial densification, these type of layers normally enter a phase of little deformation (Phase 2). During this stable phase, the rate of deformation is almost constant (linear) and strongly dependent on the layer's inherent characteristics. A material of poor initial quality and consequently a low bearing capacity, may experience premature shear failure of the layer under high traffic loadings and a very short or non-existent second phase (Jordaan, 2006).

In Phase 3, these layers exhibit an increase in the rate of deformation while showing a relatively quick decrease in effective elastic modulus at the same time. This can be as a result of an increased moisture content or due to a sudden increase in high traffic loading (Jordaan, 2006).

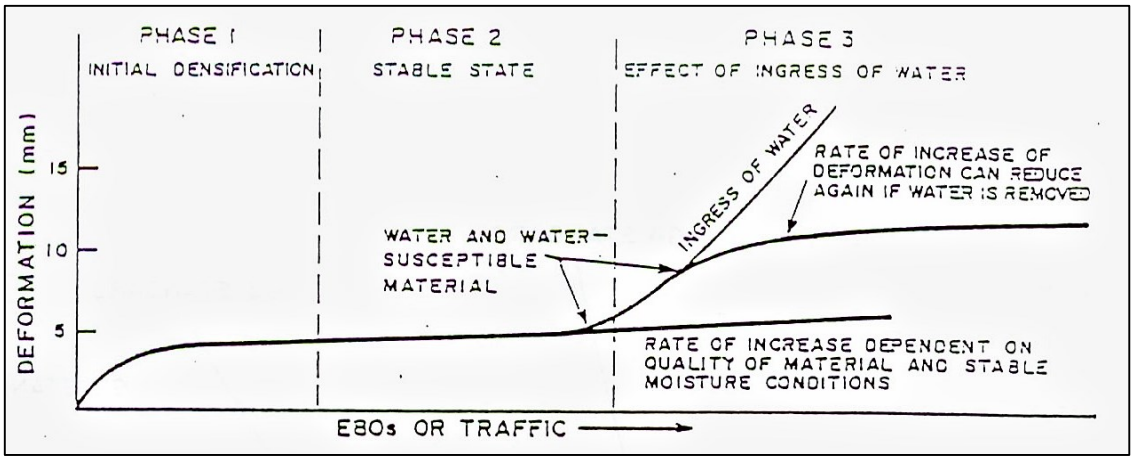

Figure 2-22: Change in permanent deformation of granular layers (Jordaan, 2006).

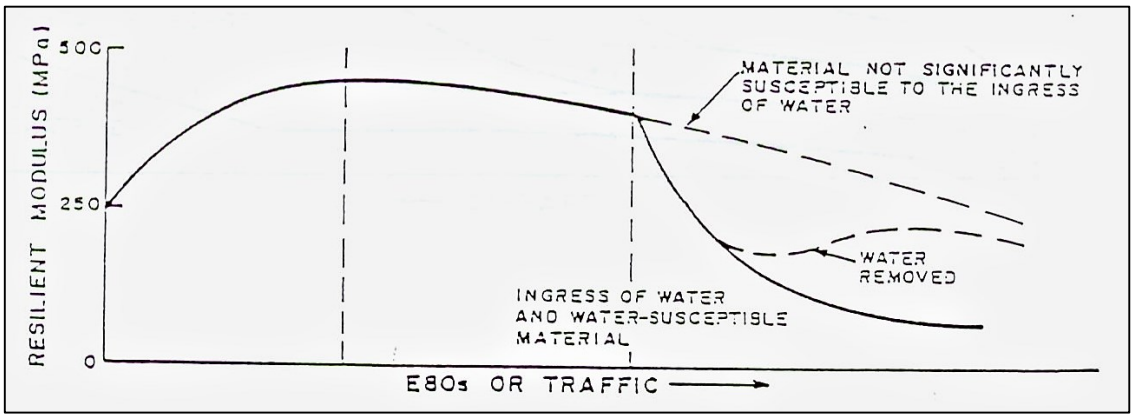

Figure 2-23: Change in effective elastic modulus of granular layers (Jordaan, 2006).

The general trends in behaviour of cemented pavement layers in terms of permanent deformation and effective elastic modulus are presented in Figures 2-24 and 2-25 respectively. The majority of the strength of a pavement with cemented layers is normally focused in these layers; consequently, these layers generally fail in tension (fatigue). At first, the cemented layer shows basically no increase in permanent deformation and has a relatively high effective elastic modulus. Typical block cracks (due to shrinkage) may develop during the early life of the pavement and will most probably reflect through to the pavement's surface (Jordaan, 2006).

Due to fatigue from trafficking and the weakness of cement in tension, a lot of cemented layers soon develop micro-cracks. These cracks cause a reduction in the effective elastic modulus of the layer. The layer still appears intact in the block cracks and the rate of permanent deformation is still very low. The development of micro-cracks continues until the layer reaches a stage where it breaks down into a granular state. This breaking down process generally happens relatively quickly after which the layer has little resemblance to the initial cemented layer (Jordaan, 2006).

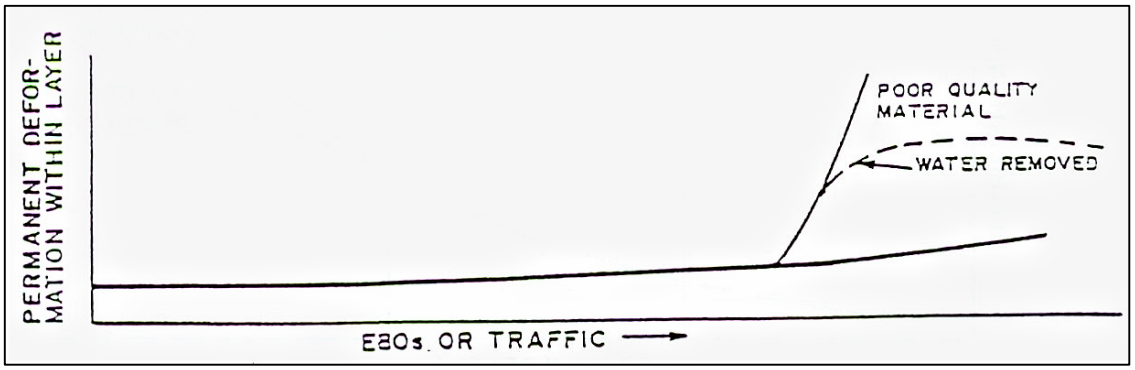

Figure 2-24: Change in permanent deformation of cemented layers (Jordaan, 2006).

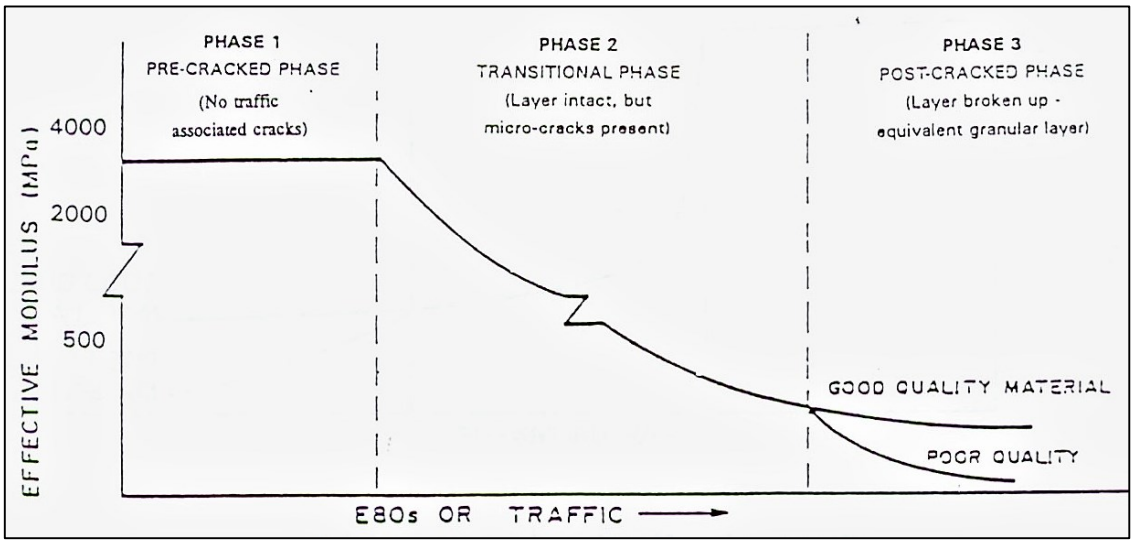

Figure 2-25: Change in effective elastic modulus of cemented layers (Jordaan, 2006).

The general trends in behaviour of bituminous pavement layers in terms of permanent deformation and effective elastic modulus are shown in Figures 2-26 and 2-27 respectively. These layers normally show a general increase in deformation under traffic loading from the time of construction. The rate of deformation of the bituminous layer is heavily dependent on the properties of the mix (especially the grading of the parent material) and operating temperatures. Due to the visco-elastic properties of bituminous layers, they are temperature susceptible and may deform at different rates, depending on the mix temperature and applied wheel load. The rate of deformation may also decrease with time as a result of an increase in stiffness of the layer due to aging of the binder; however, this will make the material more vulnerable to fatigue cracking. At the end of the layer's fatigue life, it breaks down to a granular state and has little resemblance to the original layer (Jordaan, 2006).

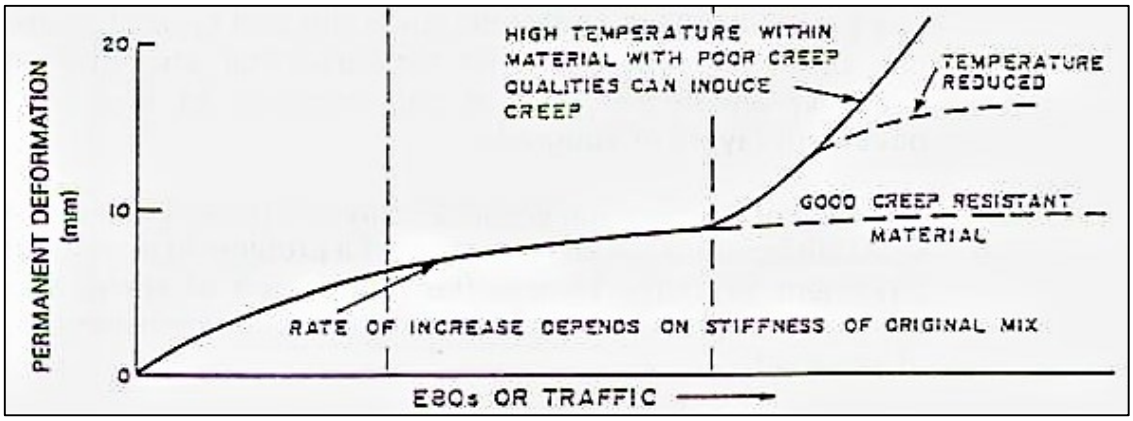

Figure 2-26: Change in permanent deformation of bituminous layers (Jordaan, 2006).

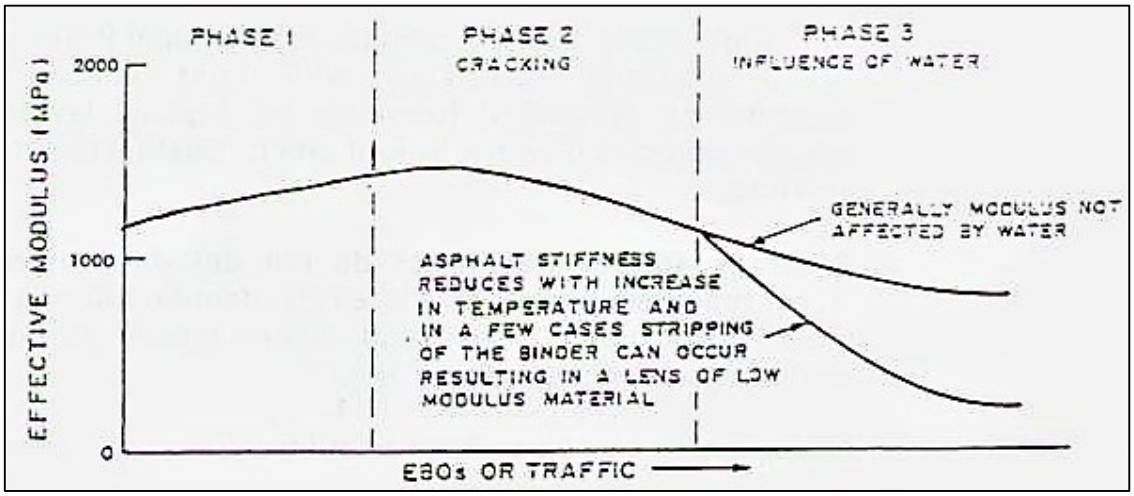

Figure 2-27: Change in effective elastic modulus of bituminous layers (Jordaan, 2006).

Theyse et al. (2006) investigated the elastic response and permanent deformation of the subgrade at the Richmond Field Station in California to calibrate a permanent deformation design model for that specific subgrade. The investigation proved that the subgrade elastic deflection is a better indicator of the subgrade permanent deformation than the vertical strain at the top of the subgrade. A much better correlation was achieved between subgrade permanent deformation and subgrade deflection. This is due to the subgrade elastic deflection being representative of the response of the total depth of the subgrade that is affected by the externally applied load. The vertical strain at the top of the subgrade is only representative of the material behaviour and conditions at the top of the subgrade.

Jordaan (2006) also showed that a general increase in permanent deformation (rut depth) can be associated with a general increase in maximum elastic deflection. He reported on two typical rural roads, P6/1 from Bapsfontein to Bronkhorstspruit (Figure 2-28) and P21/1 from Bloemfontein to Soutpan (Figure 2-29), that showcased this trend.

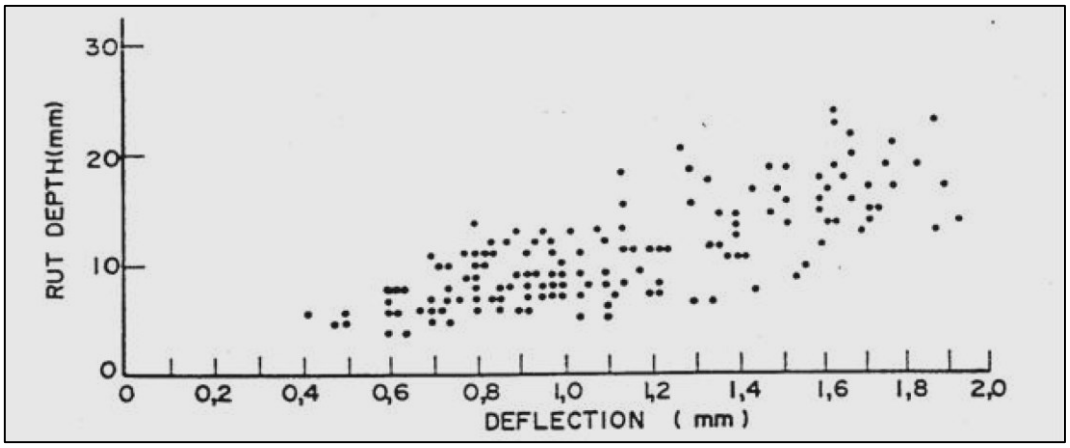

Figure 2-28: Rut depth vs deflection plot for Road P6/1 (Jordaan, 2006).

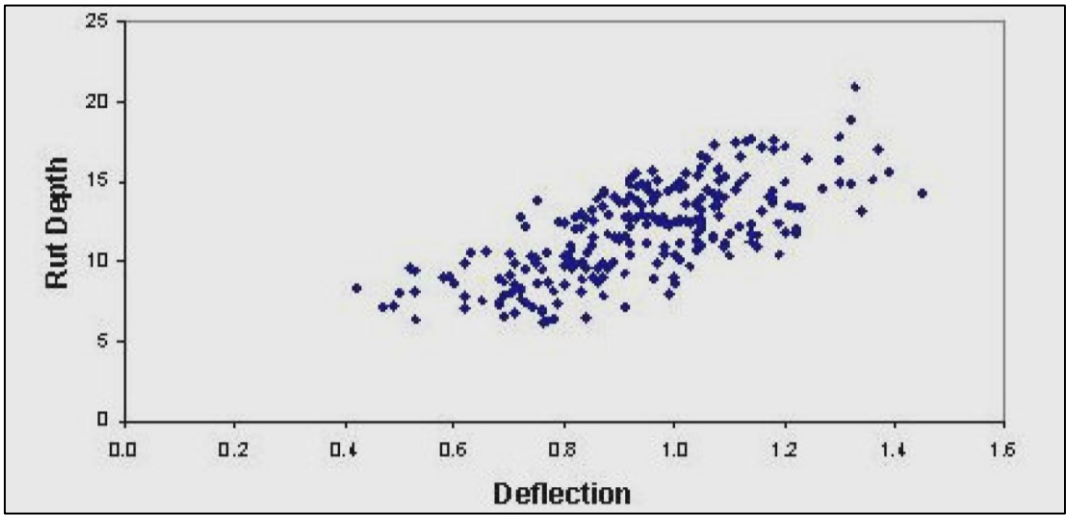

Figure 2-29: Rut depth vs deflection plot for Road P21/1 (Jordaan, 2006).

The permanent deformation of flexible pavements has been studied for a vast number of years with great success. Even though research has been focused on certain materials and layers, the deformation behaviour of various materials/layers has been investigated. Some of the most popular flexible pavement base materials that have been studied in the past and are relevant to this study include:

- Natural gravel;
- Crushed stone;
- Bitumen foam treated material;
- Bitumen emulsion treated material;
- Cemented material;
- Large aggregate mixes, and
- High modulus asphalt.

So far, Accelerated Pavement Testing (APT) has been the preferred method of data collection regarding pavement response and performance. APT is the controlled application of a prototype wheel load, at or above the appropriate legal load limit, to a prototype or actual pavement structure in order to determine pavement response and performance under a controlled and accelerated accumulation of damage in a short period of time. The acceleration of pavement damage is achieved by increased load repetitions, modified loading conditions, imposed climatic conditions, etc. Construction is done by conventional plant and processes in order to model real world conditions (Metcalf, 1996). Loading is typically provided by a traffic simulator (fixed or transportable) that imposes a rolling wheel load over a specific test length.

2.5.1. Natural Gravel

CSIR Transportek has been involved in APT with a fleet of Heavy Vehicle Simulators (HVSs) for many years in South Africa; hence, plenty of pavement response and performance data have been accumulated to date. Theyse (1997) processed the in-depth deflection and permanent deformation data from a number of the test sections and reported an average rut rate of 1.33 nanometre per cycle (nm/cycle) for a typical natural gravel base flexible pavement structure. The HVS test included a 40-kN dual-wheel (at 690 kPa tyre inflation pressure) load applied to a pavement structure that consisted of a S2 seal, a 305-mm G4 base, a 115-mm G4 subbase, and a G5 subgrade. The speed of the loading wheel was kept constant at all times.

2.5.2. Crushed Stone

The same set of HVS test data processed by Theyse (1997) included a crushed stone base test section. An average rut rate of 0.35 nm/cycle was reported for this pavement structure, which comprised a S2 and slurry seal, a 150-mm G1 base, a 245-mm C3 subbase, and a G4/G5 subgrade. The HVS loading characteristics remained the same as before.

Wu et al. (2009) evaluated the effectiveness of blended calcium sulphate as a pavement base layer, compared to conventional crushed stone. A full-scale accelerated pavement test was conducted to evaluate the field response and performance of the relevant test sections at the Louisiana Pavement Research Facility (PRF) in Port Allen, LA. An average rut rate of 6.15 nm/cycle was derived for the crushed stone base test section, which presented a 50-mm HMA surface, a 216-mm crushed stone base, a 305-mm lime treated soil subbase, and a silty-clay subgrade to the Accelerated Loading Facility (ALF). The ALF machine applied a 43.4-kN dual-wheel (at 723 kPa tyre inflation pressure) load to the test section at a constant speed of 16.8 km/h.

Theyse (1999) reported on extensive HVS testing done in South Africa to evaluate different base materials constructed through labour-intensive procedures. Due to the variety of base materials used, the response and performance assessment of these test sections was important from a labour-intensive construction point of view as well as for its contribution to a better understanding of material behaviour. The 100-mm G2 crushed stone base (150-mm cement treated subbase) test section showed an average rut rate of 0.3 nm/cycle while it was loaded with a 40-kN dual wheel at a constant speed.

2.5.3. Bitumen Foam Treated Material

Romanoschi et al. (2004) evaluated the effectiveness of bitumen foam treated Recycled Asphalt Pavement from Full-Depth Reclamation (FAS-FDR) as a base material for flexible pavements. This was achieved through full-scale APT on four pavements, one conventional granular base and three thicknesses of FAS-FDR, at the Civil Engineering Infrastructure Systems Laboratory (CISL) of Kansas State University. The 305-mm-thick FAS-FDR base performed well with an average rut rate of 2.54 nm/cycle reported for this test section under a 75.7-kN dual-wheel (at 700 kPa tyre inflation pressure) load moving at a constant speed. Apart from the base layer, each test section consisted of a 75-mm HMA (12.5-mm nominal maximum size Superpave mixture) surfacing layer and a selected subgrade soil, placed and compacted in 150-mm lifts, on top of the existing subgrade (silty clay).

A full-scale APT experiment was conducted on bitumen foam pavements at the Canterbury Accelerated Pavement Testing Indoor Facility (CAPTIF) to study the effects of adding bitumen foam to unbound granular materials when used as base courses in flexible pavements (Gonzalez et al., 2009). A total of six pavement sections were constructed within a 1.5-m-deep and 4.0-m-wide concrete tank, which stretched 58 m along a circular track. All sections had a 50-mm surfacing, which comprised a single coat chip seal covered with a skim coat of AC10 hot mix and a thin 30-mm HMA layer. The base layer varied in bitumen and cement content but remained a crushed stone blended with crusher dust at a fixed thickness of 200 mm. The top of the subgrade was a 525-mm clay, which extended in 225-, 150-, and 150-mm lifts. The average rut rate for the bitumen foam treated test sections under a 40-to 60-kN dual-wheel (at 700 kPa tyre inflation pressure) load turned out to be very similar (Table 2-4). The Simulated Loading and Vehicle Emulator (SLAVE) units applied the wheel loads to the circular test track at a constant speed of 40 km/h.

Table 2-4: Rutting behaviour of bitumen foam treated base test sections (Gonzalez et al., 2009).

	Test Section ID			
	B28C10	**B14C10**	**B12C10**	**B22C00**
Bitumen Content	2.8%	1.4%	1.2%	2.2%
Cement Content	1.0%	1.0%	1.0%	0.0%
Avg. Rut Rate	+/- 1.43 nm/cycle			2.57 nm/cycle

2.5.4. Bitumen Emulsion Treated Material

Theyse's (1999) report on extensive HVS testing done in South Africa to evaluate different base materials constructed through labour-intensive procedures included the performance assessment of an emulsion treated gravel base as well. The 150-mm ETB (150-mm cement treated subbase) test section showed an average rut rate of 0.60 nm/cycle while it was loaded with a 40-kN dual wheel at a constant speed.

Horak and Rust (1992) reported on APT done in South Africa to evaluate and model the performance of ETB pavements. One of the HVS tests included a cracked CTB pavement that was rehabilitated by means of cold-mix recycling of the base and surfacing, transforming it into an ETB with a cement treated subbase. The structural composition and permanent deformation behaviour of this test section are provided in Table 2-5. The HVS applied a 60-kN dual-wheel load to the pavement structure at a constant speed.

Table 2-5: Rutting behaviour of rehabilitated ETB test section (Horak and Rust, 1992).

Surfacing	60-mm Gap-Graded Asphalt
Base	100-mm ETB (1.0% Bitumen, 1.0% Cement)
Subbase	Cement Treated Subbase
Selected Subgrade	Sandstone Selected Subgrade
Subgrade	Clayey Subgrade
Avg. Rut Rate	1.00 nm/cycle

2.5.5. Cemented Material

Theyse (1997) looked at a CTB test section as well. This pavement structure consisted of a S2 seal, a 300-mm C3 base, a 200-mm G4 subbase, and a G5 subgrade. The HVS applied a 40-kN dual-wheel (at 700 kPa tyre inflation pressure) load to the pavement structure at a constant speed. An average rut rate of 0.59 nm/cycle was the result.

Metcalf et al. (1999) discussed accelerated testing done in Louisiana to analyse the historically prevalent flexible crushed stone base and alternative CTBs under ALF loading. He compared the performance of nine different base courses. The permanent deformation behaviour of the 10% plant mixed soil-cement CTB test section is provided in Table 2-6. Loading was provided by an ALF in the form of a dual wheel (at 724 kPa tyre inflation pressure), which could be varied between 43 and 85 kN. The speed of the loaded wheel was kept constant at 17 km/h.

Table 2-6: Rutting behaviour of CTB test section (Metcalf et al., 1999).

Surfacing	90-mm Asphalt
Base	215-mm Plant Mixed Soil-Cement (10%)
Subbase/Subgrade	Fair Silty Soil
Avg. rut rate	12.5 nm/cycle

The South African HVS programme also assessed the performance of three rehabilitated lightly cemented pavement structures under full-scale HVS loading (Steyn et al., 1997). A 40-kN HVS dual-wheel (at 520 kPa tyre inflation pressure) load was applied to a rehabilitated pavement structure that comprised a new double seal (S2) on top of an existing 140-mm C3 base, 160-mm C3 subbase, 120-mm G4 selected layer, 140-mm river sand, and G5 subgrade. An average rut rate of 0.5 nm/cycle was recorded for this pavement structure.

2.5.6. Large Aggregate Mixes

Van der Merwe et al. (1992) reported on the HVS testing of a rehabilitated BTB pavement in South Africa. The original pavement structure consisted of a 160-mm BTB (4.1% bitumen) on top of a 200-mm natural gravel subbase and a 200-mm selected layer. Rehabilitation comprised an 80-mm semi-gap-graded asphalt overlay placed over this structure (Table 2-7). The permanent deformation behaviour of this test section is provided in Table 2-7. The HVS test included a 40-kN dual-wheel load applied to the pavement structure at a constant speed.

Table 2-7: Rutting behaviour of rehabilitated BTB test section (Van der Merwe et al., 1992).

Surfacing	80-mm Semi-Gap-Graded Asphalt
Base	160-mm BTB (4.1% bitumen)
Subbase	200-mm Natural Gravel (G4)
Selected	200-mm Selected Layer
Avg. rut rate	0.23 nm/cycle

2.5.7. High Modulus Asphalt

Rohde et al. (2008) evaluated EME bases using full-scale APT at the Federal University of Rio Grande do Sul (UFRGS) campus. Two test sections with different EME base thicknesses (80 mm and 120 mm) were constructed on top of a subbase consisting of 280-mm unbound granular material compacted over lateritic soil of high bearing capacity. The two pavements were rounded off with a micro-surfacing wearing course. The EME mix consisted of basalt aggregate, sand, hydrated lime, and a bitumen modified with asphaltite, named CAPPLUS 106B. The EME mix and bitumen characteristics are provided in Table 2-8. Testing of the 120-mm EME test section was conducted at ambient air temperatures of 25°C and higher. An average rut rate of 20 nm/cycle was recorded for this test section while it was loaded with a 50-kN dual wheel (at 620 kPa tyre inflation pressure) at a constant speed of 6 km/h.

Table 2-8: EME mix and bitumen characteristics (Rohde et al., 2008).

EME Mix	
Bitumen Content	5.50%
Bitumen (CAPPLUS 106B)	
Penetration at 25°C (1/10 mm)	27
Ring and Ball Softening Point	56°C

In preparation for the inclusion of EME into the Swiss standards, three test sections were constructed in the Halle-Fosse at the Federal Institute of Technology at Lausanne, Switzerland (Perret et al., 2004). Two sections with EME bases (110-mm EME1 and 70-mm EME2) and one section with a reference HMA base (140-mm HMT 22s) were evaluated using full-scale APT at 50°C. Each pavement structure comprised two bituminous layers (wearing course and base course), a subbase of unbound granular material, and a subgrade of fine sand on top of a concrete slab. An average rut rate of 10.77 nm/cycle was recorded for the EME1 test section while it was loaded with a 57.5-kN single wheel (at 800 kPa tyre inflation pressure) at a constant speed. Table 2-9 provides the characteristics of the EME1 mix and the bitumen used.

Table 2-9: EME1 mix and bitumen characteristics (Perret et al., 2004).

EME1 Mix	
Bitumen Content	4.25%
Bitumen (BP Structure 15/25)	
Penetration at 25°C (1/10 mm)	21
Ring and Ball Softening Point	67.8°C

2.6. Pavement Instrumentation

The prediction of pavement response to tyre loading is one of the biggest challenges in pavement engineering. This is due to the complex interaction between the environment, applied load, and non-homogeneous layered pavement system. Calculating pavement response forms an important part of the pavement design process as it is used to determine pavement damages in the mechanistic-empirical pavement design procedure. However, it is still only a prediction and does not indicate how the pavement will actually behave in service.

Instrumentation embedded within the pavement structure can record the true response of a pavement exposed to tyre loading. It does not really assist in the design process as the pavement has already been constructed, but it may be useful in monitoring the health and performance of the pavement. Typical in-situ pavement instrumentation includes:

- Multi-depth deflectometers;
- Emu strain coils;
- Moisture and temperature sensors;
- Stress sensors, and
- Strain gauges.

Although the instrumentation is embedded within the pavement structure, it remains one of the biggest challenges to protect cables, plugs, and sockets from potential rodent, flood, and weather related damage. Any damage to the sensors and their components can jeopardise the ability of the instrumentation to produce accurate data or to produce any data at all. Discussion on some of the pavement instrumentation relevant to this study is to follow.

2.6.1. Multi-Depth Deflectometer

The Multi-Depth Deflectometer (MDD) is a Linear Variable Differential Transformer (LVDT) deflection measuring device used to measure transient depth deflection profiles of a pavement structure in association with a moving load. It was developed by the National Institute of Transport and Road Research (NITRR) in South Africa during the late 1970s as an integral part of their extensive full-scale APT programme (De Beer et al., 1989).

The MDD system consists of two to six LVDTs installed vertically at different depths in a pavement structure, normally at the interfaces of the pavement layers. An LVDT along with its clamping unit represent a MDD module. Figure 2-30 illustrates a typical MDD module with all its components. The clamping (or housing) unit comprises a clamping nut, spring, loading washer, steel ball bearings, rubber membrane, and cable ducting. The MDD modules are installed in a 39-mm-diameter hole lined with a neoprene sleeve (De Beer et al., 1989).

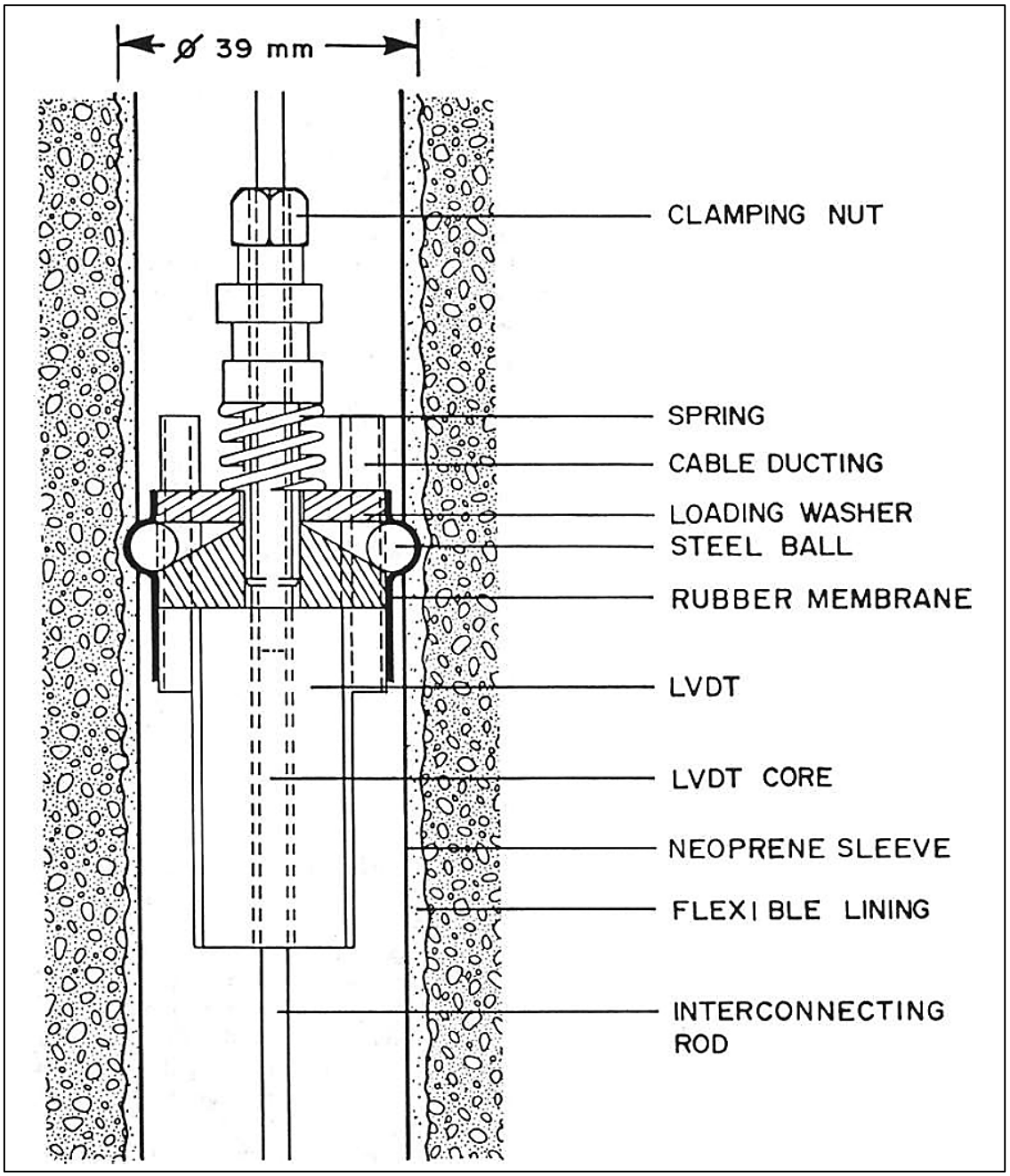

Figure 2-30: Components of a MDD module (De Beer et al., 1989).

The neoprene sleeve provides stability to both the hole and the MDD equipment during testing. The steel ball bearings are used to lock each module in position inside of the hole at the required depth. This is done by turning the clamping nut clockwise, thereby compressing the spring on top of the loading washer. The subsequent movement of the steel balls outwards ensures that the module is clamped to the side of the hole. As these ball bearings are continually under pressure from the spring unit, the unit will automatically make up for any relaxation through movement in the pavement structure as a result of stresses induced by traffic loading. Up to six MDD modules may be fixed in a single hole (De Beer et al., 1989).

The interconnecting rod is adjustable and contains LVDT cores that are spaced according to the placement of the MDD modules. It is fixed to the anchor rod, generally close to 3 m below the pavement surface, through a snap connector unit. Under normal conditions the deflection at this point is usually zero. The hole in which the MDD modules are installed highlights the one drawback of this instrument as the MDD measures displacement inside a discontinuous material, while modelling is conducted assuming no discontinuity (De Beer et al., 1989).

The MDD system can either measure the elastic (resilient) deflection or the total permanent (plastic) deformation of any layer in a pavement structure. The resilient depth deflections, normally measured at the layer interfaces, can be used to back-calculate the effective elastic modulus of each layer. The resilient deflection of a maximum of six levels can be measured at the same time. The permanent deformation at various layer depths is typically measured during the service period of the MDDs under static conditions. All measurements are made relative to the anchor located at approximately 3 m below the pavement surface (De Beer et al., 1989).

De Beer et al. (1989) used case studies for tests on an asphalt base, a granular base, and a cemented base pavement to show how the effective elastic moduli of pavement layers can be back-calculated from measured MDD deflections. Figures 2-31 through 2-33 illustrate the MDD deflections for the three different base types after various stages of HVS trafficking.

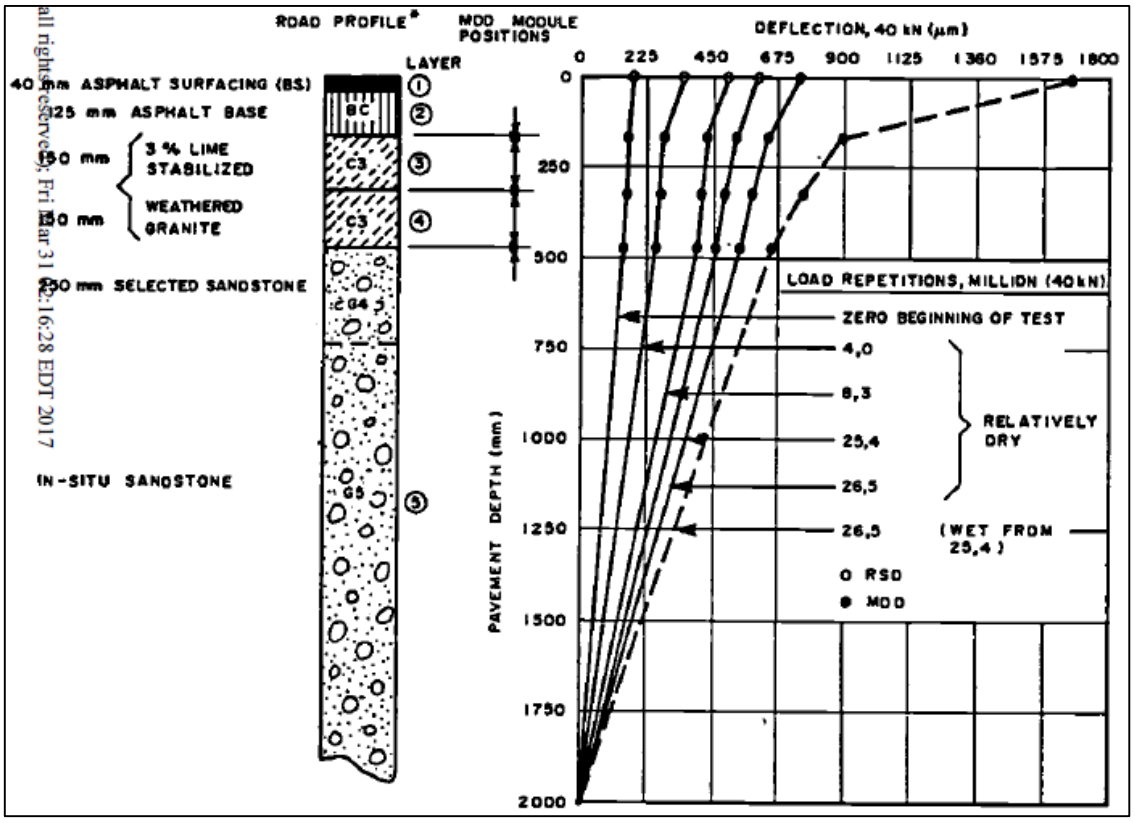

Figure 2-31: Measured MDD deflections on an asphalt base pavement (De Beer et al., 1989).

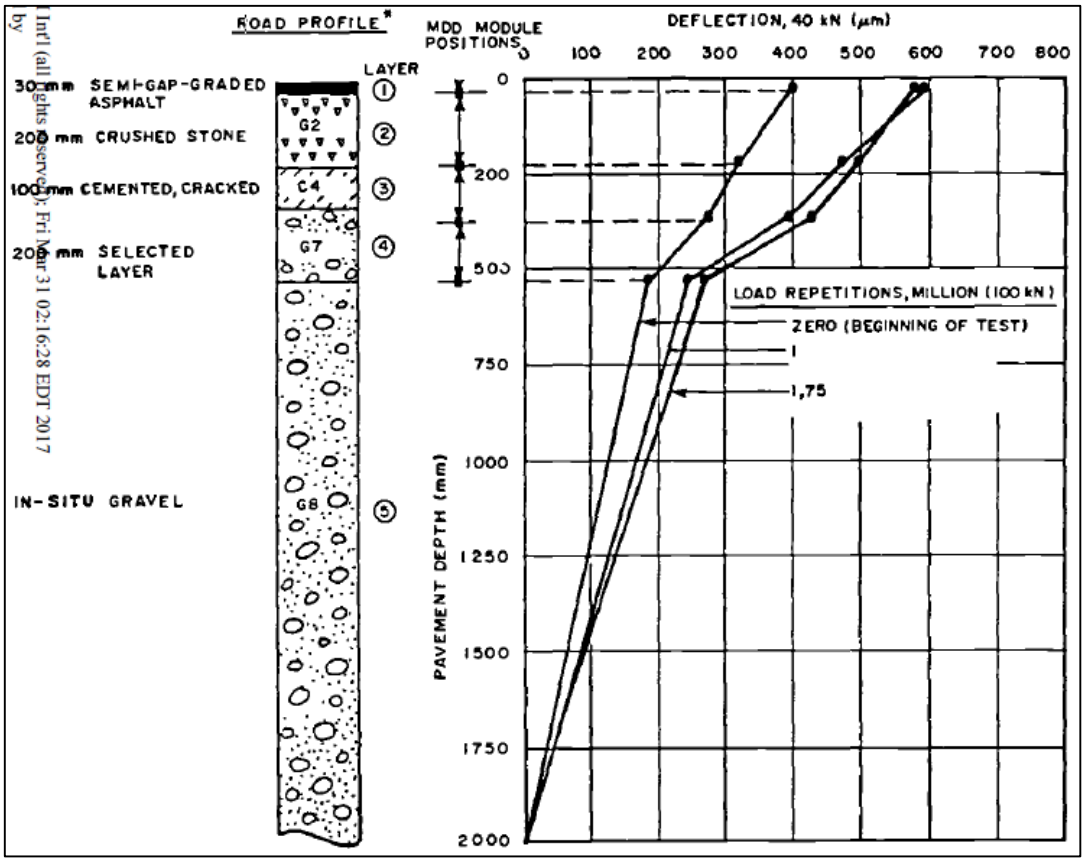

Figure 2-32: Measured MDD deflections on a granular base pavement (De Beer et al., 1989).

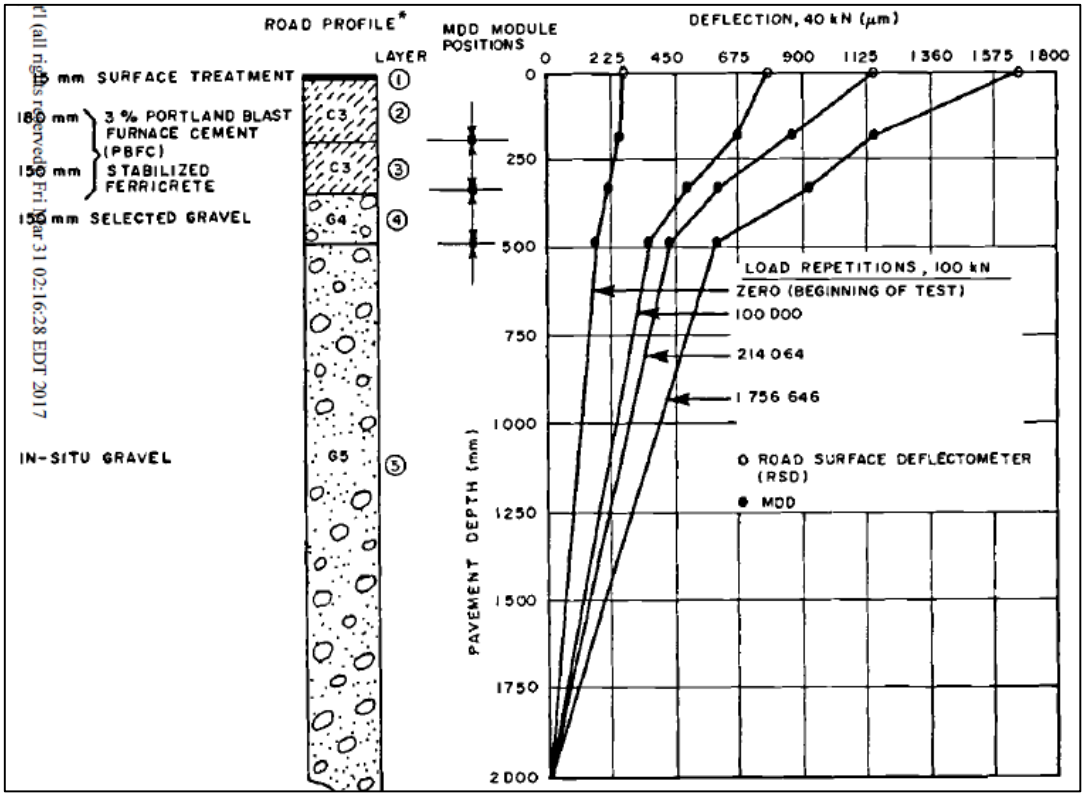

Figure 2-33: Measured MDD deflections on a cemented base pavement (De Beer et al., 1989).

The typical quasi-continuous deflection basins expected for a set of five MDDs under a moving wheel load are illustrated in Figure 2-34. The uppermost MDD is expected to experience the highest amount of deflection with each subsequent MDD deflecting less than the previous MDD above.

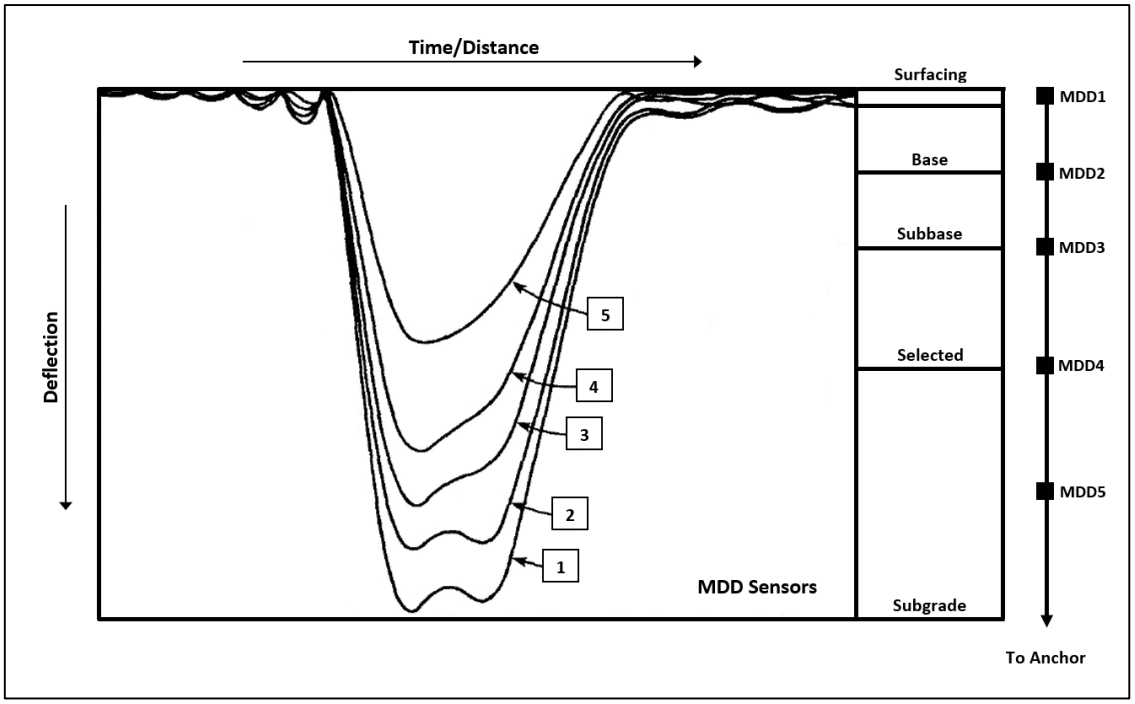

Figure 2-34: Quasi-continuous deflection basins for a set of five MDDs.

2.6.2. Strata Gauge

The strata gauge is an advanced and robust microprocessor-based instrument that measures the density and moisture in strata layers. It is an externally applied instrument that serves as an alternative to in-situ sensors. Although the strata gauge does not provide the continuous measuring capabilities some of the equivalent in-situ sensors do, it does provide better reliability and very accurate measurements.

In the Geotechnical and Civil fields, this device is regularly used to check the effectiveness of aggregate and soil compaction at various depths. Measurements are made by drilling two access holes in the pavement structure using the provided guide plate. The strata gauge is placed over the holes and the two probes inserted at a specific depth up to 600 mm, in increments of 50 mm (InstroTek, n.d.). Figure 2-35 illustrates a typical strata gauge, some of its basic components, and how it works.

The strata gauge operates by emitting radiation from two safety-sealed radioactive sources:

- For density measurements, a Cesium-137 gamma emitter emits gamma radiation through the test material (Figure 2-35). Some of the gamma radiation travels through the material and is detected by the Geiger-Mueller detector situated within the density detector rod. As high-density materials absorb more gamma radiation, a material of high density will provide a lower count per time of test than a low-density material (InstroTek, n.d.).
- For moisture measurements, an Americium-241/Beryllium neutron emitter emits neutron radiation into the test material (Figure 2-35). The high-energy neutrons experience a decrease in energy due to the collision with hydrogen atoms in the moisture of the material. As the Helium-3 detector only detects low-energy neutrons, a wet material will provide a high count per time of test, and a dry material will provide a low count for the same period of time (InstroTek, n.d.).

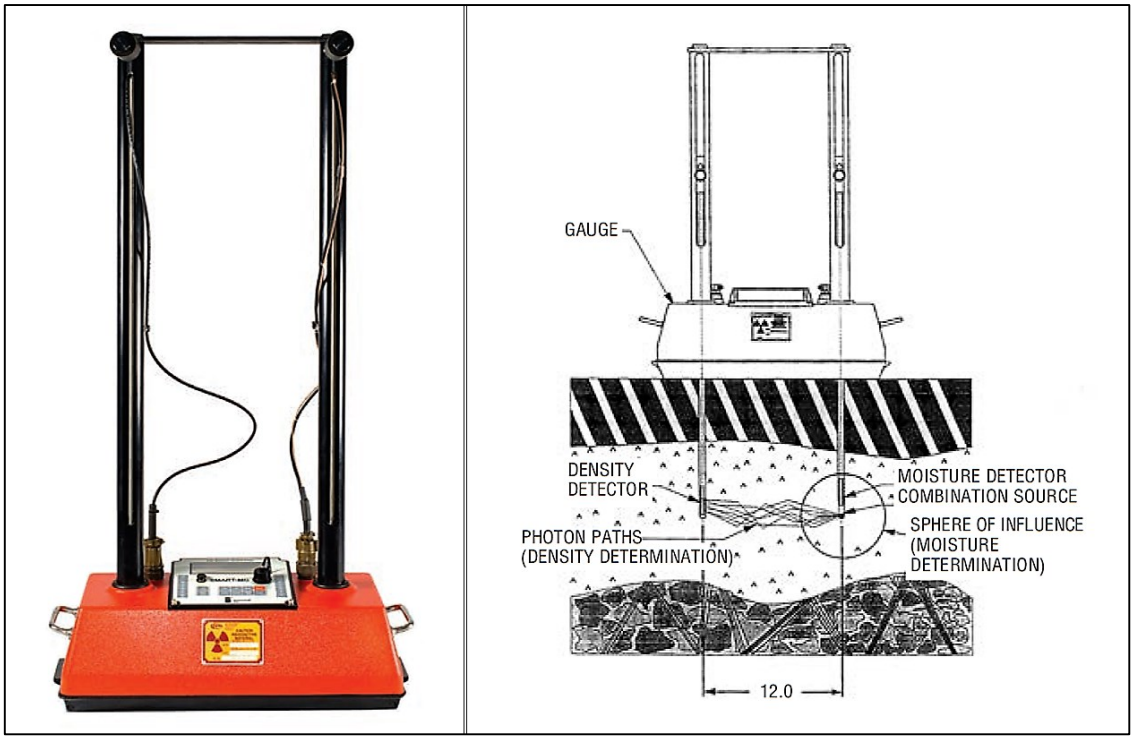

Figure 2-35: CPN MC-S-24 dual probe strata gauge (InstroTek, n.d.).

The radioactive sources of the strata gauge decay slowly over time; therefore, it is the user's responsibility to periodically take a standard count on the reference standard provided. This replaces the previous standard count on the strata gauge program, which then uses the new standard to determine the field count to standard count ratio in order to compensate for any source decay (InstroTek, n.d.).

2.7. Traffic Speed Deflectometer

The Traffic Speed Deflectometer (TSD) is a continuous deflection measuring device used to support project- and network-level pavement management decisions. It is a non-destructive pavement evaluation device that measures pavement deflections due to a moving load. Doppler technology is used to measure pavement deflection while travelling at normal traffic speeds of up to 80 km/h. No traffic control is required as the TSD is able to measure pavement deflection without the need to remain stationary (Zofka and Sudyka, 2015).

A long and rigid beam, placed inside a semi-truck, is instrumented with high-rate sensors that include Doppler sensors, laser distance sensors, and accelerometers. While the truck is in motion, vertical pavement deflection velocities are measured at a very high rate. The deflection bowl is obtained from the measured vertical deflection velocities and the horizontal driving velocity. The vertical velocities are divided by the horizontal driving velocity to produce the deflection slope at discrete points representing the deflection bowl. This principle of TSD operation is illustrated in Figure 2-36. The absolute deflections can then be calculated by integrating the deflection slopes numerically or by using a closed-form solution of a mechanical model (Zofka and Sudyka, 2015).

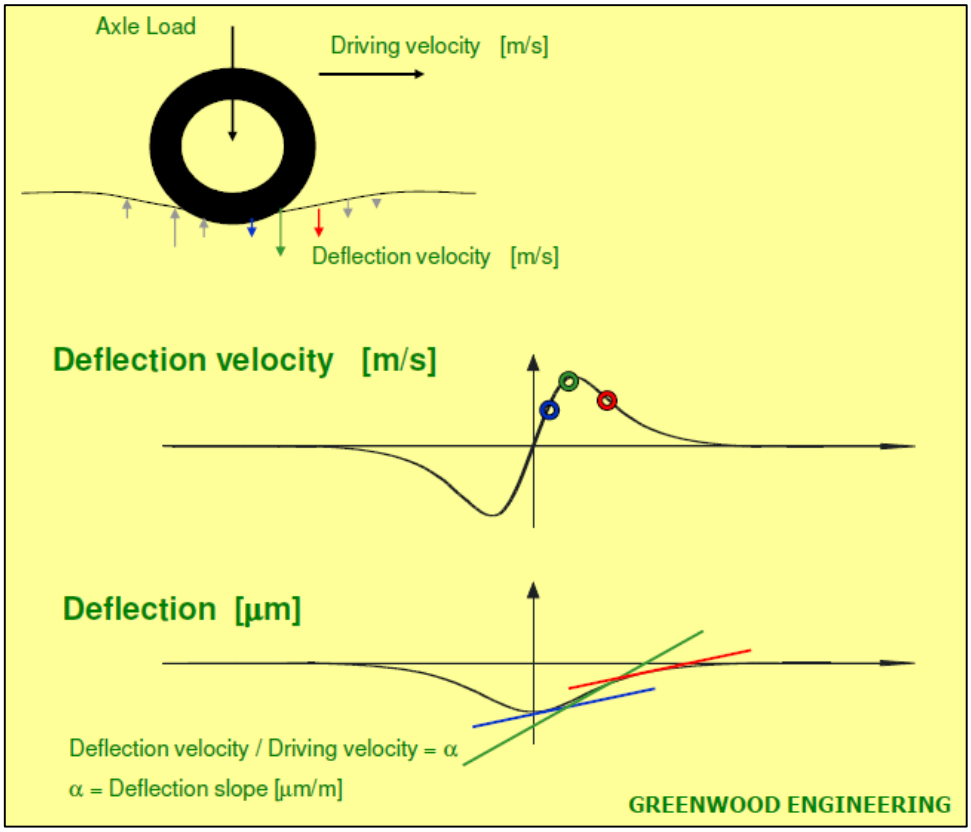

Figure 2-36: Principle of TSD operation (Krarup, 2012).

The TSD technology is developed, designed, and produced by Greenwood Engineering. During 2012 the fifth TSD was constructed for SANRAL/South Africa. This TSD, illustrated in Figure 2-37, uses 10 Doppler lasers and also includes the Greenwood LaserProf and Right-of-Way imaging system. It collects data at intervals as small as 50 mm using a variable axle load of 6 to 12 tons applied to a dual-tyred single rear axle. Strain gauges measure the dynamic axle loading at each wheel of the trailing axle (Greenwood Engineering, 2017).

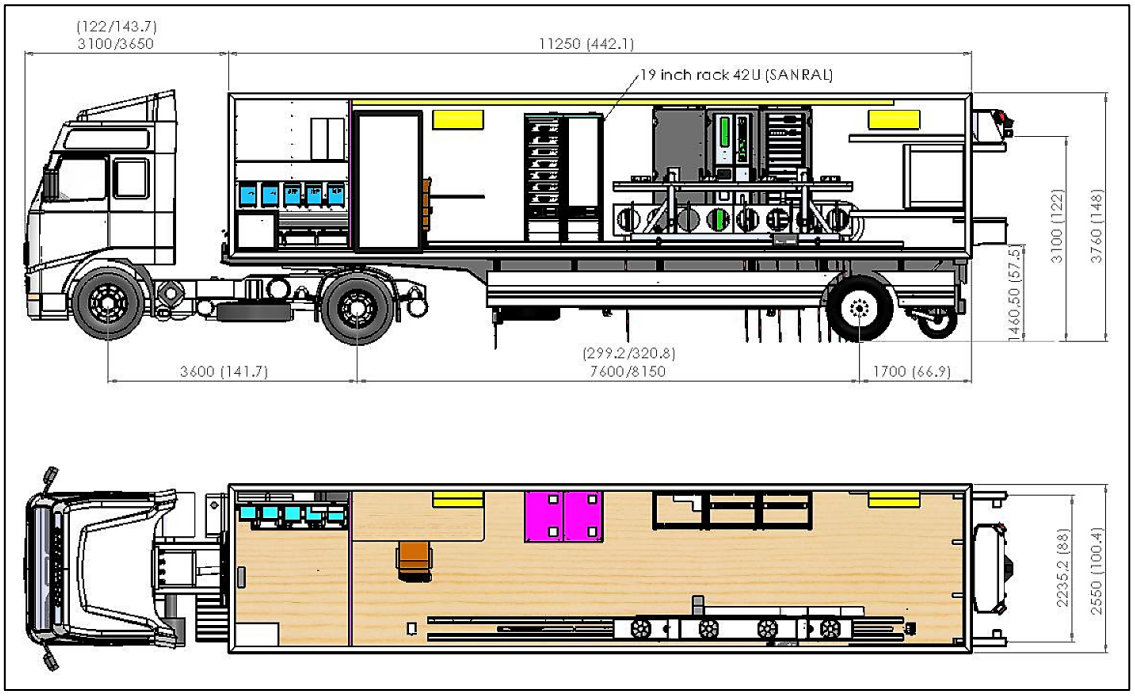

Figure 2-37: Greenwood TSD owned by SANRAL (Krarup, 2012).

2.7.1. Pavement Response Analysis

Pavement response is the manner in which a pavement reacts to applied stresses and determines how it will behave structurally. Pavement response can either be analysed through a static or dynamic solution. Stresses, strains, and deflections are usually generated as the results, or output parameters, of such a solution. Steyn (2001) evaluated the nominal differences between the two pavement response analysis procedures. A few of the inferences he made were:

- Similar trends are followed by both static and dynamic pavement response analysis for all parameters at various load levels;
- Increased load magnitudes result in increased stresses, strains, and deflections;
- Pavement response parameters normally decrease with depth;
- Stress usually remain constant with increasing speed, and
- Deflection and strain usually decrease with increasing speed.

2.7.2. Static vs Dynamic Response Analysis

Static response analysis accepts that the load is applied to the system for so long that the response of the system comes to a standstill. The applied stress (σ) and measured strain (ε) reach an equilibrium state according to Hooke's law (σ = Eε). Even though internal displacements exist within the system and hence displacement at the system boundaries, they remain constant. The acceleration and velocity of all points within the system are zero. Therefore, the externally applied load is only resisted by the stiffness of the system. The best known and most often used pavement response model is the integral transformation solution for the static analysis of a homogeneous, isotropic, multi-layered linear elastic system subjected to a uniform circular load in the form of a contact pressure (SANRAL, 2014).

Dynamic response analysis, on the other hand, takes into account the effects of load magnitude variation, change in location of load application, and the dynamic response of the system to the continuously changing load characteristics. Hence, the system reacts dynamically and has not come to rest. For this reason, the damping and inertia also need to be included in the analysis in addition to the stiffness of the system. It has been shown that the most realistic representation of pavement loading is a dynamic (time-dependent) phenomenon, which comprises a static and dynamic load component (Figure 2-38) (SANRAL, 2014).

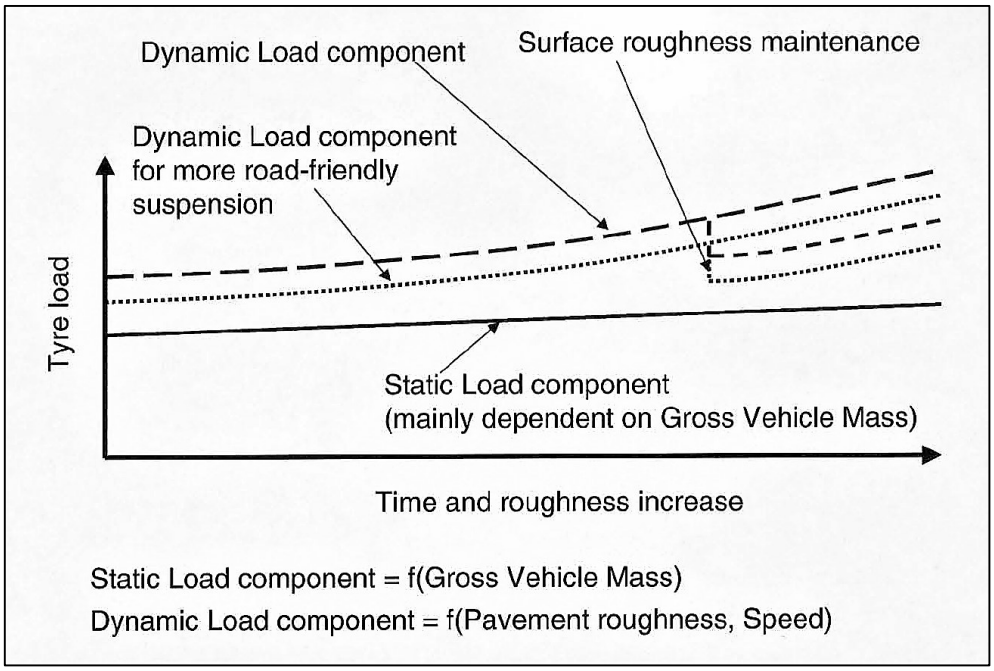

Figure 2-38: Static and dynamic components of tyre load (Steyn, 2001).

While the static load component is mainly dependent on the Gross Vehicle Mass (GVM), the dynamic load component relies on the vehicle's dynamic response, which in turn is mainly dependent on the vehicle's operating conditions (Speed) and the pavement roughness level. The dynamic load component has been shown to be between 5 and 50 per cent of the static load component, depending on these factors. The average tyre load is not affected that much by the vehicle speed and pavement roughness as a good correlation exists between average tyre load and GVM per tyre, regardless of the vehicle speed and pavement roughness. The Coefficient of Variance (COV) of the tyre load, on the other hand, presents good relationships with vehicle speed and pavement roughness (Steyn, 2001).

Investigations have shown that vehicle speed and pavement roughness are the two main influencing parameters when considering the COV of the tyre load. An increase in vehicle speed and/or pavement roughness will result in a wider distribution of the tyre loads around the same mean tyre load on the vehicle population (increased COV). Therefore, a larger fraction of peak (and minimum) loads are applied to the pavement. The damage relationship for tyre loads to a pavement is usually an exponential relationship; hence, an increase in peak loads will result in greater damage to the pavement. An increase in GVM will shift the whole distribution to the right (increased mean), but it won't have any significant effect on the COV (Steyn, 2001). This effect is illustrated graphically in Figure 2-39.

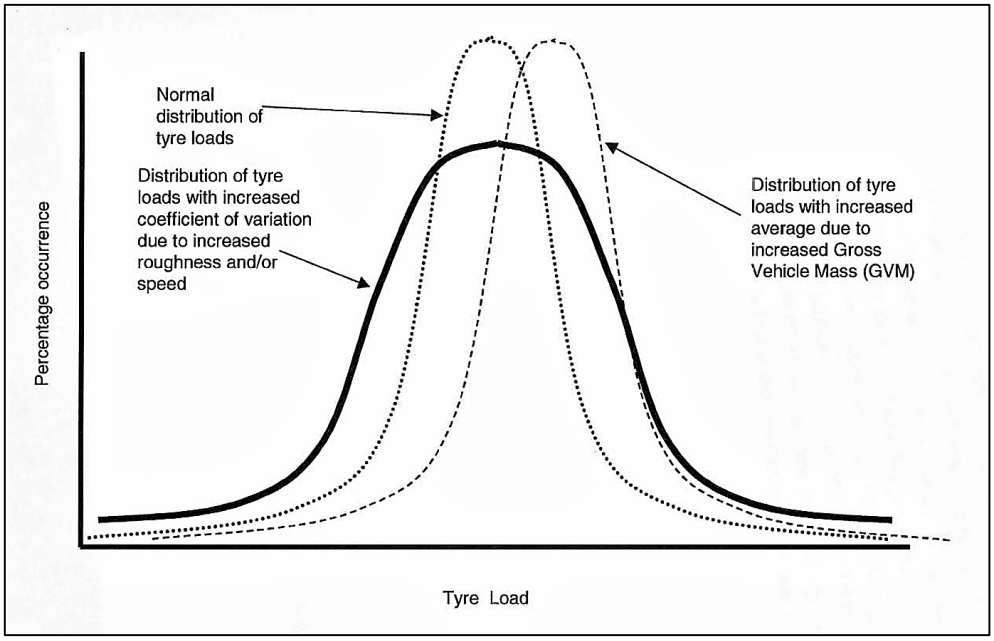

Figure 2-39: Change in mean and COV of tyre load population (Steyn, 2001).

2.8. Multi-Layer Elastic Theory

Pavement design is generally based on simplified empirical and/or mechanistic-empirical design methods. This is due to the behaviour of materials used in asphalt pavement layers as well as the mechanistic complexity of the pavement structure. The current approach used for flexible pavement design is based on the static analysis of a multi-layered elastic system for obtaining the structural response. This approach simulates the applied tyre load as a uniformly distributed vertical load on a circular contact area, assuming that the contact pressure is equal to the tyre inflation pressure. It is based on the multi-layer elastic theory.

The multi-layer elastic theory is the most often used tool to determine flexible pavement responses to truck loading since the 1940s, primarily due to its simplicity. There are a number of important assumptions that is essential to the theory. They are as follows:

- The pavement system is loaded statically over a uniform circular area;
- Each material (layer) is homogeneous, isotropic, linear elastic, and weightless;
- All layers have a finite thickness;
- The subgrade is semi-infinite with a constant modulus;
- All layers are infinite in the lateral directions;
- Full friction is present between layers;
- No surface shearing forces are present;
- Solutions are characterised by Young's modulus and Poisson's ratio, and
- The compatibility of strains and stresses is satisfied at all layer interfaces (Wang, 2011).

This is referred to as the continuum mechanics response model used in classical mechanistic-empirical design methods. It provides the stress, strain, and displacement results at any location within the pavement system. These stresses, strains, and displacements at critical locations in the pavement structure represent critical parameters, which act as primary, load related inputs to the damage model. This solution is available in a number of software packages such as BISAR, CHEV, and ELSYM for example (SANRAL, 2014).

When considering a multi-layered pavement system, the solution type used will govern the required material models and inputs (Young's modulus and Poisson's ratio). However, Young's modulus is only valid for perfectly linear elastic materials, while the majority of pavement materials behave non-linearly or inelastically. Hence, the resilient modulus, which is a linear secant modulus, is adopted as a replacement for the Young's modulus input in order to approximate the non-linear stress-strain behaviour of pavement materials.

Therefore, for linear elastic pavement analysis, each pavement layer is described by a value of resilient modulus (stress over associated elastic strain) and Poisson's ratio. Table 2-10 provides typical resilient moduli and Poisson's ratios for a few common South African road building materials (SANRAL, 2014).

Table 2-10: Resilient moduli and Poisson's ratios according to the SAMDM (SANRAL, 2014).

Material	Modulus [MPa]	Poisson's Ratio	Description
G4	75 to 350	0.35	Natural gravel (base quality) over a granular layer
G1	250 to 1000	0.35 to 0.5	High-quality crushed stone over a cemented layer
FTB	450 to 600	0.3	Medium to high strength bitumen stabilised material
ETB	450 to 600	0.3	Medium to high strength bitumen stabilised material
CTB	2000/300	0.3	New C3 cemented layer/EG4 equivalent granular state
BTB	4000	0.4 to 0.44	Coarse continuously graded HMA
EME	5000	0.4 to 0.44	Gap graded HMA

2.8.1. Moduli Back-Calculation

Pavement layer moduli can be back-calculated by means of a multi-layered linear elastic computer program such as BISAR, CHEV, and ELSYM. In the back-calculation procedure, the in-situ layer moduli of an entire pavement structure can be determined from a complete set of MDD depth deflection measurements for instance. The amount of dynamic deflection as a result of a particular wheel load has been used by engineers for numerous years as an indicator of the inherent stiffness of a pavement structure.

The procedure is based on completing numerous runs of the layered elastic program in an iterative manner in order to get the measured (from MDDs) and calculated (from computer program) depth deflections to match. The moduli of the layers are repeatedly changed until a depth deflection curve similar to that measured with the MDDs is obtained. Normally, an acceptable fit is achieved when the deviation from each MDD deflection measurement is less than 0.0015 mm (De Beer et al., 1989). Figure 2-40 illustrates a typical example of such an iterative procedure.

This fitting procedure is usually done by working from the bottom layers upwards to the top. However, it has been shown that it is more convenient to start at the top and work with the relative deflection (difference in deflection) between adjacent MDD modules. The calculated set of layer moduli is referred to as the "effective elastic moduli" of the different layers in the pavement structure (De Beer et al., 1989).

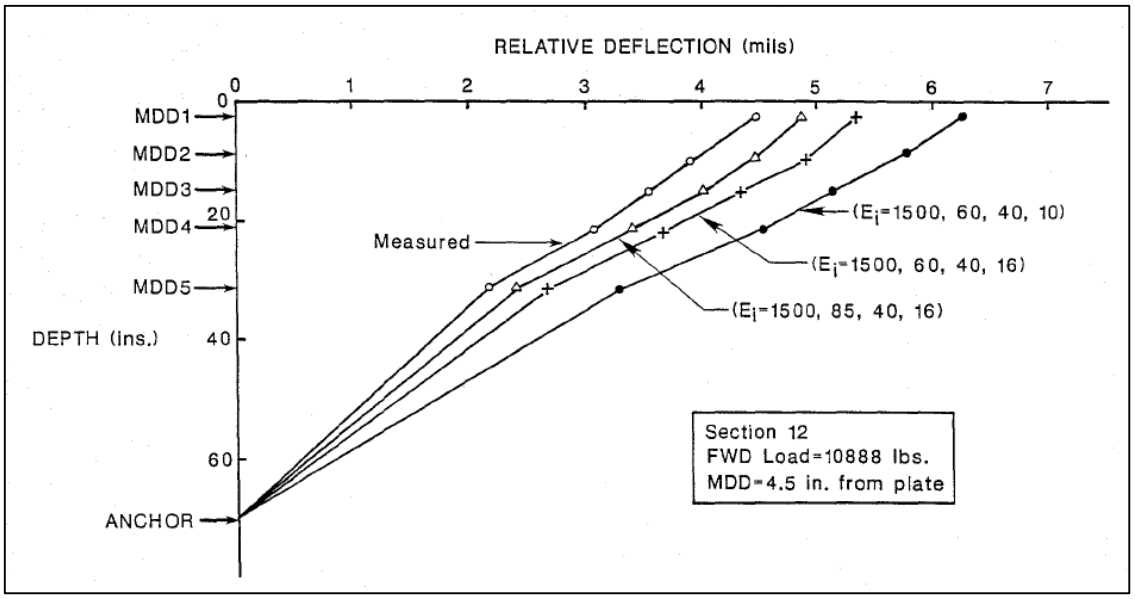

Figure 2-40: Manual iterative procedure for calculating layer moduli (Scullion et al., 1988).

2.8.2. CHEV Computer Program

CHEV, originally developed by the Chevron Oil Company, is a PC version of the FORTRAN program of the Chevron Elastic Layer Analysis Program. The program makes use of elastic analysis to determine stresses, strains, and deflections just about anywhere within a pavement structure due to a single wheel load under static conditions (Muniandy et al., 2013).

The Young's modulus, Poisson's ratio, and thickness are specified for each layer. Furthermore, the load magnitude, contact pressure, and location need to be specified for the load considered. Typical axle and wheel load configurations for design are provided in Table 2-11. The load radius is determined by the program. With these input parameters, the multi-layered elastic system computer program then calculates the various stresses, strains, and deflections in an ideal elastic layered system with a uniform circular load at the surface (Muniandy et al., 2013). Figures 2-41 and 2-42 illustrate the input screen and corresponding output of a typical CHEV analysis respectively.

The bottom layer (subgrade) of the system is considered semi-infinite, while all the other layers have a finite thickness. All of the layers are infinite in the horizontal direction. Each layer is identified by its Young's modulus (E), Poisson's ratio (υ), and thickness. The system surface is free of any shear and the layer interfaces have full continuity of stresses and strains (Muniandy et al., 2013). BISAR and ELSYM, on the other hand, present layer interfaces that vary from full continuity to frictionless; however, if conditions are chosen correctly, similar results to CHEV can be obtained.

Table 2-11: Typical axle and wheel load configurations for design (Theyse et al., 2011).

Axle Group Configuration	Wheel Configuration	Typical Half-Axle Configuration for Analysis	Static Axle Group Load [kN]	Recommended Tyre Contact Stress [kPa]
Standard Design Load	Dual	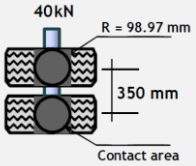	80	650
Steering Axle	Single	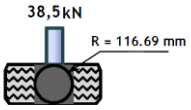	77	900
Single Axle	Single	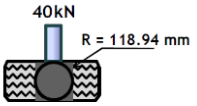	80	900
	Dual	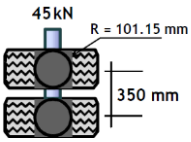	90	700
Tandem Axle	Single	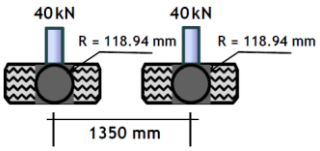	160	900
	Dual	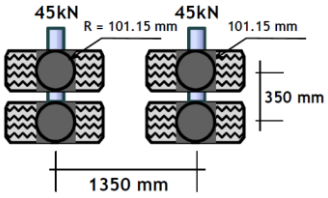	180	700
Tridem Axle	Single	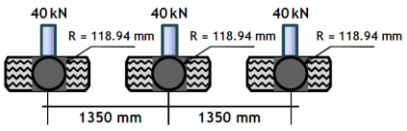	240	900
	Dual	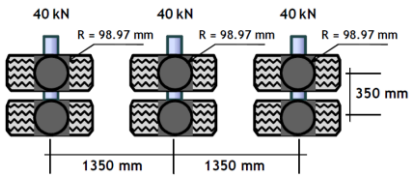	240	650

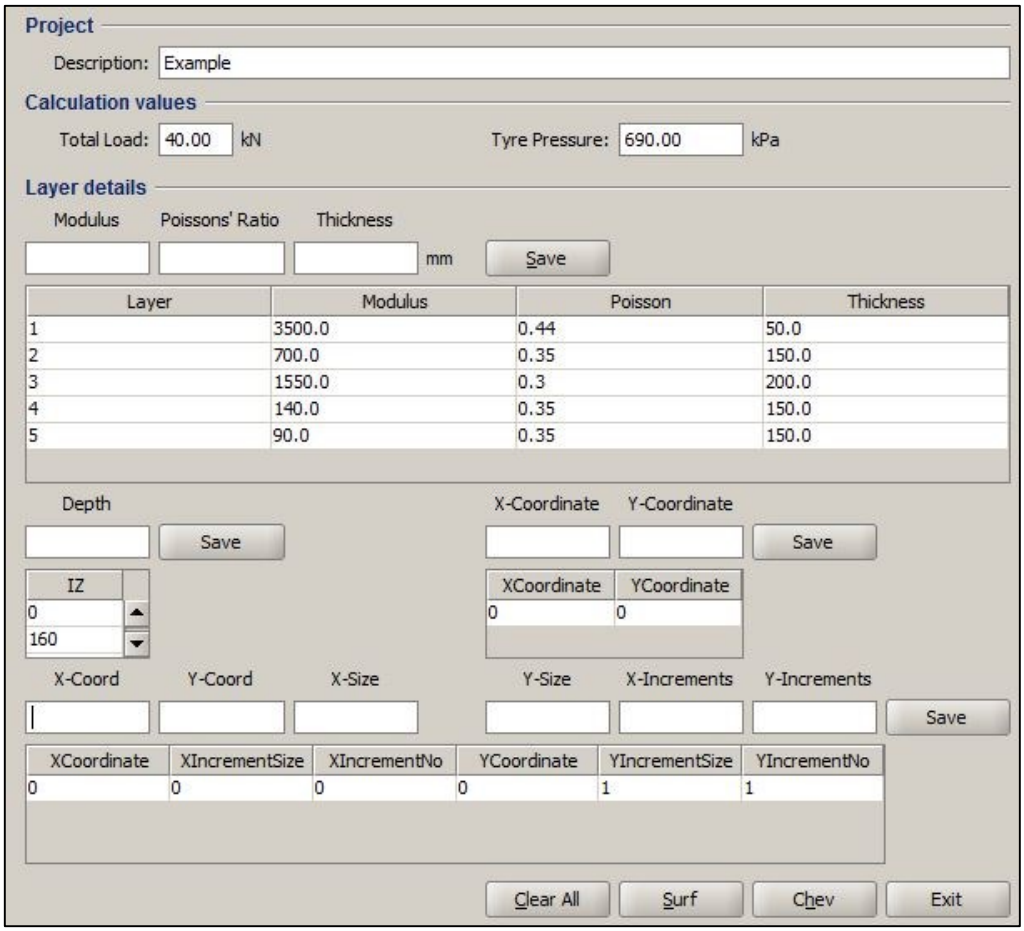

Figure 2-41: CHEV input screen.

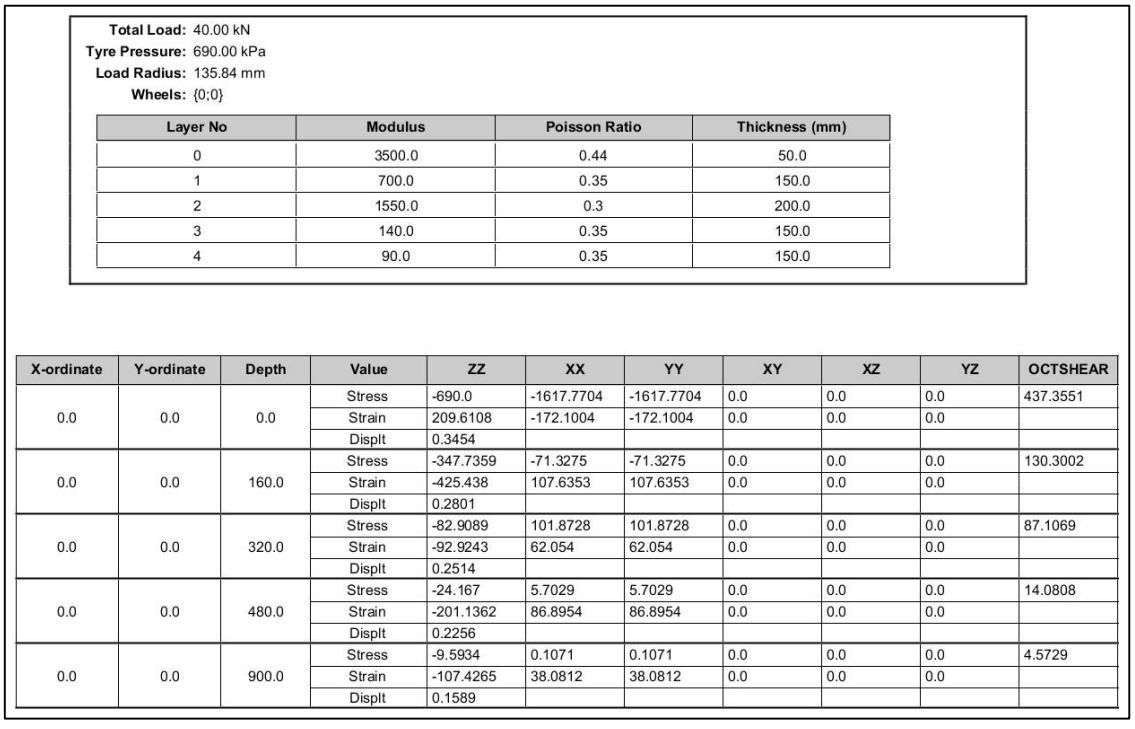

Total Load: 40.00 kN
Tyre Pressure: 690.00 kPa
Load Radius: 135.84 mm
Wheels: {0;0}

Layer No	Modulus	Poisson Ratio	Thickness (mm)
0	3500.0	0.44	50.0
1	700.0	0.35	150.0
2	1550.0	0.3	200.0
3	140.0	0.35	150.0
4	90.0	0.35	150.0

X-ordinate	Y-ordinate	Depth	Value	ZZ	XX	YY	XY	XZ	YZ	OCTSHEAR
0.0	0.0	0.0	Stress	-690.0	-1617.7704	-1617.7704	0.0	0.0	0.0	437.3551
			Strain	209.6108	-172.1004	-172.1004	0.0	0.0	0.0	
			DispIt	0.3454						
0.0	0.0	160.0	Stress	-347.7359	-71.3275	-71.3275	0.0	0.0	0.0	130.3002
			Strain	-425.438	107.6353	107.6353	0.0	0.0	0.0	
			DispIt	0.2801						
0.0	0.0	320.0	Stress	-82.9089	101.8728	101.8728	0.0	0.0	0.0	87.1069
			Strain	-92.9243	62.054	62.054	0.0	0.0	0.0	
			DispIt	0.2514						
0.0	0.0	480.0	Stress	-24.167	5.7029	5.7029	0.0	0.0	0.0	14.0808
			Strain	-201.1362	86.8954	86.8954	0.0	0.0	0.0	
			DispIt	0.2256						
0.0	0.0	900.0	Stress	-9.5934	0.1071	0.1071	0.0	0.0	0.0	4.5729
			Strain	-107.4265	38.0812	38.0812	0.0	0.0	0.0	
			DispIt	0.1589						

Figure 2-42: CHEV output.

2.9. Pavement Number Design Method

The Pavement Number (PN) design method was originally developed for the design of bituminous stabilised layers in pavements, but it is also applicable to granular and cemented materials. It is based on the Structural Number (SN) concept used in the original AASHTO methods. However, a number of shortcomings of the SN method have been overcome in the PN method. The PN design method has the following advantages:

- Data from in-service pavements were used to develop the method and therefore preclude the use of a mechanistic-empirical design method;
- The method provides a good fit to the available field data, and
- The method is robust in the way that it cannot easily be manipulated to produce inappropriate designs.

The PN method can be applied to both new and rehabilitation design; therefore, it is developed to be used in conjunction with the Design Equivalent Material Class (DEMAC) material classification method (see Chapter 2.9.7) (Asphalt Academy, 2009). The step by step PN calculation procedure is detailed in Chapter 3.3.3.

2.9.1. Applicability and Limitations

Before the PN value can be calculated, the suitability of the design method to the pavement situation should be checked. In order for the PN design method to be used, a number of conditions must be satisfied:

- The design traffic should be between 1 and 30 Million Equivalent Standard Axles (MESA). If the design traffic does not fall within this range, the PN method is considered inappropriate as it has not been validated for traffic levels outside of this range.
- The subgrade CBR should not be less than 3 per cent. If the subgrade CBR is less than 3 per cent at a depth less than 600 mm below the surface, the PN method is not recommended. This is because calibration of the method did not include any pavements that had a subgrade CBR less than 3 per cent.
- Thin, weak lenses should not be present. The presence of thin, weak lenses below the surfacing layer or between stabilised layers, especially within the upper 400 mm of the pavement, will develop zones of high slip and shear. In such circumstances, the structural capacity assessment of the PN method is not applicable (Asphalt Academy, 2009).

2.9.2. Rules of Thumb

The PN method relies on a number of basic points of departure, which reflect well-established principles of pavement behaviour and performance. These rules of thumb will make sure that a suitable pavement design solution is obtained in most situations. There are 10 rules, the first 3 relating to the pavement system in general and the last 7 relating to specific pavement layers:

1) The structural capacity of a pavement system is a function of the long-term load spreading potential of all the pavement layers as well as the relative quality of the subgrade.

2) The relative quality and stiffness of the subgrade is the starting point of design as the subgrade plays a very important role in the overall behaviour and performance of the pavement.

3) For pavements with a thin surfacing, the base layer is the most critical component of the pavement structure and failure of this layer will effectively indicate pavement failure.

4) The load spreading potential of each individual layer is a product of its thickness and its Effective Long-Term Stiffness (ELTS).

5) The ELTS of a layer depends on the material type and the layer's placement within the pavement structure.

6) Fine-grained subgrade materials are stress-softening and normally soften with decreased cover thickness. The ELTS of these materials depends mainly on the material quality and the climatic region.

7) Coarse-grained unbound layers are stress-stiffening. The ELTS of these materials mainly depends on the material quality and the relative stiffness of the supporting layer. The ELTS increases with increasing support stiffness, via the modular ratio limit, up to a maximum stiffness determined primarily by the material quality.

8) Cement stabilised materials behave like a stiff, glassy material at first, but with time, they gradually start to deteriorate into loose clumps or separate blocks, which can be solid or deteriorate further until a granular state is reached. The rate of deterioration depends primarily on the layer thickness and the stiffness of the supporting layer.

9) Asphalt surfacing layers behave either like a stiff, glassy material or a semi-stiff, rubbery material. The material state depends mainly on the temperature and binder content. With time, the asphalt is subject to deterioration by means of aging and fatigue. Fatigue breakdown depends mainly on the stiffness of the supporting layer.

10) BSMs are assumed to behave in a similar manner to coarse granular materials but with a higher cohesive strength. Due to the higher cohesive strength, they are less sensitive to the support stiffness than granular materials and can therefore tolerate greater modular ratio limits. A BSM is assumed to behave like a cemented material if the cement content exceeds 1 per cent (Asphalt Academy, 2009).

2.9.3. Effective Long-Term Stiffness (ELTS)

The ELTS is a model parameter calibrated for use in the PN design method and acts as a relative indicator for the average long-term in-situ stiffness of a pavement layer. It averages out the effects of decreasing stiffness due to traffic related deterioration as well as seasonal changes. The ELTS does not represent the stiffness of a material at a specific point in time and cannot be obtained through laboratory or field tests. Therefore, it may differ from the stiffness values typically associated with material classes (Asphalt Academy, 2009). Figure 2-43 illustrates the ELTS concept for cemented materials. The concept is applicable to all pavement materials included in the PN design method.

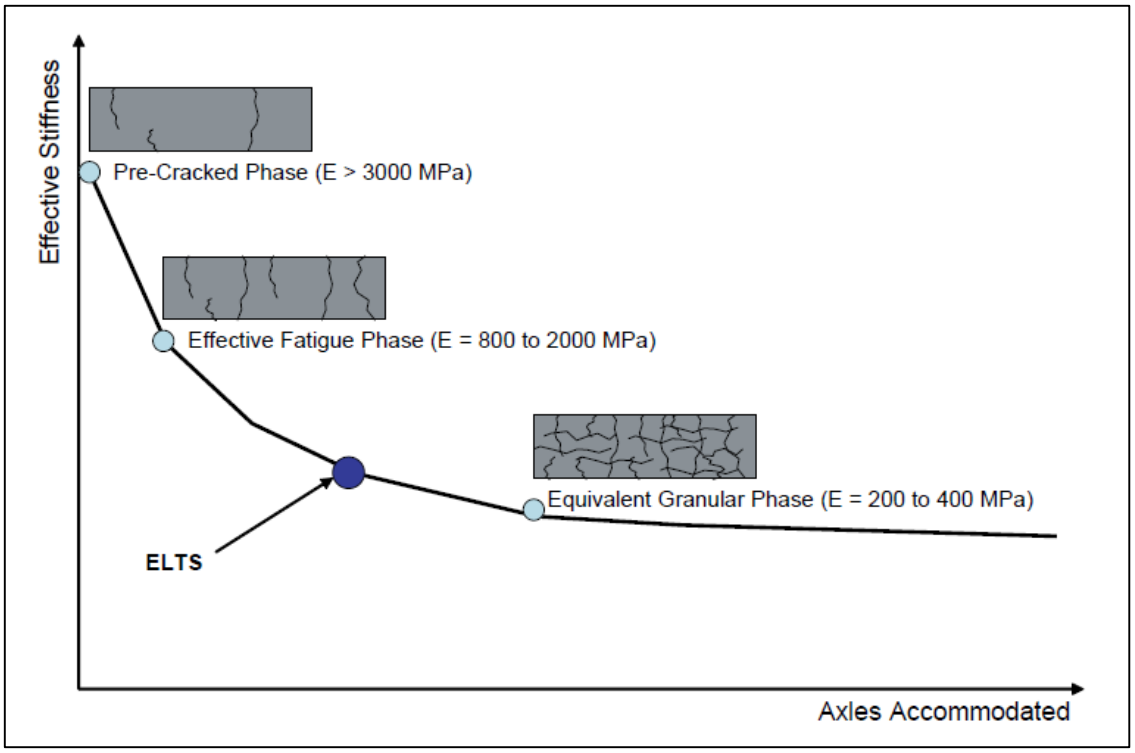

Figure 2-43: ELTS example for a lightly cemented material (Asphalt Academy, 2009).

2.9.4. Modular Ratio Limit

The modular ratio of a pavement layer is described as the ratio of the layer's stiffness relative to the stiffness of the underlying layer. It accounts for the stress-sensitive stiffness of granular materials and to a lesser extent, BSMs. Due to the stress-sensitivity, the stiffness of the material decreases when it is placed over a weaker support layer. The decrease in stiffness takes place where the support layer is soft, which causes the overlying layers to bend into the support layer. This increases the likelihood of higher shear and tensile forces in the overlying layers and therefore limits the stiffness that can be obtained (Asphalt Academy, 2009).

By placing a limit on the modular ratio a specific material can sustain, it ensures that the assumed stiffness value for that layer is realistic, given the material quality and stiffness of the support layer. This limiting concept ensures that the stress-sensitive stiffness behaviour of materials is accounted for. The modular ratio of a material changes over the lifetime of a pavement. In the PN method, this modular ratio is related to the overall long-term stiffness that a material can maintain (Asphalt Academy, 2009).

2.9.5. Maximum Allowable Stiffness

During the activity of loading, there exists a maximum stiffness that each type of material can achieve. As with the modular ratio, the maximum stiffness of a material is highly dependent on the quality of the material. A less dense and angular material will not develop very high stiffness values under loading, regardless of the stiffness of the support layer. The PN method uses the maximum allowed stiffness and modular ratio limit to determine the necessary ELTS values (Asphalt Academy, 2009).

2.9.6. Base Confidence Factor

The type of material used in the base layer of a pavement has a great effect on the overall performance of the pavement. The base layer serves as the main load bearing element in the pavement system and failure thereof will effectively result in pavement failure. Experience has shown there is a limit on the type of base materials that can be used for any given traffic situation. The number of base materials suitable for design becomes more and more limited as the design traffic increases. In the PN method, the suitability of the chosen base material is controlled by the Base Confidence Factor (BCF). The BCF is used to adjust the base layer's contribution to the PN value (Asphalt Academy, 2009).

2.9.7. Design Equivalent Material Class

The DEMAC material classification method provides a method for consistent assessment of pavement materials by means of routine tests and indicators. The material classes adopted for this method run parallel with the TG2 and TRH14 material classification systems. Both these classification systems are suitable for new and rehabilitation design as the performance and behaviour patterns of each material class are known with some certainty (Asphalt Academy, 2009).

With the DEMAC material classification method, the determined material class is considered a Design Equivalent Material Class. When a DEMAC is assigned to a material, it suggests that the material presents in-situ shear, stiffness, and flexibility properties very much like those of a newly constructed material of the same class. The material to which a DEMAC has been assigned will at least conform to or exceed the specifications for the class, as stated in TRH14, in nearly all instances (Asphalt Academy, 2009).

This material classification method is applicable to granular materials, BSMs, and cemented materials. For each material type, a wide variety of tests and indicators are used to determine a DEMAC. The more test results and indicators available for assessment, the greater the final certainty and confidence in the assigned material class will be (Asphalt Academy, 2009).

2.10. Summary

In summary, it can be said that permanent deformation (rutting) in flexible pavements is the result of densification and/or shear deformation of all individual layers within a pavement structure when subjected to traffic load. A longitudinal surface depression, which is visible within the wheel tracks of the pavement, is the result. Numerous influencing factors such as density, moisture content, and temperature play an important role in this deformation behaviour and therefore should be accounted for at all times.

Due to the usual abundance of granular materials in pavements, the typical permanent deformation behaviour of flexible pavements before failure can be described by two phases, namely an initiation (primary) phase and a propagation (secondary) phase. During the initiation phase, also known as the bedding-in phase, a fast increase in permanent deformation occurs under the first wheel passes due to post-compaction (densification). During the propagation phase, also known as the plateau phase, a slower and more linear permanent deformation rate is experienced primarily due to shear deformation. It is assumed that the initiation phase mainly occurs in the wearing course and the propagation phase in the base course (Perret et al., 2004).

Table 2-12 summarises the permanent deformation results from a number of selected APT studies that was conducted in the past. It includes a variety of base course materials that are relevant to this study. Permanent deformation is presented as an average rut rate based on the total pavement response after the initial bedding-in phase, during the plateau phase. In order to compensate for any wheel load differences between the studies, a normalised rut rate per kilonewton wheel load is also included.

Table 2-12: Summary of previous permanent deformation studies.

Ref.	Thickness [mm]	Wheel Load [kN]	Rut Rate [nm/cycle]	Rut Rate/kN [nm/cycle/kN]	Comments
1.1	305	40	1.33	0.033	-
1.2	150	40	0.35	0.009	-
2.1	216	43.4	6.15	0.142	-
3.1	100	40	0.30	0.008	-
4.1	200	40 to 60	1.43	0.029	2.8% Bitumen; 1.0% Cement
4.2	200	40 to 60	1.43	0.029	1.4% Bitumen; 1.0% Cement
4.3	200	40 to 60	1.43	0.029	1.2% Bitumen; 1.0% Cement
4.4	200	40 to 60	2.57	0.051	2.2% Bitumen; 0.0% Cement
5.1	305	75.7	2.54	0.034	Foam Treated FAS-FDR Base
3.2	150	40	0.60	0.015	-
6.1	100	60	1.00	0.017	1.0% Bitumen; 1.0% Cement
1.3	300	40	0.59	0.015	-
7.1	215	43 to 85	12.50	0.195	Plant Mixed Soil-Cement 10%
8.1	300	40	0.50	0.013	-
9.1	160	40	0.23	0.006	4.1% Bitumen
10.1	120	50	20.00	0.400	5.5% CAPPLUS 106B
11.1	110	57.5	10.77	0.187	4.25% BP Structure 15/25

References		Base Type Colour Allocation	
1	Theyse (1997) – South Africa		Natural Gravel
2	Wu et al. (2009) – United States		Crushed Stone
3	Theyse (1999) – South Africa		Bitumen Foam Treated
4	Gonzalez et al. (2009) – New Zealand		Bitumen Emulsion Treated
5	Romanoschi et al. (2004) – United States		Cemented Material
6	Horak and Rust (1992) – South Africa		Large Aggregate Mixes
7	Metcalf et al. (1999) – United States		High Modulus Asphalt
8	Steyn et al. (1997) – South Africa		
9	Van der Merwe et al. (1992) – South Africa		
10	Rohde et al. (2008) – Brazil		
11	Perret et al. (2004) – Switzerland		

Figure 2-44 presents a performance rank of the different APT test sections in terms of their resistance to permanent deformation (normalised rut rates). It is important to note that each study had unique loading characteristics and was conducted at different temperatures, moisture conditions, etc. However, some of the studies show a radical difference in testing conditions compared to the others, and the effect of this clearly reflects in the rut rates from Table 2-12. References 2.1, 7.1, and 10.1 considered lateral wandering, reference 10.1 experienced high temperatures and intense rainfalls during testing, and reference 11.1 was submitted to very harsh loading (57.5 kN single wheel load at 800 kPa tyre inflation pressure) and climatic (50°C at 3 cm) conditions. These four studies are, therefore, excluded from the comparison. Figure 2-45 illustrates an expected performance rank of different types of flexible pavement base materials (based on typical maximum in-situ stiffness) under similar testing conditions.

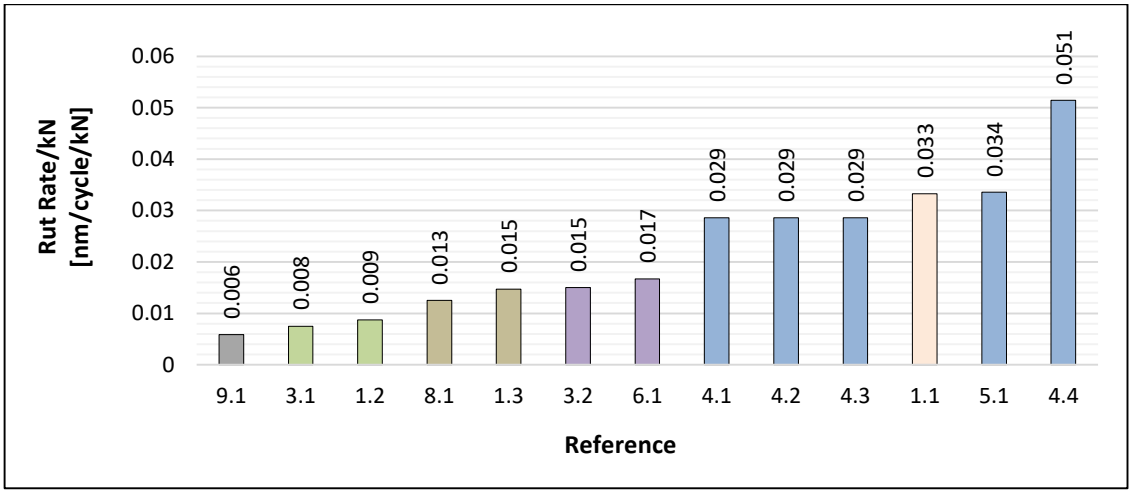

Figure 2-44: Permanent deformation performance rank for 13 APT test sections.

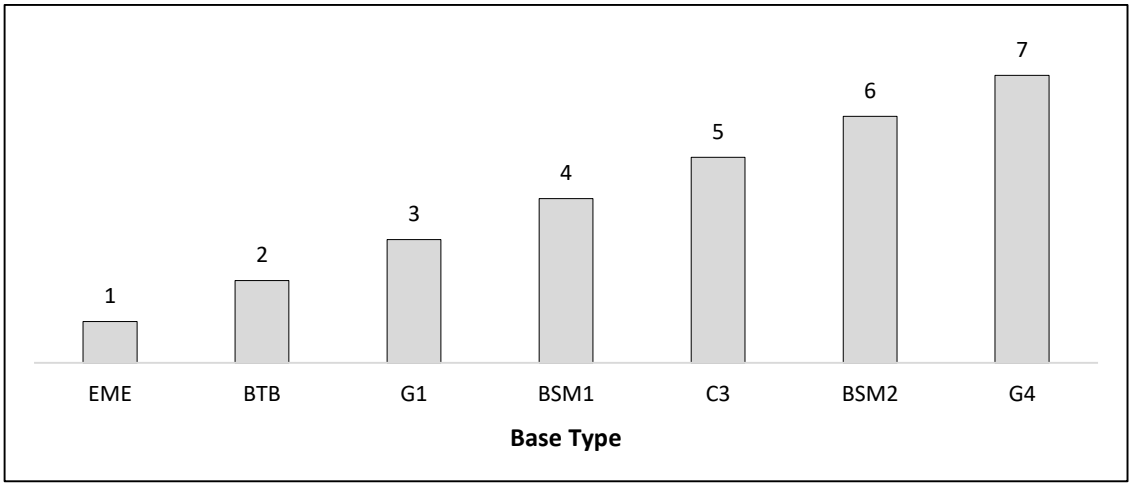

Figure 2-45: Expected permanent deformation performance rank for different base materials.

3. METHODOLOGY

3.1. Introduction

UP collected the raw pavement response and environmental related data from the SANRAL experimental site on the R104; however, this data still needed to go through numerous analysis procedures in order to obtain the required data for this study. This chapter focuses on:

- Detailing the SANRAL experimental site setup in terms of the different test sections, their structural composition, and the instrumentation utilised within each, and
- Defining the different methods used to obtain (collect) the required data for this study.

3.2. SANRAL Experimental Site Setup

The South African National Roads Agency Ltd (SANRAL) completed the construction of seven flexible and three rigid pavement sections on the R104, which is located between Pretoria and Bronkhorstspruit (Figure 3-2), during 2013. The 10 sections were all constructed in sequence over a continuous length of 1.21 km using various construction techniques. The purpose of this initiative was to provide a testing environment in which functionality data of a variety of flexible and rigid pavements can be collected and studied.

The seven flexible sections under investigation are represented in Sections 1 through 7, each having a unique structural composition. A transverse and longitudinal cross-section view of the continuous testing facility are presented in Figures 3-1 and 3-2 respectively. It should be noted that Section 7 is split into two equal 100-m-long sections, 7a and 7b, to make up a combined length of 200 m. The pavement structures differ from each other primarily in layer thickness and base layer constituent; otherwise, they are very similar.

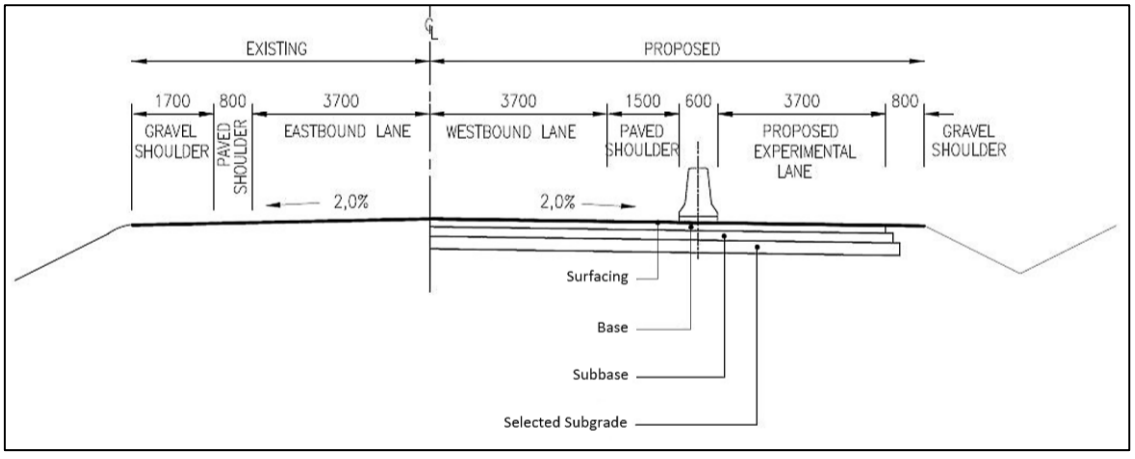

Figure 3-1: Transverse cross-section of testing facility.

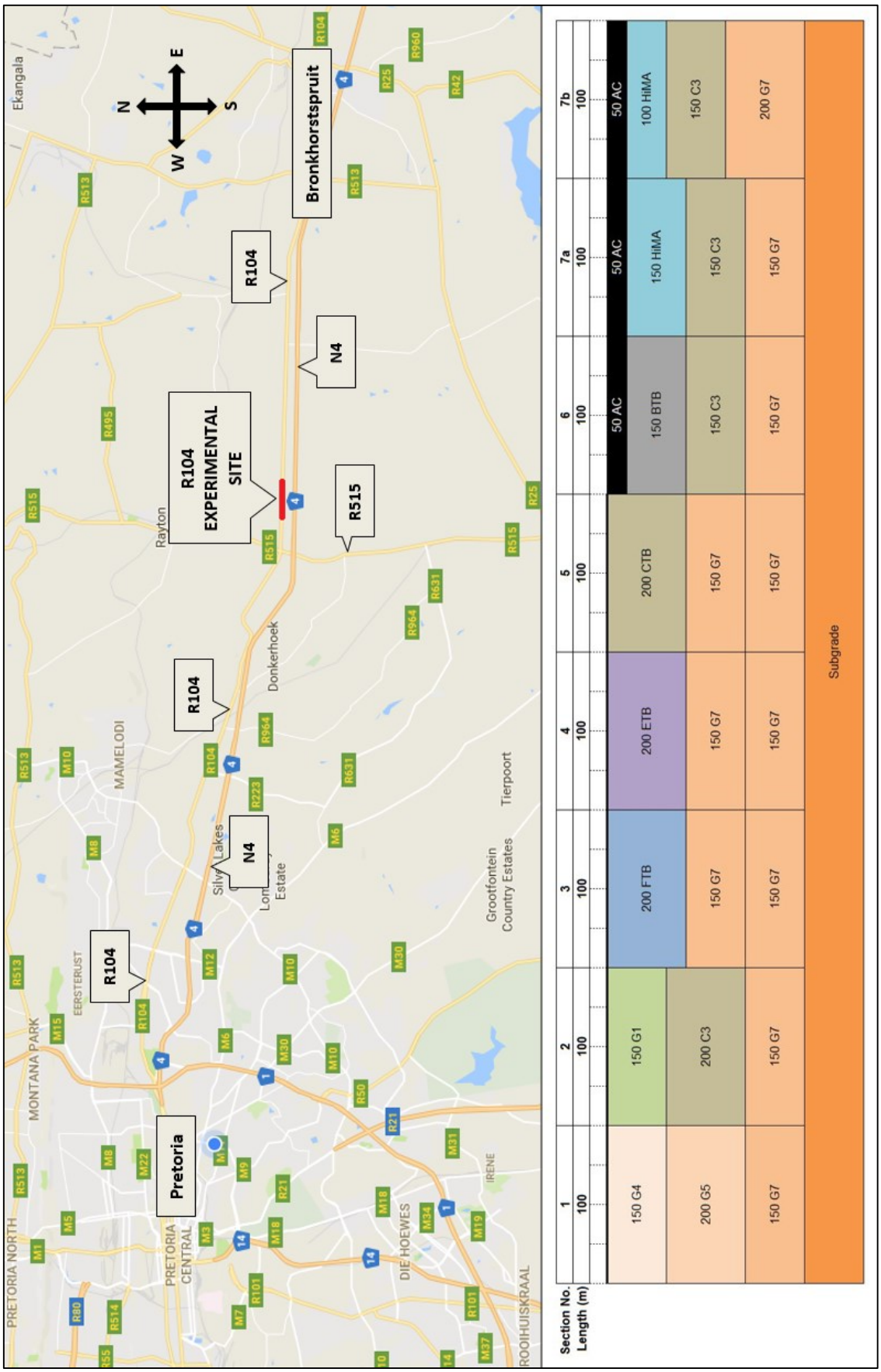

Figure 3-2: Location and longitudinal cross-section of SANRAL testing facility.

3.2.1. Material Properties

All of the materials used in the seven flexible pavement sections (Figure 3-2) are detailed in Table 3-1. They are divided into five categories: surfacing, base, subbase, selected subgrade, and subgrade materials. A layer ID has been assigned to each material in order to aid with the test section summary in Chapter 3.2.3.

Table 3-1: Material properties of flexible pavement sections.

Layer ID	Description	Thickness [mm]	Material Code	Section	Comments
Surfacing Materials					
1a	Double Seal Surfacing	19/9	S2	1 to 5	19+9 mm chips; S-E1 modified bitumen
1b	Asphalt Surfacing	50	AC	6; 7	Continuously coarse graded with 13 mm rolled-in chips; 60/70 penetration grade binder modified with 4.0% Saso-Flex wax (A-E2); 5.5% binder; 1.0% active mineral filler
Base Materials					
2a	Natural Gravel Base	150	G4	1	-
2b	Crushed Stone Base	150	G1	2	-
2c	Foam Treated Base	200	FTB	3	BSM1 equivalent quality material; G5 parent material; 80/100 penetration grade binder (2.5%); 1.0% active filler
2d	Emulsion Treated Base	200	ETB	4	BSM1 equivalent quality material; G5 parent material
2e	Cement Treated Base	200	CTB	5	C3 equivalent quality material; G5 parent material
2f	Bitumen Treated Base	150	BTB	6	Continuously graded asphalt; 40/50 penetration grade binder
2g	High Modulus Asphalt Base	150; 100	EME[1]	7	20/30 Penetration grade binder (5.0%); 1.0% active filler
Subbase Materials					
3a	Cemented Granular Material	200; 150	C3	2; 6; 7	G5 parent material
3b	Granular Material	200	G5	1	-
3c	Granular Material	150	G7	3; 4; 5	-
Selected Subgrade Materials					
4a	Granular Material	150; 200	G7	1 to 7	-
Fill/Subgrade Materials					
5a	Granular Material	Varies	G7	1 to 7	Includes additional material
5b	Roadbed	Varies	> G9	1 to 7	-

Notes: 1) Although the R104 documents refer to high modulus asphalt as HiMA, the new terminology, EME, is adopted for this study.

3.2.2. Instrumentation

During construction, each of the test sections was equipped with a variety of in-situ pavement instrumentation in order to monitor pavement response and performance (Figures 3-3 and 3-4). A detailed list of the sensors used on the R104 experimental site is provided in Table 3-2. A sensor ID has been assigned to each type of sensor to aid with the test section summary in Chapter 3.2.3.

Apart from the in-situ sensors collecting data, strata gauge readings are taken at regular time intervals to monitor moisture and density variation. A basic wireless weather station located 2 km west of the R104 experimental site, next to the Rayton Traffic Control Centre (RTCC), continuously collects weather related data (light, UV index, temperature, etc.) as well. The SANRAL TSD, which forms part of the experimental setup, is detailed in Chapter 2.7.

Table 3-2: Types of sensors monitored on the R104 experimental site.

Sensor Description	**Sensor ID**
Multi-Depth Deflectometer	MDD
Emu Strain Coils	Emu
Time Domain Reflectometery Sensors (Moisture and Temperature)	TDR
Thermocouples (Temperature)	TC
Pressure Cells	PC
Pressure Films	S
Big Mat Stress Sensors	BM
Strain Gauges	SG
Accelerometers	AM

Figure 3-3: Emu strain coils, pressure cells, big mat stress sensors, and strain gauges.

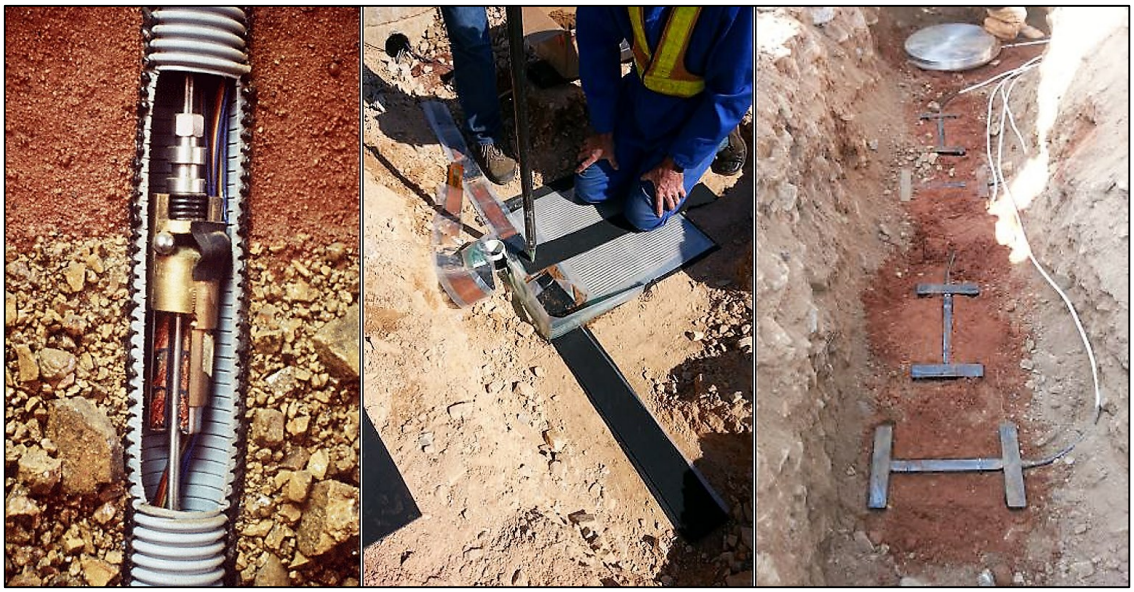

Figure 3-4: MDDs, pressure films, pressure cells, and strain gauges.

3.2.3. Test Section Summary

Table 3-3 provides a basic summary regarding the structural properties of each test section. The location and type of sensors within each section is presented schematically in Figures 3-5 through 3-12. Keeping track of the location of the sensors is essential in validating the pavement response and interpreting the results. Please refer back to Chapters 3.2.1 and 3.2.2 for the layer IDs and sensor IDs respectively.

Table 3-3: Structural properties of flexible sections.

	Section 1	**Section 2**	**Section 3**	**Section 4**	**Section 5**	**Section 6**	**Section 7a**	**Section 7b**
Chainage [km]	39.610 to 39.710	39.510 to 39.610	39.410 to 39.510	39.310 to 39.410	39.210 to 39.310	39.110 to 39.210	39.010 to 39.110	38.910 to 39.010
Length [m]	100	100	100	100	100	100	100	100
Surfacing [mm]	S2 (1a)	S2 (1a)	S2 (1a)	S2 (1a)	S2 (1a)	50 AC (1b)	50 AC (1b)	50 AC (1b)
Base [mm]	150 G4 (2a)	150 G1 (2b)	200 FTB (2c)	200 ETB (2d)	200 CTB (2e)	150 BTB (2f)	150 EME (2g)	100 EME (2g)
Subbase [mm]	200 G5 (3b)	200 C3 (3a)	150 G7 (3c)	150 G7 (3c)	150 G7 (3c)	150 C3 (3a)	150 C3 (3a)	150 C3 (3a)
Selected Subgrade [mm]	150 G7 (4a)	150 G7 (4a)	150 G7 (4a)	150 G7 (4a)	150 G7 (4a)	150 G7 (4a)	150 G7 (4a)	200 G7 (4a)
Subgrade	G7 (5a)/G9 and greater (5b)							

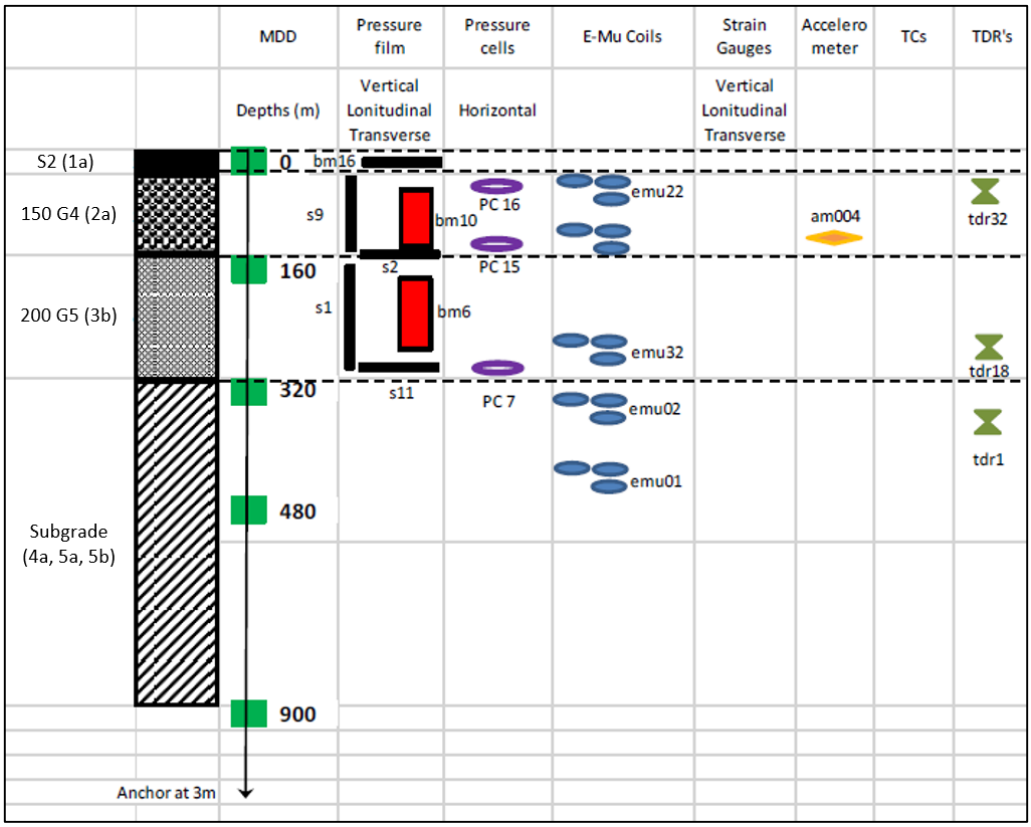

Figure 3-5: Schematic location of sensors in Section 1.

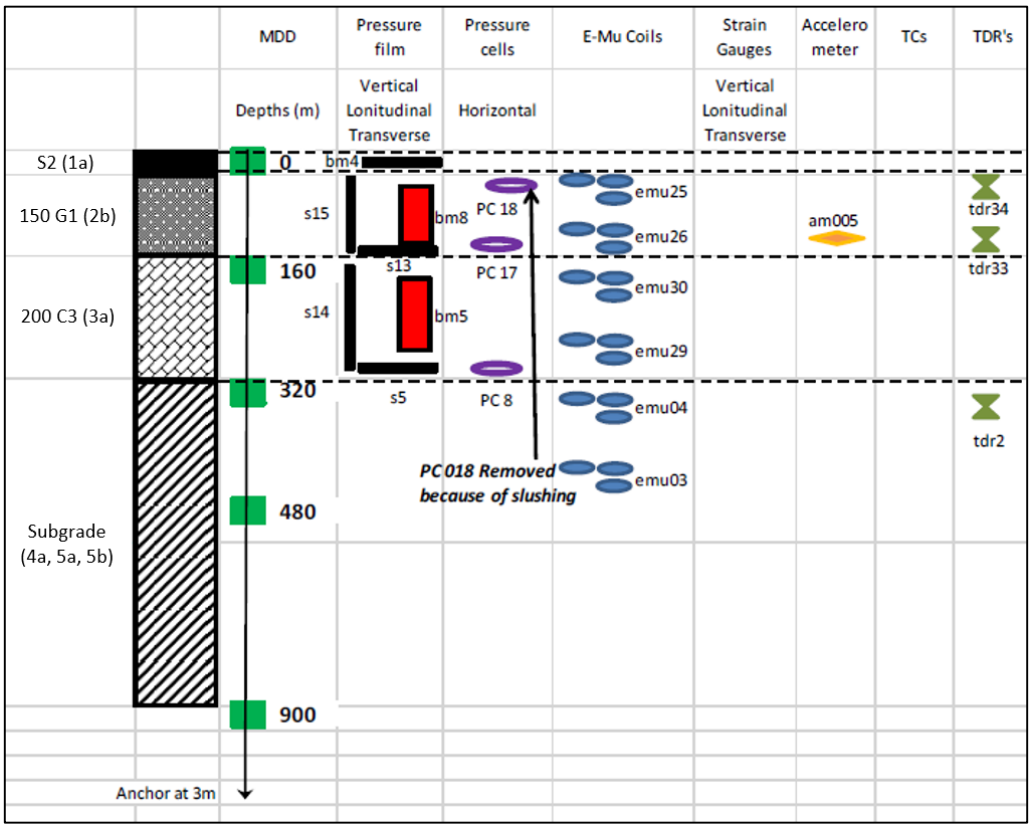

Figure 3-6: Schematic location of sensors in Section 2.

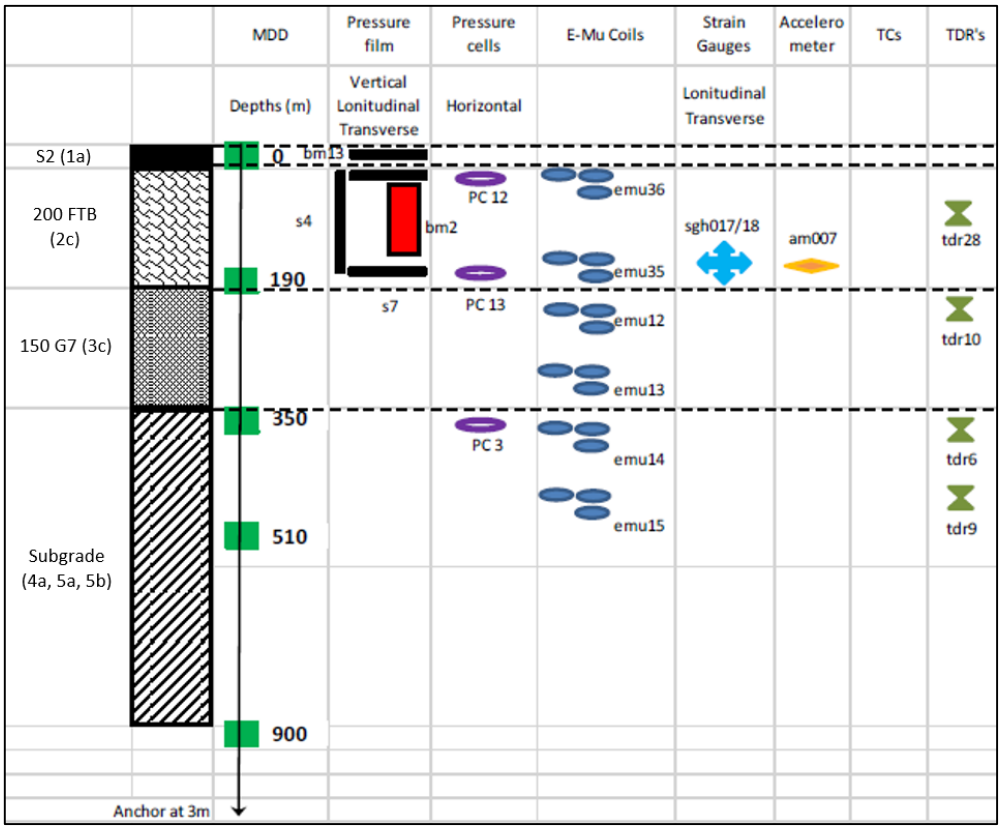

Figure 3-7: Schematic location of sensors in Section 3.

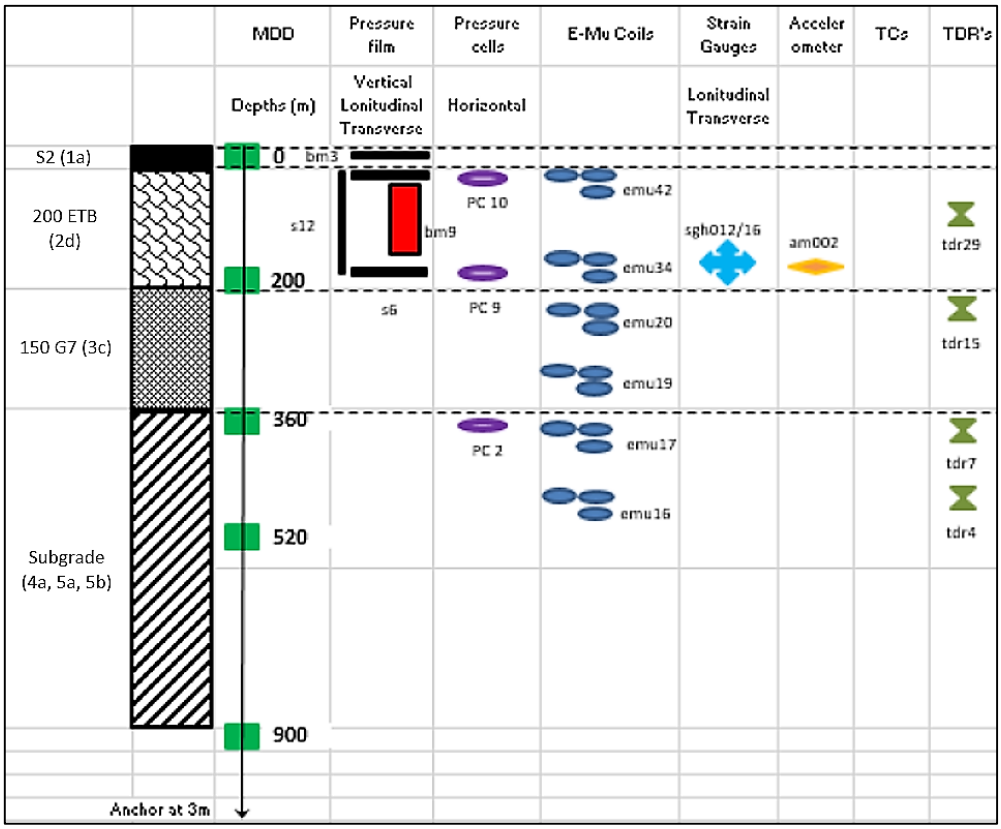

Figure 3-8: Schematic location of sensors in Section 4.

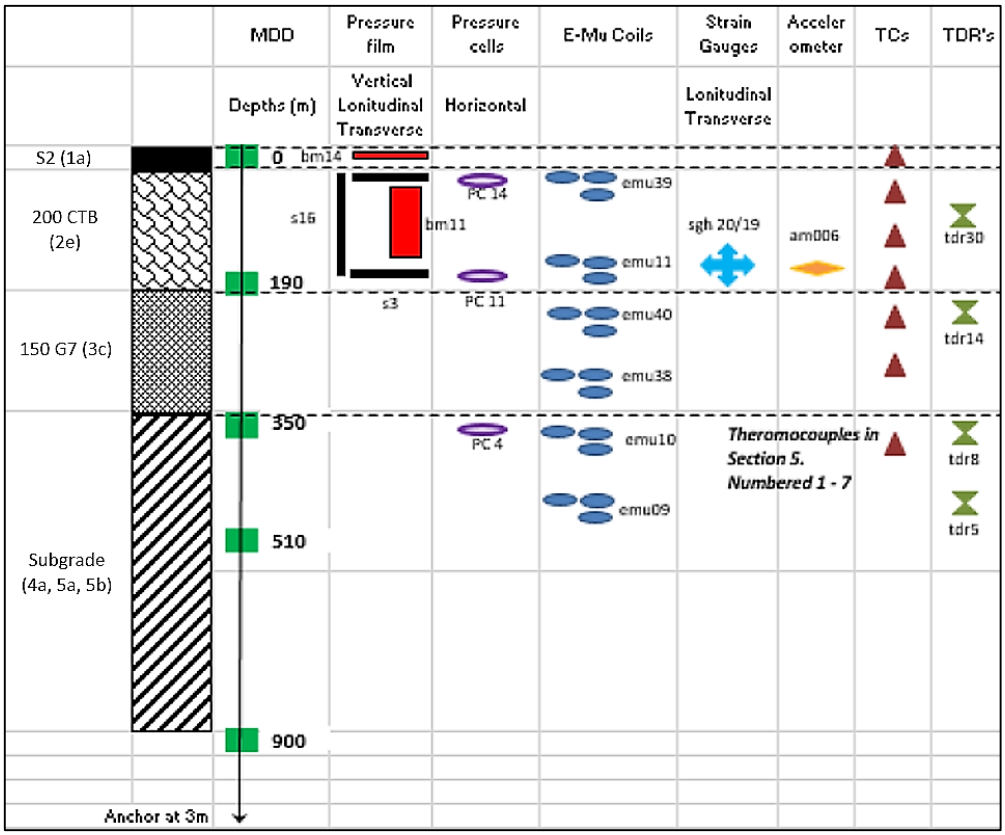

Figure 3-9: Schematic location of sensors in Section 5.

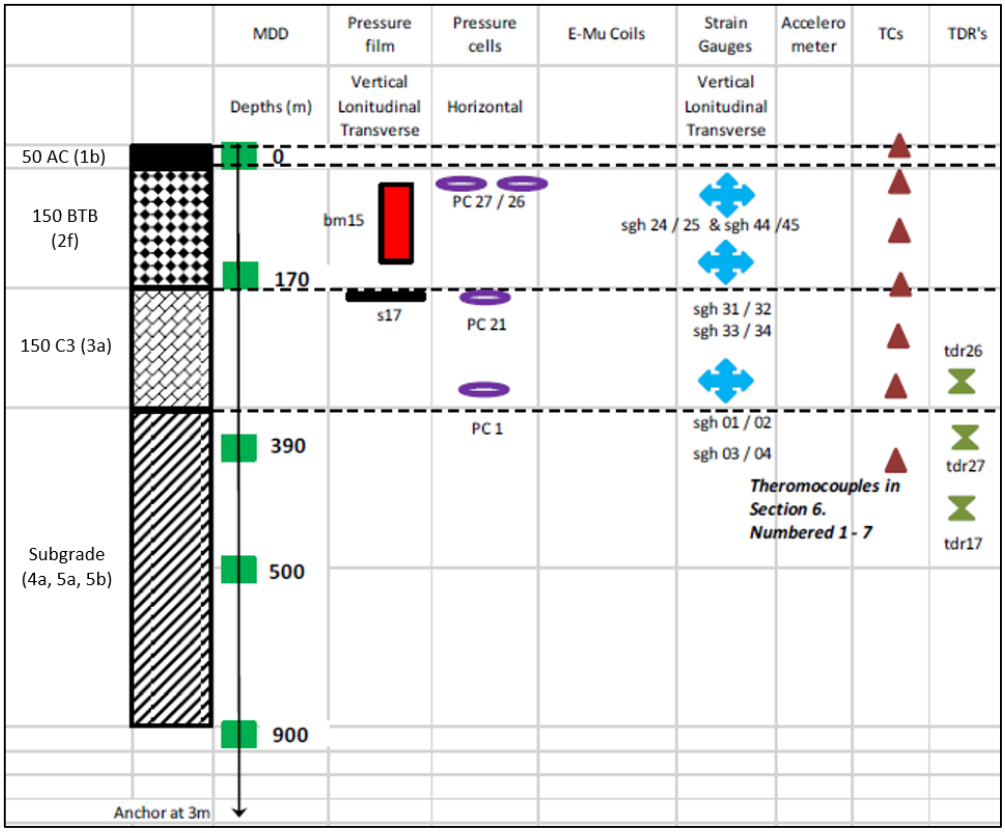

Figure 3-10: Schematic location of sensors in Section 6.

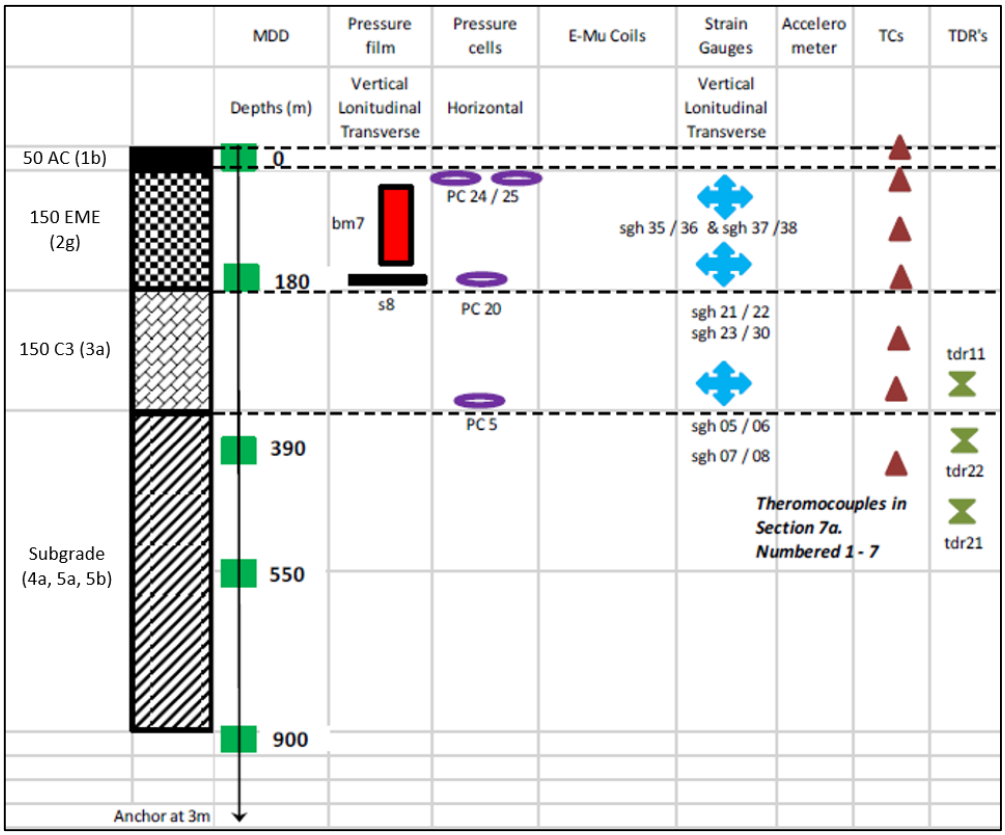

Figure 3-11: Schematic location of sensors in Section 7a.

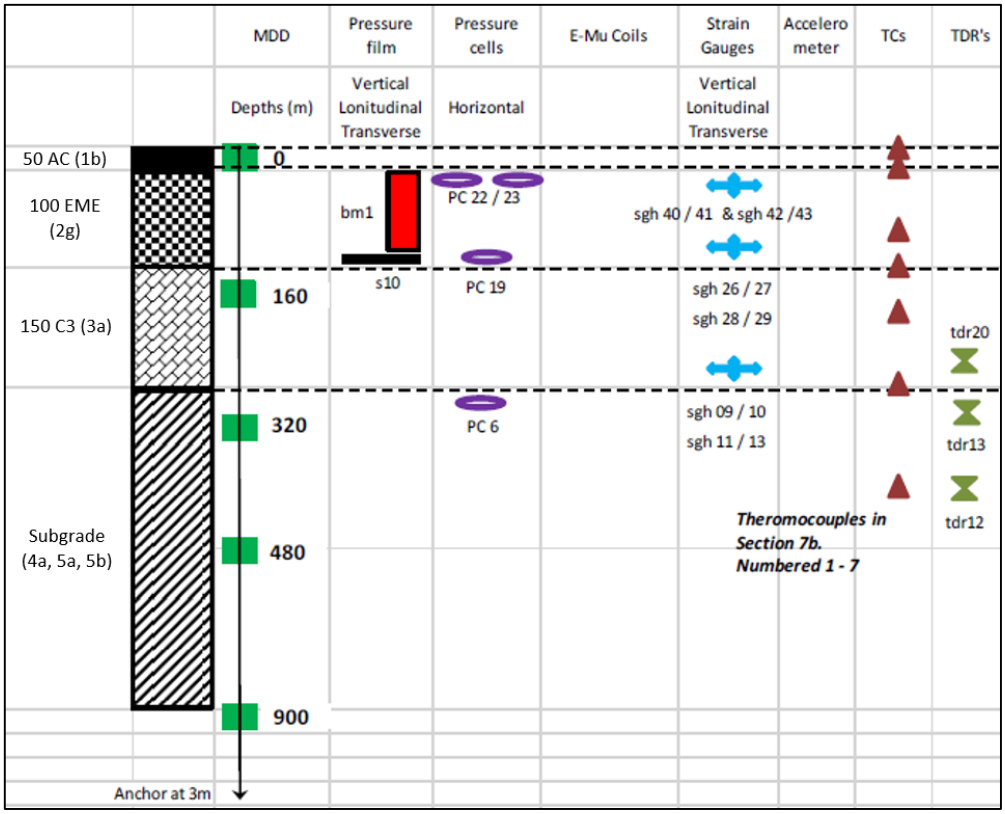

Figure 3-12: Schematic location of sensors in Section 7b.

3.3. Methods for Data Collection

All the data that formed part of this study were generated by means of a two-stage operation. First, the raw collected data relevant to this study (MDD, temperature, moisture, and density) were processed and validated for further use. Thereafter, the necessary permanent deformation behaviour, layer moduli, and PN values were calculated for each of the flexible pavement sections. Table 3-4 presents a flow diagram of the two-stage operation. The methodology of stage one is presented with the respective processed and validated data in Chapter 4.2. The procedures of stage 2 are defined in the subsections to follow.

Table 3-4: Step by step flow diagram of methodology for data collection.

Stage 1
UP collects in-situ pavement response and environmental related data from the seven flexible pavement sections on the R104 → Process and validate data relevant to the study for further use
Stage 2a
Analyse MDD data through statistical analyses, graphs, etc. → Draw inferences from the results in terms of the permanent deformation behaviour **(see Chapter 3.3.1)**
Stage 2b
Back-calculate the layer moduli of each pavement structure by means of the CHEV linear elastic static computer program and MDD measured depth deflections **(see Chapter 3.3.2)**
⇩
Use the back-calculated layer moduli to calculate the PN value of each pavement structure by means of the PN design method **(see Chapter 3.3.3)**

3.3.1. Analysis of MDD Data

From all the in-situ pavement response and environmental related data gathered, only the MDD, temperature, moisture, and density data were used to make inferences about the permanent deformation behaviour of a pavement structure. The MDD data presented a vertical response output (Figure 3-13), while the temperature, moisture, and density data provided three parameters that could alter this vertical response. The analysis procedure focused on the base layer due to the similarity of the pavement structures apart from this layer. Therefore, only the total deformation and base layer deformation were investigated (first two MDDs from the top).

The MDD data were evaluated through a process whereby only the static, non-loading state between successive load applications (TSD passes) was considered. This portion of the data, referred to as the static response, is represented by the range of data covered by orange lines in Figure 3-13, which represents a typical vertical response output from a MDD module for a single load passing over the sensor. For this study, however, the dynamic zone includes three deflection bowls, one for each of the three TSD axles.

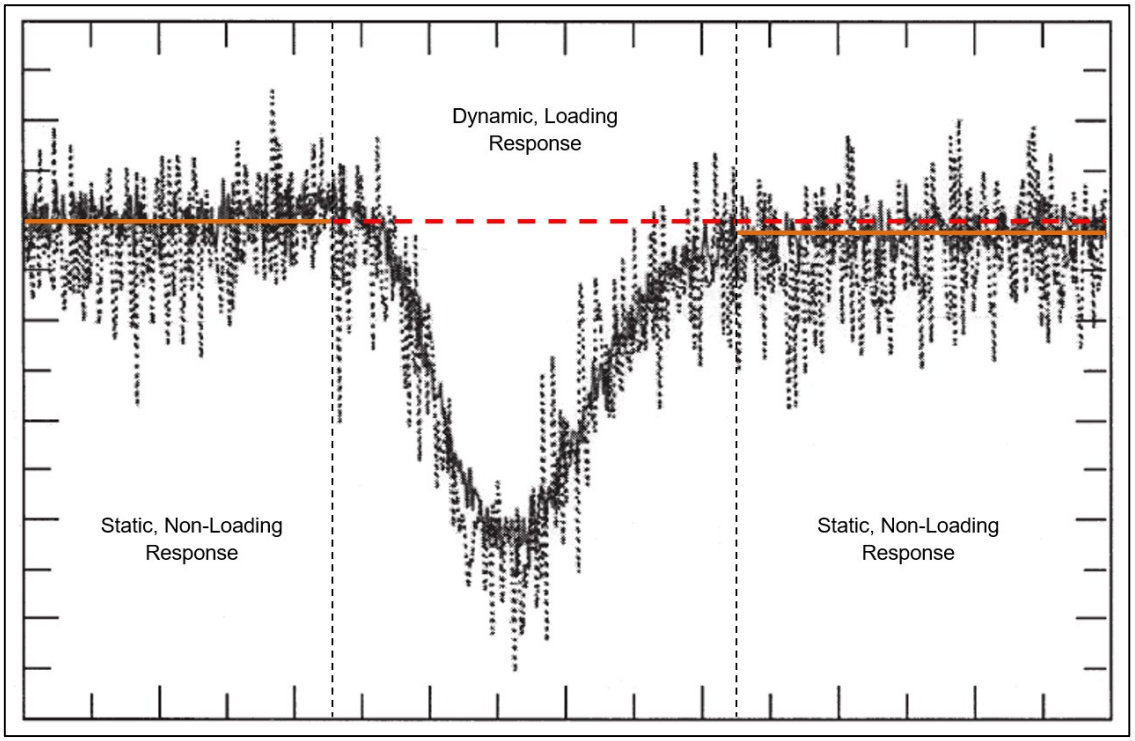

Figure 3-13: Typical vertical strain response output from a MDD module.

The orange lines represent the average vertical response before and after load application. Conservatively, the first and last second of a TSD test run were used for analysis in order to ensure static, non-loading conditions. With the first and last second representing vertical response data before and after load application respectively, a conclusion could be drawn regarding any permanent response as a result of the applied load (three TSD half-axle loads). This represented the short-term loading response (Figure 3-14).

Additionally, the last second of a test run relative to the first second of the next test run was evaluated and a conclusion was drawn regarding any permanent response recovered as a result of the time delay between consecutive test runs. This represented the longer-term recovering response (Figure 3-14). Figure 3-14 illustrates a typical test run sequence of the TSD during testing. A summary of the analysis procedure is presented schematically in Figure 3-15.

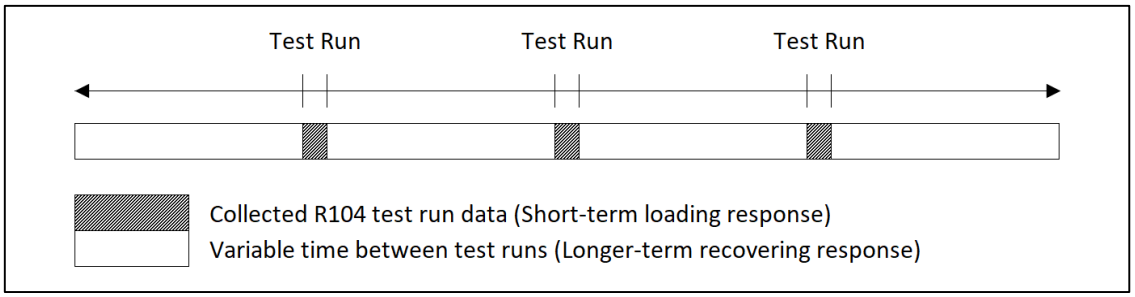

Figure 3-14: Typical TSD loading sequence.

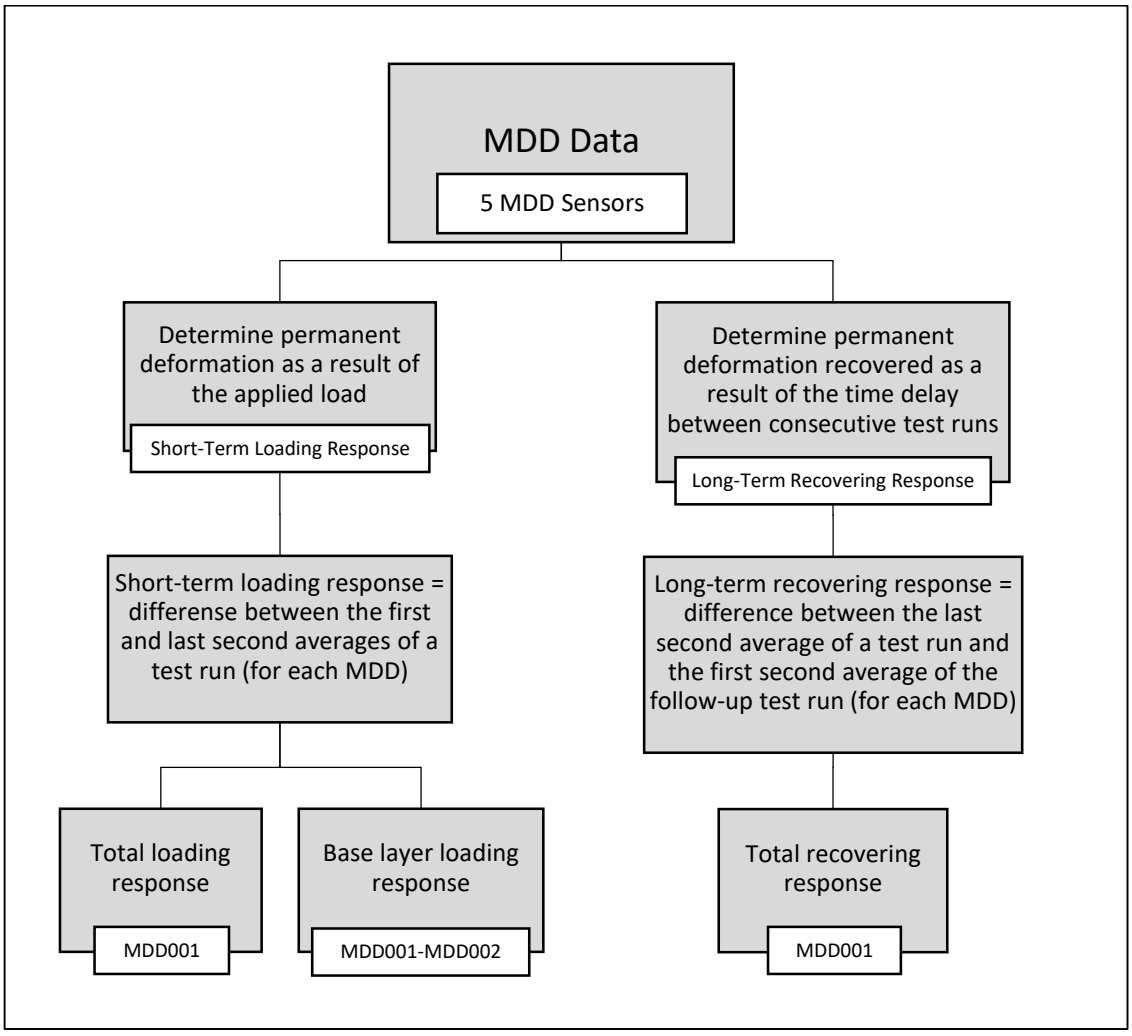

Figure 3-15: Analysis of collected MDD data for permanent deformation behaviour.

The time duration of a test run and time delay between consecutive test runs varied somewhat, but this was assumed small enough to be ignored. It should also be noted that due to the vertical positioning of the MDDs, the base layer response (MDD001-MDD002) actually included the behaviour of the surfacing layer (see Figures 3-5 to 3-12). The first MDD was installed at the top of the surfacing layer and the second at the interface of the base and subbase layer.

Permanent deformation was considered at a fixed location in the pavement (at MDD location), directly underneath the tyre load, and in the vertical z-direction only. Figure 3-16 illustrates the target transverse location of the TSD's trail dual wheel in relation to the instrumentation installed in the pavement structure; it was assumed there is no lateral wander from this location. Other transversal offsets from position 0 m were also tested but not considered in this study.

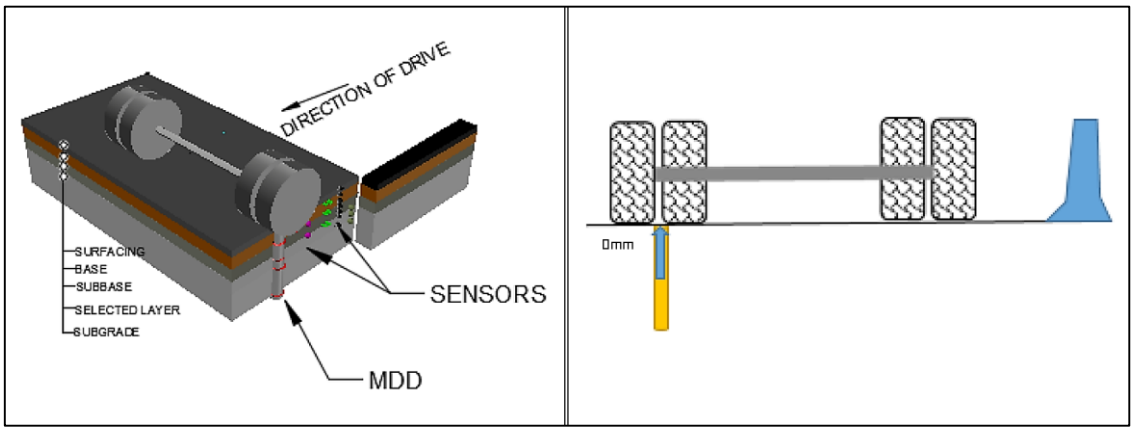

Figure 3-16: Target transverse location of the TSD trail dual wheel.

For the purpose of this study, the TSD only served as the loading mechanism. A steering, drive, and trail axle (90-kN) each applied a different load to the pavement during a test run. Both the steering and driving axle load were unknown, but this was irrelevant as identical loading conditions were considered for the seven flexible pavement test sections. A target TSD speed of 20 km/h, which is similar to typical maximum APT speeds, was considered from the range of speeds (5 to 80 km/h) used during testing at the SANRAL experimental site. It should be noted that this was not an APT setup and that permanent deformation was evaluated as a result of a single load application (three half-axle loads) from the TSD.

Some minor fluctuations in axle loading were present due to the dynamic effects of the slow moving TSD. Similarly, the speed of the TSD also fluctuated around 20 km/h (20.14 average, 1.56 standard deviation, 7.7% COV) but not significant enough to raise any concern. Therefore, for the purpose of this study, the TSD speed and axle loads were assumed to remain constant and the effect of "speed of loading" could be ignored. Furthermore, all instrumentation was assumed to be installed correctly, calibrated appropriately, and functioning properly. The quality of construction was not taken into account (quality verifications were not available), and any material characteristics not mentioned in Table 3-1 were not considered.

3.3.2. Moduli Back-Calculation Method

Layer moduli were back-calculated from the trail-axle MDD depth deflections using the CHEV linear elastic static software. This software adopts all the principles of the multi-layer elastic theory as described in Chapter 2.8.2. Although a non-linear material response analysis is a more realistic representation of the response of a pavement to loading, it falls outside the scope of this study. Therefore, a linear material response analysis was considered to accommodate the CHEV software. The back-calculation procedure included the following steps:

1) Specify the following input parameters for each layer of the pavement structure:
   - Poisson's ratio (Table 2-10), and
   - Layer thickness (known).
2) Specify the following input parameters for the applied load:
   - Load magnitude (half of TSD trail axle, 45 kN);
   - Contact pressure (700 kPa from Table 2-11), and
   - Load location (no transversal offset, x = 0, y = 0).
3) Specify the interested depths of measurement (MDD depths).
4) Assume a reasonable set of moduli for the pavement layers.
5) The multi-layered elastic system computer program calculates the vertical deflection at each MDD location (specified depths).
6) Plot the calculated (from CHEV) versus measured (from MDDs) depth deflections and take note of the difference between the values. It is assumed that the anchor point at a depth of 3 m does not move.
7) Repeat steps 4 to 6 until the deviation from each MDD deflection measurement is less than 0.02 mm (De Beer et al., 1989).

With each iteration, the assumed set of moduli was changed one layer at a time, starting from the top downwards, in order to obtain a satisfactory match between the two sets of data at each MDD location. When the measured slope was steeper than the calculated slope, the modulus of the material had to be increased, and vice versa. The end result was a set of effective elastic moduli that served as input parameters to the pavement number calculation method.

Due to the heavily time consuming nature of this manual iterative procedure, a more lenient tolerance of 0.02 mm was used instead of the 0.0015 mm specified by De Beer et al. (1989). The MDD setup at the experimental site also did not include a MDD at the surfacing-base interface as mentioned before, but due to very thin surfacing layers, the effect of this on the back-calculated moduli was assumed to be small enough to be ignored.

It should be noted that the static loading nature of the CHEV computer program does not correspond with the moving load conditions of the TSD. It is known that the speed of loading has an effect on the inherent stiffness of a pavement layer as the amount of dynamic deflection is dependent on the speed of loading. Even though smaller moduli values will be expected for a static load, the difference in speed (0 vs 20 km/h) was considered small enough to have a negligible effect. Steyn et al. (2016) also reported very small changes in dynamic deflection for speeds up to 20 km/h during testing at the R104 experimental site.

3.3.3. Pavement Number Calculation Method

Here, the stepwise method for calculating the PN value of a pavement structure is detailed; however, the exact procedure as described in TG2 was not followed. The PN design method and its counterpart, the DEMAC material classification method, each has a major issue with regards to this study. The DEMAC method is unable to classify asphaltic materials and surface seals, while the maximum allowed stiffness values used by the PN method for high quality materials bear little to no resemblance to the original back-calculated effective moduli. The top class for all three material types (granular, cemented, and bitumen stabilised) has an infinite interval, which allows materials with a great difference in performance (material stiffness) to be classified as the same DEMAC. Consequently, identical material stiffness inputs are assigned to these very different materials for PN calculation.

Due to the lack of laboratory tests and indicators available for analysis, this study relies significantly on the back-calculated layer moduli for calculating the PN values of the relevant test sections. As material stiffness plays a vital role in PN calculation and the calculated PN values are related back to permanent deformation behaviour, it is important that the back-calculated moduli are kept original to ensure that any environmental related effects that reflect in them and the deformation behaviour, reflect in the PN values as well. DEMAC material classification was, therefore, omitted and the back-calculated layer moduli incorporated directly into the calculation procedure.

Minimal traffic (testing) had been applied to the test sections prior to this study, and the sections were still relatively new at the time of testing; hence, each material was assigned the material class from the original design of the experimental site as the material characteristics should not have changed much since construction. The back-calculated layer moduli replaced the maximum allowed stiffness values from the original method but served the same purpose in the calculation procedure. These were the only two alterations that were made to the original PN method, which contributed to a more accurate structural integrity for the given conditions during testing.

The PN calculation procedure for this study included the following steps:

1) Check the applicability of the method. The five-layer system of each pavement structure (four pavement layers plus the subgrade) ensures complete compliance with the five-layer model rule required by the PN design method. All other conditions as described in Chapter 2.9.1 are assumed to apply and the method may proceed.

2) Obtain the layer thickness for each layer in the pavement structure (known).

3) Determine the subgrade's Effective Long-Term Stiffness (ELTS):
   - Determine the basic stiffness of the subgrade (Chapter 3.3.2).
   - Adjust the stiffness for the climatic region by multiplying the basic stiffness by the climate adjustment factor (Table 3-5).
   - Adjust the stiffness for depth of subgrade cover by adding the subgrade cover adjustment factor (Figure 3-17).

4) Determine the ELTS of each layer above the subgrade:
   - Determine the modular ratio limit for the assigned class (Table 3-6).
   - Determine the maximum allowed stiffness for the assigned class (Chapter 3.3.2).
   - Assigned ELTS = **Minimum** of the *maximum allowed stiffness* and the *ELTS of the support layer multiplied by the modular ratio limit*. Start at the subgrade and work upwards to the surfacing layer.

5) Determine the Base Confidence Factor (BCF) for the base layer (Table 3-6).

6) Determine the adjustment factor based on the thickness for any cement stabilised layers (Figure 3-18).

7) Calculate the contribution of each layer to the overall PN value:
   - Contribution of layer = ELTS of layer (MPa) * layer thickness (mm) / 10 000.
   - For the base layer, multiply this contribution with the BCF.
   - For any cement stabilised layers, multiply this contribution with the thickness adjustment factor.

8) Add up all the layer contributions to get the PN value of the pavement.

Table 3-5: Climate adjustment factors (Asphalt Academy, 2009).

Climate and Weinert N Values (After TRH4, 1996)	Adjustment Factor
Wet (Weinert N < 2)	0.6
Moderate (Weinert N = 2 to 5)	0.9
Dry (Weinert N > 5)	1.0

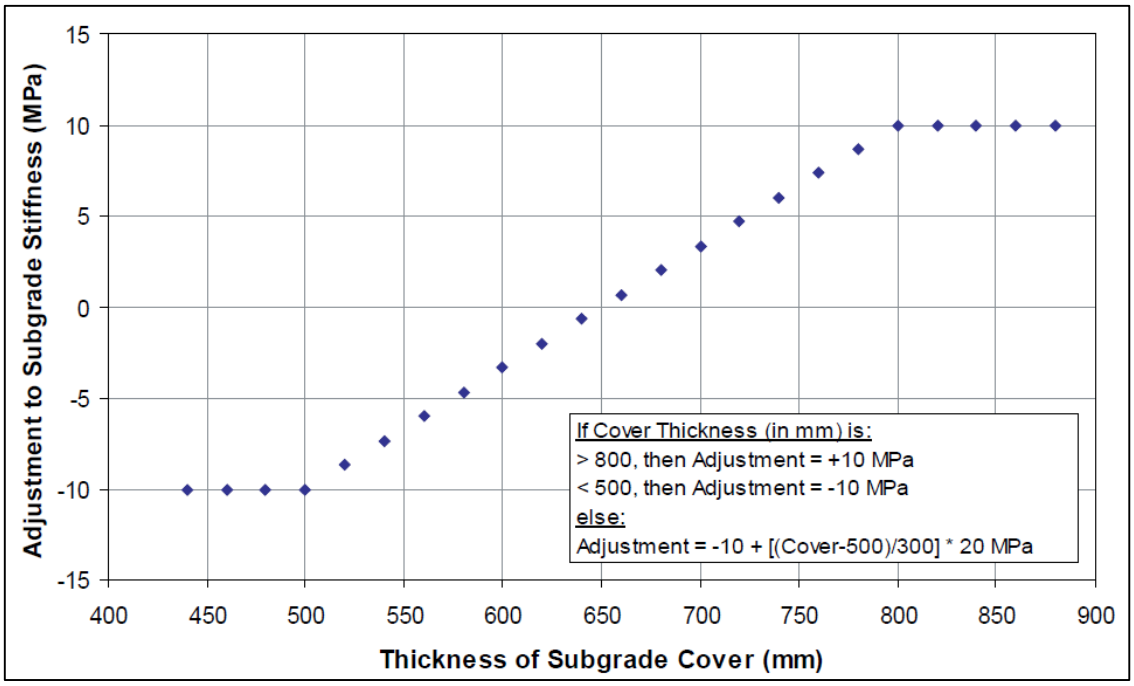

Figure 3-17: Subgrade stiffness adjustment based on cover thickness (Asphalt Academy, 2009).

Table 3-6: Modular ratio limit and base confidence factor values (Asphalt Academy, 2009).

General Material Description	Material Class	Modular Ratio Limit	BCF
HMA surfacing and base material	AG, AC, AS, AO	5.0	1.0
Surface seals	S1, S2, S3, S4, S5, S6	2.0	N/A
High strength BSM, normally using crushed stone or RA source material	BSM1	3.0	1.0
Medium strength BSM, normally using natural gravel or RA source material	BSM2	2.0	0.7
Crushed stone material	G1	2.0	1.1
	G2	1.9	0.8
	G3	1.8	0.7
Natural gravel	G4	1.8	0.2
	G5	1.8	0.1
	G6	1.8	-2.0
Gravel-soil blend	G7	1.7	-2.5
	G8	1.6	-3.0
	G9	1.4	-4.0
	G10	1.2	-5.0
Cement stabilised crushed stone	C1 and C2	9.0	0.8
Cement stabilised natural gravel	C3	4.0	0.6
	C4	3.0	0.4

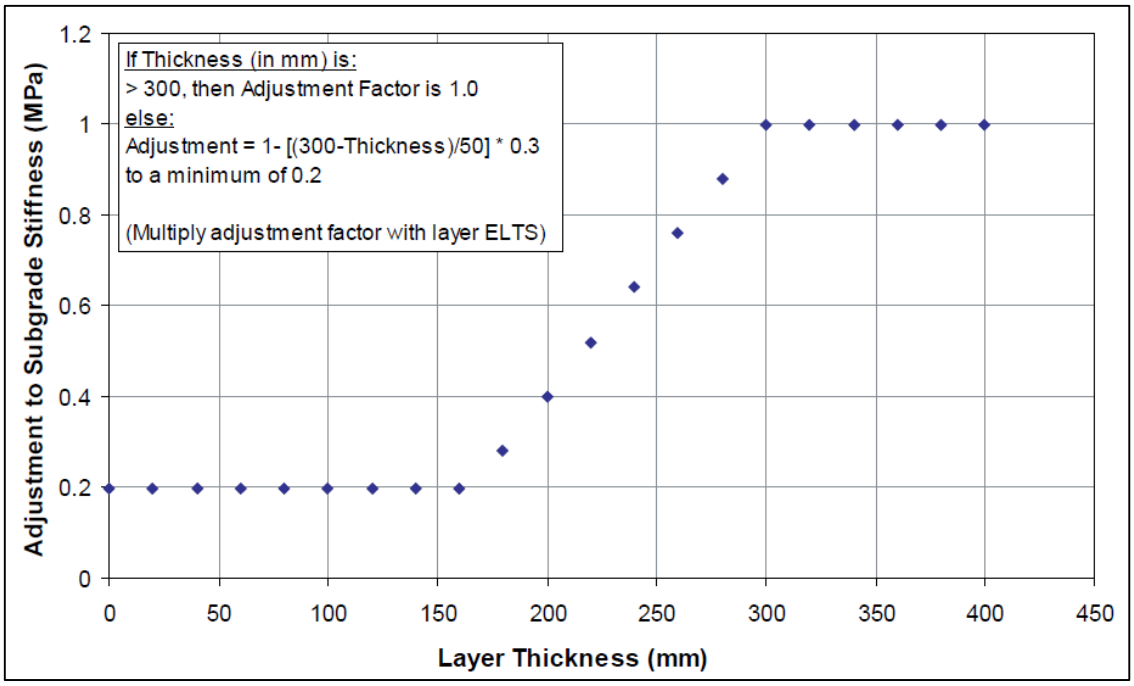

Figure 3-18: Layer thickness adjustment factor for cemented layers (Asphalt Academy, 2009).

3.4. Summary

Table 3-7 summarises all the data that formed part of this study, the information they provide, and how they were utilised in this study.

Table 3-7: Data summary.

Data Type	Description	Use
MDD	Dynamic vertical response data	To back-calculate layer moduli
	Static vertical response data	To determine the permanent deformation behaviour in terms of a short-term loading response as well as a longer-term recovering response
Temperature	Air and in-situ temperature readings	To explain any anomalies present in the permanent deformation behaviour
Moisture	In-situ moisture readings at various locations (depths) within the pavement structure	To explain any anomalies present in the permanent deformation behaviour
Density	In-situ density readings at various locations (depths) within the pavement structure	To explain any anomalies present in the permanent deformation behaviour
Layer Moduli	Stiffness information regarding individual pavement layers	To calculate the pavement number value of individual pavement layers
Pavement Number	A measure of the pavement's structural integrity (strength)	To determine a possible relationship between the permanent deformation behaviour and structural integrity of a pavement

4. DATA COLLECTION

4.1. Introduction

In this chapter, the data collection phase of the study is discussed. Data collection was divided into two separate operations. First, the raw collected data relevant to this study were processed and validated for further use. Thereafter, the permanent deformation behaviour, layer moduli, and PN values were calculated for each of the flexible pavement sections. The results for both these operations are presented in this chapter, while the discussion thereof follows in Chapter 5.

4.2. Collected Data

From 4 September 2013 to 10 June 2015 a variety of pavement response data as well as environmental related data were recorded on the seven flexible pavement sections at the SANRAL experimental site. It should be noted that only a limited amount of this data are applicable to the current study. Only MDD, temperature, moisture, and density data were considered. These four data groups were processed and validated in order to assess the credibility of each data type before it was used. The results are presented in the subsections to follow.

The in-situ pavement response and environmental related data were collected for a range of different loading speeds (TSD speeds). After a pre-assessment of all the collected data, it was decided to consider the 20 km/h data of each section to conduct the study. From all the data collected, the 20 km/h data turned out to be the most complete data set in relation to the other speeds. Matching 20 km/h runs were performed on the seven sections (between 2 February 2015 and 10 June 2015) and the results (sensor data) recorded in the respective data files. Table 4-1 provides the time and date of the test run used to represent each test section.

Table 4-1: Representative test runs for seven SANRAL test sections.

	Date of Test	Time of Test	TSD Speed [km/h]
Section 1	02-Feb-2015	13:27	19.31
Section 2	03-Feb-2015	10:19	19.17
Section 3	04-Feb-2015	09:23	17.77
Section 4	09-Jun-2015	10:25	19.22
Section 5	10-Jun-2015	10:47	19.84
Section 6	02-Mar-2015	14:27	22.42
Section 7a	03-Mar-2015	10:11	22.50
Section 7b	04-Mar-2015	09:51	20.93

4.2.1. MDD Data

From all the vertical response data collected, the MDD data turned out to be the most credible and complete. The emu coil and strain gauge data showed signs of high variability and numerous sensors did not respond to TSD loading at all. The sensors could possibly have been out of the stress range or malfunctioned due to damage suffered in service or during installation (construction). The study was, therefore, limited to MDD data for studying deformation behaviour. Table 4-2 presents a short cut-out of the MDD data from Section 1 after a nil adjustment of each MDD. Figure 4-1 shows the corresponding time-deflection plot of the data, which clearly illustrates the five elastic deflection basins measured at the layer interfaces as a result of the trail axle load of the TSD. These five basins (localised test run data) are used for moduli back-calculation purposes, while the extents (first and last second) of the full test run are used to determine permanent deformation behaviour. The MDD data for Sections 2 to 7 are provided in Appendix A.

Table 4-2: Cut-out of MDD data from Section 1.

Time [milliseconds]	MDD001 [µm]	MDD002 [µm]	MDD003 [µm]	MDD004 [µm]	MDD005 [µm]
…	…	…	…	…	…
70.83	-1.28	-1.28	-1.23	-1.15	0.04
71.67	-0.29	-0.19	-0.14	-0.18	0.09
72.50	0.48	0.68	0.66	0.62	0.14
73.33	0.79	1.09	0.97	1.03	0.14
74.17	0.84	1.15	1.04	1.20	0.14
75.00	0.80	1.07	1.02	1.23	0.18
75.83	0.75	0.96	0.99	1.14	0.19
76.67	0.69	0.81	0.97	1.02	0.12
77.50	0.52	0.53	0.82	0.79	-0.03
78.33	-0.11	-0.24	0.10	0.08	-0.15
79.17	-1.22	-1.46	-1.16	-1.09	-0.20
80.00	-1.97	-2.26	-2.01	-1.83	-0.20
80.83	-1.63	-1.88	-1.68	-1.45	-0.16
81.67	-0.63	-0.77	-0.65	-0.40	-0.08
82.50	0.23	0.23	0.26	0.54	0.03
83.33	0.65	0.78	0.76	0.99	0.11
84.17	0.78	0.96	0.96	1.08	0.14
85.00	0.80	0.94	0.99	1.04	0.13
85.83	0.80	0.86	0.95	1.04	0.05
…	…	…	…	…	…

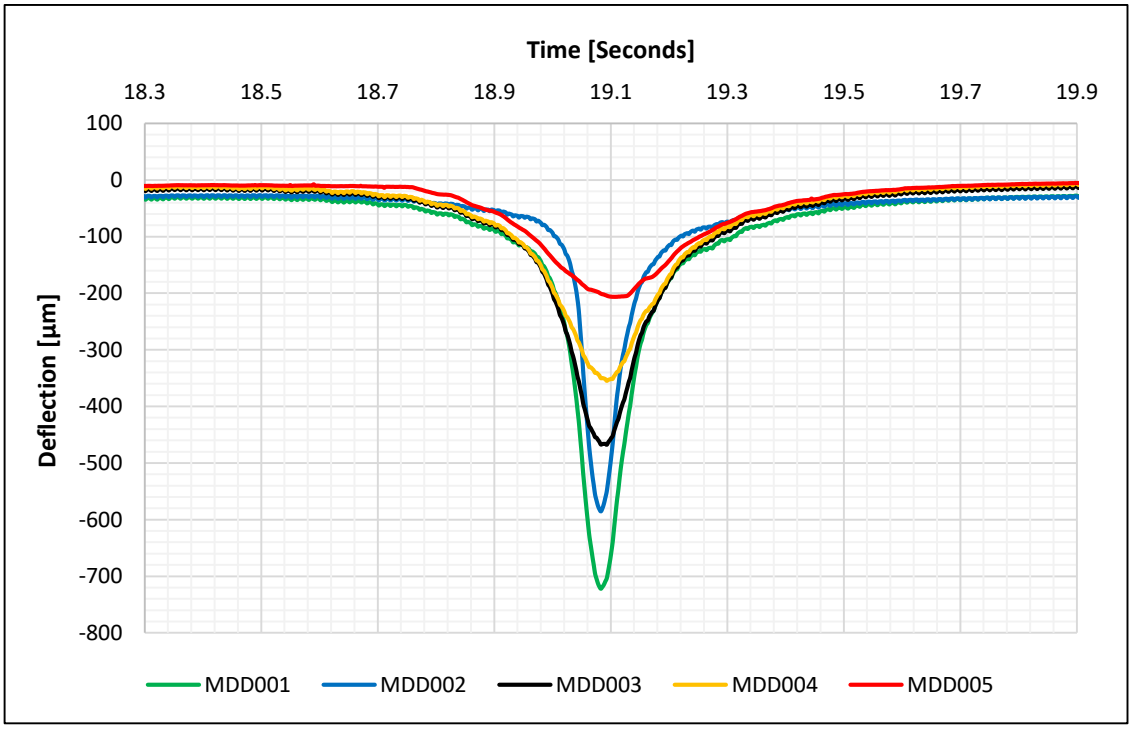

Figure 4-1: Measured MDD deflections from Section 1.

A few MDDs did not register a reading or showed uncharacteristic behaviour during TSD loading; however, these were all MDDs lower down in the pavement structure, which are not essential to determine the permanent deformation behaviour. The study focuses on total and base layer deformation; therefore, only the first two MDDs from the top are significant.

For moduli back-calculation purposes, on the other hand, all the MDDs play an equal important role in obtaining the effective modulus of each layer in the pavement structure. Therefore, where a malfunctioning MDD was identified, a realistic dynamic deflection value was assumed for it (through extrapolation from the top) in order for the back-calculation process to proceed.

For some of the sections, a few MDDs also seemed to have been mixed up during testing as some deflection basins appeared to be in the incorrect order. The MDDs seemed to function properly and registered realistic readings; they were just in the wrong order. One would expect the uppermost MDD to have the largest deflection basin and each subsequent MDD to have a basin smaller or equal to the previous one. It was, therefore, assumed that the MDD channels had accidentally been mixed up and that a logical order should be assumed where necessary (confirmed by acceptable E-values in Chapter 4.3.2). It is acknowledged that another cause may have been poorly clamped MDD modules (no movement of MDD anchors was evident).

Table 4-3 provides the rearranged MDD order for each section. The operational status of each MDD is also indicated. Where a malfunctioning MDD was identified, a realistic dynamic deflection value was assumed for moduli back-calculation purposes (indicated in brackets).

Table 4-3: MDD order rearrangement and operational status.

	MDD001	MDD002	MDD003	MDD004	MDD005
Section 1	MDD002	MDD001	MDD003	MDD004	MDD005
	✓	✓	✓	✓	✓
Section 2	MDD001	MDD003	MDD002	MDD004	MDD005
	✓	✓	✓	✓	× (71.2 µm)
Section 3	MDD001	MDD002	MDD003	MDD004	MDD005
	✓	✓	✓	✓	× (40.5 µm)
Section 4	MDD001	MDD002	MDD004	MDD003	MDD005
	✓	✓	× (89.7 µm)	✓	× (35.7 µm)
Section 5	MDD001	MDD003	MDD002	MDD005	MDD004
	✓	✓	✓	✓	× (72.6 µm)
Section 6	MDD004	MDD001	MDD005	MDD003	MDD002
	✓	✓	✓	× (63.7 µm)	× (41.3 µm)
Section 7a	MDD003	MDD004	MDD001	MDD002	MDD005
	✓	✓	✓	× (40.1 µm)	× (28.5 µm)
Section 7b	MDD001	MDD002	MDD003	MDD004	MDD005
	✓	✓	✓	✓	✓

4.2.2. Temperature Data

All temperature data under consideration were collected with Decagon Time Domain Reflectometry (TDR) sensors and DAQ units. The temperature data collected by the K-type thermocouples and stand-alone Smartreaders were incomplete and not useful to this study. Too many readings were missing from the data set and consequently no temperature data were available for the representative test runs of the test sections. Steyn and Coetzer (2015) reported water damage to some of the equipment due to flooding of the manholes (Figure 4-2).

Figure 4-2: Flooded manhole and water-damaged Smartreader unit (Steyn and Coetzer, 2015).

A short cut-out of the temperature data under consideration is presented in Table 4-4. The temperature was monitored continuously in 30-min intervals across the first five sections. Each reading included an air temperature (from the on-site weather station) and a temperature within the pavement structure, 75 mm from the surface (from TDR sensor). Even though all the sections at the SANRAL experimental site are within close proximity of each other, a difference in temperature was expected between the different base materials (granular, cemented, and bituminous) at this depth due to a difference in temperature sensitivity. However, the temperature variation between adjacent sections was very small; therefore, the road temperatures were averaged and used across all seven sections.

Table 4-4: Cut-out of temperature data from SANRAL experimental site.

Date	Time	Air Temp. [°C]	Road Temp. [°C]
…	…	…	…
26-Jan-2014	07:10	17.1	24.2
26-Jan-2014	07:40	18.6	24.7
26-Jan-2014	08:10	20.1	26.2
26-Jan-2014	08:40	20.6	27.2
26-Jan-2014	09:10	21.6	28.2
26-Jan-2014	09:40	22.6	29.2
26-Jan-2014	10:10	24.1	31.7
26-Jan-2014	10:40	26.6	35.2
26-Jan-2014	11:10	27.1	37.2
26-Jan-2014	11:40	27.6	37.7
26-Jan-2014	12:10	27.6	39.2
26-Jan-2014	12:40	26.6	39.2
26-Jan-2014	13:10	28.1	39.7
26-Jan-2014	13:40	30.6	41.6
26-Jan-2014	14:10	29.1	42.1
26-Jan-2014	14:40	29.1	41.6
26-Jan-2014	15:10	28.6	41.6
26-Jan-2014	15:40	28.1	42.1
26-Jan-2014	16:10	29.1	41.6
26-Jan-2014	16:40	27.6	40.7
26-Jan-2014	17:10	28.1	39.7
26-Jan-2014	17:40	26.1	38.2
26-Jan-2014	18:10	25.1	36.7
26-Jan-2014	18:40	23.6	35.2
…	…	…	…

Figure 4-3 presents a monthly average plot of this data. From this graph, it is clear that a credible set of data was recorded. The temperature fluctuates in a logical manner through the course of a calendar year. The temperature peaks during the summer months and reaches a minimum during the winter months. It should be noted that this plot represents an average of all the data points within each month and that no specific time of the day is targeted. The temperature data at the time of testing of each section are provided in Table 4-5. A corresponding plot of the test-specific data is illustrated in Figure 4-4.

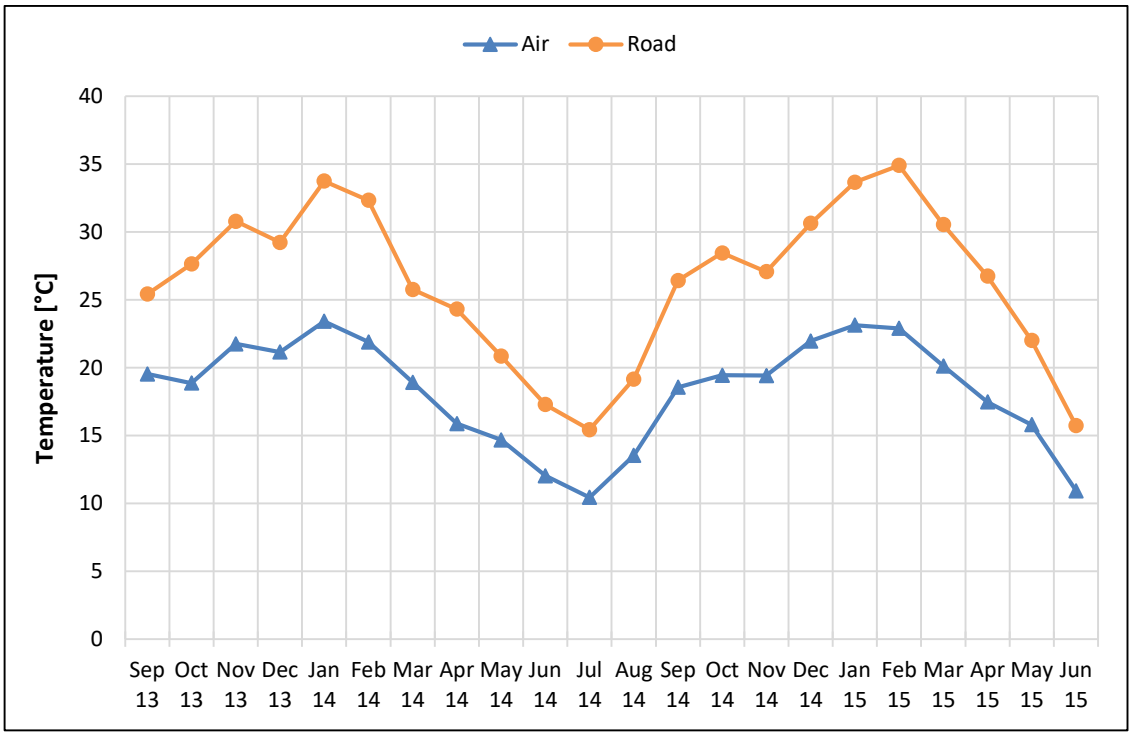

Figure 4-3: Monthly average plot of temperature data.

Table 4-5: Test-specific temperature data.

	Date	Time	Air Temp. [°C]	Road Temp. [°C]
Section 1	02-Feb-2015	13:27	27.6	39.7
Section 2	03-Feb-2015	10:19	24.2	36.5
Section 3	04-Feb-2015	09:23	24.9	32.3
Section 4	09-Jun-2015	10:25	10.1	17.0
Section 5	10-Jun-2015	10:47	10.5	18.2
Section 6	02-Mar-2015	14:27	25.1	39.0
Section 7a	03-Mar-2015	10:11	22.1	31.6
Section 7b	04-Mar-2015	09:51	22.1	32.1

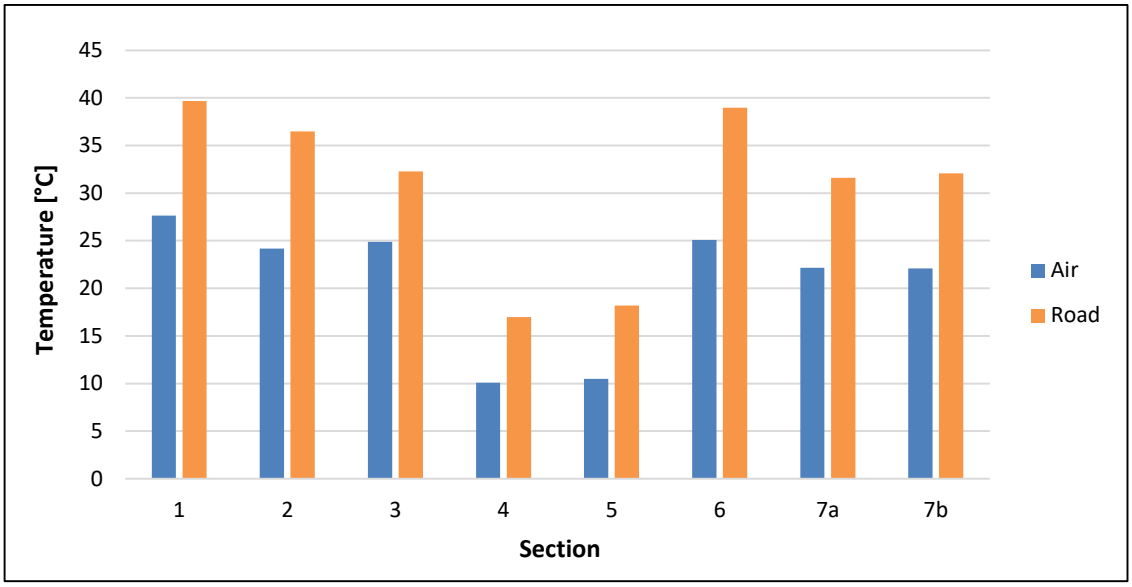

Figure 4-4: Test-specific temperature data.

4.2.3. Moisture Data

All moisture data under consideration were collected with a strata gauge. Similar to the K-type thermocouples and stand-alone Smartreaders, some of the Decagon TDR sensors and DAQ units were flooded and every now and again experienced water damage (Figure 4-5) (Steyn and Coetzer, 2015). This led to breaks in the continuous moisture data and therefore a full record of all the TDR sensors in terms of moisture data was not available. Even though the strata gauge measurements were taken a lot less frequently, a much more reliable and complete set of data was obtained.

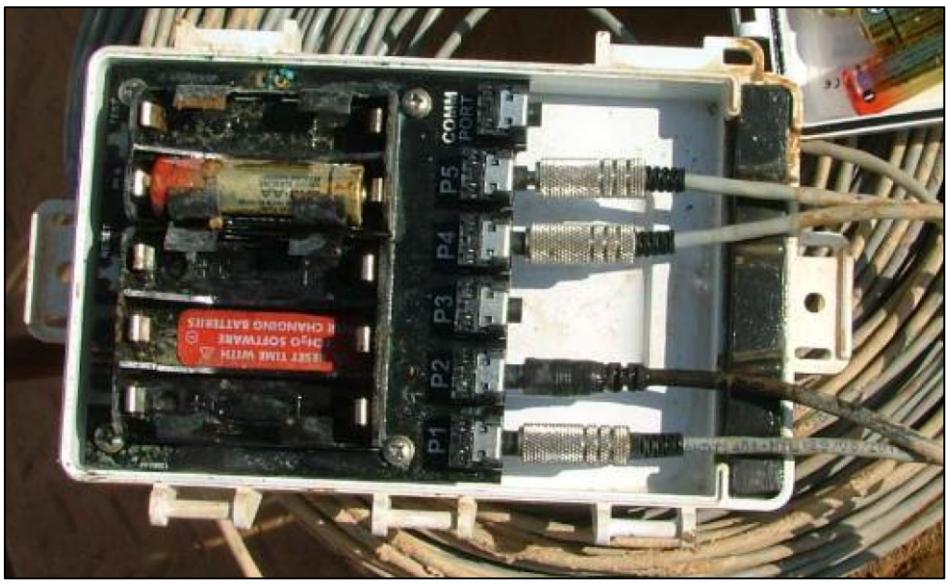

Figure 4-5: Water-damaged Decagon unit (Steyn and Coetzer, 2015).

During the data collection period (4 September 2013 to 10 June 2015), strata measurements were taken on the first five test sections on eight different occasions. With each measurement, the strata gauge took a moisture and density reading every 50 mm up to a depth of 600 mm into the pavement structure. Table 4-6 presents the moisture content with depth of Section 1 for the eight different measuring dates, while Figure 4-6 illustrates the corresponding moisture content with depth plots. The moisture data for Sections 2 to 5 are provided in Appendix B.

Table 4-6: Section 1 moisture content with depth.

Depth [mm]	27-Sep 2013 [%]	24-Oct 2013 [%]	19-Dec 2013 [%]	11-Feb 2014 [%]	03-Jul 2014 [%]	30-Oct 2014 [%]	15-Apr 2015 [%]	31-Jul 2015 [%]
50	2.83	4.03	5.14	4.87	4.63	3.76	4.66	4.43
100	3.00	3.76	4.94	4.67	4.33	3.56	4.49	4.51
150	3.44	4.56	5.95	5.14	4.76	4.33	4.69	4.52
200	4.28	5.54	6.83	6.21	5.31	5.02	5.78	5.37
250	4.74	6.65	7.67	7.20	6.40	5.79	6.34	5.94
300	5.41	7.52	8.83	7.30	6.81	6.71	6.51	6.56
350	5.76	8.19	9.94	8.47	7.45	7.53	7.62	7.27
400	7.85	10.73	13.16	11.20	9.88	10.17	10.23	9.80
450	10.10	14.10	16.47	14.57	12.42	12.44	12.89	13.09
500	13.89	18.55	19.91	18.54	15.97	17.05	16.62	17.42
550	15.64	19.17	20.18	19.97	17.07	17.98	17.44	17.17
600	16.49	19.41	20.62	20.80	18.96	20.58	19.68	19.14

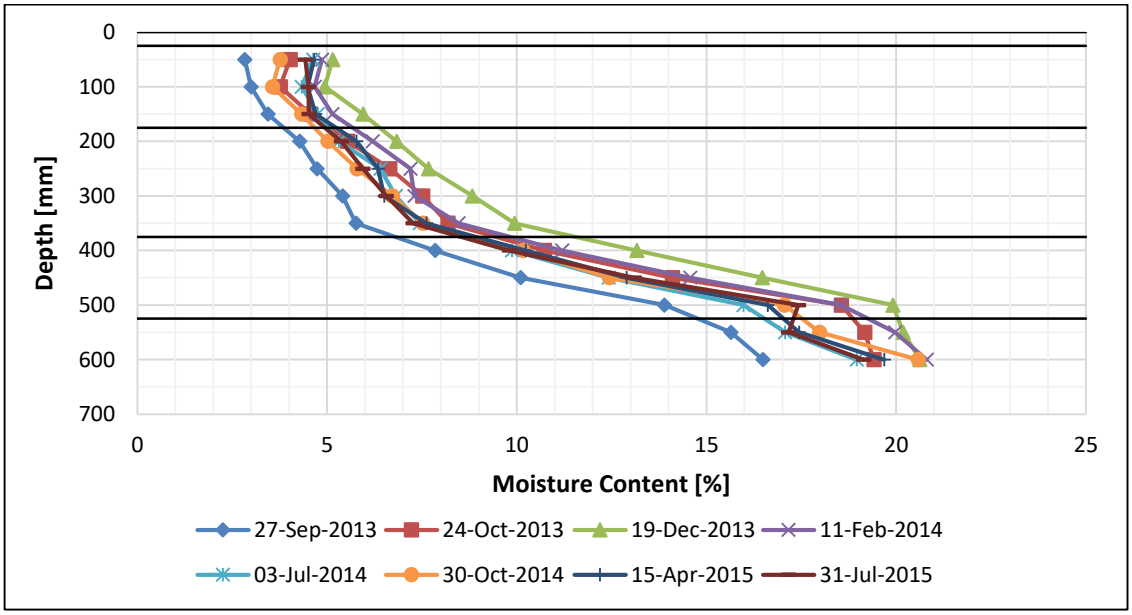

Figure 4-6: Section 1 moisture content with depth.

The moisture content with depth plots show a gradual increase in moisture content with depth as one would expect. A greater overall moisture content is visible during the expected high rainfall months and the moisture content percentages are within a realistic range. An average moisture content for each test section for the eight measuring dates is provided in Table 4-7 and presented graphically in Figure 4-7.

Table 4-7: Average section moisture content per measuring date.

	Section 1 [%]	Section 2 [%]	Section 3 [%]	Section 4 [%]	Section 5 [%]
27-Sep-2013	7.79	10.60	13.93	14.81	13.94
24-Oct-2013	10.18	11.46	14.65	16.30	15.69
19-Dec-2013	11.64	12.33	16.54	16.55	17.41
11-Feb-2014	10.74	11.91	15.48	16.81	16.09
03-Jul-2014	9.50	11.18	15.00	15.81	15.59
30-Oct-2014	9.58	11.64	15.01	15.86	16.75
15-Apr-2015	9.75	11.79	15.63	16.85	16.42
31-Jul-2015	9.60	11.66	15.60	16.46	16.36

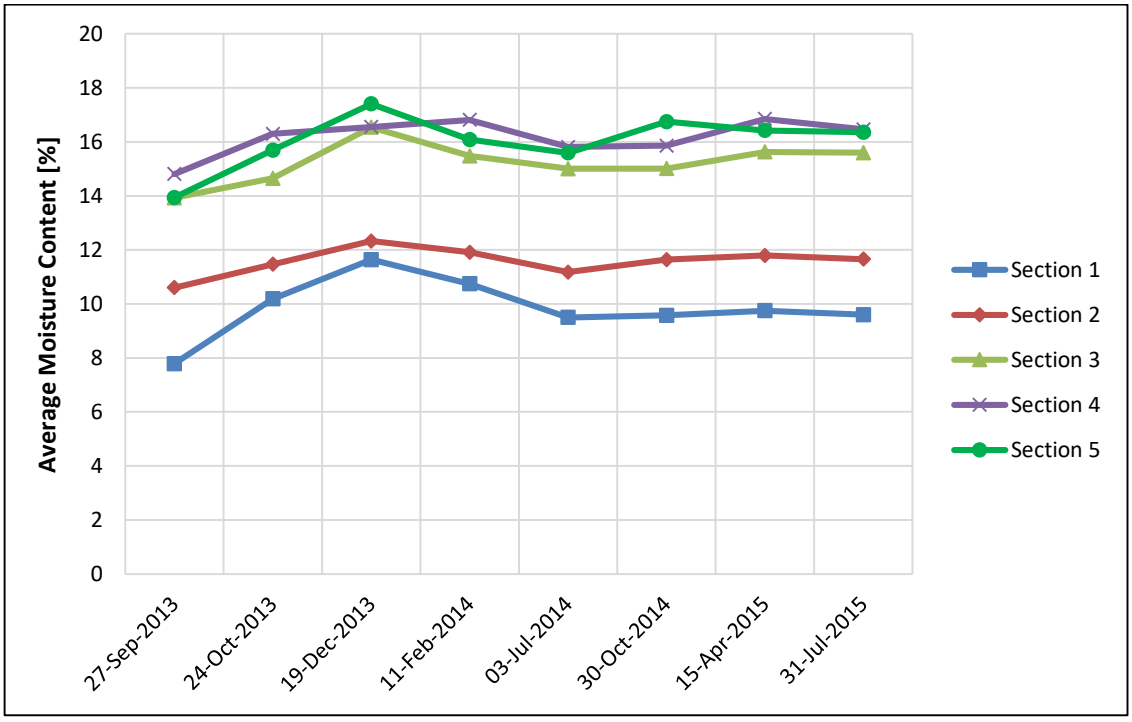

Figure 4-7: Average section moisture content per measuring date.

4.2.4. Density Data

The density data under consideration were collected in conjunction with the moisture data as previously mentioned. Table 4-8 presents the dry density with depth of Section 1 for the eight different measuring dates, while Figure 4-8 illustrates the corresponding dry density with depth plots. The density data for Sections 2 to 5 are provided in Appendix C.

Table 4-8: Section 1 dry density with depth.

Depth [mm]	27-Sep 2013 [kg/m^3]	24-Oct 2013 [kg/m^3]	19-Dec 2013 [kg/m^3]	11-Feb 2014 [kg/m^3]	03-Jul 2014 [kg/m^3]	30-Oct 2014 [kg/m^3]	15-Apr 2015 [kg/m^3]	31-Jul 2015 [kg/m^3]
50	2296	2260	2313	2341	2332	2311	2298	2305
100	2370	2366	2389	2353	2355	2359	2430	2350
150	2353	2323	2304	2334	2334	2357	2343	2365
200	2244	2257	2210	2224	2241	2251	2233	2214
250	2154	2134	2139	2112	2124	2141	2081	2120
300	2090	2075	2039	2123	2100	2085	2106	2104
350	2169	2174	2122	2173	2162	2151	2126	2174
400	2154	2172	2082	2108	2116	2124	2111	2132
450	2128	2057	2046	2059	2093	2106	2102	2070
500	2059	1989	1979	1990	2041	1976	2010	1969
550	2033	1972	1952	1968	2027	1969	2013	2039
600	1995	1973	1959	1942	1973	1963	1951	1959

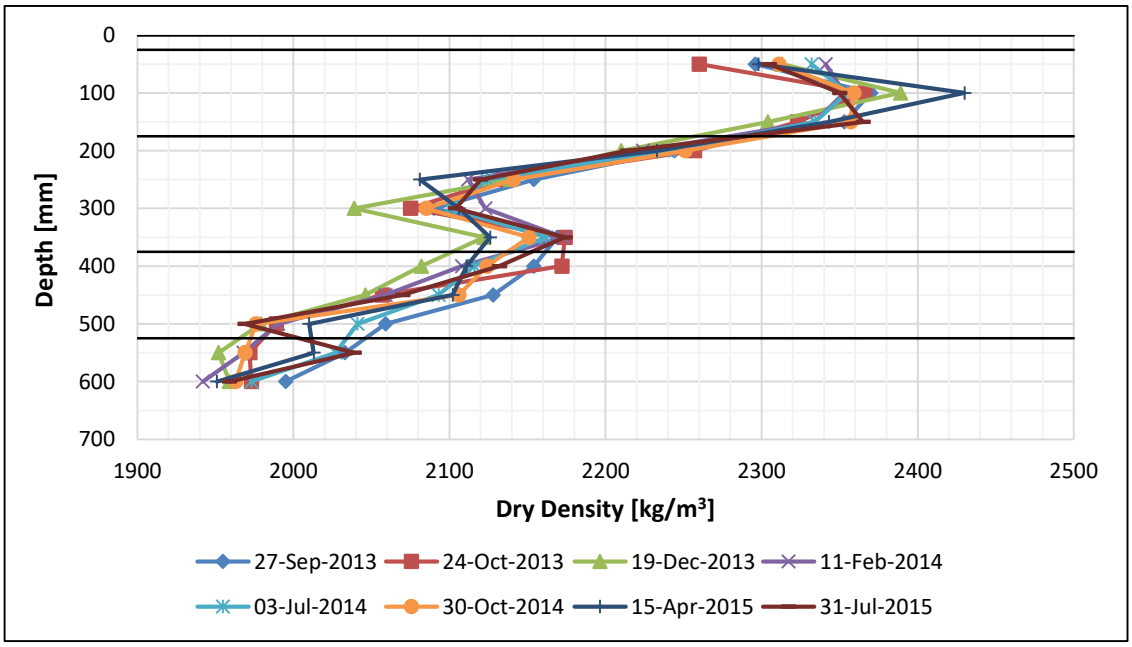

Figure 4-8: Section 1 dry density with depth.

The density values are of a realistic nature, and the dry density with depth plots show a general decrease in density with depth as one would expect. Due to their high load spreading requirements, shallower pavement layers are typically of higher quality and density than deeper layers. Layers of high structural integrity are required on top to absorb the majority of the applied stresses before they reach the deeper layers. An average dry density for each test section for the eight measuring dates is provided in Table 4-9 and presented graphically in Figure 4-9.

Table 4-9: Average section dry density per measuring date.

	Section 1 [kg/m³]	Section 2 [kg/m³]	Section 3 [kg/m³]	Section 4 [kg/m³]	Section 5 [kg/m³]
27-Sep-2013	2170	2087	1950	1900	1979
24-Oct-2013	2146	2069	1952	1890	1964
19-Dec-2013	2128	2062	1939	1885	1943
11-Feb-2014	2144	2075	1940	1884	1953
03-Jul-2014	2158	2072	1935	1898	1964
30-Oct-2014	2149	2076	1948	1889	1956
15-Apr-2015	2150	2059	1938	1862	1949
31-Jul-2015	2150	2067	1933	1867	1937

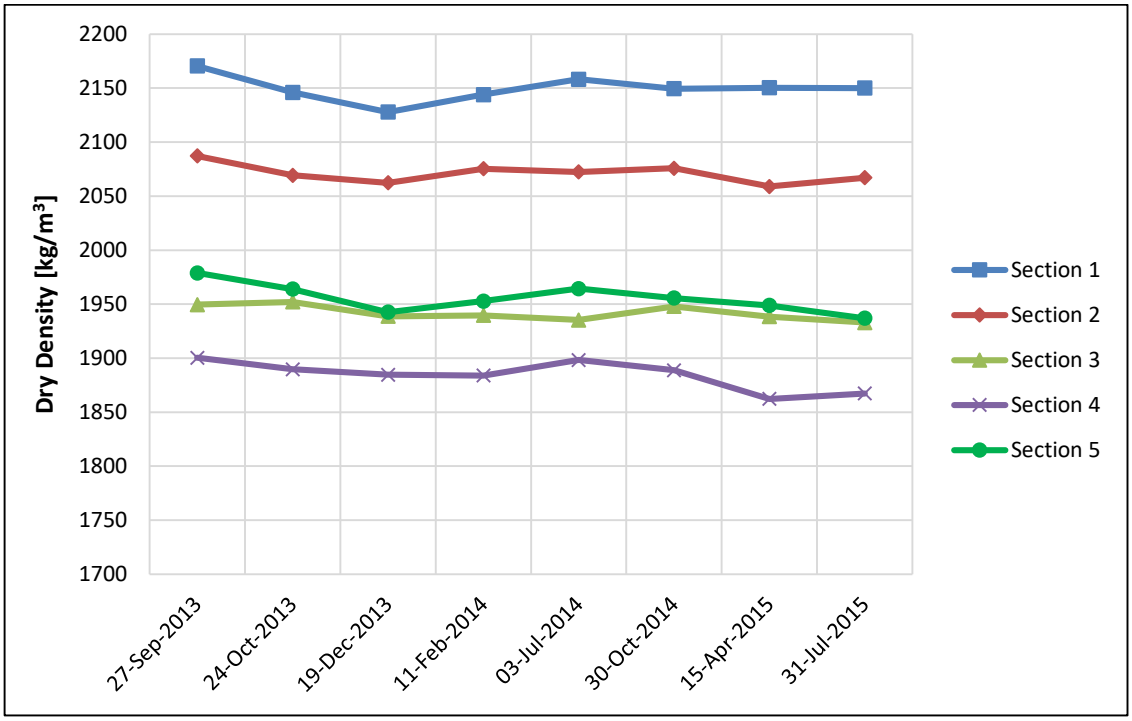

Figure 4-9: Average section dry density per measuring date.

4.3. Calculated Data

After the collected data were processed and validated, the permanent deformation behaviour, layer moduli, and PN values were determined for each of the flexible pavement sections. All calculations were done according to the procedures described in Chapter 3.3. The results are presented in the subsections to follow.

4.3.1. Permanent Deformation Behaviour

The permanent deformation behaviour of each test section was determined by means of the method described in Chapter 3.3.1. Table 4-10 provides the first and last second, static MDD vertical response averages for each of the eight representative test runs. As only total and base layer deformation are of importance, only the first two MDDs from the top (MDD001 and MDD002) were considered. It should be noted that some of the original source MDD data were in millimetres and some in micrometres. This is due to different transfer functions that were used to convert the initial MDD voltage readings. All deformation values were converted to and presented in micrometres.

Table 4-10: First and last second, static MDD vertical response averages.

	MDD001		MDD002	
	First Second [µm]	**Last Second [µm]**	**First Second [µm]**	**Last Second [µm]**
Section 1	0.02	-25.73	0.00	-23.77
Section 2	-0.04	-11.20	-0.04	-4.76
Section 3	0.28	-6.31	0.18	-1.64
Section 4	-0.08	-2.00	-0.08	-1.62
Section 5	-0.01	-7.19	0.06	-5.08
Section 6	-0.12	-19.27	0.10	-1.54
Section 7a	0.07	-2.32	-0.25	-2.14
Section 7b	-0.00	-4.71	-0.23	-4.61

From the vertical response averages in Table 4-10, the permanent deformation of each test section was determined (difference between first and last second averages) in terms of a short-term loading response. Table 4-11 presents the permanent deformation of the individual MDDs, the pavement structure as a whole (MDD001), and the base layer (MDD001 minus MDD002) all together. The base layer deformation as a percentage of the total deformation is also included.

Table 4-11: Short-term loading response per section.

	Permanent Deformation				
	MDD001 [µm]	**MDD002 [µm]**	**Total [µm]**	**Base [µm]**	**Base as % of Total**
Section 1	25.75	23.77	25.75	1.98	7.65
Section 2	11.16	4.72	11.16	6.44	57.71
Section 3	6.59	1.82	6.59	4.77	72.53
Section 4	1.92	1.54	1.92	0.38	20.31
Section 5	7.18	5.14	7.18	2.04	28.51
Section 6	19.15	1.64	19.15	17.51	91.44
Section 7a	2.39	1.89	2.39	0.50	21.11
Section 7b	4.71	4.38	4.71	0.33	7.01

For permanent deformation behaviour in terms of a longer-term recovering response, two consecutive test runs were required for analysis. However, the static MDD vertical response averages between consecutive test runs provided improbable differences in most cases; the readings implied a recovery in excess of the initial permanent deformation recorded, which is unrealistic. Only Sections 2, 3, 4, and 7a had a viable set of consecutive test runs that could be used for analysis. For Sections 3 and 7a, the original representative test runs with their respective follow-up test runs were still applicable. For Sections 2 and 4, however, alternatives had to be used.

Table 4-12 presents the longer-term recovering response for each of these four sections. The first and last second of the initial test run were used to determine the initial permanent deformation. Thereafter, the first second of the follow-up test run were used in conjunction with the last second of the initial test run to determine the amount of permanent deformation recovered as a result of the time delay between the two consecutive test runs.

Table 4-12: Longer-term recovering response per section.

	Initial Test Run		**Follow-Up Test Run**	**Permanent Deformation [µm]**	**Permanent Deformation Recovered [µm]**	**% Recovered**
	First Second [µm]	**Last Second [µm]**	**First Second [µm]**			
Section 2	1778.67	1776.33	1778.00	2.34	1.67	71.37
Section 3	0.28	-6.31	0.02	6.59	6.33	96.05
Section 4	-0.10	-1.76	-0.12	1.66	1.64	98.80
Section 7a	0.07	-3.72	0.06	3.79	3.78	99.74

4.3.2. Back-Calculated Layer Moduli

The layer moduli of each test section were back-calculated according to the method described in Chapter 3.3.2. Figure 4-10 presents the final CHEV results for Section 1. The CHEV output indicates the calculated depth deflections for the chosen set of layer moduli. Table 4-13 and Figure 4-11 illustrate the corresponding measured (from MDDs) versus calculated (from CHEV) depth deflections. The moduli back-calculation data for Sections 2 to 7 are provided in Appendix D. The back-calculated layer moduli for each section is summarised in Table 4-14 (refer to Chapter 5.3.1 for discussion).

Total Load: 45.00 kN
Tyre Pressure: 700.00 kPa
Load Radius: 143.05 mm
Wheels: {0;0}

Layer No	Modulus	Poisson Ratio	Thickness (mm)
0	3700.0	0.4	25.0
1	365.0	0.35	150.0
2	255.0	0.35	200.0
3	90.0	0.35	150.0
4	90.0	0.35	150.0

X-ordinate	Y-ordinate	Depth	Value	ZZ	XX	YY	XY	XZ	YZ	OCTSHEAR
0.0	0.0	0.0	Stress	-700.0	-2338.5697	-2338.5697	0.0	0.0	0.0	772.4292
			Strain	316.4475	-303.5519	-303.5519	0.0	0.0	0.0	
			DispIt	0.741						
0.0	0.0	160.0	Stress	-311.4115	59.6911	59.6911	0.0	0.0	0.0	174.9394
			Strain	-967.6581	404.9129	404.9129	0.0	0.0	0.0	
			DispIt	0.578						
0.0	0.0	320.0	Stress	-97.3736	57.155	57.155	0.0	0.0	0.0	72.8455
			Strain	-538.7533	279.3393	279.3393	0.0	0.0	0.0	
			DispIt	0.4519						
0.0	0.0	480.0	Stress	-47.2195	3.9555	3.9555	0.0	0.0	0.0	24.1241
			Strain	-555.4259	212.1986	212.1986	0.0	0.0	0.0	
			DispIt	0.3522						
0.0	0.0	900.0	Stress	-16.6646	0.9764	0.9764	0.0	0.0	0.0	8.3161
			Strain	-192.7572	71.859	71.859	0.0	0.0	0.0	
			DispIt	0.2155						

Figure 4-10: CHEV output for Section 1.

Table 4-13: Measured versus calculated depth deflections for Section 1.

	MDD1	MDD2	MDD3	MDD4	MDD5	Anchor
Depth [m]	0	-0.16	-0.32	-0.48	-0.90	-3.00
Measured [mm]	0.7220	0.5852	0.4677	0.3548	0.2064	0
Calculated [mm]	0.7410	0.5780	0.4519	0.3522	0.2155	0
Difference [mm]	0.0190	0.0072	0.0158	0.0026	0.0091	0

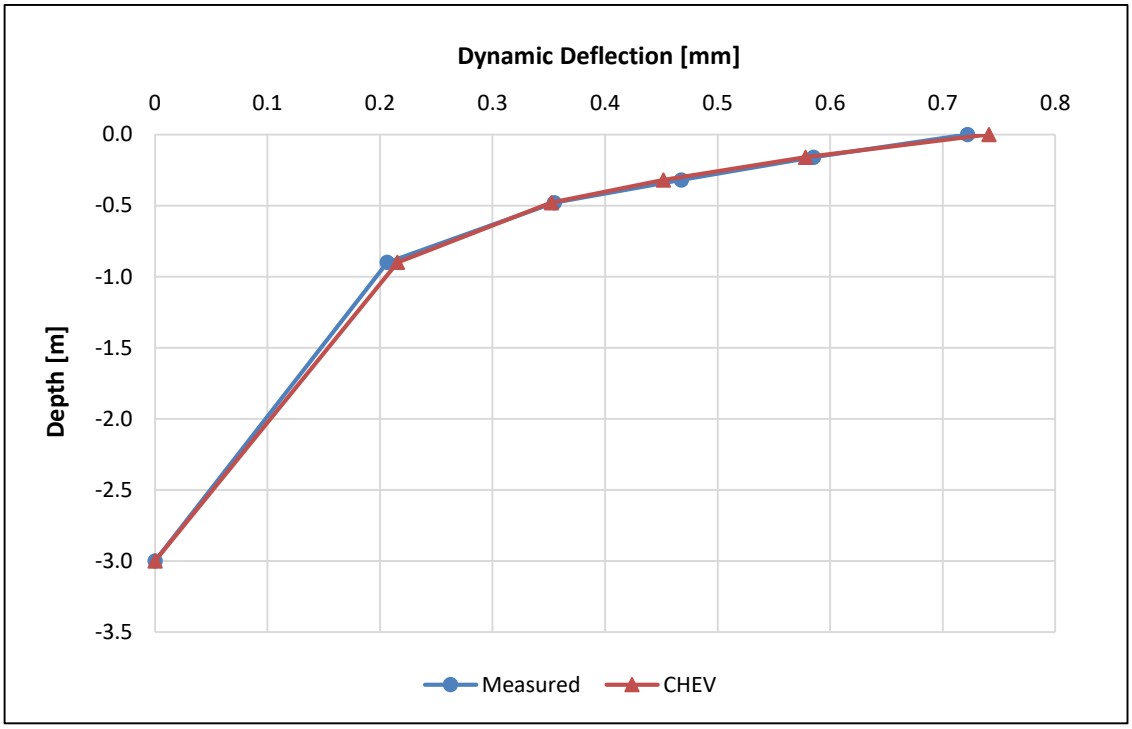

Figure 4-11: Measured versus calculated depth deflections for Section 1.

Table 4-14: Back-calculated layer moduli per section.

	Surfacing [MPa]	Base [MPa]	Subbase [MPa]	Selected [MPa]	Subgrade [MPa]
Section 1	3700	365	255	90	90
Section 2	800	320	1975	270	270
Section 3	950	600	580	580	580
Section 4	1220	1550	500	500	540
Section 5	810	950	280	280	270
Section 6	790	1150	2900	500	480
Section 7a	3150	7500	3700	750	750
Section 7b	2150	3200	2950	750	325

4.3.3. Calculated Pavement Numbers

Each pavement structure's pavement number was calculated according to the procedure described in Chapter 3.3.3. A variety of subgrade materials (G7, G9, and greater) are utilised across the entire SANRAL testing facility; however, a G8 subgrade material was assumed for all seven sections as well as moderate climatic conditions for subgrade ELTS calculation purposes. Tables 4-15 through 4-17 illustrate the results for Section 1. The pavement number data for Sections 2 to 7 are provided in Appendix E. The calculated PN values for each section is summarised in Table 4-18.

Table 4-15: Calculation of subgrade ELTS for Section 1.

Step	Data Type	Value	Source
a	Subgrade Class / Initial Stiffness	G8 / 90 MPa	Assumed / Table 4-14
b	Climate / Adjustment Factor	Moderate / 0.9	Assumed / Table 3-5
c	Cover Depth / Adjustment Factor	525 mm / -8.33 MPa	Known / Figure 3-17
d	Subgrade ELTS	(90*0.9) - 8.33 = 72.67 MPa	Calculated

Table 4-16: Calculation of ELTS for individual layers of Section 1.

Layer	Maximum Stiffness (E_{max}) & Modular Ration (MR)	Effective Long-Term Stiffness
25 mm S2 Surfacing	E_{max} = 3700 MPa, MR = 2.0	ELTS = min (3700, 2.0 x 291.6) = 583.2 MPa
150 mm G4 Base	E_{max} = 365 MPa, MR = 1.8	ELTS = min (365, 1.8 x 162) = 291.6 MPa
200 mm G5 Subbase	E_{max} = 255 MPa, MR = 1.8	ELTS = min (255, 1.8 x 90) = 162 MPa
150 mm G7 Selected	E_{max} = 90 MPa, MR = 1.7	ELTS = min (90, 1.7 x 72.67) = 90 MPa
G8 Subgrade		ELTS = 72.67 MPa (from Table 4-15)

Table 4-17: Calculation of pavement number for Section 1.

Layer	Thickness [mm]	Material Class	ELTS [MPa]	Thickness Adjustment Factor	BCF	Layer Contribution
Surfacing	25	S2	583.2	n/a	n/a	1.46
Base	150	G4	291.6	n/a	0.2	0.87
Subbase	200	G5	162	n/a	n/a	3.24
Selected	150	G7	90	n/a	n/a	1.35
Subgrade	Semi-Infinite	G8	72.67	n/a	n/a	n/a
				Pavement Number =		6.92

Table 4-18: Pavement number values per section.

	Surfacing	Base	Subbase	Selected	Total
Section 1	1.46	0.87	3.24	1.35	6.92
Section 2	1.60	0.96	8.64	4.05	15.25
Section 3	2.38	12.00	8.70	8.70	31.78
Section 4	3.05	30.00	7.50	7.50	48.05
Section 5	2.03	3.04	4.20	4.20	13.47
Section 6	3.95	17.25	6.00	7.50	34.70
Section 7a	15.75	112.50	9.00	11.25	148.50
Section 7b	10.75	32.00	5.76	9.61	58.12

4.4. Summary

A summary of the essential deformation and environmental related data for the seven flexible test sections under investigation is provided in Tables 4-19 and 4-20 respectively. An average of the overall strata readings (Tables 4-7 and 4-9) represents the moisture and density data for each section. The temperature and strata data are only applicable to the loading response data; in some cases, the recovering response data were derived from different test runs than the representative test runs. The data blacked out were not collected/calculated/available.

Table 4-19: Deformation data summary.

	Dynamic Deformation	Permanent Deformation			Pavement Number
		Loading Response		Recovering Response	
	Total	Total	Base	Total	
Section 1 (G4)	722 µm	25.75 µm	1.98 µm / 7.69%		6.92
Section 2 (G1)	415 µm	11.16 µm	6.44 µm / 57.71%	71.37%	15.25
Section 3 (FTB)	287 µm	6.59 µm	4.77 µm / 72.38%	96.05%	31.78
Section 4 (ETB)	178 µm	1.92 µm	0.38 µm / 19.79%	98.80%	48.05
Section 5 (CTB)	344 µm	7.18 µm	2.04 µm / 28.41%		13.47
Section 6 (BTB)	175 µm	19.15 µm	17.51 µm / 91.44%		34.70
Section 7a (EME150)	67 µm	2.39 µm	0.50 µm / 20.92%	99.74%	148.50
Section 7b (EME100)	140 µm	4.71 µm	0.33 µm / 7.01%		58.12

Table 4-20: Environmental related data summary.

	Temperature		Moisture Content	Dry Density
	Air	Road	Pavement Average	Pavement Average
Section 1 (G4)	27.6 °C	39.7 °C	9.85%	2150 kg/m^3
Section 2 (G1)	24.2 °C	36.5 °C	11.57%	2071 kg/m^3
Section 3 (FTB)	24.9 °C	32.3 °C	15.23%	1942 kg/m^3
Section 4 (ETB)	10.1 °C	17.0 °C	16.18%	1884 kg/m^3
Section 5 (CTB)	10.5 °C	18.2 °C	16.03%	1955 kg/m^3
Section 6 (BTB)	25.1 °C	39.0 °C		
Section 7a (EME150)	22.1 °C	31.6 °C		
Section 7b (EME100)	22.1 °C	32.1 °C		

5. DISCUSSION

5.1. Introduction

In this chapter, the data from Chapter 4 are analysed and discussed in terms of:

- The permanent deformation behaviour of the seven flexible pavement sections, and
- How well the permanent deformation behaviour of the seven flexible pavement sections relates to their structural integrity.

5.2. Permanent Deformation Behaviour

In terms of a short-term loading response, the permanent deformation behaviour (total) of the seven flexible pavements (Tables 4-19 and 4-20) follows similar trends to that of previous studies (Table 2-12 and Figure 2-44). Although the permanent deformation values (rut rates) are all much bigger than those recorded in previous studies, the permanent deformation of the different pavement structures relative to each other still corresponds with the expected behaviour to a satisfactory extent. The crushed stone (G1) base pavement performs better than the natural gravel (G4) base pavement and the ETB better than the FTB for example.

Construction of the test sections was completed in 2013 and the relevant tests done about a year and a half later. Minimal traffic (testing) had been applied to these sections prior to the relevant test dates, and the sections were still quite new at the time of testing. All seven flexible pavements were most probably still within the bedding-in phase of their permanent deformation life cycle, while the previous studies, which are all APT setups, present permanent deformation information from the plateau phase, hence the larger than expected rut rates. It should also be remembered that the rut rates from this study represent the permanent deformation for a single load application of three half-axle loads (from the TSD), while APT studies consider a single half-axle load.

The similarities between previous studies and this study are very limited. Differences in structural composition, loading conditions, environmental conditions, etc. make a direct comparison difficult and unrealistic. Therefore, a more relative approach is followed where the permanent deformation behaviour of the different flexible pavements relative to each other is more important than the actual values. That is also why this study proves to be meaningful because a variety of flexible pavements can be studied with minimum to no variation in the experimental setup. Structurally, the seven sections have a lot in common. The layerworks below the subbase are identical for all seven sections. The base layer is the only constantly changing layer between the sections, while three types of subbase layers and two different

surfacing layers are utilised across the seven sections. The sections are also within close proximity (all sections over an 800-m stretch of road) of each other, which lessens the effect of environmental factors to some extent. All seven sections are the same age and have received roughly the same amount of trafficking since construction. Loading conditions are kept the same for every test performed, which is probably one of the most important similarities. Table 5-1 provides a performance rank of the seven different flexible pavements at the SANRAL experimental site in terms of their resistance to permanent deformation (total).

Table 5-1: Permanent deformation performance rank for seven flexible pavements.

Rank	Flexible Pavement Type (Base Layer)	Section No.	Rut Rate [µm/cycle]
1	Emulsion Treated Base	Section 4	1.92
2	High Modulus Asphalt Base (150 mm)	Section 7a	2.39
	High Modulus Asphalt Base (100 mm)	Section 7b	4.71
3	Foam Treated Base	Section 3	6.59
4	Cement Treated Base	Section 5	7.18
5	Crushed Stone (G1) Base	Section 2	11.16
6	Bitumen Treated Base	Section 6	19.15
7	Natural Gravel (G4) Base	Section 1	25.75

Based on previous studies and some theoretical engineering knowledge, it can be said that, with the consideration of the environmental conditions during testing, all of the sections pretty much perform as expected; a few irregularities are present but with good reason. The following unusual observations are made:

- The BTB pavement is expected to rank towards the top of the list but only ranks sixth out of a total of seven pavements;
- The EME pavements rank among the top as expected but is expected to be more rut resistant in relation to the other pavements;
- The ETB pavement is expected to rank among the FTB and CTB pavements but instead shows impeccable performance at the top of the list, and
- The G1 pavement should rank higher up, above the BSM and CTB pavements.

It is primarily the bituminous type of pavements that show uncharacteristic behaviour. Bituminous materials are much more temperature susceptible than the rest of the materials used in flexible pavements. Due to their visco-elastic properties, they can achieve very high stiffness values at low operating temperatures, while the opposite applies when they operate at high

temperatures. This is exactly the case for Section 6 where a high pavement temperature (see Table 4-20) during testing is most probably partly responsible for the larger than expected permanent deformation; the bituminous surfacing and base accounts for more than 70% of the total permanent deformation recorded. One would argue that the grading of the BTB should play a significant role under severe temperature conditions when the bitumen becomes unable to provide much stiffness to the layer, but this is probably eliminated by the effect of post-compaction. The rut resistant EME sections (7a and 7b) also seem to be less efficient at higher pavement temperatures. Both Sections 6 and 7 have a 50-mm asphalt surfacing on top of a bituminous base; hence, the effect of temperature will certainly reflect in these sections.

Section 3 performs quite well at a relatively high pavement temperature, but the joint surfacing and base permanent deformation is in excess of 70% as well. Section 4, on the other hand, probably benefited from its low pavement temperature during testing as excellent performance is observed from this section. All of the sections are actually affected by temperature to some extent due to a bituminous surfacing layer, but the ones with bituminous bases are affected significantly more. What is interesting though, is that the BSM bases of Sections 3 and 4 follow similar trends to that of bituminous materials, while they are expected to exhibit a more granular type of behaviour instead. This can possibly be attributed to a higher than normal binder content and the relatively young age of the sections.

As mentioned before, the effects of post-compaction (large permanent deformation values) are visible in all of the sections. However, some of the sections are affected more than others. It has been known that smaller particles have a better initial density than larger particles. This phenomenon can be seen in the base layer of the respective pavement sections. Sections 2 and 6 show a large amount of base layer deformation in relation to total permanent deformation. The crushed stone (G1) base and BTB are both coarse grained materials and, due to their bigger particle sizes, are more prone to large amounts of permanent deformation initially. However, it is worth noting that the G1 base also presents a smaller than expected back-calculated stiffness (see Table 4-14), possibly due to a poor construction (slushing) process. Sections 1 and 7 show the opposite end of this phenomenon in comparison with Sections 2 and 6 respectively. The finer grained granular base of Section 1 shows much better performance and so does the fine grained (sand-skeleton) high modulus asphalt base of Section 7, even at high temperatures.

Of the three types of environmental related data, only the temperature data turn out to be useful for making inferences about the permanent deformation behaviour. Unlike the moisture and density data, the temperature data provide test-specific data at the time of testing for all seven sections. Pavement temperature is also a short-term effect (hourly for example) ideal to the single load cycle approach of this study, while moisture content and density are long-term

(seasonal for example) effects and more suiting to APT setups. However, it is still acknowledged that moisture and density may be very influential. For interest sake though, an anomaly is present in the moisture and density data. The FTB, ETB, and CTB sections show higher moisture contents than the granular pavements, which reflects in the density data as well, while they are expected to be less susceptible to moisture effects (but can be wetter).

For permanent deformation behaviour in terms of a longer-term recovery response, a very limited amount of data is available for analysis (only four sections). Despite a lack of environmental related data and base layer deformation data, a trend is still visible. As expected, the bituminous type of pavements (Sections 3, 4, and 7a) recovered more of their short-term permanent deformation between successive test runs than the granular type of pavement (Section 2). This can probably be attributed to the delayed elasticity (visco-elastic properties) of bituminous materials.

5.3. Permanent Deformation vs Structural Integrity

When the permanent deformation behaviour (total) of the seven flexible pavement sections are compared with their calculated pavement number (from dynamic MDD depth deflections), a simple pattern can be observed. There is a general tendency that a higher PN value corresponds to a smaller permanent deformation value (rut rate), which makes sense. The PN value of a pavement is a measure of its structural integrity (strength) and subsequently is an indication of its structural capacity. A higher PN value relates to a pavement that can carry a larger amount of traffic before failure. With the cumulative amount of permanent deformation as failing criteria, a smaller amount of permanent deformation per cycle must be accompanied by a larger PN value.

A power function with a R-squared value (coefficient of determination) of 0.77 is the most suitable and best fit relationship for the data (Figure 5-1). However, a better relationship is attained when using the raw dynamic MDD depth deflection data (maximum total) before PN calculation (Figure 5-2). Theyse et al. (2006) and Jordaan (2006) similarly showed that good correlations exist between the accumulated permanent deformation (rut depth) and maximum elastic deflection of a specific subgrade and two typical rural roads respectively.

For both relationships, the Section 6 data point is eliminated as a statistical outlier. This is the only data point that deviates significantly from the proposed relationship in both cases. As discussed before, this section probably shows the most uncharacteristic behaviour of all seven sections, probably due to post-compaction and high operating temperatures, but theoretically, temperature variations and post-compaction should not affect the relationship. Any difference

in deformation values should reflect in the back-calculated layer moduli and therefore the PN values as well. The reason for deviation from the relationship can possibly be attributed to an experimental error or variability in MDD measurements. This can be as a result of MDDs not installed at the correct depths, MDD modules not properly clamped to the sides of the 39-mm hole in the pavement structure, faulty MDDs, etc. The dynamic MDD depth deflection data also goes through a two-stage process (moduli back-calculation and pavement number calculation) in order to obtain the necessary PN data. Along the way, some form of accuracy and certainty is most likely lost during these procedures, which affects the fit of the relationship as well.

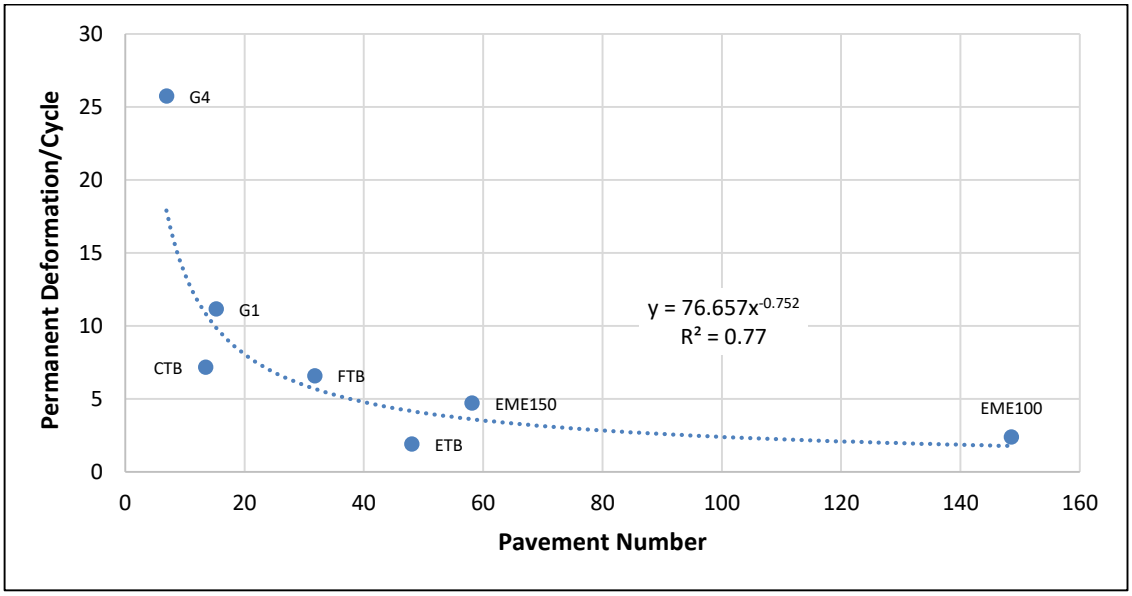

Figure 5-1: Permanent deformation per cycle vs pavement number.

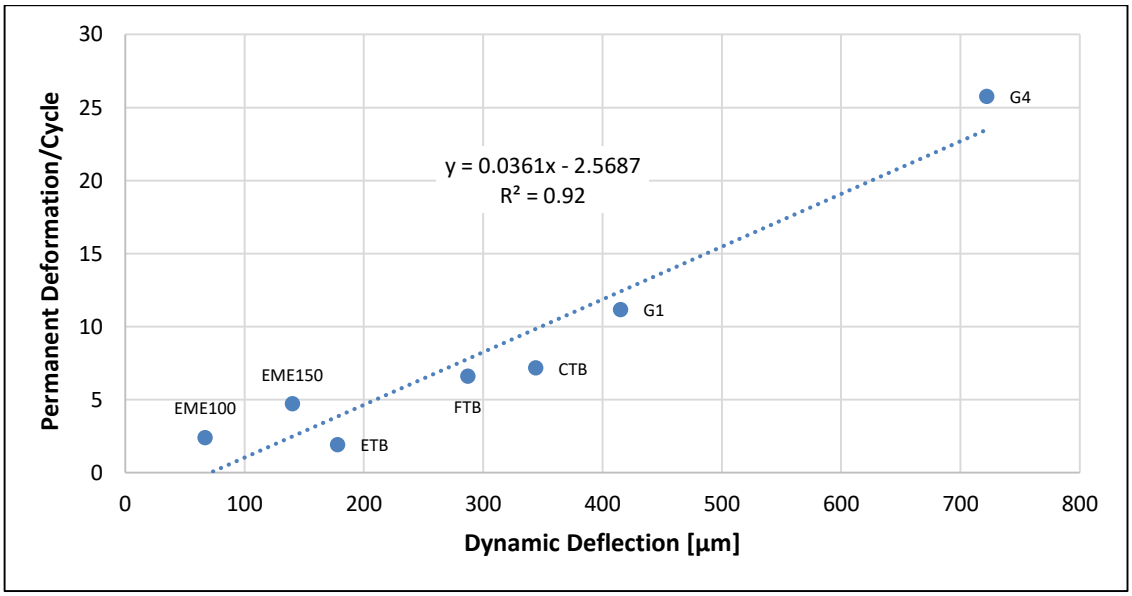

Figure 5-2: Permanent deformation per cycle vs dynamic deflection.

5.3.1. Moduli Back-Calculation

The back-calculated layer moduli from Table 4.14 illustrate the type of pavement strength distribution one would expect from each section. However, the actual stiffness values do not show complete compliance with the typical stiffness values from Table 2-10; some of them are within an acceptable range, but the majority are larger than the expected (especially the granular layers lower down in the pavement). It is only the G1 base, BTB, and Section 6 surfacing that show a lower than expected stiffness. For the bituminous type of materials, however, large variations in stiffness are possible. These materials are highly temperature susceptible; hence, the stiffness can vary, depending on the operating temperature.

Even though the quality of construction could have played a role in the layer moduli obtained, the reason for improbable moduli values can most probably be attributed to the back-calculation method itself. Although the CHEV software is the best suited software of the few computer programs considered, it has two vital limitations that can alter the results obtained. It can only simulate linear-elastic materials while the majority of pavement materials do not or do not only behave in this manner. Secondly, the software is unable to simulate a dynamic moving load for analysis. However, all three computer programs considered have these limitations.

It should be remembered that the base layer deformation actually includes the behaviour of the surfacing layer as well (see Chapter 3.3.2). The first MDD is located at the top of the surfacing layer and the second at the interface of the base and subbase layer; hence, the depth deflection at the surfacing-base interface is not measured and one less reference point is available for back-calculation purposes. The more depth deflections one can get to match, the more certain one can be of the chosen set of layer moduli. This as well as the fact that a bigger tolerance (0.02 mm instead of 0.0015 mm) is used during the iteration process (to match the calculated and measured depth deflections) can affect the accuracy of the moduli values obtained.

5.3.2. Pavement Number Calculation

Although the back-calculated layer moduli can affect the accuracy of the calculated PN values, the PN method itself can also be a contributor. The PN design method is an empirical method, suitable for new and rehabilitation design, that was originally developed for the design of bitumen stabilised layers in pavements; however, it is also applicable to granular and cemented layers but not ideal. Additionally, numerous conditions need to apply in order for the PN method to be used (see Chapter 2.9.1). The majority of the pavement layers in this study are not bituminous and all the necessary conditions for the method are assumed in order to ensure applicability of the method.

6. CONCLUSIONS AND RECOMMENDATIONS

6.1. Introduction

In this chapter, conclusions are drawn and recommendations are made based on the information in this dissertation. The study focuses on investigating and comparing the permanent deformation behaviour of a number of specific flexible pavements. Additionally, it is determined how well this behaviour relates to the structural integrity of a pavement. Therefore, two sets of conclusions are drawn, one for each focus point. Some of the conclusions may confirm existing knowledge but are highlighted once more as they are considered important for a clear understanding of some aspects regarding this study. Recommendations are made from an academic and practical standpoint for future work.

6.2. Conclusions

The following primary conclusions are drawn regarding the permanent deformation behaviour of flexible pavements:

a) Flexible pavements with different material compositions behave differently with regards to permanent deformation, regardless of the conditions under which they operate.

b) For permanent deformation behaviour in terms of a short-term loading response and under normal operating conditions, bituminous pavements show superior performance to cement/bitumen stabilised pavements, while the latter performs better than granular pavements. CTB and ETB pavements are very similar with FTB pavements closely behind. The only granular exceptions are inverted crushed stone pavements, which should closely follow bituminous pavements at the top end of the performance range.

c) For permanent deformation behaviour in terms of a longer-term recovering response, bituminous pavements tend to recover a larger amount of the permanent deformation attained after load application than granular pavements.

d) Post-compaction has a significant effect on the permanent deformation behaviour of flexible pavements during the initial stages of their life cycle.

e) Temperature variations can have a major influence on the in-situ performance and behaviour of bituminous layers in the field.

f) FTB and ETB pavements may show signs of bituminous behaviour at high and low operating temperatures even though a more granular type of behaviour is expected from them.

g) It is possible to determine the permanent deformation behaviour of a pavement by assessing the difference in static MDD readings at different locations within the pavement structure; however, this is an indicator of potential permanent deformation only. A number of limitations and constraints, which influenced the applied methodology, lead to assumptions that prevent the results to be regarded as absolute true measures of permanent deformation.

The following primary conclusions are drawn regarding how well the permanent deformation behaviour of flexible pavements relates to their structural integrity:

a) The permanent deformation behaviour of flexible pavements relates relatively well to their structural integrity as a general decrease in permanent deformation (rut rate) is observed with an increase in pavement number. A transfer function for linking permanent deformation behaviour to structural integrity is proposed as per Figure 5-1 (negative power function, $y = 76.657x^{-0.752}$, $R^2 = 0.77$).

b) The permanent deformation behaviour of flexible pavements correlates positively with the corresponding dynamic response as an increase in permanent deformation (rut rate) is observed with an increase in maximum dynamic MDD deflection (positive linear function, $y = 0.0361x - 2.5687$, $R^2 = 0.92$).

c) It is possible to determine the effective elastic moduli of different layers in a pavement structure by means of a complete set of MDD depth deflections and a multi-layered linear elastic computer program.

6.3. Recommendations

The following primary recommendations are made from an academic standpoint:

a) This exact study should be repeated in the future to avoid the possible effects of post-compaction as this has a significant impact on the permanent deformation behaviour.

b) The effect of in-situ moisture and density on the permanent deformation behaviour of flexible pavements should be investigated.

c) The effect of the transversal offset of the loading wheel from the measuring point (instrumentation) on the permanent deformation behaviour should be investigated.

d) The effect of lateral wander of the loading wheel on the permanent deformation behaviour should be investigated.

e) The effect of the time duration between consecutive load cycles on the amount of permanent deformation recovered should be investigated.

f) An alternative to the CHEV computer program that can simulate non-linear materials and dynamic moving loads should be investigated for back-calculating the layer moduli of a pavement structure.

g) A study should be performed to investigate the material behaviour and temperature susceptibility of bitumen stabilised materials with different binder contents.

The following primary recommendations are made from a practical standpoint:

a) A greater number of measuring points should be implemented along each test section to improve the certainty and credibility of measured response data. For this study, the response data from a single measuring point represented the behaviour of a 100-m-long test section.

b) From a short-term loading response point of view, the first and last second used from the test run data should be kept as close to the dynamic region (and constant) as possible to limit any delayed recovery of deformation and ensure consistency of data collection between the different test sections. For this study, the chosen interval across the dynamic zone was too long (upper and lower limits of test run data), which allowed for recovery in some instances, and varied between the different test sections.

c) From a longer-term recovering response point of view, the time delay between consecutive test run load applications should be kept as constant as possible during testing to ensure consistency of the time duration for which the recovery behaviour is evaluated. For this study, the time delay between consecutive test run load applications varied for the different test sections.

d) The quality of construction (base layer bearing capacity, stiffness, etc.) should be used to explain any anomalies present in the permanent deformation behaviour. The construction quality verifications applicable to this study were not available for analysis.

e) A more stringent tolerance and more time efficient method are recommended for the iterative matching procedure during moduli back-calculation for improved accuracy. Due to the heavily time consuming nature of the manual iterative procedure, a more lenient tolerance had to be used in this study.

7. REFERENCES

AG Peltz. (no date). *Runway Reconstruction Pensacola Regional Airport*. Available at: http://www.agpeltz.com/rcc-projects/runway-reconstruction-pensacola-regional-airport/ [Accessed: 25 April 2017].

Al-Mosawe, H. 2016. *Prediction of permanent deformation in asphalt mixtures*. PhD thesis. University of Nottingham.

American Association of State Highway and Transportation Officials (AASHTO). 1993. *AASHTO guide for design of pavement structures*. 1993 edition. Washington D.C.: AASHTO.

American Association of State Highway and Transportation Officials (AASHTO). 2004. *Guide for mechanistic-empirical design of new and rehabilitated pavement structures*. Washington D.C.: Transportation Research Board, National Research Council.

Arnold, G.K. 2004. *Rutting of granular pavements*. PhD thesis. University of Nottingham and Queens University Belfast.

Asphalt Academy. 2009. *Technical Guideline: Bitumen stabilized materials, A guideline for the design and construction of bitumen emulsion and foamed bitumen stabilized materials*. Technical Guideline 2 (TG2). 2nd edition. Pretoria, South Africa: Asphalt Academy.

Barksdale, R.D. 1972. 'Laboratory evaluation of rutting in base course materials'. *Proceedings of the 3rd international conference on the structural design of asphalt pavements*, Grosvenor House, Park Lane, London, England, 11-15 September 1972, pp. 161-174.

Battiato, G., Ronca, G. and Verga, C. 1977. 'Moving loads on a viscoelastic double layer: Prediction of recoverable and permanent deformations'. *Proceedings of the 4th international conference on the structural design of asphalt pavements*, Ann Arbor, Michigan, 22-26 August 1977, pp. 459.

Boudreau, R., Vaughan, K. and Frost, D. 2016. *Inverted Pavements.* [Webinar], *AFP70: Mineral Aggregates*. Transportation Research Board (TRB). 18 July. Available at: http://onlinepubs.trb.org/onlinepubs/webinars/160718.pdf [Accessed: 6 April 2017].

Brown, S.F. 1978. Chapter 2: Material characteristics for analytical pavement design. *Developments in highway pavement engineering.* Volume 1. Elsevier Science Ltd.

Croney, D. and Bulman, J.N. 1972. 'The influence of climatic factors on the structural design of flexible pavements'. *Proceedings of the 3rd international conference on the structural design of asphalt pavements*, Grosvenor House, Park Lane, London, England, 11-15 September 1972, pp. 67-71.

Dawson, A.R. 1990. *Introduction to soils and granular materials*. Lecture notes from residential course, bituminous pavements – materials, design and evaluation. Department of Civil Engineering, University of Nottingham.

De Beer, M., Horak, E. and Visser, A.T. 1989. 'The multidepth deflectometer (MDD) system for determining the effective elastic moduli of pavement layers'. *Nondestructive testing of pavements and backcalculation of moduli, ASTM STP 1026*. Philadelphia: American Society for Testing and Materials.

Eisenmann, J. and Hilmer, A. 1987. 'Influence of wheel load and inflation pressure on the rutting effect of asphalt pavements – Experiments and theoretical investigations'. *Proceedings of the 6th international conference on structural design of asphalt pavements*, University of Michigan, Ann Arbor, Michigan, 13-17 July 1987, pp. 392-403.

Garba, R. 2002. *Permanent deformation properties of asphalt concrete mixtures*. PhD thesis. Norwegian University of Science and Technology.

Gibb, J.M. 1996. *Evaluation of resistance to permanent deformation in the design of bituminous paving mixtures*. PhD thesis. University of Nottingham.

Gonzalez, A., Cubrinovski, M., Pidwerbesky, B. and Alabaster, D. 2009. 'Full scale experiment on foam bitumen pavements in CAPTIF accelerated testing facility'. *Proceedings of the 88th annual meeting of the transportation research board*, Washington D.C., United States, 11-15 January 2009.

Greenwood Engineering. 2017. *Traffic Speed Deflectometer*. Available at: https://www.greenwood.dk/tsd.php [Accessed: 5 May 2017].

Haynes, J.H. and Yoder, E.J. 1963. *Effects of repeated loading on gravel and stone base course materials used in the AASHO road test*. Highway Research Record 39.

Hicks, R.G. and Monismith, C.L. 1971. *Factors influencing the resilient properties of granular materials*. Highway Research Record 345, pp. 15-31. Washington D.C.: Highway Research Board.

Holubec, I. 1969. *Cyclic creep of granular materials*. Ontario: Department of Highways. (Report no. RR147)

Horak, E. and Rust, F.C. 1992. 'The performance and behaviour of bitumen emulsion treated road bases in South Africa'. *Proceedings of the 7th international conference on asphalt pavements*, Nottingham, United Kingdom, August 1992.

Horak, E., Hefer, A. and Maina, J.W. 2015. 'Determination of pavement number for flexible pavements using FWD deflection bowl information'. *Paper presented at the 34th annual Southern African Transport Conference (SATC),* CSIR International Convention Centre, Pretoria, South Africa, 6-9 July 2015, pp. 187-200.

InstroTek. (no date). *MC-S-24 Operating Manual*. Available at: https://www.instrotek.com/pages/downloads#product-manuals [Accessed: 18 May 2017].

Jordaan, G.J. 2006. 'Practical approach to pavement rehabilitation investigations and design'. 1st edition. Pretoria, South Africa.

Kleyn, E. and Steyn, W.J.vdM. 2010. 'Utilizing traffic molding of pavement sublayers towards more cost efficient pavement design and management'. *International Journal of Pavements (IJP)*, 9(1-2-3), pp. 14-24.

Kleyn, E. 2012. 'Successful G1 crushed stone basecourse construction'. *Abstracts of the 31st annual Southern African Transport Conference (SATC)*, CSIR International Convention Centre, Pretoria, South Africa, 9-12 July 2012, pp. 110-118.

Kleyn, E. and Steyn, W.J.vdM. 2015. 'Towards composing an ideal flexible pavement'. *Proceedings of the 11th Conference on Asphalt Pavements for South Africa (CAPSA)*, Sun City, South Africa, 16-19 August 2015.

Krarup, J. 2012. *Measuring systems for infrastructure, for roads, and for railroads*. [PowerPoint Presentation]. Available at: ftp://ftp.greenwood.dk/tsd/pdf/tsd_fwdusersgroup 2012.pdf [Accessed: 5 May 2017].

Kolisoja, P. and Dawson, A. 2004. *Permanent deformation*. Unpublished report for ROADEX Northern Periphery II. (Report on Task 2.1, October 2004)

Korkiala-Tanttu, L. 2009. *Calculation method for permanent deformation of unbound pavement materials*. PhD dissertation. Helsinki University of Technology.

Lekarp, F. 1999. *Resilient and permanent deformation behaviour of unbound aggregates under repeated loading*. PhD thesis. Kungliga Tekniska Högskolan, Royal Institute of Technology, Stockholm, Sweden.

Metcalf, J.B. 1996. *Synthesis of Highway Practice 235: Application of full-scale accelerated pavement testing*. Washington D.C.: Transportation Research Board, National Research Council.

Metcalf, J.B., Romanoschi, S.A., Li, Y. and Rasoulian, M. 1999. 'The first full-scale accelerated pavement test in Louisiana: Development and findings'. *Proceedings of the 1st international conference on accelerated pavement testing*, Reno, Nev., 18-20 October 1999.

Muniandy, R., Aburkaba, E. and Thamer, N. 2013. 'Comparison of flexible pavement performance using Kenlayer and Chev PC software program'. *Australian Journal of Basic and Applied Sciences*, 7(9), pp. 112-119.

Nkgapele, M., Denneman, E. and Anochie-Boateng, J.K. 2012. 'Construction of a high modulus asphalt (HiMA) trial section Ethekwini: South Africa's first practical experience with design, manufacturing and paving of HiMA'. *Paper presented at the 31st annual Southern African Transport Conference (SATC)*, CSIR International Convention Centre, Pretoria, South Africa, 9-12 July 2012, pp. 396-407.

Pavement Interactive. 2012a. *Asphalt Concrete Base (ACB)*. Available at: http://www.pavementinteractive.org/pavement-typesasphalt-concrete-base-acb/ [Accessed: 29 April 2017].

Pavement Interactive. 2012b. *HMA Pavement*. Available at: http://www.pavementinteractive.org/hma-pavement/ [Accessed: 29 April 2017].

Perret, J., Dumont, A.G. and Turtschy, J.C. 2004. 'Assessment of resistance to rutting of high modulus bituminous mixtures using full-scale accelerated loading tests'. *Proceedings of the 3rd Eurasphalt & Eurobitume congress*, Vienna, Austria, 22 May 2004.

Rohde, L., Ceratti, J.A.P., Núñez, W.P. and Vitorello, T. 2008. 'Using APT and laboratory testing to evaluate the performance of high modulus asphalt concrete for base courses in Brazil'. *Proceedings of the 3rd international conference on accelerated pavement testing*, Madrid, Spain, 1-3 October 2008.

Romanoschi, S.A., Hossain, M., Gisi, A. and Heitzmann, M. 2004. 'Accelerated pavement testing evaluation of the structural contribution of full-depth reclamation material when stabilized with foamed asphalt'. *Journal of the Transportation Research Board*, No. 1896, pp. 199-207.

Scullion, T., Uzan, J., Yazdani, J.I. and Chan, P. 1988. *Field evaluation of the multi-depth deflectometers*. College Station, Texas: The Texas A&M University, Texas Transportation Institute. (Interim Research Report 1123-2)

Steyn, W.J.vdM., De Beer, M. and Visser, A.T. 1997. 'Thin asphalt and double seal rehabilitated lightly cemented pavements: Evaluation of structural behaviour and life cycle costs'. *Proceedings of the 8th international conference on asphalt pavements*, Seattle, Washington, 10-14 August 1997.

Steyn, W.J.vdM. 2001. *Considerations of vehicle-pavement interaction for pavement design*. PhD thesis. University of Pretoria.

Steyn, W.J.vdM., Denneman, E. and Mahlangu, S. 2008. 'A comparison between the permanent deformation behaviour of a standard and a rut resistant HMA mix'. *Paper presented at the 27th annual Southern African Transport Conference (SATC),* CSIR International Convention Centre, Pretoria, South Africa, 7-11 July 2008.

Steyn, W.J.vdM. and Denneman, E. 2008. 'Simulation of temperature conditions on ATP of HMA mixes'. *Proceedings of the 3rd international conference on accelerated pavement testing*, Madrid, Spain, 1-3 October 2008.

Steyn, W.J.vdM. 2012. *Synthesis of Highway Practice 433: Significant findings from full-scale accelerated pavement testing*. Washington D.C.: Transportation Research Board, National Research Council.

Steyn, W.J.vdM. and Coetzer, S. 2015. *Revision of the South African Pavement Design Method: SAPDM/C-2 A benchmark of measured stresses and strains collected on a variety of pavements for various loads: Weather, temperature and moisture data*. Unpublished report for the South African National Roads Agency Ltd, Pretoria. (Draft contract report SANRAL/SAPDM/C-2/2015-01)

Steyn, W.J.vdM., Mshali, M. and Coetzer, S. 2016. *Revision of the South African Pavement Design Method: SAPDM/C-2 A benchmark of measured stresses and strains collected on a variety of pavements for various loads: Data report R104 December 2015*. Unpublished report for the South African National Roads Agency Ltd, Pretoria. (Draft contract report SANRAL/SAPDM/C-2/2016-01)

Taherkhani, H. 2006. *Experimental characterisation of the compressive permanent deformation behaviour in asphaltic mixtures*. PhD thesis. University of Nottingham.

The South African National Roads Agency Ltd (SANRAL). 2014. *South African Pavement Engineering Manual.* 2nd edition. South Africa: SANRAL.

Theyse, H.L. 1997. *Permanent deformation and in-depth deflection records for selected HVS tests*. Unpublished report for STEP. (Technical Report TR-97/004)

Theyse, H.L. 1999. 'Accelerated pavement and laboratory testing of materials suited to labour-intensive road construction'. *Proceedings of the 1st international conference on accelerated pavement testing*, Reno, Nev., 18-20 October 1999.

Theyse, H.L., Hoover, T.P., Harvey, J.T., Monismith, C.L. and Coetzee, N.F. 2006. 'A mechanistic-empirical subgrade design model based on Heavy Vehicle Simulator test results'. *Geotechnical Special Publication No. 154*. Reston, VA: American Society of Civil Engineers.

Theyse, H.L., Legge, F.T.H., Pretorius, P.C. and Wolff, H. 2007. 'A yield strength model for partially saturated unbound granular material'. *Road Materials and Pavement Design*, 8(3), pp. 423-448.

Theyse, H.L., De Beer, M., Maina, J.W. and Kannemeyer, L. 2011. 'Interim revision of the South African mechanistic-empirical pavement design method for flexible pavements'. *Proceedings of the 10th Conference on Asphalt Pavements for South Africa (CAPSA)*, Champagne Sports Resorts, KwaZulu-Natal, South Africa, 11-14 September 2011.

Thom, N.H. and Brown, S.F. 1987. 'Effect of moisture on the structural performance of a crushed-limestone road base'. *Proceedings of the 66th annual meeting of the transportation research board*, Washington D.C., United States, 12-15 January 1987, pp. 50-56. Washington D.C.: Transportation Research Board. (Transportation Research Record 1121)

TRH14. 1985. *Guidelines for road construction materials.* Pretoria: Department of Transport. (Technical Recommendations for Highways; TRH14)

TRH13. 1986. *Cement stabilizers in road construction.* Draft. Pretoria: Department of Transport. (Technical Recommendations for Highways; TRH13)

TRH8. 1987. *Design and use of hot-mix asphalt in pavements.* Draft. Pretoria: Department of Transport. (Technical Recommendations for Highways; TRH8)

TRH4. 1996. *Structural design of flexible pavements for interurban and rural roads.* Draft. Pretoria: Department of Transport. (Technical Recommendations for Highways; TRH4)

Uthus, L. 2007. *Deformation properties of unbound granular aggregates*. PhD thesis. Norwegian University of Science and Technology.

Van der Merwe, C.J., Theyse, H.L., Horak, E., Hugo, F. and Du Plessis, H.A. 1992. 'Evaluation of the rehabilitation design of a BTB pavement and the effects of artificial ageing using accelerated wheel load testing'. *Proceedings of the 7th international conference on asphalt pavements*, Nottingham, United Kingdom, August 1992.

Wang, H. 2011. *Analysis of tire-pavement interaction and pavement responses using a decoupled modelling approach*. PhD dissertation. University of Illinois at Urbana-Champaign.

Wu, Z., Chen, X., Mohammad, L.N. and Zhang, Z. 2009. 'Field performance of stabilized blended calcium sulfate materials under accelerated pavement testing'. *Proceedings of the 88th annual meeting of the transportation research board*, Washington D.C., United States, 11-15 January 2009.

Werkmeister, S. 2003. *Permanent deformation behaviour of unbound granular materials in pavement constructions*. PhD dissertation. Dresden University of Technology.

Zofka, A. and Sudyka, J. 2015. 'Traffic speed deflectometer (TSD) measurements for pavement evaluation'. *International symposium on Non-Destructive Testing in Civil Engineering (NDT-CE),* Berlin, Germany*,* 15-17 September 2015.

8. APPENDICES

8.1. Appendix A: MDD Data

Appendix A provides the MDD data for Sections 2 to 7. Figures 8-1 to 8-7 present the time-deflection plots for Sections 2 to 7b respectively. Each plot illustrates the five quasi-continuous deflection basins from the trail axle load of the TSD for the respective test section. The necessary MDD rearrangements have already been made, but the dynamic deflections for the malfunctioning MDDs have yet to be assumed. This is done prior to the moduli back-calculation procedure.

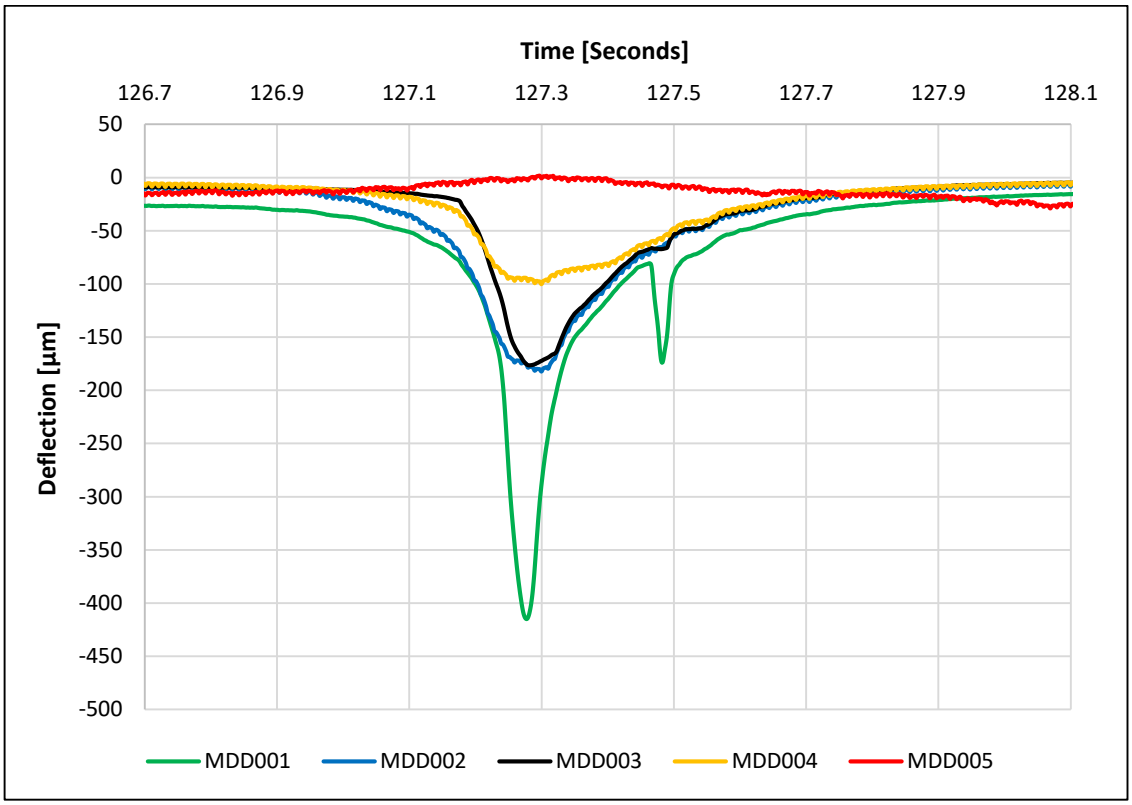

Figure 8-1: Measured MDD deflections from Section 2.

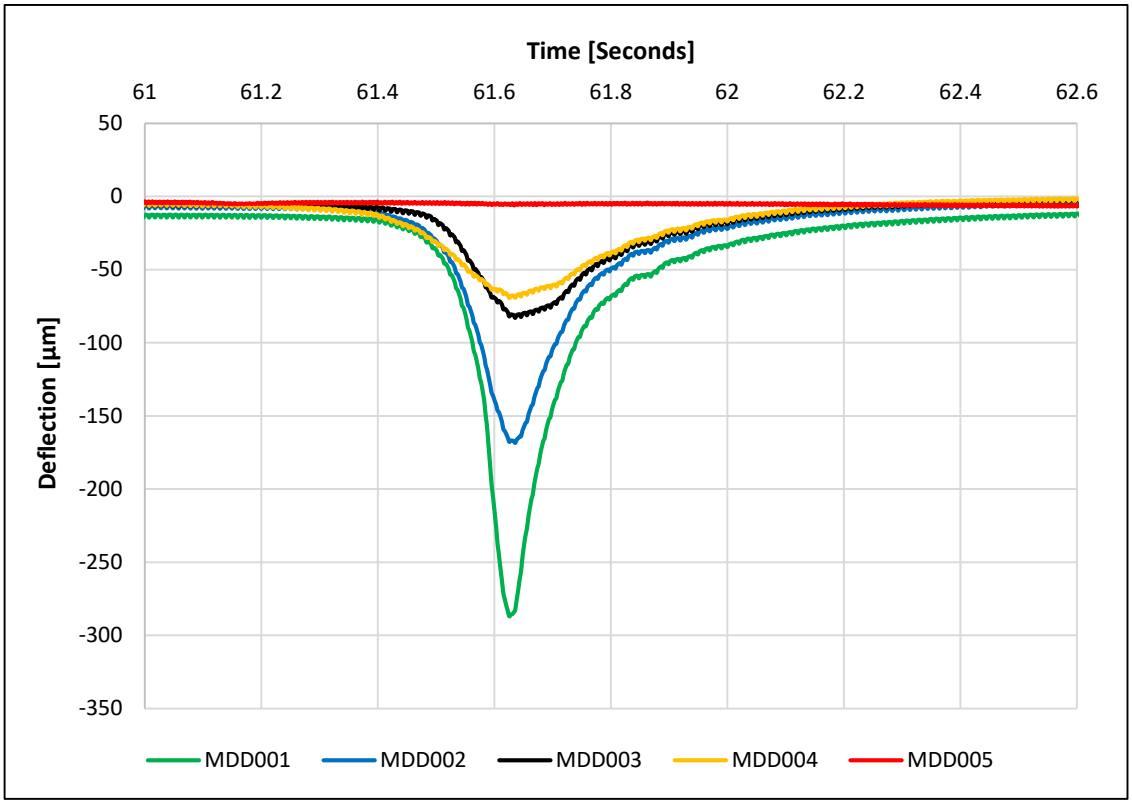

Figure 8-2: Measured MDD deflections from Section 3.

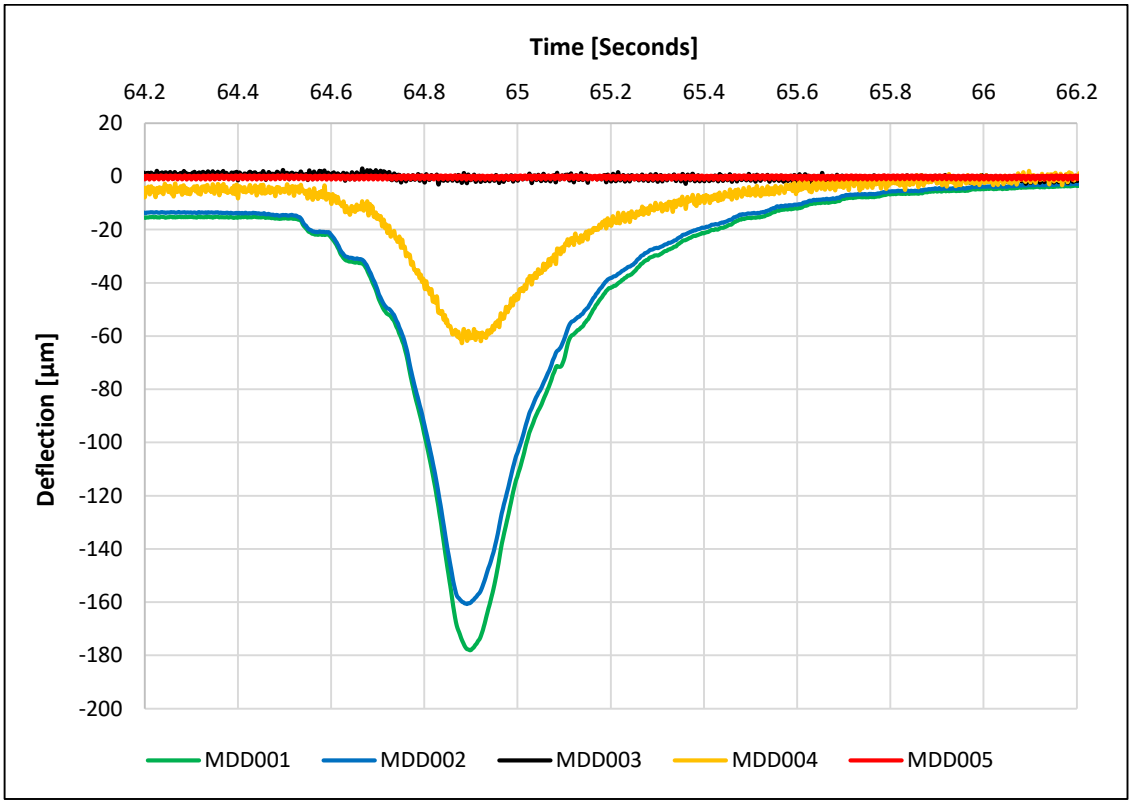

Figure 8-3: Measured MDD deflections from Section 4.

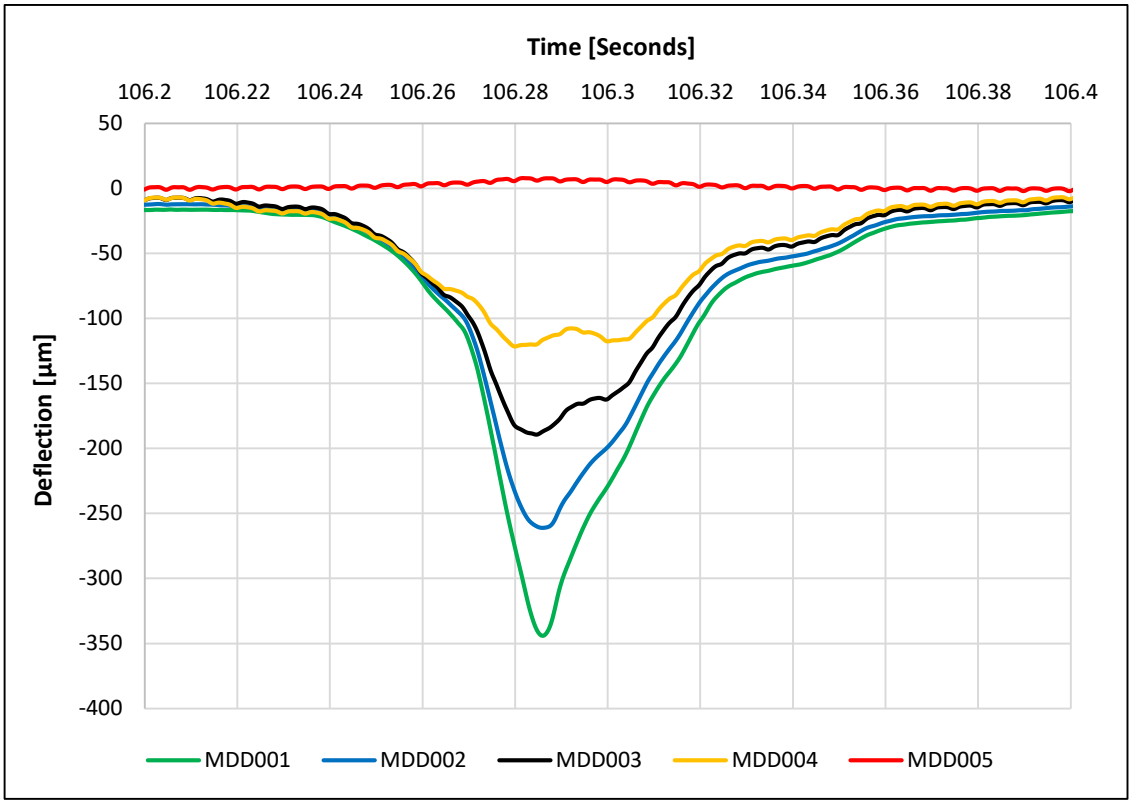

Figure 8-4: Measured MDD deflections from Section 5.

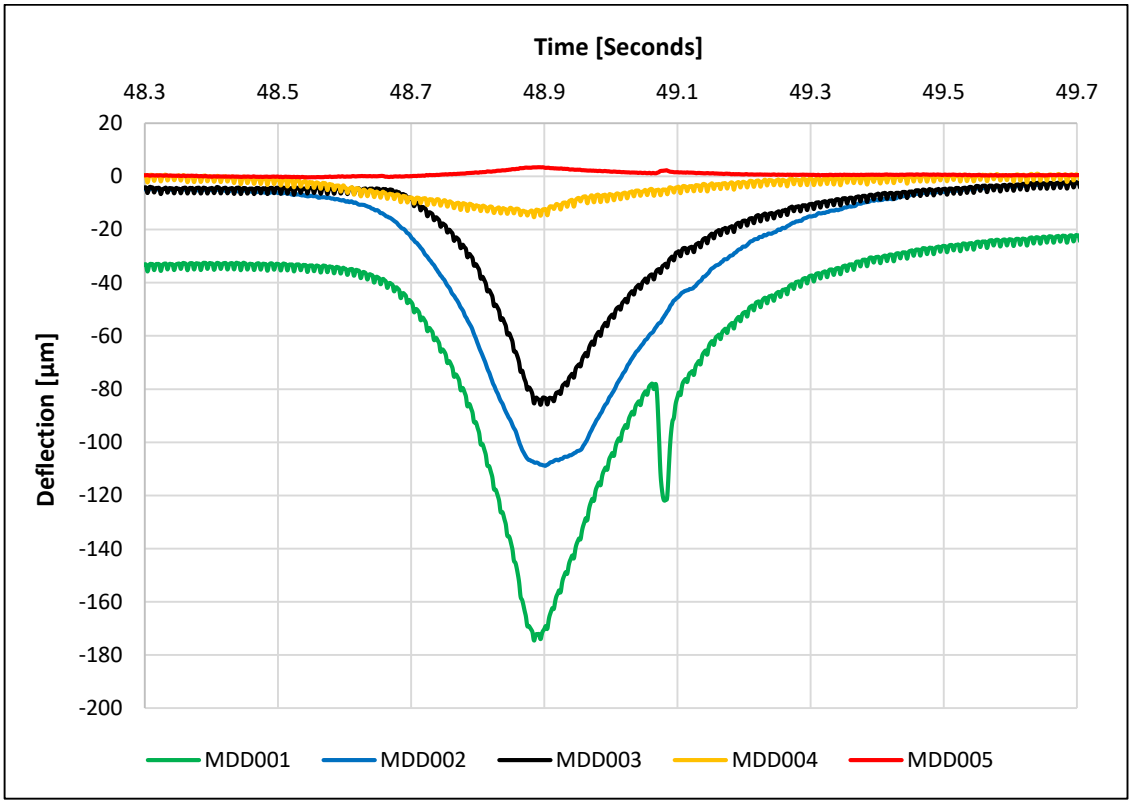

Figure 8-5: Measured MDD deflections from Section 6.

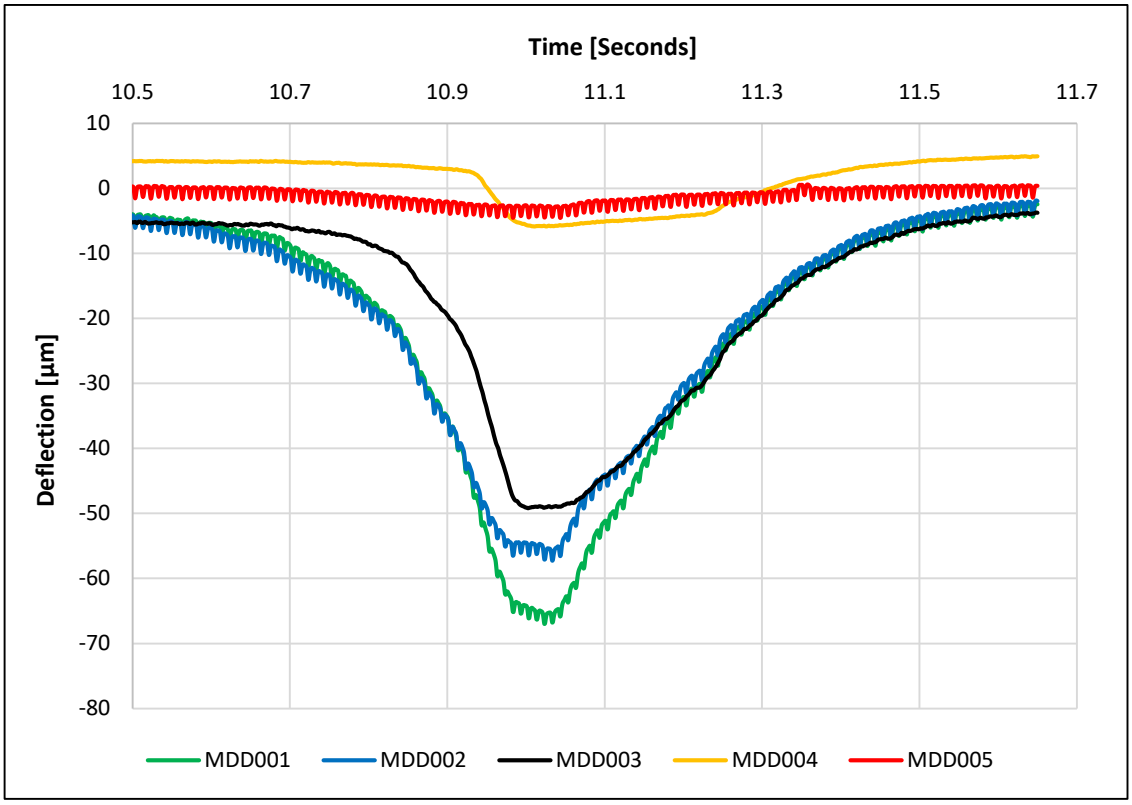

Figure 8-6: Measured MDD deflections from Section 7a.

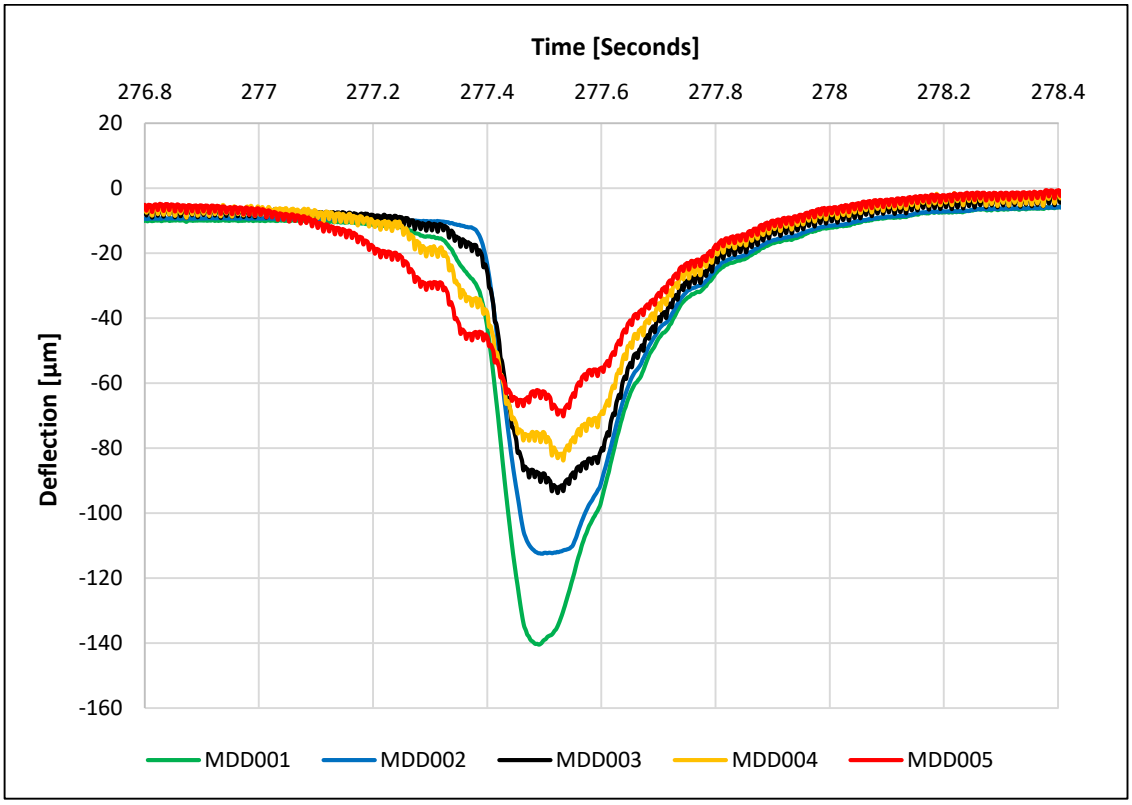

Figure 8-7: Measured MDD deflections from Section 7b.

8.2. Appendix B: Moisture Data

Appendix B provides the moisture data for Sections 2 to 5. Tables 8-1 to 8-4 present the moisture content with depth (for eight measuring dates) of Sections 2 to 5 respectively. Figures 8-8 through 8-11 illustrate the corresponding moisture content with depth plots.

Table 8-1: Section 2 moisture content with depth.

Depth [mm]	27-Sep 2013 [%]	24-Oct 2013 [%]	19-Dec 2013 [%]	11-Feb 2014 [%]	03-Jul 2014 [%]	30-Oct 2014 [%]	15-Apr 2015 [%]	31-Jul 2015 [%]
50	3.79	3.99	4.40	4.47	3.21	3.06	5.45	3.90
100	3.61	3.74	3.95	3.88	3.80	3.66	4.57	4.02
150	4.48	5.12	5.52	5.30	5.18	5.00	5.33	5.48
200	6.99	7.84	8.22	7.76	7.44	7.50	5.75	7.90
250	9.99	10.47	11.12	11.19	10.85	10.56	11.20	10.72
300	12.62	13.02	13.62	13.23	13.49	13.33	13.85	13.80
350	13.03	13.48	14.16	13.86	13.40	13.73	14.18	14.32
400	11.76	12.48	14.48	13.00	12.30	13.09	12.78	12.76
450	12.66	13.91	15.32	14.95	13.35	13.82	14.03	14.34
500	14.48	15.67	17.17	16.42	15.24	16.65	16.28	15.68
550	16.02	18.34	19.18	18.68	16.84	18.83	18.12	17.49
600	17.77	19.51	20.81	20.23	19.01	20.42	19.95	19.48

Table 8-2: Section 3 moisture content with depth.

Depth [mm]	27-Sep 2013 [%]	24-Oct 2013 [%]	19-Dec 2013 [%]	11-Feb 2014 [%]	03-Jul 2014 [%]	30-Oct 2014 [%]	15-Apr 2015 [%]	31-Jul 2015 [%]
50	12.92	10.89	12.25	13.63	12.10	12.30	13.47	12.61
100	11.25	11.07	13.15	12.78	12.99	11.56	13.40	14.09
150	13.15	13.54	15.26	14.27	14.52	13.84	14.76	14.89
200	14.05	14.51	17.56	14.64	14.43	14.74	15.43	14.87
250	13.63	14.05	16.33	14.61	14.18	13.74	14.41	14.72
300	12.60	14.18	15.75	14.72	13.75	14.36	14.11	14.47
350	14.56	16.02	17.14	16.38	15.68	16.17	17.00	16.73
400	15.58	16.08	17.75	17.14	17.65	17.30	18.05	17.97
450	15.37	15.98	18.26	17.14	16.12	17.16	17.04	16.80
500	14.81	16.23	18.62	17.03	16.43	16.46	16.61	17.00
550	14.85	16.37	17.98	16.78	16.26	16.13	16.52	16.76
600	14.34	16.90	18.42	16.67	15.95	16.41	16.70	16.30

Table 8-3: Section 4 moisture content with depth.

Depth [mm]	27-Sep 2013 [%]	24-Oct 2013 [%]	19-Dec 2013 [%]	11-Feb 2014 [%]	03-Jul 2014 [%]	30-Oct 2014 [%]	15-Apr 2015 [%]	31-Jul 2015 [%]
50	10.06	9.93	10.87	11.72	9.78	11.36	10.82	10.73
100	9.80	10.11	11.51	11.42	10.73	10.69	13.50	11.98
150	12.74	13.31	14.34	13.80	13.98	11.23	14.51	13.84
200	13.69	15.29	15.42	14.84	15.25	15.10	15.83	15.70
250	15.38	15.76	16.99	16.03	16.37	16.25	17.22	16.86
300	15.31	15.41	16.87	16.65	15.95	16.68	16.90	16.74
350	15.58	17.01	17.87	17.49	16.71	17.27	17.72	17.30
400	16.22	18.09	18.91	18.76	17.71	18.46	18.48	18.44
450	15.96	19.99	18.36	19.28	17.77	17.11	17.93	17.90
500	17.79	20.98	19.56	20.39	18.46	18.69	19.16	19.03
550	17.40	19.59	19.12	20.54	18.60	18.25	19.60	19.20
600	17.74	20.11	18.84	20.83	18.46	19.22	20.52	19.81

Table 8-4: Section 5 moisture content with depth.

Depth [mm]	27-Sep 2013 [%]	24-Oct 2013 [%]	19-Dec 2013 [%]	11-Feb 2014 [%]	03-Jul 2014 [%]	30-Oct 2014 [%]	15-Apr 2015 [%]	31-Jul 2015 [%]
50	8.53	9.05	11.21	12.03	10.48	12.30	12.35	10.84
100	9.02	10.08	11.40	11.08	10.72	11.51	12.76	13.29
150	11.11	13.20	14.88	13.65	13.68	13.81	14.36	14.05
200	12.00	14.13	15.79	14.81	13.85	15.17	14.98	14.99
250	12.58	14.43	16.75	15.26	14.36	15.31	14.77	14.53
300	13.48	15.61	17.08	16.01	15.24	16.32	15.74	15.81
350	15.06	16.50	18.87	17.78	17.02	17.34	17.33	17.68
400	16.32	17.66	20.03	18.28	18.23	18.57	18.13	18.17
450	16.64	19.01	20.37	18.63	17.86	19.74	19.10	18.46
500	16.79	18.09	20.20	18.41	17.98	19.32	18.83	18.66
550	17.10	19.07	19.84	17.49	18.51	19.89	18.34	18.99
600	18.67	21.47	22.45	19.59	19.20	21.67	20.35	20.80

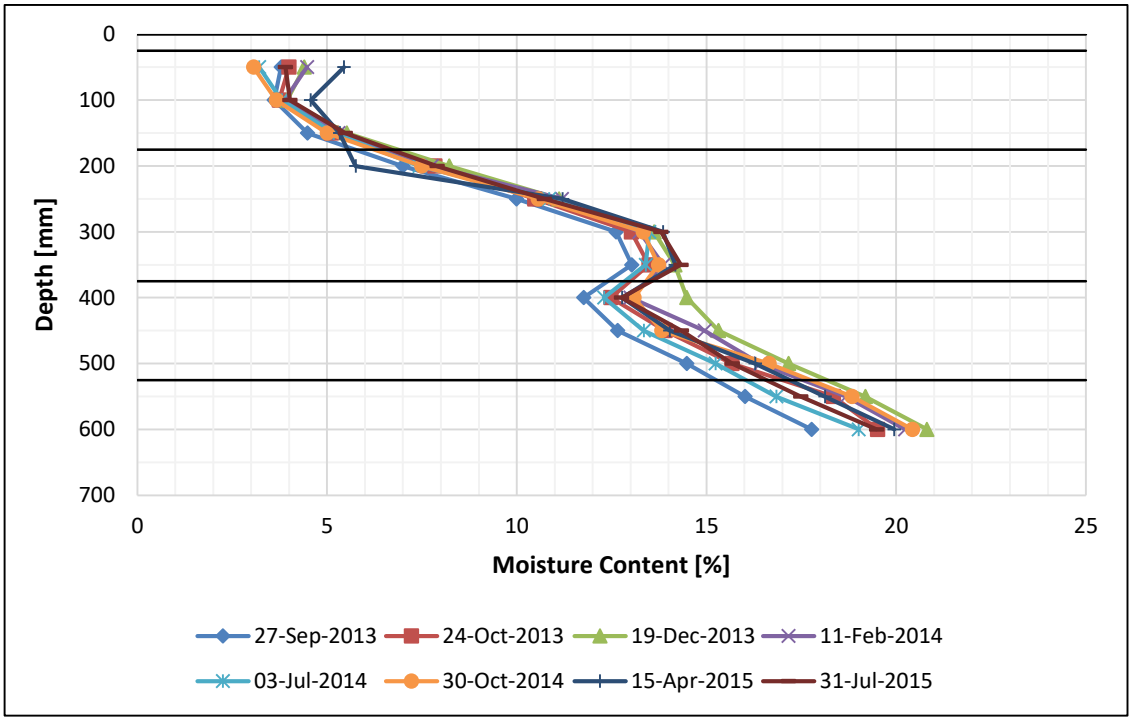

Figure 8-8: Section 2 moisture content with depth.

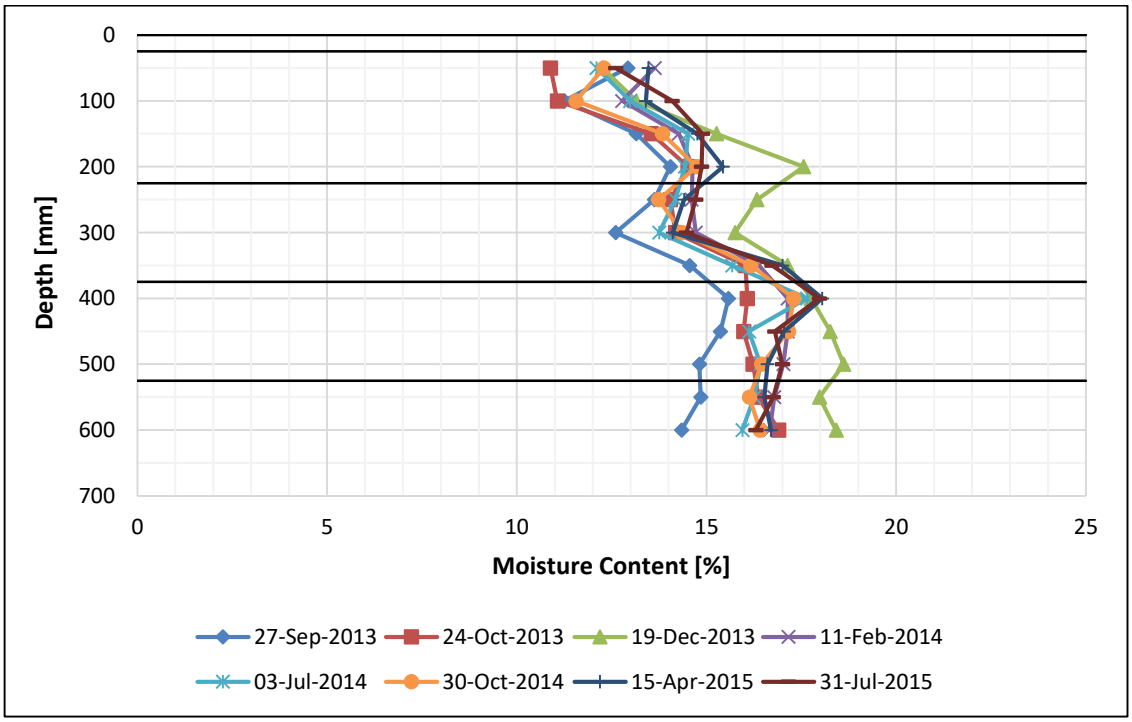

Figure 8-9: Section 3 moisture content with depth.

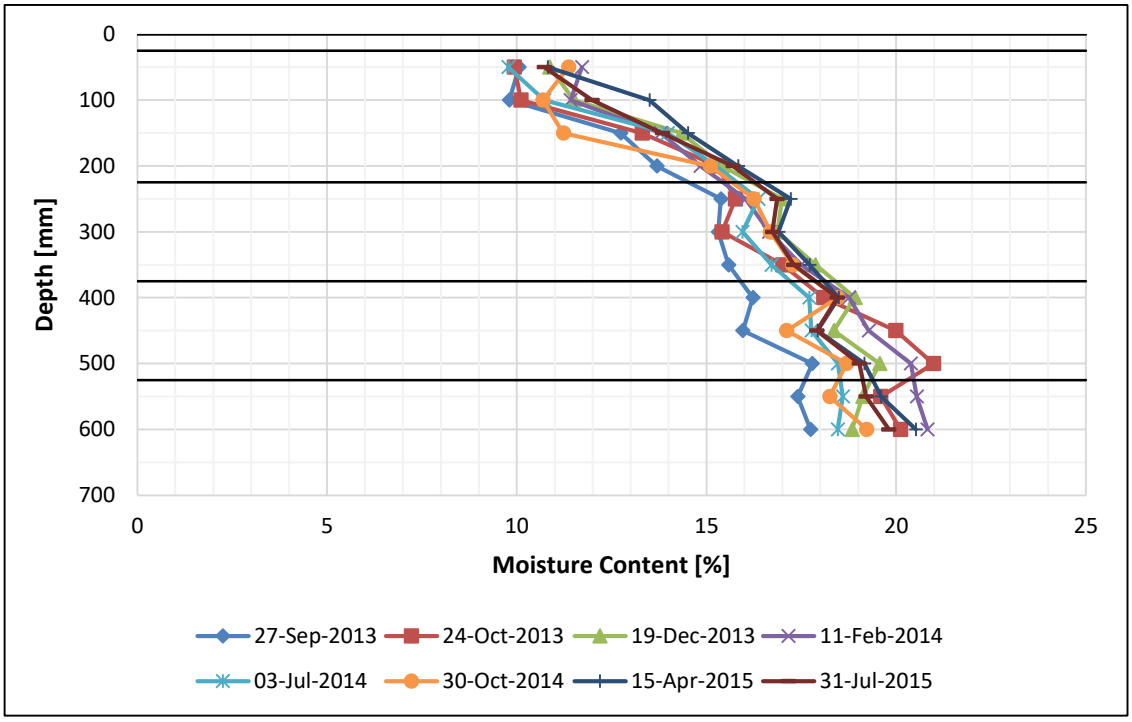

Figure 8-10: Section 4 moisture content with depth.

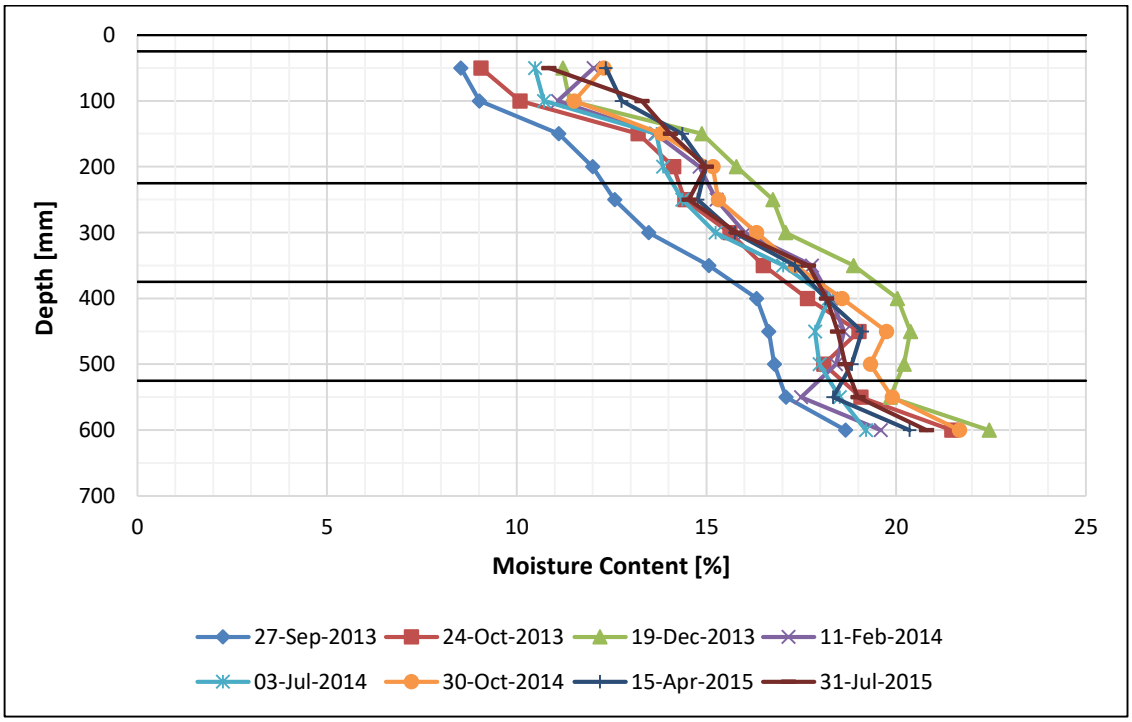

Figure 8-11: Section 5 moisture content with depth.

8.3. Appendix C: Density Data

Appendix C provides the density data for Sections 2 to 5. Tables 8-5 to 8-8 present the dry density with depth (for eight measuring dates) of Sections 2 to 5 respectively. Figures 8-12 through 8-15 illustrate the corresponding dry density with depth plots.

Table 8-5: Section 2 dry density with depth.

Depth [mm]	27-Sep 2013 [kg/m^3]	24-Oct 2013 [kg/m^3]	19-Dec 2013 [kg/m^3]	11-Feb 2014 [kg/m^3]	03-Jul 2014 [kg/m^3]	30-Oct 2014 [kg/m^3]	15-Apr 2015 [kg/m^3]	31-Jul 2015 [kg/m^3]
50	2269	2279	2272	2303	2305	2319	2295	2333
100	2411	2409	2433	2374	2392	2375	2342	2389
150	2386	2326	2355	2340	2337	2339	2345	2317
200	2259	2168	2165	2243	2205	2188	2225	2191
250	2122	2110	2087	2064	2101	2121	2080	2126
300	1926	1951	1946	1965	1927	1973	1949	1928
350	1880	1884	1892	1890	1866	1886	1848	1836
400	2024	2003	1954	2016	2016	1994	2019	2014
450	1967	1963	1965	1953	1978	1968	1974	1939
500	1975	1959	1905	1937	1962	1940	1904	1945
550	1948	1908	1913	1927	1918	1922	1876	1933
600	1880	1871	1860	1893	1862	1885	1850	1853

Table 8-6: Section 3 dry density with depth.

Depth [mm]	27-Sep 2013 [kg/m^3]	24-Oct 2013 [kg/m^3]	19-Dec 2013 [kg/m^3]	11-Feb 2014 [kg/m^3]	03-Jul 2014 [kg/m^3]	30-Oct 2014 [kg/m^3]	15-Apr 2015 [kg/m^3]	31-Jul 2015 [kg/m^3]
50	1950	1975	1984	1966	1975	1960	1990	1999
100	2008	2069	2000	2035	1971	2033	1985	1937
150	1894	1890	1874	1878	1860	1886	1877	1880
200	1737	1723	1737	1749	1753	1730	1704	1742
250	1908	1943	1917	1910	1897	1958	1936	1896
300	2071	2031	1987	1991	2065	2027	2048	2038
350	1951	1947	1984	1941	1945	1973	1929	1955
400	1932	1916	1915	1937	1887	1919	1878	1875
450	1985	2015	1966	1972	1991	1987	1942	1970
500	1978	1935	1950	1950	1936	1969	1987	1959
550	1987	1992	1980	1978	1956	1959	1985	1957
600	1994	1988	1971	1968	1988	1974	2000	1988

Table 8-7: Section 4 dry density with depth.

Depth [mm]	27-Sep 2013 [kg/m^3]	24-Oct 2013 [kg/m^3]	19-Dec 2013 [kg/m^3]	11-Feb 2014 [kg/m^3]	03-Jul 2014 [kg/m^3]	30-Oct 2014 [kg/m^3]	15-Apr 2015 [kg/m^3]	31-Jul 2015 [kg/m^3]
50	2077	2074	2070	2065	2117	2103	2098	2107
100	2142	2156	2103	2128	2172	2114	2037	2078
150	1994	1969	1994	1993	1995	2048	1964	2002
200	1950	1858	1907	1920	1882	1907	1863	1866
250	1853	1903	1872	1878	1827	1858	1812	1821
300	1881	1947	1915	1886	1931	1906	1882	1864
350	1893	1893	1852	1858	1873	1847	1840	1850
400	1837	1841	1787	1818	1841	1804	1807	1800
450	1861	1806	1841	1800	1829	1823	1852	1804
500	1754	1730	1738	1766	1771	1755	1748	1750
550	1764	1720	1747	1728	1737	1748	1709	1708
600	1798	1780	1789	1767	1804	1753	1735	1757

Table 8-8: Section 5 dry density with depth.

Depth [mm]	27-Sep 2013 [kg/m^3]	24-Oct 2013 [kg/m^3]	19-Dec 2013 [kg/m^3]	11-Feb 2014 [kg/m^3]	03-Jul 2014 [kg/m^3]	30-Oct 2014 [kg/m^3]	15-Apr 2015 [kg/m^3]	31-Jul 2015 [kg/m^3]
50	2111	2132	2105	2054	2100	2041	2065	2103
100	2174	2133	2141	2102	2137	2128	2069	2031
150	1981	1955	1956	1992	1966	2013	1971	1943
200	1984	1946	1957	1944	1949	1945	1936	1928
250	2027	2024	1958	2018	2005	2005	2045	2009
300	2018	1979	1961	1992	2028	1973	1982	1974
350	1992	1970	1897	1918	1951	1938	1933	1889
400	1924	1897	1872	1876	1882	1885	1875	1877
450	1887	1867	1870	1868	1887	1869	1848	1891
500	1888	1929	1861	1863	1880	1915	1864	1849
550	1901	1909	1920	1938	1912	1900	1936	1880
600	1859	1826	1813	1868	1875	1855	1862	1870

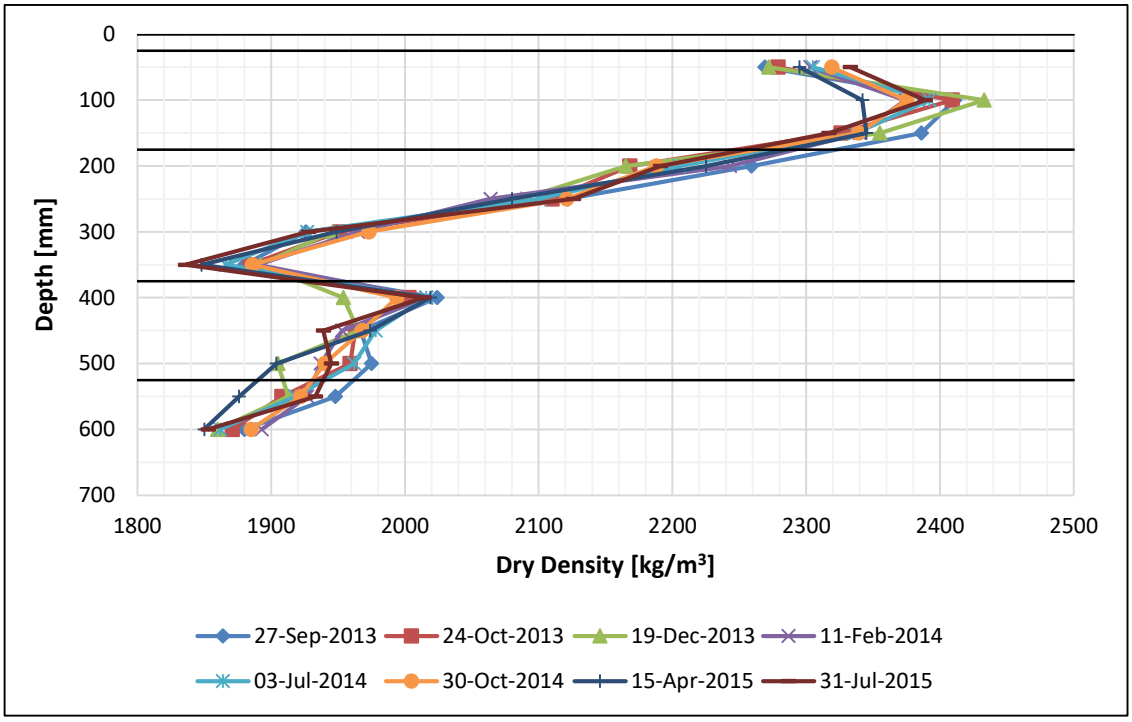

Figure 8-12: Section 2 dry density with depth.

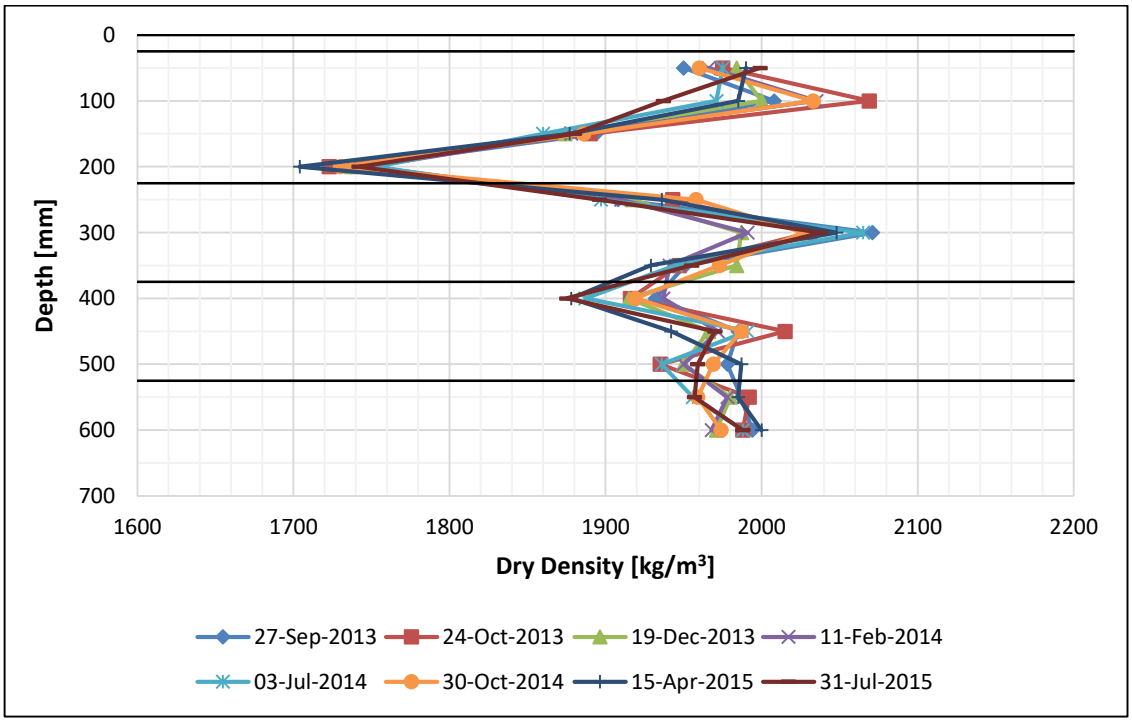

Figure 8-13: Section 3 dry density with depth.

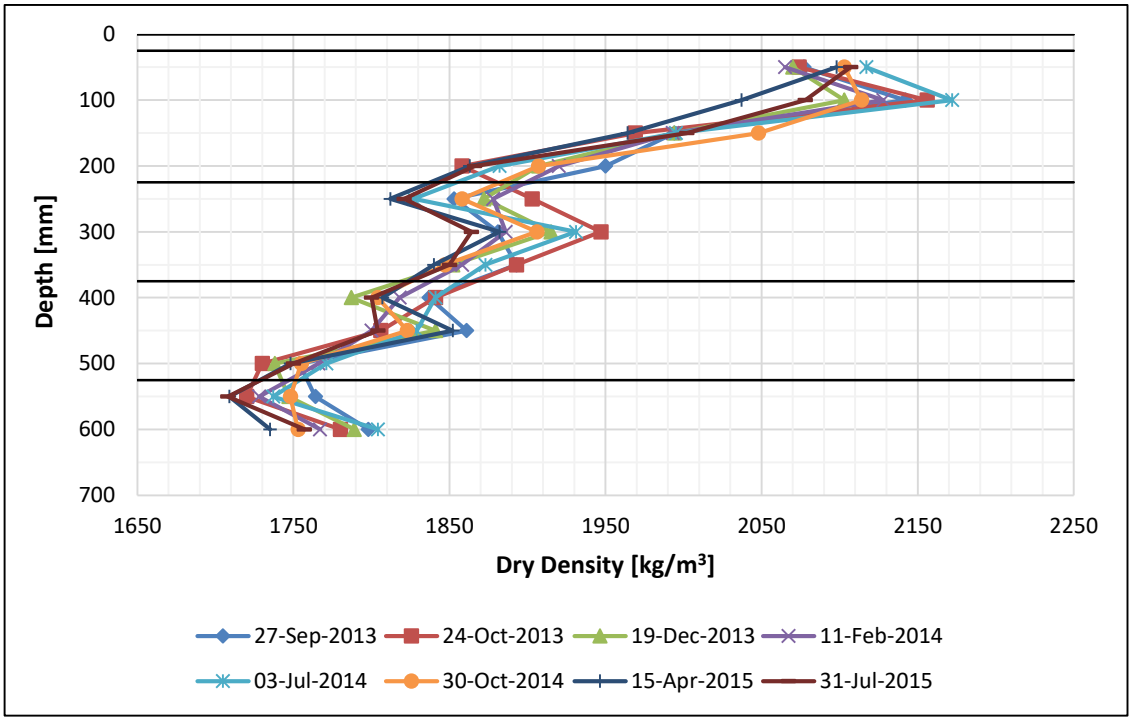

Figure 8-14: Section 4 dry density with depth.

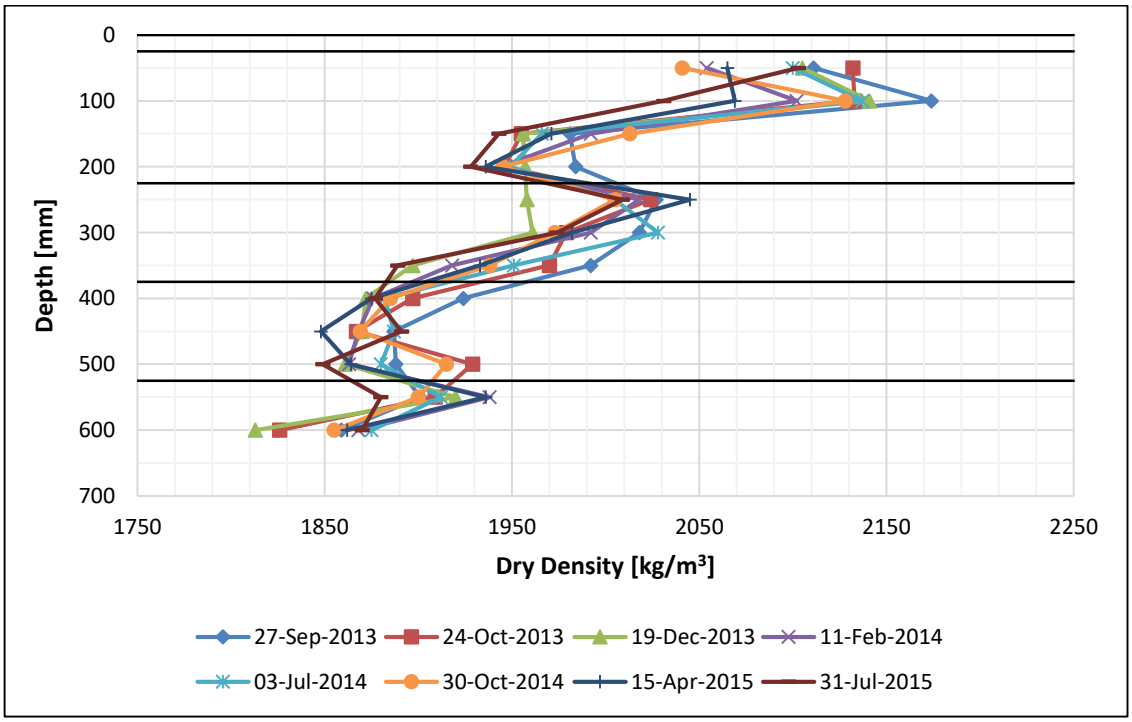

Figure 8-15: Section 5 dry density with depth.

8.4. Appendix D: Moduli Back-Calculation Data

Appendix D provides the moduli back-calculation data for Sections 2 to 7. Figures 8-16 to 8-22 present the final CHEV output data for Sections 2 to 7b respectively. The measured (from MDDs) versus calculated (from CHEV) depth deflections for each section are provided in Tables 8-9 through 8-15. The corresponding measured versus calculated depth deflection plots are illustrated in Figures 8-23 through 8-29.

Total Load: 45.00 kN
Tyre Pressure: 700.00 kPa
Load Radius: 143.05 mm
Wheels: {0;0}

Layer No	Modulus	Poisson Ratio	Thickness (mm)
0	800.0	0.4	25.0
1	320.0	0.35	150.0
2	1975.0	0.3	200.0
3	270.0	0.35	150.0
4	270.0	0.35	150.0

X-ordinate	Y-ordinate	Depth	Value	ZZ	XX	YY	XY	XZ	YZ	OCTSHEAR
0.0	0.0	0.0	Stress	-700.0	-710.8991	-710.8991	0.0	0.0	0.0	5.1379
			Strain	-164.1009	-183.1743	-183.1743	0.0	0.0	0.0	
			Displt	0.4104						
0.0	0.0	160.0	Stress	-477.3587	-193.4199	-193.4199	0.0	0.0	0.0	133.85
			Strain	-1068.6398	129.2268	129.2268	0.0	0.0	0.0	
			Displt	0.2						
0.0	0.0	320.0	Stress	-128.9266	119.1505	119.1505	0.0	0.0	0.0	116.9446
			Strain	-101.4769	61.8143	61.8143	0.0	0.0	0.0	
			Displt	0.1665						
0.0	0.0	480.0	Stress	-56.3661	-0.6652	-0.6652	0.0	0.0	0.0	26.2577
			Strain	-207.0389	71.4658	71.4658	0.0	0.0	0.0	
			Displt	0.1347						
0.0	0.0	900.0	Stress	-20.6446	0.3991	0.3991	0.0	0.0	0.0	9.9201
			Strain	-77.4961	27.7223	27.7223	0.0	0.0	0.0	
			Displt	0.0816						

Figure 8-16: CHEV output for Section 2.

Total Load: 45.00 kN
Tyre Pressure: 700.00 kPa
Load Radius: 143.05 mm
Wheels: {0;0}

Layer No	Modulus	Poisson Ratio	Thickness (mm)
0	950.0	0.4	25.0
1	600.0	0.3	200.0
2	580.0	0.35	150.0
3	580.0	0.35	150.0
4	580.0	0.35	150.0

X-ordinate	Y-ordinate	Depth	Value	ZZ	XX	YY	XY	XZ	YZ	OCTSHEAR
0.0	0.0	0.0	Stress	-700.0	-832.8465	-832.8465	0.0	0.0	0.0	62.6245
			Strain	-35.4976	-231.2715	-231.2715	0.0	0.0	0.0	
			DispIt	0.2887						
0.0	0.0	190.0	Stress	-323.4322	1.2211	1.2211	0.0	0.0	0.0	153.043
			Strain	-540.2748	163.1408	163.1408	0.0	0.0	0.0	
			DispIt	0.1586						
0.0	0.0	350.0	Stress	-139.2774	0.5917	0.5917	0.0	0.0	0.0	65.9349
			Strain	-240.8476	84.7099	84.7099	0.0	0.0	0.0	
			DispIt	0.1003						
0.0	0.0	510.0	Stress	-73.4487	1.8352	1.8352	0.0	0.0	0.0	35.4892
			Strain	-128.8506	46.3792	46.3792	0.0	0.0	0.0	
			DispIt	0.072						
0.0	0.0	900.0	Stress	-25.4991	0.9684	0.9684	0.0	0.0	0.0	12.4769
			Strain	-45.1327	16.4726	16.4726	0.0	0.0	0.0	
			DispIt	0.0421						

Figure 8-17: CHEV output for Section 3.

Total Load: 45.00 kN
Tyre Pressure: 700.00 kPa
Load Radius: 143.05 mm
Wheels: {0;0}

Layer No	Modulus	Poisson Ratio	Thickness (mm)
0	1220.0	0.4	25.0
1	1550.0	0.3	200.0
2	500.0	0.35	150.0
3	500.0	0.35	150.0
4	540.0	0.35	150.0

X-ordinate	Y-ordinate	Depth	Value	ZZ	XX	YY	XY	XZ	YZ	OCTSHEAR
0.0	0.0	0.0	Stress	-700.0	-795.6147	-795.6147	0.0	0.0	0.0	45.0732
			Strain	-52.0559	-161.7777	-161.7777	0.0	0.0	0.0	
			DispIt	0.1879						
0.0	0.0	200.0	Stress	-232.66	140.2857	140.2857	0.0	0.0	0.0	175.8083
			Strain	-204.4074	108.3858	108.3858	0.0	0.0	0.0	
			DispIt	0.1384						
0.0	0.0	360.0	Stress	-103.8503	0.5509	0.5509	0.0	0.0	0.0	49.2152
			Strain	-208.4719	73.4114	73.4114	0.0	0.0	0.0	
			DispIt	0.0948						
0.0	0.0	520.0	Stress	-59.25	-1.057	-1.057	0.0	0.0	0.0	27.4324
			Strain	-117.0201	40.1008	40.1008	0.0	0.0	0.0	
			DispIt	0.0697						
0.0	0.0	900.0	Stress	-23.058	0.865	0.865	0.0	0.0	0.0	11.2774
			Strain	-43.8213	15.9862	15.9862	0.0	0.0	0.0	
			DispIt	0.043						

Figure 8-18: CHEV output for Section 4.

Total Load: 45.00 kN
Tyre Pressure: 700.00 kPa
Load Radius: 143.05 mm
Wheels: {0;0}

Layer No	Modulus	Poisson Ratio	Thickness (mm)
0	810.0	0.4	25.0
1	950.0	0.3	200.0
2	280.0	0.35	150.0
3	280.0	0.35	150.0
4	270.0	0.35	150.0

X-ordinate	Y-ordinate	Depth	Value	ZZ	XX	YY	XY	XZ	YZ	OCTSHEAR
0.0	0.0	0.0	Stress	-700.0	-835.3048	-835.3048	0.0	0.0	0.0	63.7833
			Strain	-39.2051	-273.0653	-273.0653	0.0	0.0	0.0	
			DispIt	0.3308						
0.0	0.0	190.0	Stress	-244.0966	127.9368	127.9368	0.0	0.0	0.0	175.3782
			Strain	-337.7459	171.3523	171.3523	0.0	0.0	0.0	
			DispIt	0.2552						
0.0	0.0	350.0	Stress	-102.8118	1.8618	1.8618	0.0	0.0	0.0	49.3436
			Strain	-371.8395	132.8368	132.8368	0.0	0.0	0.0	
			DispIt	0.1812						
0.0	0.0	510.0	Stress	-57.4791	2.6548	2.6548	0.0	0.0	0.0	28.3474
			Strain	-211.9195	78.0119	78.0119	0.0	0.0	0.0	
			DispIt	0.1364						
0.0	0.0	900.0	Stress	-21.9614	0.8872	0.8872	0.0	0.0	0.0	10.7709
			Strain	-83.6385	30.6043	30.6043	0.0	0.0	0.0	
			DispIt	0.0838						

Figure 8-19: CHEV output for Section 5.

Total Load: 45.00 kN
Tyre Pressure: 700.00 kPa
Load Radius: 143.05 mm
Wheels: {0;0}

Layer No	Modulus	Poisson Ratio	Thickness (mm)
0	790.0	0.44	50.0
1	1150.0	0.44	150.0
2	2900.0	0.3	150.0
3	500.0	0.35	150.0
4	480.0	0.35	150.0

X-ordinate	Y-ordinate	Depth	Value	ZZ	XX	YY	XY	XZ	YZ	OCTSHEAR
0.0	0.0	0.0	Stress	-700.0	-576.1091	-576.1091	0.0	0.0	0.0	58.4027
			Strain	-244.3342	-18.5077	-18.5077	0.0	0.0	0.0	
			DispIt	0.1683						
0.0	0.0	170.0	Stress	-422.2212	-165.5636	-165.5636	0.0	0.0	0.0	120.9896
			Strain	-240.4567	80.9232	80.9232	0.0	0.0	0.0	
			DispIt	0.1114						
0.0	0.0	390.0	Stress	-76.6883	1.4604	1.4604	0.0	0.0	0.0	36.8397
			Strain	-155.4212	55.5803	55.5803	0.0	0.0	0.0	
			DispIt	0.0864						
0.0	0.0	550.0	Stress	-44.8021	0.8305	0.8305	0.0	0.0	0.0	21.5114
			Strain	-94.5488	33.7928	33.7928	0.0	0.0	0.0	
			DispIt	0.0671						
0.0	0.0	900.0	Stress	-19.9642	0.5949	0.5949	0.0	0.0	0.0	9.6916
			Strain	-42.4596	15.3628	15.3628	0.0	0.0	0.0	
			DispIt	0.045						

Figure 8-20: CHEV output for Section 6.

Total Load: 45.00 kN
Tyre Pressure: 700.00 kPa
Load Radius: 143.05 mm
Wheels: {0;0}

Layer No	Modulus	Poisson Ratio	Thickness (mm)
0	3150.0	0.44	50.0
1	7500.0	0.44	150.0
2	3700.0	0.3	150.0
3	750.0	0.35	150.0
4	750.0	0.35	150.0

X-ordinate	Y-ordinate	Depth	Value	ZZ	XX	YY	XY	XZ	YZ	OCTSHEAR
0.0	0.0	0.0	Stress	-700.0	-670.5544	-670.5544	0.0	0.0	0.0	13.8808
			Strain	-34.8927	-21.4319	-21.4319	0.0	0.0	0.0	
			DispIt	0.0672						
0.0	0.0	180.0	Stress	-275.9374	110.2334	110.2334	0.0	0.0	0.0	182.0427
			Strain	-49.7257	24.4191	24.4191	0.0	0.0	0.0	
			DispIt	0.0589						
0.0	0.0	390.0	Stress	-56.3428	3.4916	3.4916	0.0	0.0	0.0	28.2062
			Strain	-78.3826	29.3194	29.3194	0.0	0.0	0.0	
			DispIt	0.0471						
0.0	0.0	550.0	Stress	-34.3745	1.586	1.586	0.0	0.0	0.0	16.9519
			Strain	-47.3129	17.416	17.416	0.0	0.0	0.0	
			DispIt	0.0374						
0.0	0.0	900.0	Stress	-16.3703	0.6471	0.6471	0.0	0.0	0.0	8.0221
			Strain	-22.431	8.2003	8.2003	0.0	0.0	0.0	
			DispIt	0.026						

Figure 8-21: CHEV output for Section 7a.

Total Load: 45.00 kN
Tyre Pressure: 700.00 kPa
Load Radius: 143.05 mm
Wheels: {0;0}

Layer No	Modulus	Poisson Ratio	Thickness (mm)
0	2150.0	0.44	50.0
1	3200.0	0.44	100.0
2	2950.0	0.3	150.0
3	750.0	0.35	200.0
4	325.0	0.35	150.0

X-ordinate	Y-ordinate	Depth	Value	ZZ	XX	YY	XY	XZ	YZ	OCTSHEAR
0.0	0.0	0.0	Stress	-700.0	-726.6202	-726.6202	0.0	0.0	0.0	12.5489
			Strain	-28.174	-46.0034	-46.0034	0.0	0.0	0.0	
			DispIt	0.134						
0.0	0.0	160.0	Stress	-356.077	13.5698	13.5698	0.0	0.0	0.0	174.2532
			Strain	-123.464	39.4312	39.4312	0.0	0.0	0.0	
			DispIt	0.1188						
0.0	0.0	320.0	Stress	-86.0714	17.6559	17.6559	0.0	0.0	0.0	48.8975
			Strain	-131.2407	55.4685	55.4685	0.0	0.0	0.0	
			DispIt	0.1037						
0.0	0.0	480.0	Stress	-38.8634	29.4999	29.4999	0.0	0.0	0.0	32.2268
			Strain	-79.3511	43.7029	43.7029	0.0	0.0	0.0	
			DispIt	0.0881						
0.0	0.0	900.0	Stress	-14.7259	0.7419	0.7419	0.0	0.0	0.0	7.2916
			Strain	-46.9083	17.3424	17.3424	0.0	0.0	0.0	
			DispIt	0.0569						

Figure 8-22: CHEV output for Section 7b.

Table 8-9: Measured versus calculated depth deflections for Section 2.

	MDD1	MDD2	MDD3	MDD4	MDD5	Anchor
Depth [m]	0	-0.16	-0.32	-0.48	-0.90	-3.00
Measured [mm]	0.4150	0.1823	0.1765	0.1202	0.0712	0
Calculated [mm]	0.4104	0.2000	0.1665	0.1347	0.0816	0
Difference [mm]	0.0046	0.0177	0.0100	0.0145	0.0104	0

Table 8-10: Measured versus calculated depth deflections for Section 3.

	MDD1	MDD2	MDD3	MDD4	MDD5	Anchor
Depth [m]	0	-0.19	-0.35	-0.51	-0.90	-3.00
Measured [mm]	0.2870	0.1685	0.0830	0.0694	0.0405	0
Calculated [mm]	0.2887	0.1586	0.1003	0.072	0.0421	0
Difference [mm]	0.0017	0.0099	0.0173	0.0026	0.0016	0

Table 8-11: Measured versus calculated depth deflections for Section 4.

	MDD1	MDD2	MDD3	MDD4	MDD5	Anchor
Depth [m]	0	-0.20	-0.36	-0.52	-0.90	-3.00
Measured [mm]	0.1781	0.1607	0.0897	0.0627	0.0357	0
Calculated [mm]	0.1879	0.1384	0.0948	0.0697	0.0430	0
Difference [mm]	0.0098	0.0223	0.0051	0.0070	0.0073	0

Table 8-12: Measured versus calculated depth deflections for Section 5.

	MDD1	MDD2	MDD3	MDD4	MDD5	Anchor
Depth [m]	0	-0.19	-0.35	-0.51	-0.90	-3.00
Measured [mm]	0.3441	0.2611	0.1894	0.1216	0.0726	0
Calculated [mm]	0.3308	0.2552	0.1812	0.1364	0.0838	0
Difference [mm]	0.0133	0.0059	0.0082	0.0148	0.0112	0

Table 8-13: Measured versus calculated depth deflections for Section 6.

	MDD1	MDD2	MDD3	MDD4	MDD5	Anchor
Depth [m]	0	-0.17	-0.39	-0.55	-0.90	-3.00
Measured [mm]	0.1746	0.1088	0.0858	0.0637	0.0413	0
Calculated [mm]	0.1683	0.1114	0.0864	0.0671	0.045	0
Difference [mm]	0.0063	0.0026	0.0006	0.0034	0.0037	0

Table 8-14: Measured versus calculated depth deflections for Section 7a.

	MDD1	MDD2	MDD3	MDD4	MDD5	Anchor
Depth [m]	0	-0.18	-0.39	-0.55	-0.90	-3.00
Measured [mm]	0.0670	0.0573	0.0492	0.0401	0.0285	0
Calculated [mm]	0.0672	0.0589	0.0471	0.0374	0.0260	0
Difference [mm]	0.0002	0.0016	0.0021	0.0027	0.0025	0

Table 8-15: Measured versus calculated depth deflections for Section 7b.

	MDD1	MDD2	MDD3	MDD4	MDD5	Anchor
Depth [m]	0	-0.16	-0.32	-0.48	-0.90	-3.00
Measured [mm]	0.1404	0.1125	0.0938	0.0838	0.0702	0
Calculated [mm]	0.1340	0.1188	0.1037	0.0881	0.0569	0
Difference [mm]	0.0064	0.0063	0.0099	0.0043	0.0133	0

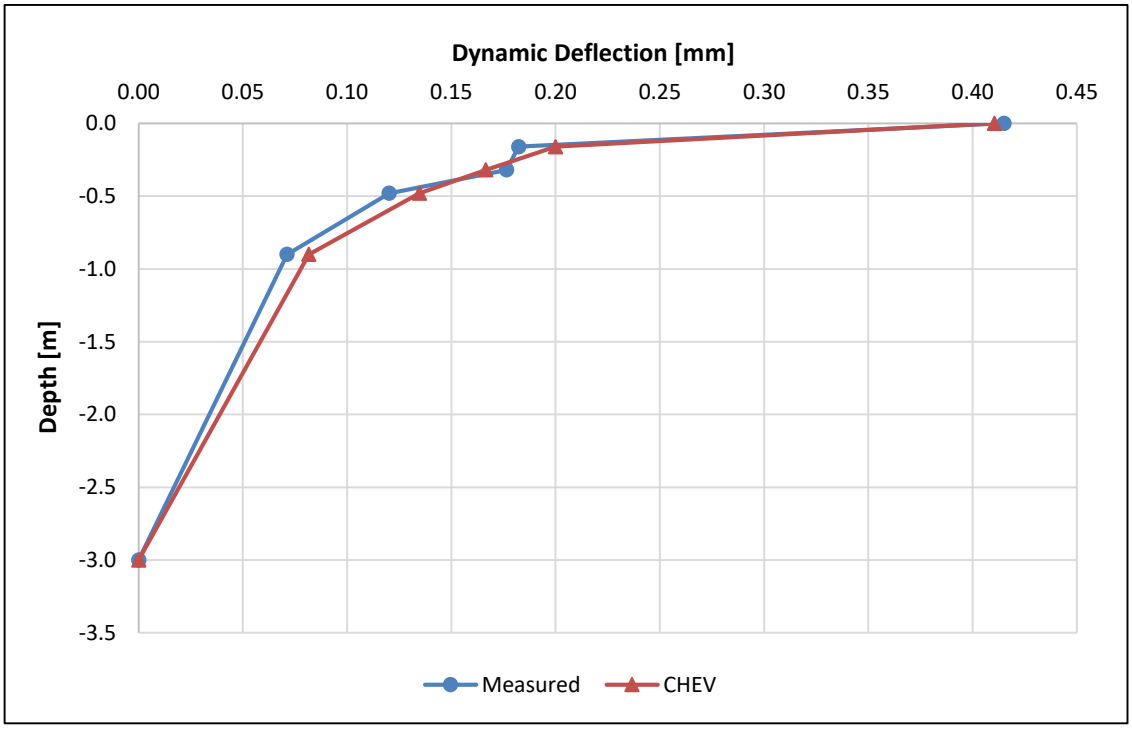

Figure 8-23: Measured versus calculated depth deflections for Section 2.

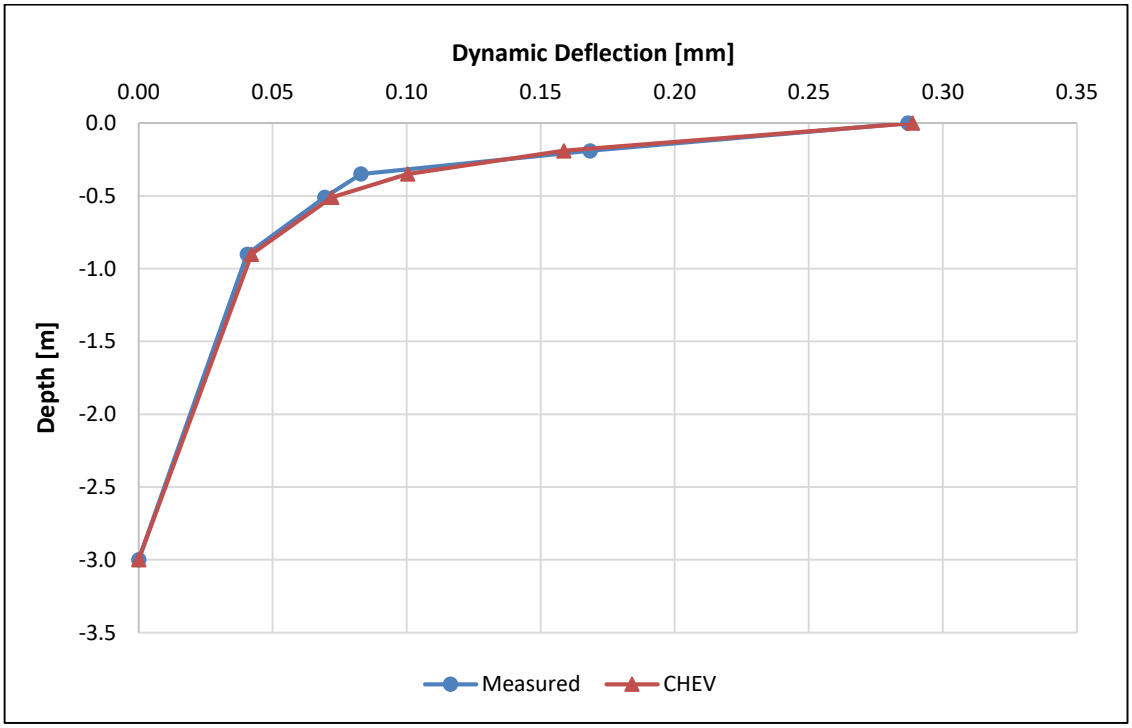

Figure 8-24: Measured versus calculated depth deflections for Section 3.

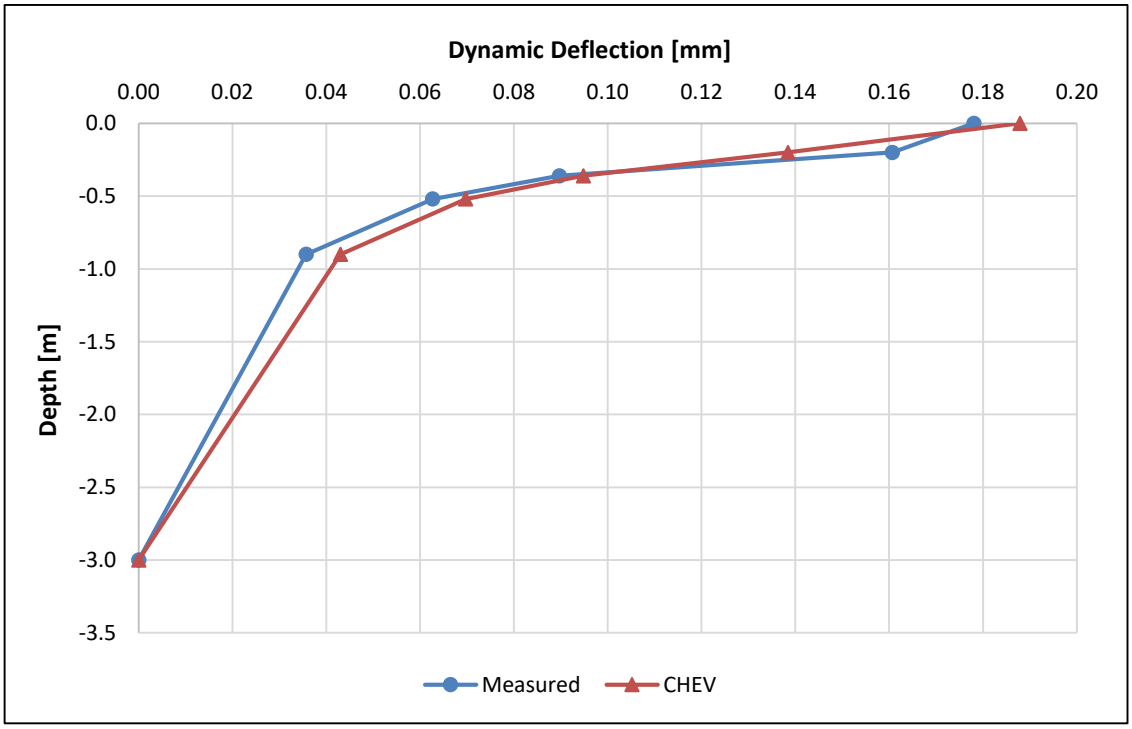

Figure 8-25: Measured versus calculated depth deflections for Section 4.

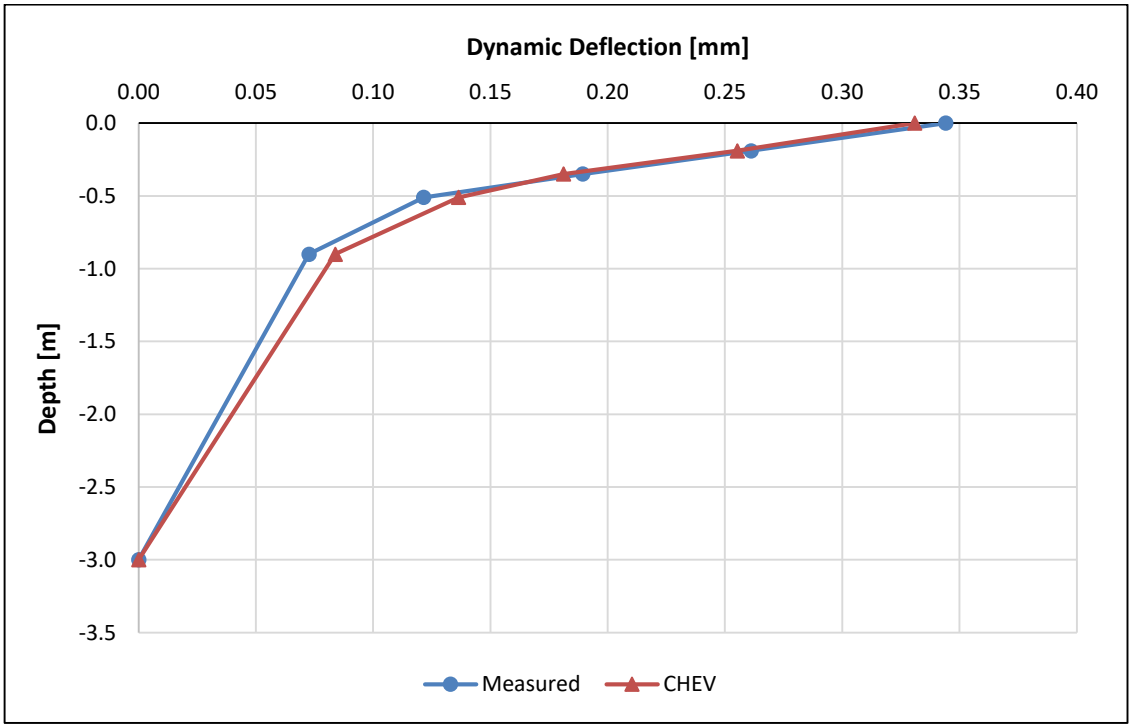

Figure 8-26: Measured versus calculated depth deflections for Section 5.

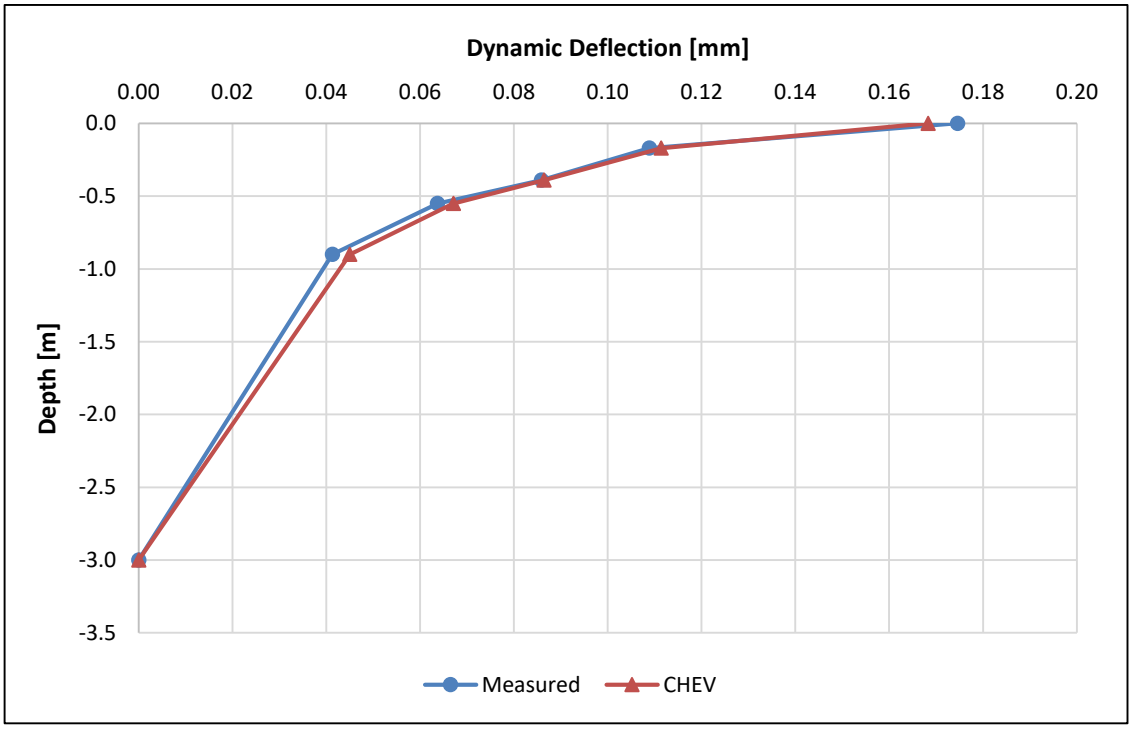

Figure 8-27: Measured versus calculated depth deflections for Section 6.

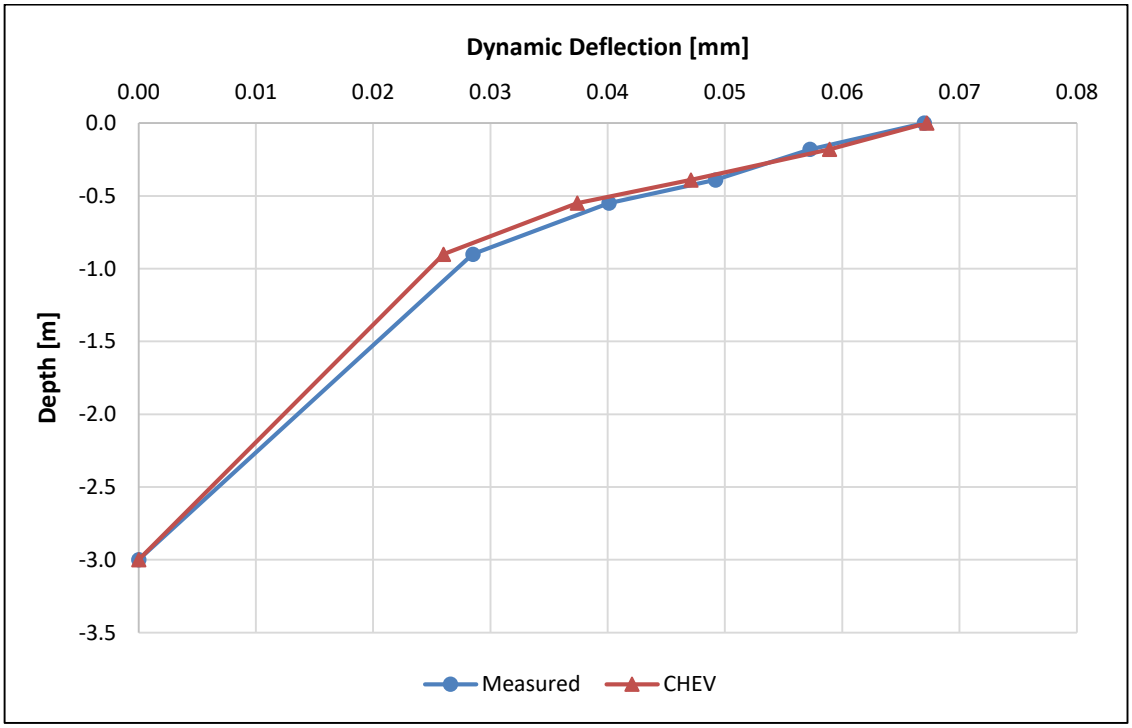

Figure 8-28: Measured versus calculated depth deflections for Section 7a.

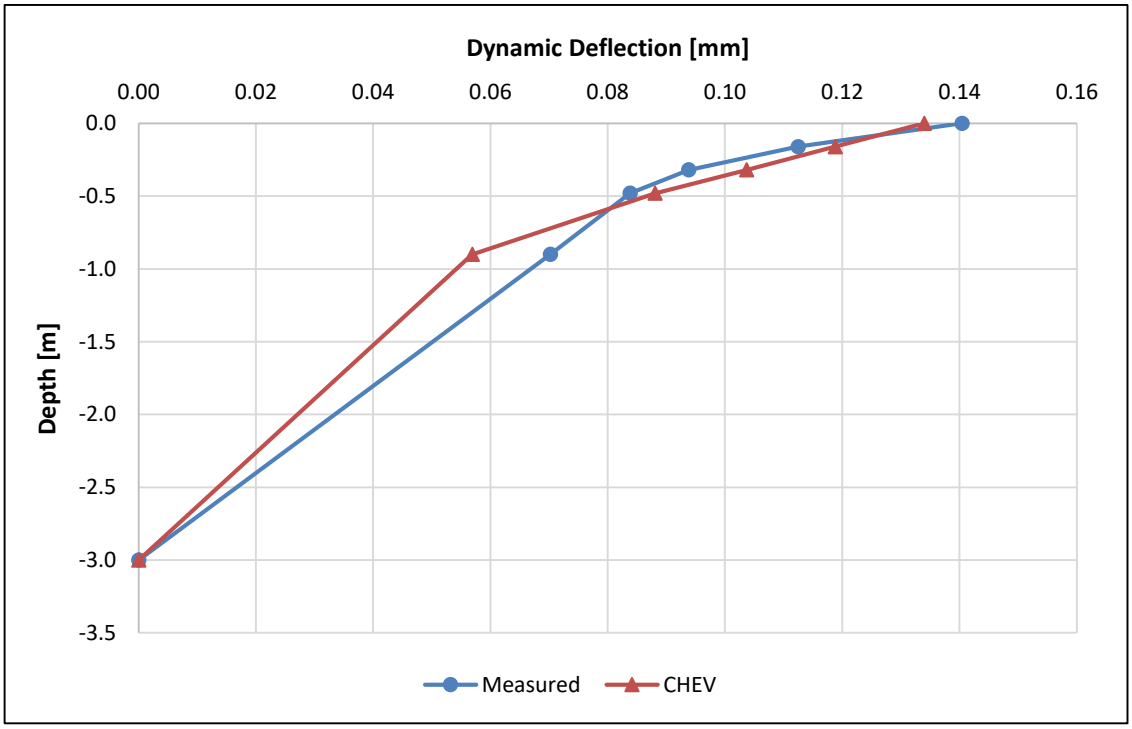

Figure 8-29: Measured versus calculated depth deflections for Section 7b.

8.5. Appendix E: Pavement Number Data

Appendix E provides the pavement number data for Sections 2 to 7. Tables 8-16 through 8-36 show the results for Sections 2 through 7b.

Table 8-16: Calculation of subgrade ELTS for Section 2.

Step	Data Type	Value	Source
a	Subgrade Class / Initial Stiffness	G8 / 270 MPa	Assumed / Table 4-14
b	Climate / Adjustment Factor	Moderate / 0.9	Assumed / Table 3-5
c	Cover Depth / Adjustment Factor	525 mm / -8.33 MPa	Known / Figure 3-17
d	Subgrade ELTS	(270*0.9) - 8.33 = 234.67 MPa	Calculated

Table 8-17: Calculation of ELTS for individual layers of Section 2.

Layer	Maximum Stiffness (E_{max}) & Modular Ration (MR)	Effective Long-Term Stiffness
25 mm S2 Surfacing	E_{max} = 800 MPa, MR = 2.0	ELTS = min (800, 2.0 x 320) = 640 MPa
150 mm G1 Base	E_{max} = 320 MPa, MR = 2.0	ELTS = min (320, 2.0 x 1080) = 320 MPa
200 mm C3 Subbase	E_{max} = 1975 MPa, MR = 4.0	ELTS = min (1975, 4.0 x 270) = 1080 MPa
150 mm G7 Selected	E_{max} = 270 MPa, MR = 1.7	ELTS = min (270, 1.7 x 234.67) = 270 MPa
G8 Subgrade		ELTS = 234.67 MPa (from Table 8-16)

Table 8-18: Calculation of pavement number for Section 2.

Layer	Thickness [mm]	Material Class	ELTS [MPa]	Thickness Adjustment Factor	BCF	Layer Contribution
Surfacing	25	S2	640	n/a	n/a	1.60
Base	150	G1	320	n/a	0.2	0.96
Subbase	200	C3	1080	0.4	n/a	8.64
Selected	150	G7	270	n/a	n/a	4.05
Subgrade	Semi-Infinite	G8	234.67	n/a	n/a	n/a
				Pavement Number =		15.25

Table 8-19: Calculation of subgrade ELTS for Section 3.

Step	Data Type	Value	Source
a	Subgrade Class / Initial Stiffness	G8 / 580 MPa	Assumed / Table 4-14
b	Climate / Adjustment Factor	Moderate / 0.9	Assumed / Table 3-5
c	Cover Depth / Adjustment Factor	525 mm / -8.33 MPa	Known / Figure 3-17
d	Subgrade ELTS	(580*0.9) - 8.33 = 513.67 MPa	Calculated

Table 8-20: Calculation of ELTS for individual layers of Section 3.

Layer	Maximum Stiffness (E_{max}) & Modular Ration (MR)	Effective Long-Term Stiffness
25 mm S2 Surfacing	E_{max} = 950 MPa, MR = 2.0	ELTS = min (950, 2.0 x 600) = 950 MPa
200 mm BSM1 Base	E_{max} = 600 MPa, MR = 3.0	ELTS = min (600, 3.0 x 580) = 600 MPa
150 mm G7 Subbase	E_{max} = 580 MPa, MR = 1.7	ELTS = min (580, 1.7 x 580) = 580 MPa
150 mm G7 Selected	E_{max} = 580 MPa, MR = 1.7	ELTS = min (580, 1.7 x 513.67) = 580 MPa
G8 Subgrade		ELTS = 513.67 MPa (from Table 8-19)

Table 8-21: Calculation of pavement number for Section 3.

Layer	Thickness [mm]	Material Class	ELTS [MPa]	Thickness Adjustment Factor	BCF	Layer Contribution
Surfacing	25	S2	950	n/a	n/a	2.38
Base	200	BSM1	600	n/a	1.0	12.00
Subbase	150	G7	580	n/a	n/a	8.70
Selected	150	G7	580	n/a	n/a	8.70
Subgrade	Semi-Infinite	G8	513.67	n/a	n/a	n/a
				Pavement Number =		31.78

Table 8-22: Calculation of subgrade ELTS for Section 4.

Step	Data Type	Value	Source
a	Subgrade Class / Initial Stiffness	G8 / 540 MPa	Assumed / Table 4-14
b	Climate / Adjustment Factor	Moderate / 0.9	Assumed / Table 3-5
c	Cover Depth / Adjustment Factor	525 mm / -8.33 MPa	Known / Figure 3-17
d	Subgrade ELTS	(540*0.9) - 8.33 = 477.67 MPa	Calculated

Table 8-23: Calculation of ELTS for individual layers of Section 4.

Layer	Maximum Stiffness (E_{max}) & Modular Ration (MR)	Effective Long-Term Stiffness
25 mm S2 Surfacing	E_{max} = 1220 MPa, MR = 2.0	ELTS = min (1220, 2.0 x 1500) = 1220 MPa
200 mm BSM1 Base	E_{max} = 1550 MPa, MR = 3.0	ELTS = min (1550, 3.0 x 500) = 1500 MPa
150 mm G7 Subbase	E_{max} = 500 MPa, MR = 1.7	ELTS = min (500, 1.7 x 500) = 500 MPa
150 mm G7 Selected	E_{max} = 500 MPa, MR = 1.7	ELTS = min (500, 1.7 x 477.67) = 500 MPa
G8 Subgrade		ELTS = 477.67 MPa (from Table 8-22)

Table 8-24: Calculation of pavement number for Section 4.

Layer	Thickness [mm]	Material Class	ELTS [MPa]	Thickness Adjustment Factor	BCF	Layer Contribution
Surfacing	25	S2	1220	n/a	n/a	3.05
Base	200	BSM1	1500	n/a	1.0	30.00
Subbase	150	G7	500	n/a	n/a	7.50
Selected	150	G7	500	n/a	n/a	7.50
Subgrade	Semi-Infinite	G8	477.67	n/a	n/a	n/a
				Pavement Number =		48.05

Table 8-25: Calculation of subgrade ELTS for Section 5.

Step	Data Type	Value	Source
a	Subgrade Class / Initial Stiffness	G8 / 270 MPa	Assumed / Table 4-14
b	Climate / Adjustment Factor	Moderate / 0.9	Assumed / Table 3-5
c	Cover Depth / Adjustment Factor	525 mm / -8.33 MPa	Known / Figure 3-17
d	Subgrade ELTS	(270*0.9) - 8.33 = 234.67 MPa	Calculated

Table 8-26: Calculation of ELTS for individual layers of Section 5.

Layer	Maximum Stiffness (E_{max}) & Modular Ration (MR)	Effective Long-Term Stiffness
25 mm S2 Surfacing	E_{max} = 810 MPa, MR = 2.0	ELTS = min (810, 2.0 x 950) = 810 MPa
200 mm C3 Base	E_{max} = 950 MPa, MR = 4.0	ELTS = min (950, 4.0 x 280) = 950 MPa
150 mm G7 Subbase	E_{max} = 280 MPa, MR = 1.7	ELTS = min (280, 1.7 x 280) = 280 MPa
150 mm G7 Selected	E_{max} = 280 MPa, MR = 1.7	ELTS = min (280, 1.7 x 234.67) = 280 MPa
G8 Subgrade		ELTS = 234.67 MPa (from Table 8-25)

Table 8-27: Calculation of pavement number for Section 5.

Layer	Thickness [mm]	Material Class	ELTS [MPa]	Thickness Adjustment Factor	BCF	Layer Contribution
Surfacing	25	S2	810	n/a	n/a	2.03
Base	200	C3	950	0.4	0.4	3.04
Subbase	150	G7	280	n/a	n/a	4.20
Selected	150	G7	280	n/a	n/a	4.20
Subgrade	Semi-Infinite	G8	234.67	n/a	n/a	n/a
				Pavement Number =		13.47

Table 8-28: Calculation of subgrade ELTS for Section 6.

Step	Data Type	Value	Source
a	Subgrade Class / Initial Stiffness	G8 / 480 MPa	Assumed / Table 4-14
b	Climate / Adjustment Factor	Moderate / 0.9	Assumed / Table 3-5
c	Cover Depth / Adjustment Factor	500 mm / -10 MPa	Known / Figure 3-17
d	Subgrade ELTS	(480*0.9) - 10 = 422 MPa	Calculated

Table 8-29: Calculation of ELTS for individual layers of Section 6.

Layer	Maximum Stiffness (E_{max}) & Modular Ration (MR)	Effective Long-Term Stiffness
50 mm AC Surfacing	E_{max} = 790 MPa, MR = 5.0	ELTS = min (790, 5.0 x 1150) = 790 MPa
150 mm AC Base	E_{max} = 1150 MPa, MR = 5.0	ELTS = min (1150, 5.0 x 2000) = 1150 MPa
150 mm C3 Subbase	E_{max} = 2900 MPa, MR = 4.0	ELTS = min (2900, 4.0 x 500) = 2000 MPa
150 mm G7 Selected	E_{max} = 500 MPa, MR = 1.7	ELTS = min (500, 1.7 x 422) = 500 MPa
G8 Subgrade		ELTS = 422 MPa (from Table 8-28)

Table 8-30: Calculation of pavement number for Section 6.

Layer	Thickness [mm]	Material Class	ELTS [MPa]	Thickness Adjustment Factor	BCF	Layer Contribution
Surfacing	50	AC	790	n/a	n/a	3.95
Base	150	AC	1150	n/a	1.0	17.25
Subbase	150	C3	2000	0.2	n/a	6.00
Selected	150	G7	500	n/a	n/a	7.50
Subgrade	Semi-Infinite	G8	422	n/a	n/a	n/a
				Pavement Number =		34.70

Table 8-31: Calculation of subgrade ELTS for Section 7a.

Step	Data Type	Value	Source
a	Subgrade Class / Initial Stiffness	G8 / 750 MPa	Assumed / Table 4-14
b	Climate / Adjustment Factor	Moderate / 0.9	Assumed / Table 3-5
c	Cover Depth / Adjustment Factor	500 mm / -10 MPa	Known / Figure 3-17
d	Subgrade ELTS	(750*0.9) - 10 = 665 MPa	Calculated

Table 8-32: Calculation of ELTS for individual layers of Section 7a.

Layer	Maximum Stiffness (E_{max}) & Modular Ration (MR)	Effective Long-Term Stiffness
50 mm AC Surfacing	E_{max} = 3150 MPa, MR = 5.0	ELTS = min (3150, 5.0 x 7500) = 3150 MPa
150 mm AC Base	E_{max} = 7500 MPa, MR = 5.0	ELTS = min (7500, 5.0 x 3000) = 7500 MPa
150 mm C3 Subbase	E_{max} = 3700 MPa, MR = 4.0	ELTS = min (3700, 4.0 x 750) = 3000 MPa
150 mm G7 Selected	E_{max} = 750 MPa, MR = 1.7	ELTS = min (750, 1.7 x 665) = 750 MPa
G8 Subgrade		ELTS = 665 MPa (from Table 8-31)

Table 8-33: Calculation of pavement number for Section 7a.

Layer	Thickness [mm]	Material Class	ELTS [MPa]	Thickness Adjustment Factor	BCF	Layer Contribution
Surfacing	50	AC	3150	n/a	n/a	15.75
Base	150	AC	7500	n/a	1.0	112.50
Subbase	150	C3	3000	0.2	n/a	9.00
Selected	150	G7	750	n/a	n/a	11.25
Subgrade	Semi-Infinite	G8	665	n/a	n/a	n/a
				Pavement Number =		148.50

Table 8-34: Calculation of subgrade ELTS for Section 7b.

Step	Data Type	Value	Source
a	Subgrade Class / Initial Stiffness	G8 / 325 MPa	Assumed / Table 4-14
b	Climate / Adjustment Factor	Moderate / 0.9	Assumed / Table 3-5
c	Cover Depth / Adjustment Factor	500 mm / -10 MPa	Known / Figure 3-17
d	Subgrade ELTS	(325*0.9) - 10 = 282.5 MPa	Calculated

Table 8-35: Calculation of ELTS for individual layers of Section 7b.

Layer	Maximum Stiffness (E_{max}) & Modular Ration (MR)	Effective Long-Term Stiffness
50 mm AC Surfacing	E_{max} = 2150 MPa, MR = 5.0	ELTS = min (2150, 5.0 x 3200) = 2150 MPa
100 mm AC Base	E_{max} = 3200 MPa, MR = 5.0	ELTS = min (3200, 5.0 x 1921) = 3200 MPa
150 mm C3 Subbase	E_{max} = 2950 MPa, MR = 4.0	ELTS = min (2950, 4.0 x 480.25) = 1921 MPa
200 mm G7 Selected	E_{max} = 750 MPa, MR = 1.7	ELTS = min (750, 1.7 x 282.5) = 480.25 MPa
G8 Subgrade		ELTS = 282.5 MPa (from Table 8-34)

Table 8-36: Calculation of pavement number for Section 7b.

Layer	Thickness [mm]	Material Class	ELTS [MPa]	Thickness Adjustment Factor	BCF	Layer Contribution
Surfacing	50	AC	2150	n/a	n/a	10.75
Base	100	AC	3200	n/a	1.0	32.00
Subbase	150	C3	1921	0.2	n/a	5.76
Selected	200	G7	480.25	n/a	n/a	9.61
Subgrade	Semi-Infinite	G8	282.5	n/a	n/a	n/a
				Pavement Number =		58.12